In pursuit of RAFT-functional polyethylene: exploration of a novel class of Sn-RAFT agents and the preparation and application of RAFT-functional polyethylene-like poly(ω-pentadecalactone)

ROBIN L. PFLUGHAUPT

A THESIS SUBMITTED IN PARTIAL FULFILLMENT OF THE REQUIREMENTS FOR THE DEGREE OF

DOCTOR OF PHILOSOPHY IN CHEMISTRY

DEPARTMENT OF CHEMISTRY

THE UNIVERSITY OF
WARWICK

FEBRUARY 2014

Table of Contents

List of Figures

List of Schemes

List of Tables

Abbreviations

δ	Chemical shift
λ	Wavelength
ºC	Degrees Centigrade
%	Percent
AIBN	2,2′-Azobis(2-methylpropionitrile)
AICN	1,1′-Azobis(cyclohexanecarbonitrile)
AM	Acrylamide
Am	Ambrettolide
AmE	epoxide of Ambrettolide
AN	Acrylonitrile
ATRP	Atom Transfer Radical Polymerization
b	block
B#	Biodiesel content (%) in blends with petroleum diesel
BA	Butyl acrylate
^{t}BA	*tert*-Butyl acrylate
BenzCL	γ-Benzoyl-ε-caprolactone
^{t}BMA	*tert*-Butyl methacrylate
Bn	Benzyl
BnOH	Benzyl Alcohol
bs	broad singlet
Calc.	Calculated
CCG	Catalysed Chain Growth
$CDCl_3$	Deuterated Chloroform
cEA	1-oxa-8-aza-cyclotetradecan-9,14-dione
CFPP	Cold Filter Plugging Point
$CHCl_3$	Chloroform
CL	ε-Caprolactone
COSY	Correlation Spectroscopy
CRP	Controlled Radical Polymerization
CTA	Chain Transfer Agent
d	doublet
DBSA	Dodecylbenzenesulfonic acid
dd	doublet of doublets

DCM	Dichloromethane
DCTB	*trans*-2-[3-(4-*tert*-butylphenyl)-2-methyl-2-propyl-lidene]malonitrile
DDL	12-Dodecanolide
DEPT	Distortionless Enhancement by Polarization Transfer
$Đ_M$	Dispersity
dm	doublet of multiplets
DMAP	4-(Dimethylamino)pyridine
DP	Degree of Polymerization
DPP	Diphenyl phosphate
DRI	Differential Refractive Index
DSC	Differential Scanning Calorimetry
DVB	Divinyl benzene
DXO	1,5-Dioxepan-2-one
EAM	Enzyme-activated monomer
EGDMA	Ethylene glycol dimethacrylate
EHA	2-Ethylhexyl acrylate
EHMPP	Ethyl 3-(4-(hydroxymethyl)piperidin-1-yl)propanoate
eq.	Equivalent(s)
eROP	Enzymatic Ring-Opening Polymerization
EtOAc	Ethyl acetate
EVA	Ethylene-*co*-Vinyl Acetate copolymer
FAME	Fatty Acid Methyl Ester
FR	Free radical
FT-IR	Fourier-transform infra-red
g	Gram
GPC	Gel Permeation Chromatography
HDL	16-Hexadecanolide
HDPE	High Density Polyethylene
2-HEA	2-Hydroxyethyl acrylate
2-HEMA	2-Hydroxyethyl methacrylate
HiC	*Humicola insolens*
HMBC	Heteronuclear Multiple-Bond Correlation
HMQC	Heteronuclear Multiple-Quantum Correlation
IDA	Isodecyl acrylate
IFDF	Isopropylfluorodithioformate

IR	Infra-red
J/Hz	Coupling constant
kV	Kilovolts
L	Litre
LA	Lauryl acrylate
LAM	Less Activated Monomer
LDPE	Low Density Polyethylene
LS	Light Scattering
m	multiplet
M	Molar
$[M]_0/[I]_0$	Initial molar ratio of monomer to initiator
$[M]_t/[M]_0$	Monomer conversion at time = t
MA	Methyl acrylate
MAO	Methylaluminoxane
MALDI-ToF MS	Matrix-Assisted Laser Desorption and Ionisation Time-of-Flight Mass Spectrometry
MAM	More Activated Monomer
McrCL	γ-Methacryloyl-ε-caprolactone
MDFI	Middle Distillate Flow Improver
MDO	2-methylene-1,3-dioxepane
4MeCL	4-Methyl-caprolactone
MeOH	Methanol
MHz	Megahertz
min	Minutes
mL	Millilitre
mm	Millimetre
MMA	Methyl methacrylate
mmol	Millimole
M_n	Number-averaged molecular weight
mol	Mole
M_p	Molecular weight of the highest peak
m.p.	Melting point
MPa	Megapascals
M_w	Weight-averaged molecular weight
m/z	Mass-to-charge ratio

NIPAM	*N*-isopropylacrylamide
nm	Nanometer
NMP	Nitroxide-Mediated Polymerization
NMR	Nuclear Magnetic Resonance
ns	Nanosecond
NVC	*N*-vinylcarbazole
NVP	*N*-vinylpyrrolidone
Obs.	Observed
PCL	Poly(ε-Caprolactone)
PDL	ω-Pentadecalactone
PE	Polyethylene
PEG	Poly(Ethylene glycol)
PEGMA	ω-hydroxyl-ω'-methacrylate-poly(ethylene glycol)
PEHA	Poly(2-ethylhexyl acrylate)
PFOMA	1*H*,1*H*,2*H*,2*H*-perfluorooctyl methacrylate
PIDA	Poly(Isodecyl acrylate)
PLA	Poly(Lauryl acrylate)
PMA	Poly(Methyl acrylate)
PPDL	Poly(ω-Pentadecalactone)
ppm	parts per million
PS	Polystyrene
PSA	Poly(Stearyl acrylate)
q	quartet
RAFT	Reversible Addition-Fragmentation chain Transfer
RI	Refractive Index
ROP	Ring-Opening Polymerization
s	singlet
S	Styrene
SA	Stearyl acrylate
scCO$_2$	Supercritical carbon dioxide
sept	septet
StB	4-(3-butenyl)styrene
t	Time or triplet
TBD	1,5,7-Triazabicyclo[4.4.0]dec-5-ene
TEMPO	2,2,6,6-Tetramethylpiperidin-1-yl)oxyl

TfOH	Trifluoromethanesulfonic acid
T_g	Glass transition temperature
TGA	Thermogravimetric analysis
THF	Tetrahydrofuran
TLC	Thin Layer Chromatography
T_m	Melting transition temperature
TMC	Trimethylene carbonate
pTSA	p-Toluene sulfonic acid
μ	micro
UDL	11-Undecanolide
UV	Ultraviolet
VAc	Vinyl acetate
vis	visible
WASA	Wax Anti-Settling Agent
WCM	Wax Crystal Modifiers
wt.%	Weight Percent

Acknowledgements

Declaration and Inclusion of Material from a Prior Thesis

Experimental work contained in this thesis is the original research carried out by the author, unless otherwise stated, in the Department of Chemistry at the University of Warwick or at Infineum UK Ltd, Milton Hill, Oxfordshire between November 2009 and February 2014. No material herein has been submitted for any other degree or at any other institution.

Results from other authors are referenced in the usual manner throughout the text.

Signed: _____   Date: _____

Robin L. Pflughaupt

Abstract

This work explores the preparation of Reversible Addition-Fragmentation chain-Transfer (RAFT)-functional polyethylene (PE). Challenges in developing methods to control the polymerization of primary radicals and prepare functional polyethylene are significant. Modest control over ethylene polymerization demonstrated *via* F-RAFT polymerization inspired our interest in RAFT agent design and we envisaged that metallo-RAFT agents could present different reactivities towards primary radicals. Considering the challenge of attempting to develop chemistry for the controlled radical polymerization of primary radicals, preparation of RAFT-functional polyethylene-like poly(ω-pentadecalactone) (PPDL) was also investigated. We envisaged the preparation of RAFT-functional PPDL to be more convenient than reported strategies to prepare functional polyethylene all whilst being a "green" alternative to PE that may be suitable for some applications.

Chapter 1 discusses challenges in preparing functional polyethylene *via* controlled radical polymerization techniques. Furthermore, metallo-RAFT chemistry and the ring-opening polymerization of macrocyclic esters are reviewed.

Chapter 2 describes the synthesis of PPDL *via* enzymatic ring-opening polymerization (eROP). Using a bifunctional initiator appropriate for the RAFT polymerization of acrylic and styrenic monomers, RAFT-functional poly(ω-pentadecalactone) was prepared. Furthermore, chain extension of the macro-chain-transfer agent was utilized to prepare acrylic and styrenic block copolymers of PPDL. To our knowledge, this is the first preparation of block copolymers of poly(ω-pentadecalactone) *via* a combination of eROP and RAFT polymerization techniques.

Chapter 3 describes the large scale synthesis and characterization of a selection of acrylic block copolymers of PPDL suitable for fuels applications. Furthermore, the fuels testing of these copolymers for cold flow applications is described. In general, all block copolymers of PPDL, in particular poly(ω-pentadecalactone)-*b*-poly(isodecyl acrylate) improved the cold flow performance of various diesel fuels.

Chapter 4 reports the synthesis of Sn-RAFT agents and their subsequent use in the controlled radical polymerization of several vinylic monomers.

Chapter 5 summarizes the findings in chapters 2 – 4 and Chapter 6 communicates the associated experimental data.

Chapter 1

Introduction

1.1 Block Copolymers and Higher Architectures of Polyethylene

Polyethylene (PE) is the most widely used material, with annual production exceeding 80 million metric tons.[1] Its ubiquity arises from the range of versatile properties exhibited by polyethylene depending on its density and degree of branching, and the fact that it is relatively cheap and easy to prepare. The cost of producing polyethylene products, however, is increased where essential post-polymerization modifications are required since polyethylene is highly hydrophobic and difficult to functionalize. Therefore, if appropriate copolymers of ethylene that do not require material modification could be prepared, costly steps in the production of countless products could be reduced or eliminated. Furthermore, since efficient techniques to functionalize polyethylene are limited, potentially interesting and useful defined copolymer architectures of polyethylene have yet to be fully explored.

Although polyethylene can be prepared *via* free radical polymerization, it is generally commercially prepared *via* coordination polymerization since the free radical process requires high-pressure (1000-4000 bar), high-temperature (200-300 ℃) bulk conditions to minimize branching resulting from uncontrolled chain transfer.[2] Both of these techniques, however, do not afford end-group control of the polymer product and consequently greatly limit the preparation of defined architectures of polyethylene and copolymers thereof. Therefore, the preparation of polyethylene *via* living or controlled radical polymerization (CRP) techniques is highly desirable. Preparation of polyethylene *via* CRP techniques, however, has not been achieved to date since these processes cannot control the polymerization of monomers generating primary propagating radicals, such as ethylene. The preparation of block copolymers of polyethylene using living and CRP techniques, however, has been demonstrated by applying atom transfer radical polymerization (ATRP), nitroxide-mediated polymerization (NMP), reversible addition-fragmentation chain transfer (RAFT) polymerization, and ring-opening polymerization (ROP) techniques to appropriately modified polyethylene prepared *via* coordination polymerization.[3] An interesting example includes preparing polyethylene *via* catalysed chain growth (CCG),[4,5] specifically neodymium catalysed chain growth on magnesium, reacting elemental sulfur with the resulting $MgPE_2$ species, and reducing the resulting sulfide species to generate thiol terminated PE, which can be transformed into a RAFT macromonomer from which block copolymers can be readily prepared.[6,7]

1.2 Controlled Radical Polymerization

Free radical polymerization enables the polymerization of a multitude of vinylic monomers under relatively undemanding reaction conditions compared to ionic and condensation polymerization techniques. Free radical polymerization, however, suffers from a lack of control. Since the lifetime of a radical chain is short (1-10 s), new chains are continually being formed, which results in high molecular weight chains being produced, through termination, early on in the reaction.[8] In conventional living polymerization however, all chains are initiated at the start of the process and molecular weight (M_w) increases linearly and with narrow molecular weight distribution or dispersity ($Đ_M$) until all of the monomer is consumed (Figure 1.1). Therefore, the ability to control radical polymerizations such that they exhibit *pseudo*-living rates of reactions achieves a handle on the M_w and $Đ_M$ of the polymer product.
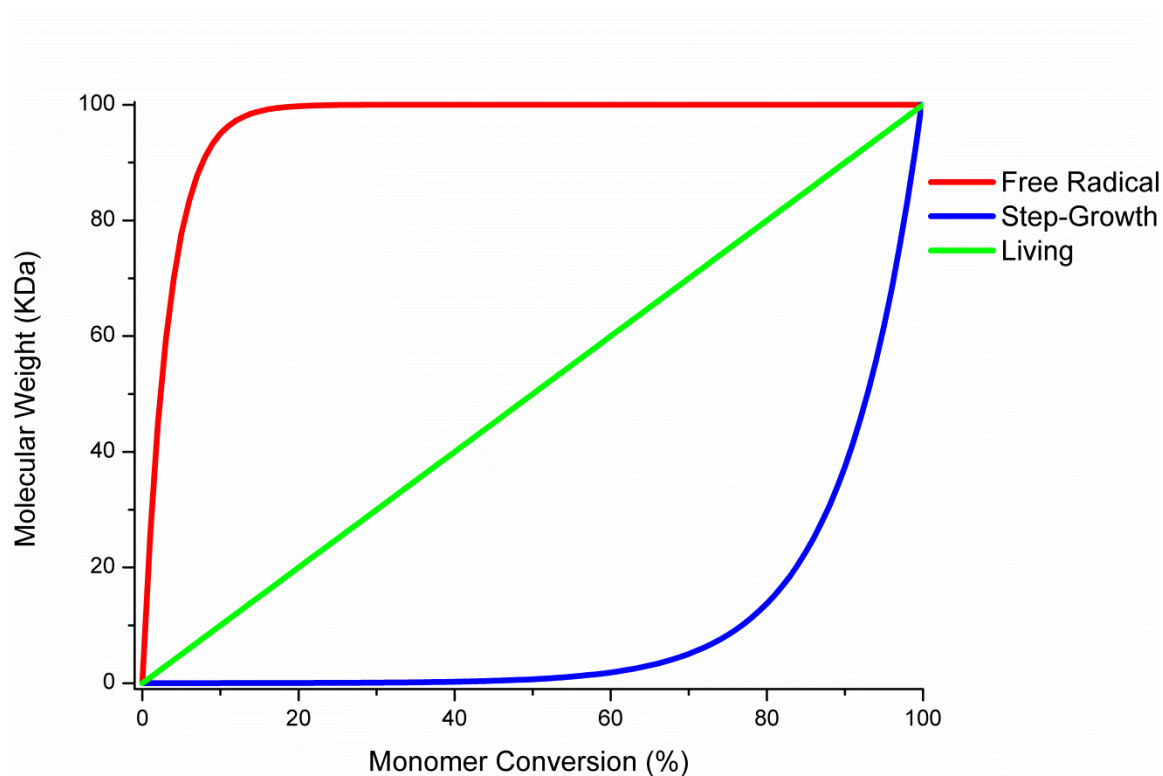
Figure 1.1: Relative reaction kinetics in living, free radical, and step-growth polymerization.

Free radical polymerization also suffers from its inability to access higher polymer architectures including block copolymers since end-group control is absent. During the 1990s, however, a multitude of techniques to achieve control of radical polymerization were developed, including reversible activation-deactivation radical processes, notably nitroxide-mediated polymerization (NMP),[9] atom transfer radical polymerization (ATRP),[10] and reversible addition-

fragmentation chain transfer (RAFT) polymerization.[11-13] These processes achieve control of radical polymerization by reversibly deactivating propagating radical chains, reducing the concentration of propagating radicals ($< 10^{-7}$ M) and ultimately reducing the incidence of termination relative to propagation.[8] NMP (Scheme 1.1) and ATRP (Scheme 1.2) achieve this through generating a reversibly dormant radical species, whereas the RAFT process does so through reversible chain transfer (Scheme 1.3).
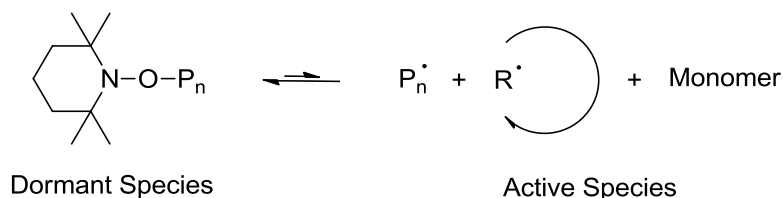
Scheme 1.1: Mechanism of NMP using TEMPO (2,2,6,6-tetramethylpiperidin-1-yl)oxyl).[9]
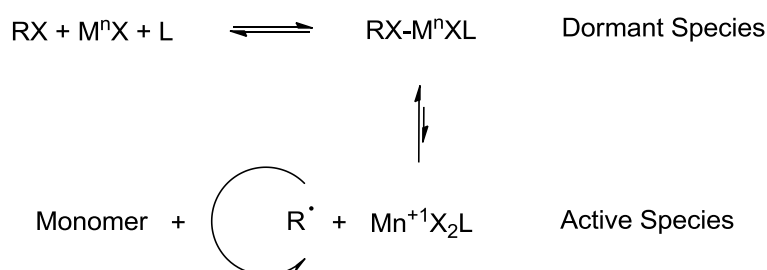
Scheme 1.2: Mechanism of ATRP.[10]

NMP is routinely employed for its excellent end-group fidelity, however suffers from the limited number of vinylic monomers to which it can be applied and the high-temperature reaction conditions it generally requires. ATRP is a widely applicable technique since virtually any appropriate initiator can be synthesized. The process, however, yields a large amount of residual transition metal catalyst in the product mixture. RAFT polymerization is currently a highly desirable process since it can be applied to many vinylic monomers and is highly tolerant of functional side-groups, facilitating access to more complex polymer architectures. Since all of these techniques achieve good end-group control such that the majority of polymer chains generated can be reactivated, they can be employed to prepare end-functional polymers, high purity block copolymers, and polymers of more complex architectures. Consequently, controlled radical polymerization has rapidly become the industrially preferred method of preparing polymers of defined architecture, molecular number (M_n), and $Đ_M$.

1.2.1 RAFT Polymerization

1.2.1.1 The RAFT Process

RAFT polymerization achieves control of radical polymerization on the basis of a degenerative chain transfer process (Scheme 1.3). As in conventional free radical polymerization, polymerization is initiated through a radical source, such as the azo- initiator 2,2'-azodiisobutyronitrile (AIBN), which thermally cleaves homolytically to generate a stable tertiary radical, which in turn reacts with monomer to generate a radical chain. In the RAFT process, radical chains react with the thiocarbonyl of a chain-transfer agent (CTA) or RAFT agent to generate a radical adduct. Where the RAFT agent is appropriately designed, the so-called R group leaves as a radical species, capable of re-initiating polymerization, and regenerates the thiocarbonyl in the addition-fragmentation stage of the mechanism. Once a second radical chain adds to the thiocarbonyl, the chain transfer process commences. Where appropriate reaction conditions are employed, at least 90% of polymer chains are terminated with the RAFT agent upon monomer consumption. The RAFT process does not exhibit 100% end-group fidelity since radical-radical termination is unavoidable. The incidence of termination, however, can be reduced by optimizing reaction conditions, in particular through increasing the ratio of RAFT agent to initiator. Critically, re-initiation of RAFT-terminated polymers in the presence of a different monomer enables access to higher polymer architectures.

Initiation
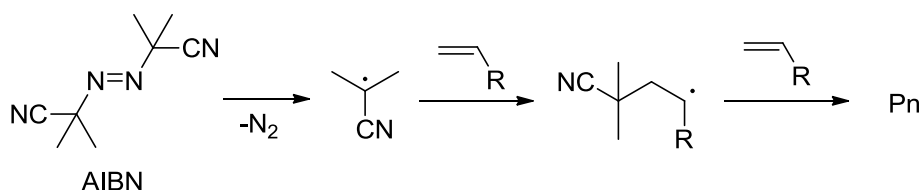
Addition Fragmentation
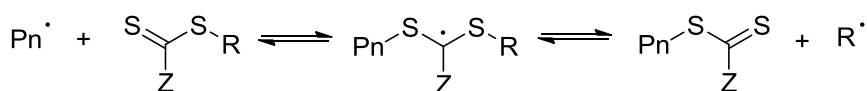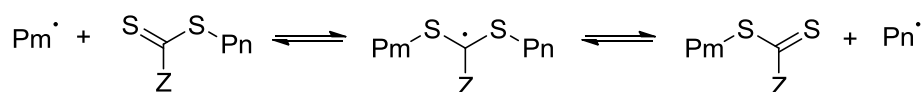
Chain Transfer

Scheme 1.3: Mechanism of the RAFT process.[14]

In order for the RAFT process to control radical polymerization, the chain transfer process must compete with the free radical process. This is achieved by tuning the reactivity of the thiocarbonyl relative to the monomer vinyl group through the so-called Z group of the RAFT agent. Furthermore, the leaving group must generate a more stable radical than the propagating radical chain in order for addition-fragmentation to occur and it is often useful, where possible, for this leaving group to have a similar structure to the monomer so that it does not interfere with the properties of the polymer chain. Therefore, RAFT agents are routinely designed with activating and leaving groups appropriate for the monomer(s) being polymerized (Figure 1.2).
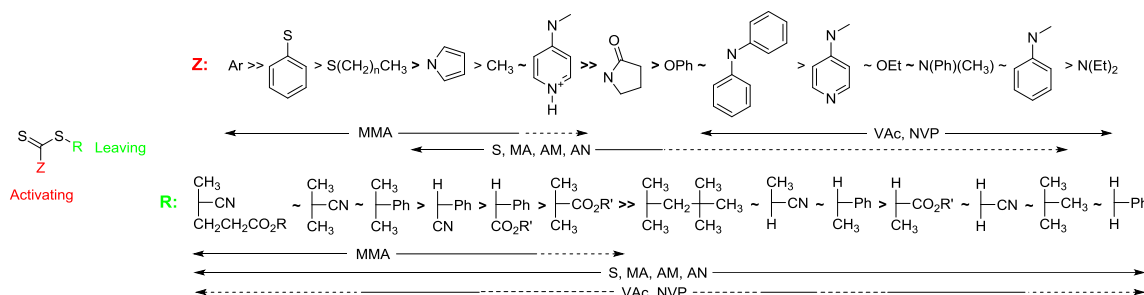
Figure 1.2: RAFT agent Z and R group monomer suitability. Solid line indicates control whilst dashed line indicates moderate control (some broadening of $Đ_M$). Monomers presented include methyl methacrylate (MMA), vinyl acetate (VAc), N-vinylpyrrolidone (NVP), styrene (S), methylacrylate (MA), acrylamide (AM), and acrylonitrile (AN). Figure adapted from Barner-Kowollik[14] and Keddie.[15]

1.2.1.1.1 Limitations of the RAFT Process

1.2.1.1.2 Switchable RAFT Agents

Despite its advantages, RAFT polymerization suffers from its inability to accommodate disparate monomer reactivities, such as those exhibited by styrene and vinyl acetate, which has consequently limited the preparation of many block copolymers *via* the RAFT process. Structure dictates monomer reactivity towards radical addition and is influenced by resonance, steric, and polar effects of both the monomer and the radical generated. Consider, for example, the polarity of the double bond in a monomer's reactivity towards a radical, or substituent resonance effects in stabilizing the generated radical - ultimately, substituents that increase monomer reactivity do so through stabilizing and therefore decreasing the reactivity of the corresponding radical.[16] Although reactivity ratios of monomers cannot be universally reported, relative reactivity ratios of two different monomers in a copolymerization reaction can be calculated according to the Mayo-Lewis equation and dictate the distribution of monomers in a copolymer and therefore the type of copolymer obtained (i.e.: block, alternating, statistical, or periodic).[16] Vinylic monomers display varied reactivates, however it is useful to broadly classify these monomers as either "more-

activated" monomers (MAMs), including styrenics, acrylates, methacrylates, and acrylamides, or "less activated" monomers (LAMs), including vinyl acetate, *N*-vinylpyrrolidone, and *N*-vinylcarbazole for the purpose of discussing the RAFT process. Theoretically, only two RAFT agents are required to control polymerization of all monomers such that a xanthate or *N,N*-disubstituted dithiocarbamate can be employed for LAMs and a di- or trithioester can be employed for MAMs.[14,17] RAFT agents suitable for MAMs limit the polymerization of LAMs following the poor leaving-group ability of propagating radicals maintaining a terminal LAM unit. Furthermore, RAFT agents suitable for LAMs are less reactive towards radical addition of propagating MAMs since the double-bond character of the thiocarbonyl is reduced by the contribution of zwitterionic canonical forms localizing a positive charge on the Z group heteroatom and a negative charge on sulfur (Figure 1.3).[17] Preparation of poly(MAM)-*b*-poly(LAM)s remains a significant challenge within RAFT polymerization and therefore there is an urgent requirement for a universal RAFT agent.

$$X = O, N$$
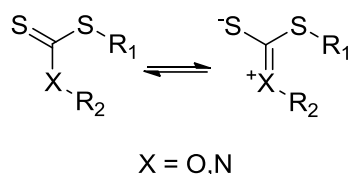
Figure 1.3: Zwitterionic canonical forms of xanthates and dithiocarbamates.

Alternative strategies to prepare poly(MAM)-*b*-poly(LAM)s are numerous and include first preparing the MAM block *via* ATRP, converting the ATRP bromine end-group into a xanthate, and polymerizing the LAM from the resultant macro-RAFT agent.[18] Furthermore, it has been demonstrated that organostibine-mediated radical polymerization (SMRP)[19] or a bifunctional RAFT agent maintaining ATRP initiator functionality[20] can be employed to prepare poly(MAM)-*b*-poly(LAM)s, as can a copper-catalysed 1,3-dipolar click addition of RAFT synthesized polyLAM and polyMAM blocks.[21] Although ingenious, these strategies are both challenging and expensive to execute on an industrial scale.

The concept of a switchable or universal RAFT agent has only recently been experimentally realised.[17,22-24] Specifically, it has been demonstrated that *N*-(4-pyridinyl)-*N*-methyldithiocarbamates can control the polymerization of LAMs and when reduced, can control the polymerization of MAMs (Scheme 1.4) enabling the preparation of poly(MAM)-*b*-poly(LAM)s with narrow molecular weight distributions. This process functions by manipulating the contribution of the zwitterionic resonance form of the dithiocarbamate such that it is favoured where the RAFT agent is unaltered, tuning the reactivity of the thiocarbonyl to LAMs, and disfavoured following reduction of the heterocycle, tuning the reactivity of the thiocarbonyl to

MAMs since the zwitterionic form unfavourably leads to loss of aromaticity. Polystyrene-*b*-poly(vinyl acetate) has been prepared using this method, however, it was discovered that the MAM block must be prepared first since the polyLAM RAFT macromonomer maintains a low transfer constant for MAM polymerizations following the relatively poor leaving group ability of the polyLAM radical. Thus, significant further investigations are required to truly realize a universal RAFT agent.

1 R= CH$_2$CN
2 R= CH(CH$_3$)CO$_2$CH$_3$
3 R= C(CH$_3$)$_2$CN

1-H$^+$ R= CH$_2$CN
2-H$^+$ R= CH(CH$_3$)CO$_2$CH$_3$
3-H$^+$ R= C(CH$_3$)$_2$CN

RAFT
Controls
VAc, NVP, NVC

RAFT
Controls
MMA, MA, S
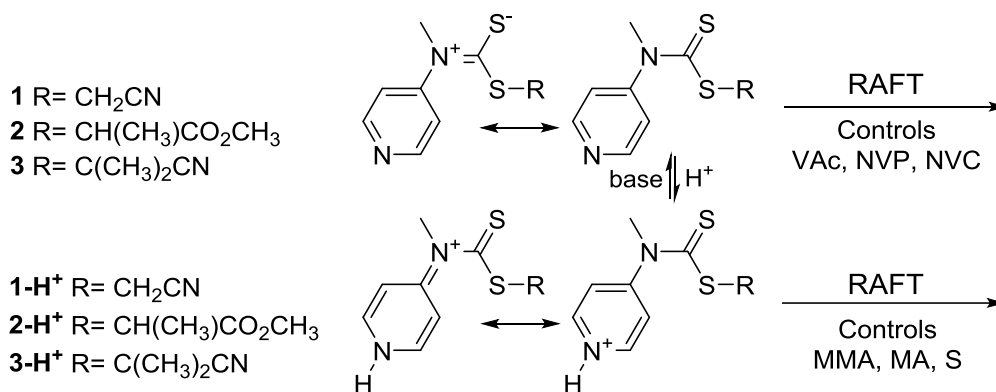
Scheme 1.4: Outline of *N*-(4-pyridinyl)-*N*-methyldithiocarbamates as universal RAFT agents.[17]

1.2.1.1.3 Control of Primary Radicals

An additional challenge with RAFT polymerization is to achieve control of currently uncontrollable monomers, in particular those generating primary radicals, such as ethylene. The challenge in the application of the RAFT process to monomers that generate a primary radical is that the radical adduct yielded during chain-transfer (Figure 1.4) is too stable following the poor leaving group ability of primary polymer macroradicals. This limits regeneration of the thiocarbonyl and therefore prevents the chain transfer process from competing with the free radical process in order to control free radical polymerization.

$$Pm \overset{S}{\diagup} \overset{\cdot}{\underset{Z}{\diagdown}} \overset{S}{\diagup} Pn$$
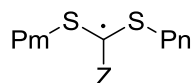
Figure 1.4: Radical adduct intermediate in RAFT chain-transfer.

Modest control of radical ethylene polymerization, however, has been demonstrated using the RAFT agent isopropylfluorodithioformate (IFDF) (Figure 1.5), specifically reducing the high molecular weight shoulder observed in the free radical case.[25] The fluorine Z group of the so-called F-RAFT agent is thought to sufficiently destabilize the chain transfer adduct radical to release polyethylene macroradicals whilst maintaining the reactivity of the thiocarbonyl towards propagating polyethylene radicals since, unlike with conventional RAFT agent Z groups, fluorine

withdraws electron density solely along a sigma bond. This insight into F-RAFT agents, which are proposed although remain to be demonstrated as universal RAFT agents,[26] will inform future investigations into the RAFT polymerization of currently uncontrollable monomers.
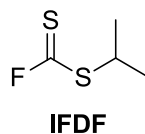
IFDF

Figure 1.5: Structure of the F-RAFT agent isopropylfluorodithioformate (IFDF).

1.2.2 Metallo-RAFT Agents

Although the RAFT process was developed as a metal-free radical approach to preparing defined polymers, considering the potential scope of the F-RAFT process for the preparation of polyethylene, we envisaged that the use of metals in RAFT agent design could significantly alter the electronics of RAFT agents, either by strongly withdrawing electron density along the RAFT agent Z group or destabilizing the chain transfer adduct radical, to control the radical polymerization of primary radicals. Furthermore, incorporation of metals into RAFT agent design could potentially inspire the development of alternate switchable RAFT agents, in particular to overcome the current limitation of having to polymerize MAMs in advance of LAMs using *N*-(4-pyridinyl)-*N*-methyldithiocarbamates as switchable RAFT agents. Four potential sites of interaction between metals and RAFT agents have been identified (Figure 1.6) and inspire possible directions for the development of metallo-RAFT agents. Xanthates and to a lesser extent dithiocarbamates[27] are well known to coordinate metals *via* the dithioester moiety and it is envisaged that metal coordination could be exploited to influence both the reactivity of the thiocarbonyl and stability of the chain transfer adduct radical. Furthermore, rational design of organometallic RAFT agents whereby the reactivity of the Z group is tuned by a coordinated metal is a promising strategy for the development of both switchable RAFT agents and CTAs capable of controlling the radical polymerization of primary radicals. Finally, direct coordination of a metal complex to the thiocarbonyl carbon of a RAFT agent presents an excellent opportunity to finely influence the electron withdrawing character of the RAFT agent Z group for controlled polymerization of primary radicals.
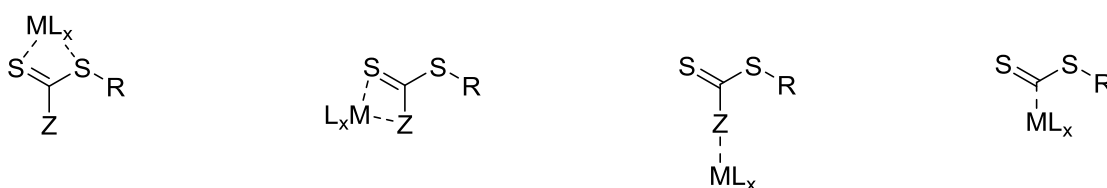
Figure 1.6: Potential metal-RAFT agent interaction sites.

Increasing interest in polymers terminated with organometallic groups for applications in opto-electrical materials, dispersants, and nanotechnologies has inspired the development of several organometallic RAFT agents and RAFT agents incorporating metal ligating functionality (Tables 1.1-1.3).[28] These RAFT agents have been developed to prepare metallopolymers of exclusively MAMs with end-group metal functionality for opto-electrical materials, and to access metallo-supramolecular polymers. Furthermore, Lo *et al.*[29] claim controlled radical polymerization and increased curing rates using organometallic RAFT agents with Z group organometallic functionality (Figure 1.7).

Table 1.1: RAFT agents with organometallic functionality in 'Z'. Table reproduced from Moad *et al.*[28] Monomers presented include butyl acrylate (BA).
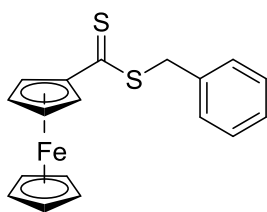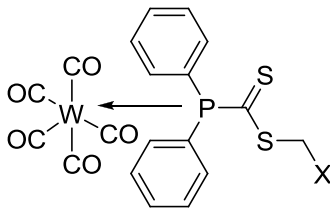
Raft Agent	Polymers
I[30]	S[30]
II X = CH$_2$CN[31] **III** X = CH$_2$Ph[32] **IV** X = CH$_2$CH=CH$_2$[32]	S, BA[31,32]

Table 1.2: RAFT agents with organometallic functionality in 'R'. Table reproduced from Moad *et al.*[28] Monomers presented include *N*-isopropylacrylamide (NIPAM), 4-(3-butenyl)styrene (StB), ethylene glycol dimethacrylate (EGDMA), and divinyl benzene (DVB).
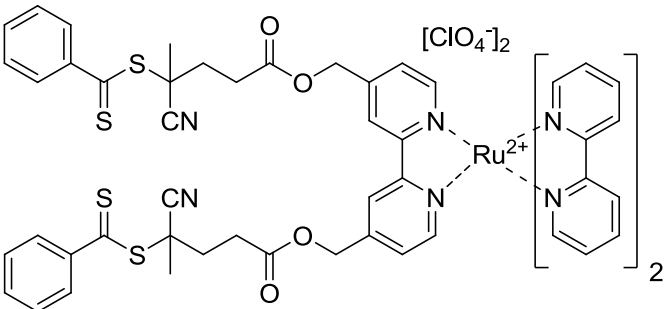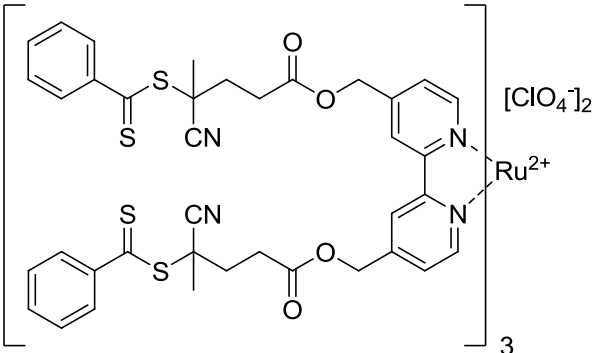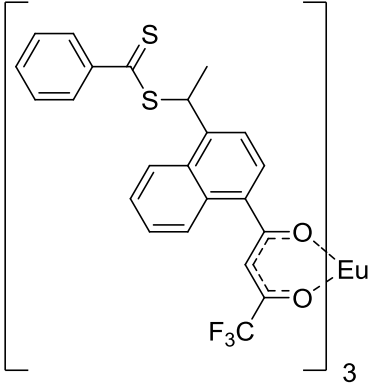
Raft Agent	Polymers
V[33]	S-Coumarin[33]
VI[33]	S-Coumarin[33-35] S-Coumarin-*b*-NIPAM[34,35]
VII[36,37]	S/StB[36] S/StB-*b*-MMA[36] EGDMA/MMA[37] DVB/S[37]

Table 1.2 Continued

StB[36]

StB-*b*-S[36]

VIII[36]

S[30]
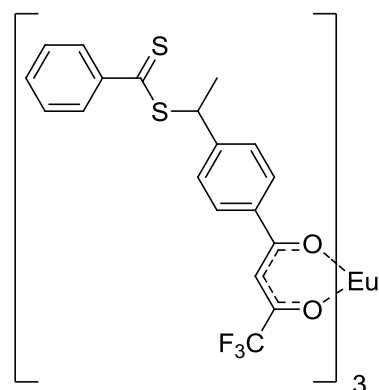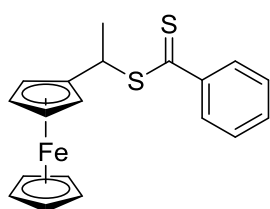
IV[30]

Table 1.3: RAFT agents containing metal ligating functionality. Table reproduced from Moad *et al.*[28] Monomers presented include *tert*-butyl acrylate (*t*BA).

RAFT Agent	Metal	Polymer
 X[38]	Pd	MA[32] MA-*b*-*t*BA[32]
 XI[39]	Ru	S[39,40] NIPAM[17,33]

Table 1.3 Continued

XII[41]	Ru	S[18,41]
XIII[42]		[t]BA[42] S[42]
XIV[42]	Ru[II], Eu[III], Fe[II]	MMA[42] [t]BA[42] S[42] S-*b*-[t]BA[42]
XV[43]	Ru	S[43] NIPAM[41]

Table 1.3 Continued

XVI[44]

Ru   S[44]

       BA[44]

       S-*b*-BA[44]

       BA-*b*-S[44]

T = P, C, O, N, S.

M = **Ti**, **Zr**, Hf, V, Nb, Ta, **Cr**, **Mo**, **W**, Mn, Tc, Re, **Fe**, **Ru**, **Os**, Co, **Rh**, **Ir**, **Ni**, **Pd**, **Pt**, Sc.

R_1, R_2 (same or different) = H, saturated or unsaturated alkyl, cycloalkyl, heterocycloalkyl, polycyclic alkyl, aryl, heteroaryl, alkylaryl.

R_3 = alkyl, aryl, alkylaryl, aminoalkyl, alkylamino, alkyloxy, cycloalkyl, heterocycloalkyl, polycyclic alkyl, -R"CN or R"COOH where R" is a saturated or unsaturated alkyl group having 1-20 carbon atoms. Preferably -CH_2Ph or -CH_2CN.

R_4 = alkylene, arylene, or alkylarylene.

Figure 1.7: Organometallic RAFT agents claimed by Lo *et al.*[29]

   Beyond organometallic RAFT agents, polymers maintaining thiocarbonylthio or derived thiol functionality have also been reported to bind metals *via* the RAFT agent thiocarboxylate moiety.[45-47] Additionally, metals have been employed alongside the RAFT process. For example, it has been demonstrated that the presence of molecular ferrocene [48] and iron[49] accelerate and decelerate the rate of RAFT polymerizations, respectively. Furthermore, it has been demonstrated that RAFT agents can be activated to behave like *pseudo* halides in ATRP, reducing the requirement for a radical source where the RAFT process is conducted in the presence of suitable ATRP catalysts.[50]

1.3 Ring-Opening Polymerization of Macrocyclic Esters

Considering the significant challenge of attempting to develop chemistry for the CRP of primary radicals, alternative strategies towards obtaining RAFT-functional PE were concurrently considered. Reports that poly(ω-pentadecalactone) (PPDL) maintains similar properties to low density polyethylene (LDPE)[51] and can be prepared *via* the ring-opening polymerization (ROP) of the macrocyclic lactone ω-pentadecalactone (PDL) motivated our interest in the preparation of RAFT-functional PPDL. We envisaged the preparation of RAFT-functional PPDL to be both more convenient and commercially applicable than reported strategies to prepare RAFT-functional PE, critically not requiring transformations on the polymer chain-end since ROP techniques afford α-chain-end functional polymers *via* choice of initiator. Furthermore, since PPDL can be prepared from the PDL using metal-free catalysts, and maintains hydrolysable ester linkages, PPDL upholds the added potential of becoming a "green" alternative to PE.

1.3.1 Introduction to ROP

Poly(ester)s are widely applied in biomedical and pharmaceutical, particularly drug-delivery applications since they maintain appropriate mechanical properties and are frequently both biodegradable and biocompatible (degradation products inclusive).[52-54] Although poly(ester)s are more cumbersome and expensive to prepare than conventional commodity plastics, they are receiving increasing interest as environmentally-friendly materials since they are both biodegradable and frequently prepared from sustainable monomer feedstocks. Aliphatic poly(ester)s were originally prepared *via* condensation polymerization of hydroxyl acids or diacids and diols (Scheme 1.5).[55] Disadvantages of polycondensation reactions, however, include the requirement for stringent monomer purification, precise stoichiometry in reactions between diacids and diols, and high reaction temperatures which promote undesirable side reactions. Critically, since condensation polymerization proceeds *via* step-growth polymerization kinetics, the ability to both control the reaction and obtain high molecular weight material is incredibly difficult to achieve.
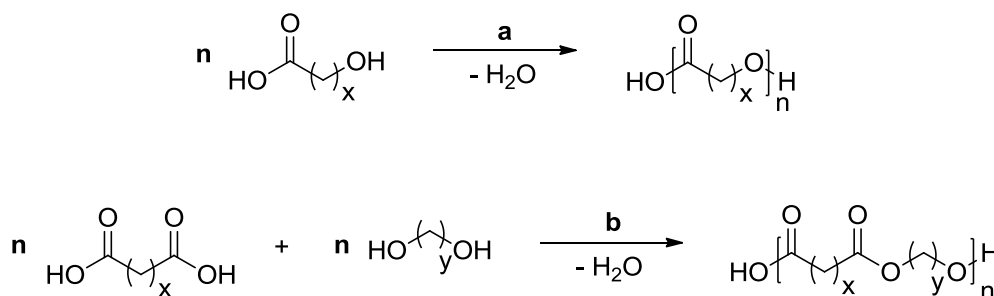
Scheme 1.5: Preparation of poly(ester)s *via* condensation polymerization of a) hydroxyl acids and b) diacids and diols.

The modern preparation of aliphatic poly(ester)s *via* ROP of cyclic esters affords excellent control over the polymerization through to high molecular weight material and under relatively mild reaction conditions (Scheme 1.6). ROP techniques are regarded as living polymerization systems since 1) they proceed *via* chain-growth kinetics, resulting in a linear increase in the molecular weight of the polymer with increasing monomer conversion, 2) the molecular weight of the polymer can be directly controlled by the ratio of monomer to initiator in the initial reaction mixture, 3) the resulting polymer maintains a narrow dispersity, and 4) high end-group fidelity is preserved throughout the polymerization. The ability to perform a polymerization with living characteristics ultimately facilitates control of the bulk properties of a material, which is crucial for a number of applications.

β-Propiolactone   γ-Butyrolactone   δ-Valerolactone   ε-Caprolactone
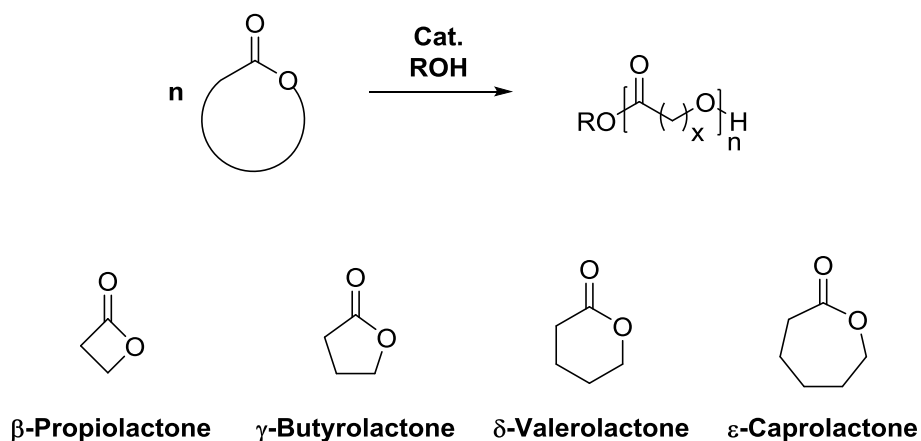
Scheme 1.6: ROP of cyclic esters to yield aliphatic poly(ester)s.

ROP techniques are employed in the polymerization of numerous classes of cyclic monomers, and monomers that are frequently polymerized alongside aliphatic cyclic esters include glycolide, *p*-dioxanone, 1,5-dioxepan-2-one (DXO), lactide, and trimethylene carbonate (TMC) (Figure 1.8). Since both nucleophiles and electrophiles can initiate the ionic polymerization of polarized monomers, the range of catalysts appropriate for ROP is vast and

includes metal complexes, organic compounds, and enzymes.[56] Ultimately, initiation in ROP proceeds *via* either an anionic, cationic, coordination-insertion, or activated monomer mechanism. Alkali and earth-alkali alkoxides are amongst the first class of catalysts demonstrated to initiate the anionic polymerization of cyclic esters. Specifically, the alkoxide anion undergoes nucleophilic addition to the carbonyl carbon of the cyclic ester, releasing an alkoxide end-group which propagates in the same manner (Scheme 1.7). A significant disadvantage of this strategy, however, is that the propagation step is frequently accompanied by numerous side reactions, in particular backbiting to regenerate the monomer or yield macrocyclic oligomers.

p-dioxanone   1,5-dioxepan-2-one (DXO)   Glycolide   Lactide   Trimethylene carbonate (TMC)
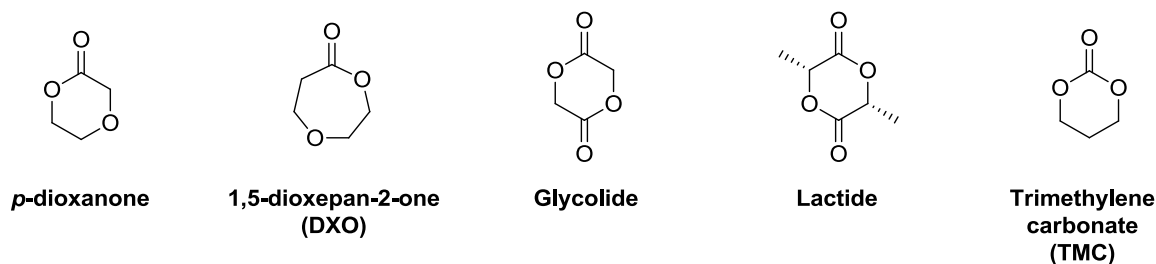
Figure 1.8: Cyclic monomers frequently polymerized alongside aliphatic cyclic esters.
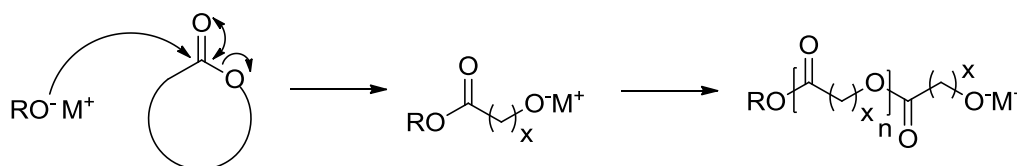
Scheme 1.7: Mechanism for metal-catalysed anionic ring-opening polymerization of cyclic esters.

Consequently, transition and rare-earth metal catalyst-initiator systems have been developed for ROP and proceed *via* a co-ordination-insertion mechanism. Specifically, co-ordination of the carbonyl oxygen of the monomer to the metal alkoxide complex activates the monomer and results in nucleophilic addition of the alkoxide to the monomer carbonyl carbon. Acyl bond cleavage ring-opens the monomer and generates a metal alkoxide from which the polymerization can propagate (Scheme 1.8).[55] Modification of the catalyst ligands has been demonstrated to reduce side reactions and enable the attainment of high molecular weight and stereoregular polymers.[57,58]
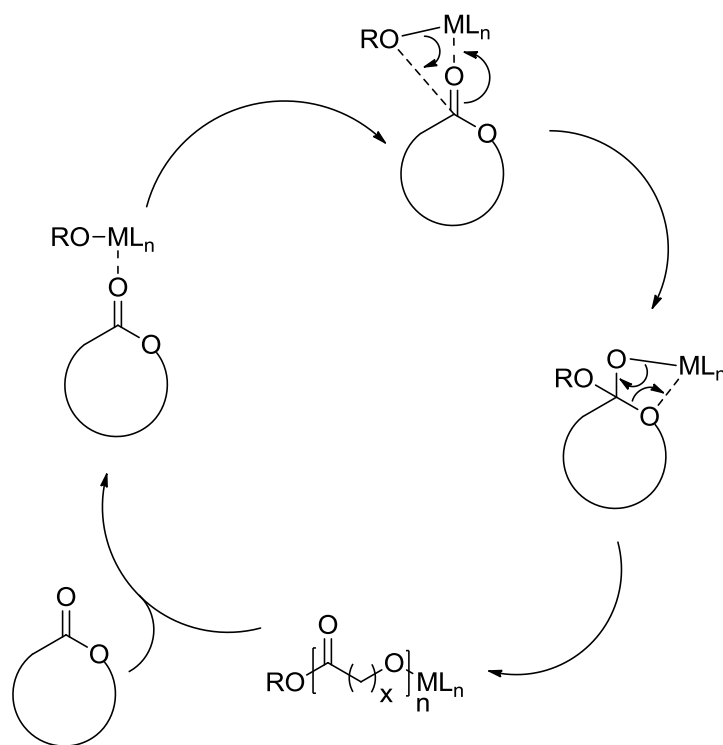
Scheme 1.8: Mechanism for metal-catalysed co-ordination/insertion ring-opening polymerization of cyclic estsers. Scheme adapted from Williams.[55]

Although metal-catalysed ROPs are highly efficient, the requirement for metal-free processes for biomedical and microelectronic applications, where metals are incompatible even in trace amounts, has driven the development of organic catalysts for ROP. The majority of organic-catalysed ROPs proceed *via* an activated monomer mechanisms. For example, the simple pyridine-based organo-catalyst 4-(dimethylamino)pyridine (DMAP) undergoes nucleophilic addition to the carbonyl carbon of the monomer to form a zwitterion intermediate, which undergoes ring-opening of the monomer acyl bond. The resulting alkoxide deprotonates the initiator or propagating alcohol species to generate another anion that undergoes a nucleophilic addition to the monomer carbonyl carbon to regenerate the catalyst and yield the hydroxyl-terminated propagating species (Scheme 1.9).
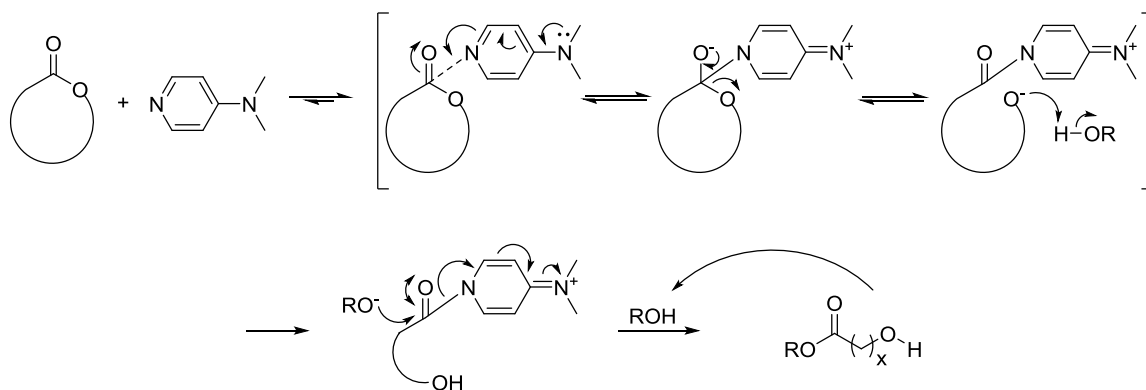
Scheme 1.9: Mechanism for ring-opening polymerization of cyclic esters mediated by DMAP. Scheme adapted from Nederberg *et al*.[59]

Another important organic catalyst for ROP is the "superbase" 1,5,7-triazabicyclo[4.4.0]dec-5-ene (TBD) which has demonstrated tremendous versatility in the range of monomers that it is capable of polymerizing. Interestingly, TBD catalyses the ROP of cyclic esters *via* dual activation of the monomer and initiating species (Scheme 1.10). Significant research concerns modulating the physio-chemical properties of polymers prepared from cyclic monomers including glass transition temperature, hydrophobicity, degradability, and Young's modulus through the preparation of higher polymer architectures, copolymerization with other monomers, and the preparation and polymerization of novel, non-aliphatic cyclic monomers possessing side-chain functionality that can undergo post-polymerization modification. Consequently, the development of new organic catalysts for ROP frequently concerns the development of highly efficient, mild catalysts that can tolerate particular functional groups.[60] Additional classes of organic catalysts reported for ROP include carbenes, phosphazenes, bifunctional catalyst systems, and electrophiles, such as acids.[56]
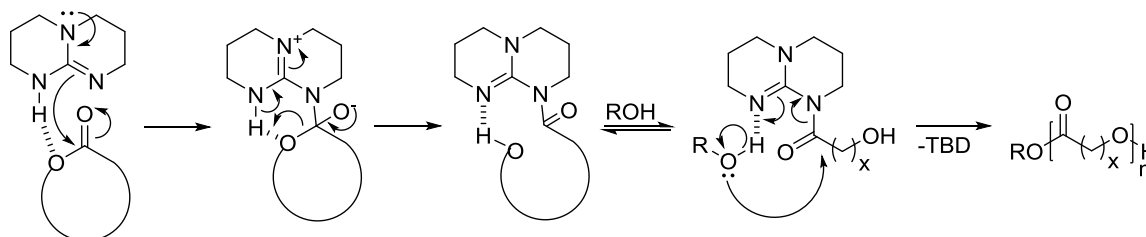
Scheme 1.10: Mechanism for the ring-opening polymerization of cyclic esters mediated by TBD. Scheme adapted from Pratt *et al*.[61]

A final class of catalysts that can be employed in ROP are enzymes. There is a tremendous amount of interest in utilizing enzymes for chemical transformations since they perform biochemical transformations with remarkable precision and efficiency, specifically with a

high degree of chemo-, regio-, and enantio-selectivity, all under mild conditions. Furthermore, enzymes are non-toxic and recyclable, and therefore a "green" alternative to conventional catalysts. Where they are immobilized on a solid support, they have the added advantage of being easy to remove from a reaction mixture or polymer product, unlike most conventional catalysts, and consequently are receiving increasing interest in polymerization reactions.[62,63] A popular class of enzymes explored for organic transformations are lipases, which hydrolyse fatty acid esters *in vivo*, and have additionally been demonstrated to polymerize cyclic esters. The hydrophobic lipase catalytic site consists of a serine, histidine, and aspartate residue and it is proposed that a cyclic ester substrate undergoes nucleophilic addition by the serine alcohol to generate an intermediate which cleaves the monomer acyl bond and releases an alkoxy anion to generate the enzyme-activated monomer (EAM) species.[56] The resulting EAM subsequently undergoes nucleophilic addition of the initiating or propagating alcohol species to generate a new intermediate, the final product of which is released *via* cleavage of the acyl bond to regenerate the enzyme (Scheme 1.11). Interestingly, lipases have a strong preference for *R*-secondary alcohols in the deacylation step and consequently can be utilized to prepare stereoregular poly(ester)s *via* kinetic resolution polymerization.[56] Enzymatic ring-opening polymerization (eROP)[64,65] is considered to proceed *via* an activated monomer mechanism. However, since the enzyme does not discriminate between ester groups, transesterification reactions occur, resulting in chain scission and the production of cyclic and linear polymer products. Therefore, eROP cannot be considered a living polymerization process even though reasonable control of molecular weight and end-group functionality can be achieved using an initiating nucleophile such as water, an alcohol, an amine, or a thiol. Regardless, eROP has proven to be an important catalyst for the preparation of new polymeric materials, particularly from macrocyclic esters, which are difficult to polymerize using conventional ROP catalysts.
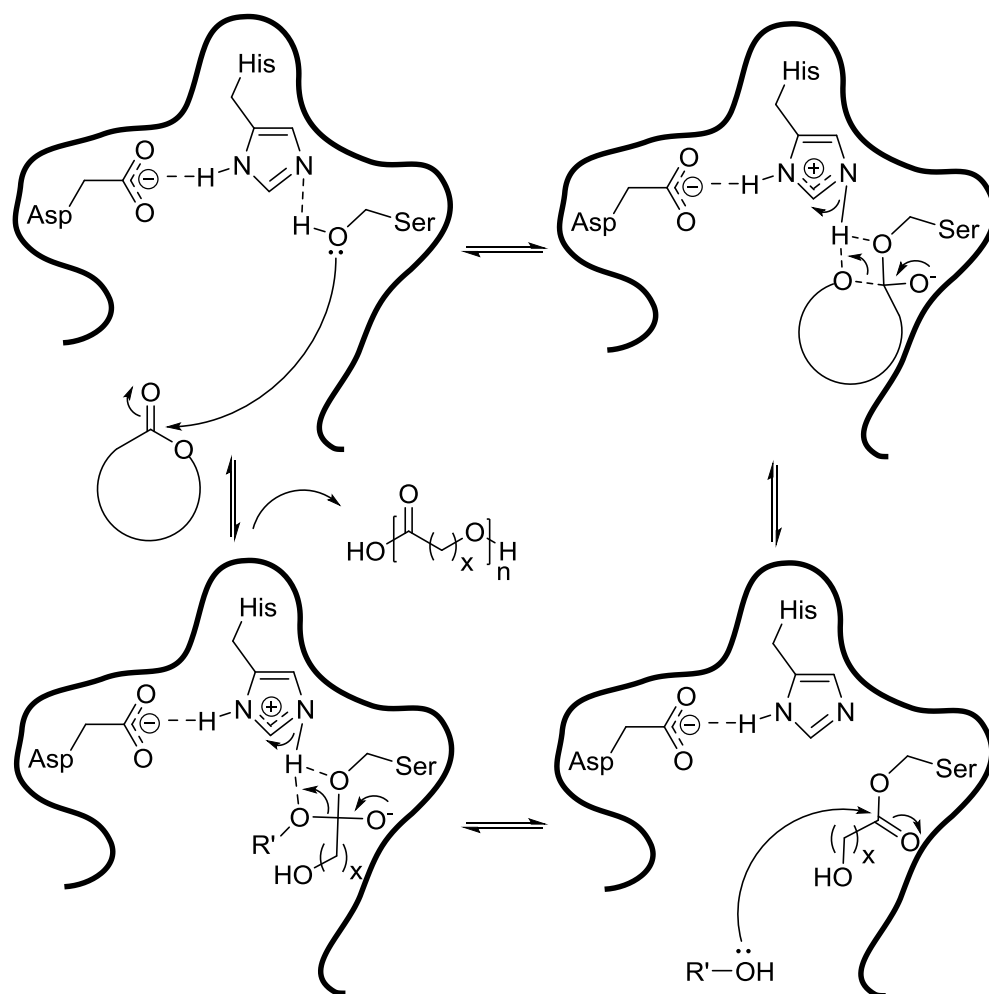
Scheme 1.11: Proposed ping-pong mechanism for the enzymatic ring-opening polymerization of cyclic esters. Scheme adapted from Dubois *et al.*[56]

ROP performed on small (up to 6 atom) and medium (between 7 and 11 atom) lactones is well-understood and thermodynamically driven by a negative change in entropy during the release of angular or transannular strains, respectively. Macrocyclic esters (containing ring sizes of 12 or more atoms), however, have little or no ring strain and consequently attempts to polymerize macrocyclic esters using conventional, non-enzymatic catalysts typically yield only oligomeric material.[56] Beginning in the 1990s, enzymes were explored as catalysts for the ROP of macrocyclic esters and the success of eROP has resulted in the preparation of novel polymeric material and the development of new processes in polymer synthesis.

1.3.2 Ring-Opening Polymerization of Macrocyclic Esters

1.3.2.1 Homopolymerization of Macrocyclic Esters

Initial eROP reactions were attempted on conventional ROP monomers such as CL,[66-68] and an initial bulk copolymerization of CL and PDL using the lipase *Pseudomonas fluorescens* reported only trace incorporation of PDL after 10 days.[69] Thereafter, the eROP of 11-undecalactone (UDL), 12-dodecalactone (DDL), and PDL (Figure 1.9) was investigated using various lipases, notably lipases derived from *Pseudomonas fluorescens* (lipase P) and *Candida cylindracea* (lipase B) in bulk conditions and at various temperatures. Uyama and co-workers[70-72] discovered that the rate of eROP varies depending on the origin of the lipase, increases with temperature and immobilization on Celite, and proceeds more rapidly for macrocyclic esters than for CL. Subsequently, it was discovered that the rate of the eROP of PDL could be increased 100-fold, further increasing the M_n and conversion, and improving the $Đ_M$ of the polymer product, by utilizing immobilized, surfactant-coated lipases in organic media, notably toluene.[56,73-75]

11-Undecanolide　　**12-Dodecanolide**　　**15-Pentadecanolide**　　**16-Hexadecanolide**
(UDL)　　　　　　　(DDL)　　　　　　　(PDL)　　　　　　　(HDL)
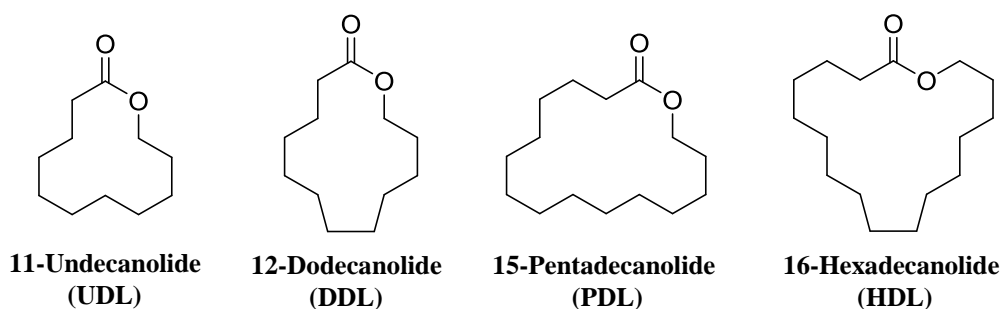
Figure 1.9: Structures of commercially available aliphatic macrocyclic lactones.

Bisht *et al.*[76] further investigated lipase choice in the eROP of PDL in bulk conditions at 80 °C by screening commercially available lipases over 24 hours. Novozyme-435, specifically *Candida antartica* immobilized on an acrylic resin, notably yielded the highest conversion and has since become the enzyme of choice for eROP reactions. Although an extensive range of enzymes have been studied for the eROP of macrocyclic esters, they have all been lipases with the exception of a cutinase from *Humicola insolens* (HiC),[77] which exhibits similar kinetics for the eROP of macrolactones as Novozyme-435.[78] Kinetic studies have been performed for the Novozyme-435 catalysed polymerization of 6-, 13-, and 16-membered lactones.[79] Temperature was determined to be an important factor such that increasing the temperature from 60 °C to 80 °C increases both the rate of the polymerization and the M_n of the polymer product, however, further increasing the temperature to 110 °C decreases both the rate and M_n. Therefore, it can be concluded that elevated reaction temperatures denature the native structure of the enzyme, impairing its ability to perform transesterification reactions. Bisht *et al.*[76] additionally investigated

the effect of water content, which was found to affect both the rate and M_n such that increasing the water content increases the rate polymerization however decreases the M_n of the polymer product. This result is consistent with the conclusion of Matsumoto *et al.*,[80] that water is the initiating species. Although the rate of eROP reactions can be increased by using an alcohol as an initiating species,[81] which is more efficient than using a thiol since thiols maintain higher binding affinities to lipases than alcohols,[82] the presence of some water is critical for the enzyme to adopt the correct structure *via* non-covalent bonding, and consequently too little water greatly reduces enzymatic activity.[56]

Duda and co-workers[83] compared the polymerization kinetics of various sized cyclic lactones *via* a zinc 2-ethylhexanoate (Zn(Oct)$_2$)/butyl alcohol catalyst-initiator system and eROP at 100 °C and discovered a reverse trend. Specifically, the orders of polymerization rates were determined to be 2500:330:21:0.9:1.0:0.9:1.0 for 6-, 7-, 9-, 12-, 13-, 16-, and 17-membered lactones, respectively using zinc 2-ethylhexanoate, and 0.1:0.13:0.19:0.74:1.0 for 7-, 12-, 13-, 16-, and 17-membered lactones using Novozyme-435, clearly indicating that eROP is a more appropriate polymerization technique for macrocyclic lactones. Ultimately, eROP proceeds more rapidly for larger rather than smaller cyclic lactones since formation of the EAM is promoted by increasing the hydrophobicity of the monomer following the hydrophobic nature of the enzyme active site.[83] Furthermore, numerous studies into the enantioselective eROP of substituted lactones report varied selectivities and rates, however, these differences can be attributed to the lactone ester conformation, which can exist either in the higher-energy *cisoid* or lower-energy *transoid* conformation, the latter of which exhibits dramatically increased rates of eROP (Figure 1.10).[56,79] Critically, seven-membered rings and smaller can only exist in the *cisoid* conformation whereas ten-membered rings and larger exist exclusively in the *transoid* conformation.[56] Although the eROP of monomers that can adopt both ester conformations is non-selective, polymerizations are *S*-selective with exclusively *cisoid* monomers and *R*-selective with exclusively *transoid* monomers in order to afford the *R*-secondary alcohol as a nucleophile, which propagates considerably more rapidly than the *S*-stereoisomer.[56] Interestingly, the rate of eROP decreases for substituted macrolactones where a methyl group is present in the α-position.[84]
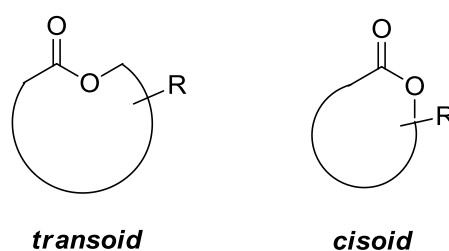
transoid   **cisoid**

Figure 1.10: *Cisoid* and *transoid* conformations of ester bonds. Figure adapted from Dubois *et al.*[56]

The rate of eROP can be further increased by performing the polymerization in a miniemulsion,[85] which Taden *et al.*[86] report as a useful method for preparing PPDL nanoparticles. Furthermore, Wosnick *et al.*[87] demonstrate that poly(ester)s including PPDL can be prepared *via* continuous-flow eROP using a packed-bed reactor. This method reduces the amount of solvent required to separate the enzyme from the polymer product, therefore greatly reducing the amount of solvent consumed in polymer purification.

1.3.2.2 Copolymerization of Macrocyclic Esters

Block copolymers of poly(ester)s can be readily prepared *via* eROP by initiating from a hydroxyl terminated polymer that does not contain any ester functionality. This strategy has been employed to prepare poly(butadiene)-*b*-PPDL,[88] in addition to block and triblock copolymers of poly(ethylene glycol) (PEG) and CL and/or DXO.[89,90] The copolymerization of PDL and TMC using stannous octanoate, methylaluminoxane (MAO), or aluminium isopropoxide as a catalyst yielded either TMC homopolymer or PPDL-*b*-poly(TMC) copolymers since these catalysts polymerize TMC more rapidly than PDL.[91] Interestingly, block copolymers of CL and lactide have been prepared *via* the eROP of CL followed by carbene catalysed ROP of lactide in one pot.[92]

The majority of copolymers prepared *via* eROP are statistical, the sequence composition for which can be evaluated by ^{13}C NMR spectroscopic analysis.[93] Kumar *et al.*[94] investigated the copolymerization of CL and PDL using Novozyme-435, optimizing the reaction temperature (70 °C) and volume of toluene (1:1 wt./vol.) and obtained a statistical copolymer (M_n = 22,300 g mol^{-1}, $Đ_M$ 1.97) after 6 hours despite the fact that PDL is 13 times more reactive than CL with this enzyme. Ultimately, Kumar *et al.*[95] highlighted the ability of lipases to not only polymerize cyclic esters but to also perform intermolecular transesterification reactions by combining poly(caprolactone) (PCL) (M_n = 44000 g mol^{-1}, $Đ_M$ 1.65), PPDL (M_n = 40,000 g mol^{-1}, $Đ_M$ 1.71), and Novozyme-435 to yield multiblock copolymers (M_n = 18,200 g mol^{-1}, $Đ_M$ 1.92) within the first hour and statistical copolymers (M_n = 31,200 g mol^{-1}, $Đ_M$ 1.87) after 30 hours. This novel synthetic strategy towards copoly(ester)s has been utilized to prepare statistical copolymers *via* polymerization of macrolactones in the presence of aliphatic poly(ester)s.[96] Similarly, microblock copoly(ester)s were prepared *via* sequential copolymerization of CL and DXO.[97] Furthermore, this strategy has been utilized to prepare statistical copolymers of PDL and TMC,[91] *p*-dioxanone,[98] glycolide,[45,46] γ-methacryloyl-ε-caprolactone (McrCL),[99] and γ-benzoyl-ε-caprolactone (BenzCL),[99] ambrettolide (Am),[99] the corresponding epoxide of ambrettolide (AmE),[99] and 1-oxa-8-aza-cyclotetradecan-9,14-dione (cEA) (Figure 1.11).[99] Interestingly, porous

scaffolds prepared from random copolymerization of PDL and CL *via* supercritical carbon dioxide foaming have been investigated for tissue regeneration applications,[100] and copolymer networks containing PPDL and CL crystalline segments have been employed for triple-shape polymer systems[101-107] and hydrogels.[108]
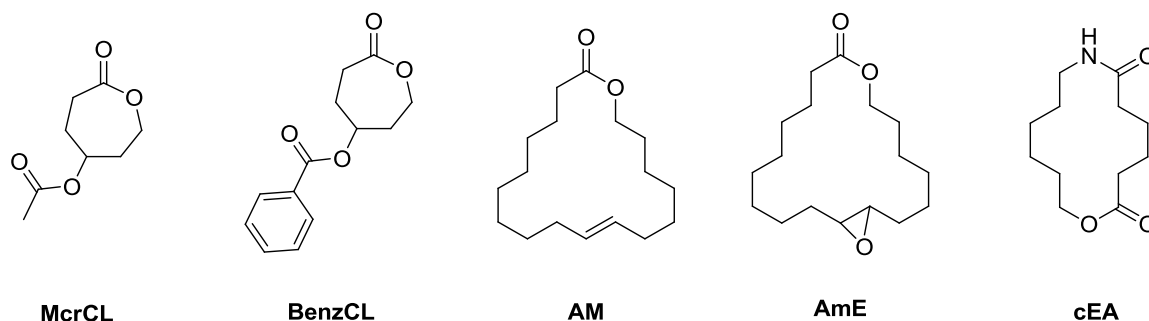
Figure 1.11: Structures of selected functional cyclic monomers γ-methacryloyl-ε-caprolactone (McrCL), γ-benzoyl-ε-caprolactone (BenzCL), ambrettolide (Am), ambrettolide (AmE), and 1-oxa-8-aza-cyclotetradecan-9,14-dione (cEA).

Statistical copolymerization importantly enables the ability to tailor the crystallinity and degradability of a polymer product. For example, oxo-crown-ethers have been copolymerized with CL and PDL to improve biodegradability.[109,110] Copolymerization with functional cyclic esters also enables the incorporation of added functionality into polymers, and the preparation of novel poly(ester)s.[111] For example, unsaturated macrolactones including globalide and ambrettolide have been copolymerized with CL, DXO, and 4-methyl-caprolactone (4MeCL) in order to prepare cross-linked networks *via* subsequent free radical or thiol-ene reactions.[112,113] Cross-linked gels have similarly been prepared *via* eROP of α-methylenemacrolides including 2-methylene-4-oxa-12-dodecanolide and subsequent radical polymerization of the pendant methacrylic groups.[114]

Simultaneous eROP and polycondensation reactions have additionally been reported. For example, Namekawa *et al.*[115] report the preparation of copolymers from macrolactones, divinyl esters of adipic and sebacic acid, and α,ω-glycols. Similarly, the copolymerization of diethyl succinate, 1,4-butane diol, and PDL has been reported to form aliphatic poly(ester)s.[116,117] The latter reaction was performed at 95 °C in the following two stages: 1) oligomerization under low vacuum to prevent monomer evaporation, followed by 2) polymerization under high vacuum to drive the equilibrium transesterification to high conversion (Scheme 1.12).[116] This method has been additionally extended to prepare a poly(carbonate-*co*-ester)[118] from diethyl carbonate, 1,4-butanediol, and PDL, and poly(lactone-*co*-β-amino ester) from PDL and ethyl 3-(4-(hydroxymethyl)piperidin-1-yl)propanoate (EHMPP).[119] PPDL is not cytotoxic[120] and numerous

microspheres prepared from copolymerization and simultaneous eROP and polycondensation of PDL have been investigated for encapsulation and drug delivery applications.[121-123] Interestingly, poly(PDL-*co*-butylene-*co*-succinate) particles (100-300 nm) were demonstrated to deliver camptothecin to tumour cells following intravenous administration.[124]
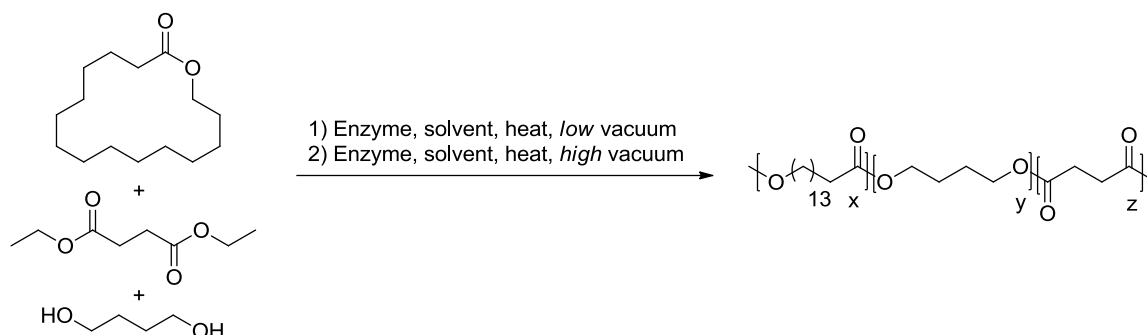
Scheme 1.12: Two-stage process for the copolymerization of PDL, diethyl succinate, and 1,4-butane diol. Scheme reproduced from Jiang.[116]

1.3.2.3 Preparation of Telechelic Poly(ester)s via eROP

End-group functionality can be introduced onto the chain-ends of polymers prepared *via* eROP through choice of initiator and/or end-capping compound, as with ROP, and has enabled the preparation of complex architectures from hyperbranched CL[125] through to CL initiated from a decorated sugar core.[126] Interestingly, Kobayashi and co-workers[127] demonstrated that the transesterase activity of lipases can be exploited to prepare methacryl macromonomers (Scheme 1.13) and α,ω-carboxylic acid terminated poly(ester)s by performing eROP in the presence of vinyl methacrylate and divinyl sebacate, respectively. This strategy has similarly been reported using ethylene glycol diacrylate to yield α,ω-diacrylate end-groups.[128]
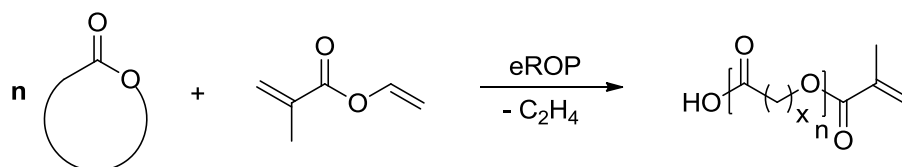
Scheme 1.13: Preparation of a poly(ester) macromonomer *via* eROP in the presence of a vinyl ester. Scheme adapted from Uyama *et al.*[129]

Kalra *et al.*[130] prepared brush copolymers using 2-hydroxyethylmethacrylate (2-HEMA) and ω-hydroxyl-ω'-methacrylate-poly(ethylene glycol) (PEGMA) (M_n 360 g mol^{-1}) as initiators for the eROP of PDL, and subsequently polymerized the corresponding macromonomers using AIBN at 70 °C in toluene (Scheme 1.14). Furthermore, Srivastava *et al.*[131] initiated the eROP of CL and DXO from 2-HEMA to yield methacrylate terminated macromonomers that were

subsequently homo or copolymerized with methacrylic monomers *via* free radical polymerization. Importantly, Takwa *et al.*[132] report that the polymerization of PDL and CL using 2-HEMA as an initiator results in a mixture of polymers with either zero, one, or two methacrylate end-groups since lipases catalyse the cleavage of the ester bond in the 2-HEMA end-group of poly(ester)s, substantiated by evidence for the incorporation of the 1,2-ethanediol moiety of 2-HEMA within the poly(ester). Therefore, the use of initiators with cleavable ester bonds in eROP yields polymers with mixed composition and end-groups, although this can be minimized through careful initiator selection and reducing reaction times. For example, Xiao *et al.*[133] report that 2-hydroxyethyl acrylate (2-HEA) and 2-HEMA have similar initiator efficiencies, however, transacylation occurs 15 times faster with 2-HEA than 2-HEMA. Methacrylate end-functional PPDL has alternatively been prepared by initiating from 2-HEMA and end-capping with vinyl methacrylate.[132]
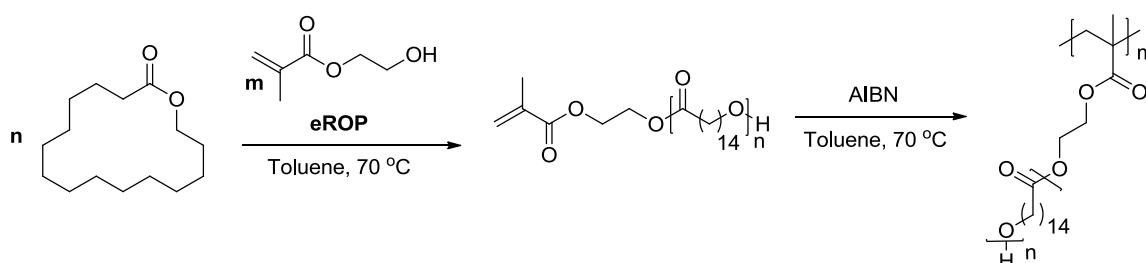
Scheme 1.14: Preparation of brush copolymers using 2-HEMA as an initiator in the eROP of PDL and subsequent polymerization of the resulting macromonomers. Scheme adapted from Kalra *et al.*[130]

Thiol-terminated CL has been prepared by initiating from 2-mercaptoethanol without the requirement for protection and deprotection steps following the disparate rates of reactivity between alcohols and thiols with lipases, or end-capping the polymer with γ-thiobutyrolactone or 3-mercaptopropionic acid (Scheme 1.15).[134,135] Similarly, α,ω-functional PPDL macromonomers have been prepared *via* the eROP of PDL initiated from 6-mercapto-1-hexanol and end-capped with γ-thiobutyrolactone, 11-mercapto-1-undecanoic acid, or vinyl acrylate.[128,136] Thiol-terminated CL has been utilized to prepare CL-*b*-PS *via* macromolecular radical chain transfer[135] and α,ω-thiol-functional PPDL has been used to prepare cross-linked films by irradiating molten polymer alongside ene monomers including tetrafunctional norbornene and trifunctional allyl ether maleate species in the presence of a photoinitiator.[137] Diepoxy-functional macromonomer prepared from PDL, glycidol, and adipic acid has additionally been copolymerized with cycloaliphatic diepoxide using a cationic photoinitiator to yield highly crystalline cross-linked films.[138]
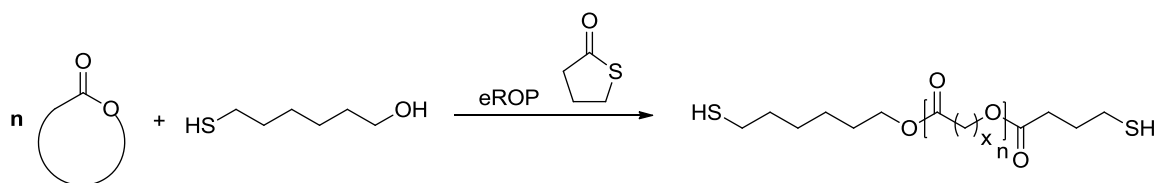
Scheme 1.15: Preparation of an α,ω-thiol functional poly(ester) *via* eROP, initiating from 6-mercaptohexanol and terminating with γ-thiobutyrolactone. Scheme adapted from Takwa *et al.*[136]

CRP and eROP have additionally been combined through the use of bifunctional initiators to prepare PCL-*b*-PS,[139] for example, in two steps. Furthermore, using a bifunctional NMP initiator, PCL-*b*-PS was prepared both *via* a two-step macroinitiation and a one pot cascade reaction. The concept was extended to include the enzymatic resolution polymerization of racemic 4-methyl-*ε*-caprolactone in order to prepare block copolymers with a high enantiomeric excess in the poly(ester) block. PCL-*b*-PS has similarly been prepared using a bifunctional ATRP initiator in two steps.[140] The one pot synthesis of block copolymers of CL and MMA was investigated using a bifunctional ATRP initiator.[141] It was determined that ATRP catalysts inhibit enzyme activity, which was less pronounced where the catalyst maintained multivalent ligands such as dinonyl bipyridine, and that the enzyme transesterifies MMA but not *t*-butyl methacrylate (*t*BMA). Block copolymers of CL and *t*BMA were therefore successfully prepared in one pot by adding the ATRP catalyst following the completion of the eROP. Where the reaction was performed by combining all reagents in one pot, significant poly(*t*BMA) was detected. Using the bifunctional initiator 2-hydroxyetheyl α-bromoisobutyrate, the eROP of CL and subsequent incorporation of vinyl acrylate was performed to generate a macroinimer, which was polymerized *via* ATRP to prepare branched block copolymers.[142] Interestingly, the controlled preparation of block copolymers has been demonstrated *via* simultaneous eROP of CL and ATRP of MMA in supercritical CO_2 (scCO_2) (Scheme 1.16),[143,144] and this strategy has been extended to prepare block copolymers of CL and 1*H*,1*H*,2*H*,2*H*-perfluorooctyl methacrylate (PFOMA).[145] Similarly, the copolymerization of CL and PS has been achieved using a bifunctional RAFT initiator in scCO_2.[146] One-pot eROP and CRP in scCO_2 is the subject of a recent review.[147]
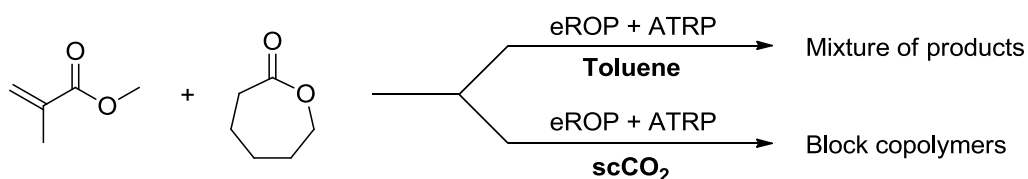
Scheme 1.16: One-pot synthesis of block copolymers of MMA and CL *via* eROP and ATRP.

Challenges associated with eROP include the indiscriminate transesterification reactions catalyzed by the enzyme, which make it difficult to utilize some materials, including acrylates and methacrylates. Lipase catalyzed transesterification, however, has been exploited to perform some interesting chemistry, including the preparation of graft copolymers[148,149] and surface grafted poly(ester)s.[150,151] For example, lipase was used to selectively graft onto the *R* enantiomer of copolymers of styrene and *p*-vinylphenylethanol (Scheme 1.17).[152,153] Furthermore, lipase has been shown to transesterify the side chains of poly(methacrylates) prepared by ATRP[154-156] or RAFT[157] with simple alcohols or hydroxyl terminated polymers. Interestingly, the synthesis of optically active polymer *via* concurrent cooperation of enzymatic kinetic resolution and ATRP has been reported all in one pot.[158]
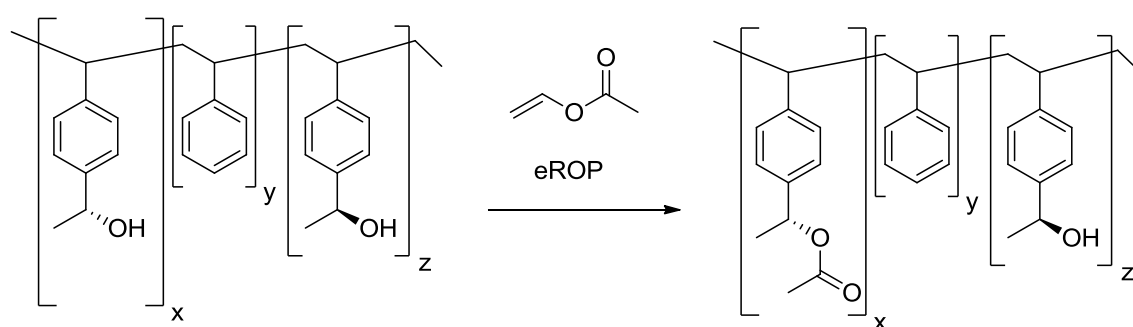
Scheme 1.17: *R*-selective enzymatic grafting of copolymers of styrene and *p*-vinylphenylethanol with vinyl acetate. Scheme adapted from Duxbury *et al*.[152]

1.3.2.4 Physical Properties of Poly(ω-Pentadecalactone) and Poly(ω-Pentadecalactone)-Containing Materials

The physical properties of poly(ester)s prepared from macrocyclic lactones range between those reported for CL, a semi-crystalline polymer (T_g of -60 °C, T_m of 60 °C, Young's modulus of 400 MPa, and a tensile strength of 15 MPa) and PE, and vary significantly with molecular weight.[56] An initial report on the physical properties of PPDL (M_n 5500, $Đ_M$ 3.53) included a T_m of 82-89 °C and a T_g between -3 and -28 °C.[159,160] A subsequent analysis of PPDL reported a T_m between 95-106 °C and the failure to detect a T_g by DSC analysis, even with rapid quenching from the melt, indicating that the material is highly crystalline.[161] Focarete *et al*.[51] similarly evaluated the physical properties of PPDL (M_w of 64,500, $Đ_M$ 2.0) and have likened it to LDPE. They report 1) thermal properties including a T_m of 97 °C, a T_g of -27 °C (detected by dynamic mechanical and dielectric spectroscopies) and a main thermal loss at 425 °C, 2) mechanical properties including elongation at break between 100-200%, a tensile strength of 14.5 MPa, and a modulus of 370 MPa, and 3) a degree of crystallinity between 54% (calculated by wide angle X-

ray diffraction measurements) and 64% (calculated from DSC heat of fusion).[51] The crystal structure of PPDL is similar to that of PCL, however exhibits lower crystal symmetry due to an even number of atoms in its backbone.[162] Numerous other physical properties of PPDL have been reported including its dipole moment[163] and crystallisation kinetics.[164] Interestingly, high molecular weight PPDL melted into fibres and elongated 9-10 times their original length exhibit tensile strengths up to 0.7GPa[165] and high molecular weight PPDL (>189,000 g mol^{-1}) exhibits strain hardening following chain entanglement.[166,167]

Random copolymers of PPDL and PCL are highly crystalline across composition ranges and the melt temperatures of these materials differ linearly with composition from PPDL (97 °C) to PCL (59 °C).[168] It has also been reported that random copolymerization of large lactones enhances aliphatic polycarbonate crystallinity.[169] The thermal stability of PPDL-poly(TMC) copolymers also changes with microstructure such that it improves with randomization, indicating that the monomers co-crystallize. [170] Ultimately, as with other poly(ester)s, the T_m of PPDL can be significantly modulated *via* copolymerization with other monomers, which is an important consideration in tuning both the crystallinity and hydrophobicity of PPDL ester linkages for numerous applications, in particular for degradation applications, in order to increase accessibility for hydrolysis.[171,172] Interestingly, Zotzmann *et al*.[101,173] report that polymer networks containing PPDL and PCL segments exhibit a triple-shape effect such that its crystalline domains recover its permanent shape due to entropic elasticity. Finally, the PE-like properties of PPDL make it attractive for modulating physical properties of materials. For example, blending PPDL into poly(*L*-lactic acid)[174] and polyurethane[175] has been shown to increase both the Young's Modulus and T_g of these materials.

1.3.2.5 Chemically Catalysed Ring-Opening Polymerization of Macrocyclic Lactones

Despite the ability of enzymes to successfully polymerize macrocyclic lactones, conventional ROP of macrocyclic lactones has also been demonstrated using several catalysts. For example, the anionic polymerization of UDL and the 13-membered lactone laurolactone was performed in bulk at 120 °C, initiating from lithium, sodium, or potassium methoxide to obtain material up to M_n 11,000 g mol^{-1}.[176] The polymerization of PDL initiated from potassium alkoxides in THF at 35 °C, however yielded high molecular weight polymers (M_n up to 100,000 g mol^{-1}).[177] Finally, yttrium isopropoxide has been reported to initiate the controlled ROP of PDL in toluene and in bulk conditions, proceeding to full monomer conversion within as little as 5 minutes.[161]

Tetrahydroborate complexes of rare earth metals lanthanum, neodymium, and ytterbium have additionally been determined to be highly active catalysts for the polymerization of PDL.[178] Furthermore, macrocyclic lactones have been polymerized in bulk and in aqueous miniemulsion conditions using acid catalysts, specifically dodecylbenzenesulfonic acid (DBSA), diphenyl phosphate (DPP), and trifluoromethanesulfonic acid (TfOH).[179] Yttrium triflate, using isopropanol as an initiator has been reported to catalyse the ROP of CL in the absence of inert conditions, however copolymerization with PDL resulted in minimal incorporation of PDL.[180] Aluminum triflate, using glycerol as an initiator, however catalysed the ROP of PDL in bulk anhydrous conditions, although with reduced reaction rates (49% conversion at 110 °C for 6 h - M_n 12,400, $Đ_M$ 2.24).[181] Finally, aluminium-salen complexes,[182,183] TBD,[184] and magnesium 2,6-di-*tert*-butyl-4-methylphenoxide (Mg(BHT)$_2$(THF)$_2$)[185] have recently been reported to control the ROP of PDL through to high molecular weight material. Importantly, (Mg(BHT)$_2$(THF)$_2$) catalyses the polymerization of PDL in the absence of both inert conditions and initiation from water.[185]

1.4 Conclusions

Efficient methods to prepare functional PE in order to access block copolymers and higher architectures of polyethylene are highly desirable. The RAFT process is a robust CRP technique and therefore RAFT-functional PE is a versatile polymer to target for both industrial and research applications. Development of F-RAFT agents in an attempt to control the radical polymerization of ethylene inspired our consideration of metallo-RAFT agents since we envisage that metallo-RAFT agents could potentially exhibit a greater range of reactivity towards vinylic monomers than organic CTAs. Considering the significant challenge in attempting to develop chemistry for the CRP of primary radicals, RAFT-functional polyethylene-like poly(ω-pentadecalactone) is identified as an interesting target material that can be readily functionalized through ROP techniques.

1.5 References

(1)   Piringer, O. G.; Baner., A. L. *Plastic packaging: interactions with food and pharmaceuticals*; 2nd ed.; Wiley-VCH: Weinheim, 2008.

(2)   Grau, E.; Broyer, J.-P.; Boisson, C.; Spitz, R.; Monteil, V. *Macromolecules* **2009**, *42*, 7279.

(3)   Zhao, Y.; Wang, L.; Xiao, A.; Yu, H. *Prog. Polym. Sci.* **2010**, *35*, 1195.

(4)   Britovsek, G. J. P.; Cohen, S. A.; Gibson, V. C.; van Meurs, M. *JACS* **2004**, *126*, 10701.

(5)   Gibson, V. C. *Science* **2006**, *312*, 703.

(6)   Mazzolini, J.; Espinosa, E.; D'Agosto, F.; Boisson, C. *Polym. Chem.* **2010**, *1*, 793.

(7)   Mazzolini, J.; Mokthari, I.; Briquet, R.; Boyron, O.; Delolme, F.; Monteil, V.; Bertin, D.; Gigmes, D.; D'Agosto, F.; Boisson, C. *Macromolecules* **2010**, *43*, 7495.

(8)   Moad, G.; Solomon, D. H. *The Chemistry of Radical Polymerization*; 2nd ed.; Elsevier: Kidlington, Oxford, 2006.

(9)   Hawker, C. J.; Bosman, A. W.; Harth, E. *Chem. Rev.* **2001**, *101*, 3661.

(10)   Matyjaszewski, K.; Xia, J. H. *Chem. Rev.* **2001**, *101*, 2921.

(11)   Moad, G.; Rizzardo, E.; Thang, S. H. *Aust. J. Chem.* **2005**, *58*, 379.

(12)   Moad, G.; Rizzardo, E.; Thang, S. H. *Aust. J. Chem.* **2006**, *59*, 669.

(13)   Moad, G.; Rizzardo, E.; Thang, S. H. *Aust. J. Chem.* **2009**, *62*, 1402.

(14)   *Handbook of RAFT Polymerization*; Barner-Kowollik, C., Ed.; Wiley-VCH: Weinheim, 2008.

(15)   Keddie, D. J. *Chem. Soc. Rev.* **2014**, *43*, 496.

(16)   Odian, G. *Principles of Polymerization*; 4th ed.; John Wiley & sons, Inc.: Hoboken, New Jersey, 2004.

(17)   Benaglia, M.; Chiefari, J.; Chong, Y. K.; Moad, G.; Rizzardo, E.; Thang, S. H. *JACS* **2009**, *131*, 6914.

(18)   Petruczok, C. D.; Barlow, R. F.; Shipp, D. A. *J. Polym. Sci., Part A: Polym. Chem.* **2008**, *46*, 7200.

(19)   Ray, B.; Kotani, M.; Yamago, S. *Macromolecules* **2006**, *39*, 5259.

(20)   Tong, Y.-Y.; Dong, Y.-Q.; Du, F.-S.; Li, Z.-C. *Macromolecules* **2008**, *41*, 7339.

(21)   Quemener, D.; Davis, T. P.; Barner-Kowollik, C.; Stenzel, M. H. *Chem. Commun.* **2006**, 5051.

(22)   Benaglia, M.; Chen, M.; Chong, Y. K.; Moad, G.; Rizzardo, E.; Thang, S. H. *Macromolecules* **2009**, *42*, 9384.

(23)   Keddie, D. J.; Guerrero-Sanchez, C.; Moad, G.; Rizzardo, E.; Thang, S. H. *Macromolecules* **2011**, *44*, 6738.

(24)   Keddie, D. J.; Guerrero-Sanchez, C.; Moad, G.; Mulder, R. J.; Rizzardo, E.; Thang, S. H. *Macromolecules* **2012**, *45*, 4205.

(25)   Busch, M.; Roth, M.; Stenzel, M. H.; Davis, T. P.; Barner-Kowollik, C. *Aust. J. Chem.* **2007**, *60*, 788.

(26)   Theis, A.; Stenzel, M. H.; Davis, T. P.; Coote, M. L.; Barner-Kowollik, C. *Aust. J. Chem.* **2005**, *58*, 437.

(27)   Hogarth, G.; Rainford-Brent, E.-J. C. R. C. R.; Kabir, S. E.; Richards, I.; Wilton-Ely, J. D. E. T.; Zhang, Q. *Inorg. Chim. Acta* **2009**, *362*, 2020.

(28)   Moad, G.; Chen, M.; Haeussler, M.; Postma, A.; Rizzardo, E.; Thang, S. H. *Polym. Chem.* **2011**, *2*, 492.

(29)   Lo, Y.-H., Shih, K.-C., Chen, Y.-C., Wang, M.H., Hsu, F. Y., Hsiao, M. S. 2006; Vol. US Patent 7,132,491 B2, November 7, 2006.

(30)   Zhou, N.; Zhang, Z.; Zhu, J.; Cheng, Z.; Zhu, X. *Macromolecules* **2009**, *42*, 3898.

(31)   Geagea, R. S., R.; Mazieres, S.; Destarac, M. *Polym. Prepr. (Am. Chem. Soc., Div. Polym. Chem.)* **2008**, *49*, 250.

(32)   Chen, C.-L.; Lo, Y.-H.; Lee, C.-Y.; Fong, Y.-H.; Shih, K.-C.; Huang, C.-C. *Inorg. Chem. Commun.* **2010**, *13*, 603.

(33)   Chen, M.; Ghiggino, K. P.; Launikonis, A.; Mau, A. W. H.; Rizzardo, E.; Sasse, W. H. F.; Thang, S. H.; Wilson, G. J. *J. Mat. Chem.* **2003**, *13*, 2696.

(34)   Chen, M.; Ghiggino, K. P.; Thang, S. H.; Wilson, G. J. *Angew. Chem. Int. Ed.* **2005**, *44*, 4368.

(35)   Chen, M.; Ghiggino, K. P.; Thang, S. H.; Wilson, G. J. *J. Chin. Chem. Soc.* **2006**, *53*, 79.

(36)   Southard, G. E.; Van Houten, K. A.; Murray, G. M. *Macromolecules* **2007**, *40*, 1395.

(37)   Southard, G. E.; Van Houten, K. A.; Ott, E. W., Jr.; Murray, G. M. *Anal. Chim. Acta* **2007**, *581*, 202.

(38)   Moughton, A. O.; Stubenrauch, K.; O'Reilly, R. K. *Soft Matter* **2009**, *5*, 2361.

(39)   Zhou, G.; He, J.; Harruna, I. I. *J. Polym. Sci., Part A: Polym. Chem.* **2007**, *45*, 4225.

(40)   Zhou, G.; Harruna, I. I. *Anal. Chem.* **2007**, *79*, 2722.

(41)   Zhou, G. C.; Harruna, II *Macromolecules* **2005**, *38*, 4114.

(42)   Munuera, L.; O'Reilly, R. K. *Dalton Trans.* **2010**, *39*, 388.

(43)   Zhou, G. C.; Harruna, II *Macromolecules* **2004**, *37*, 7132.

(44)   Zhang, L.; Zhang, Y.; Chen, Y. *Eur. Polym. J.* **2006**, *42*, 2398.

(45)   Hasell, T.; Thurecht, K. J.; Jones, R. D. W.; Brown, P. D.; Howdle, S. M. *Chem. Commun.* **2007**, 3933.

(46)   Fustin, C.-A.; Colard, C.; Filali, M.; Guillet, P.; Duwez, A.-S.; Meier, M. A. R.; Schubert, U. S.; Gohy, J.-F. *Langmuir* **2006**, *22*, 6690.

(47)   Beer, P. D.; Cowley, A. R.; Jeffery, J. C.; Paul, R. L.; Wong, W. W. H. *Polyhedron* **2003**, *22*, 795.

(48)   Chen, Q. Z., Z.; Zhou, N.; Zhu, J., Pan, Q.; Zhu, X. *J. Polym. Sci., Part A: Polym. Chem.* **2009**, *47*, 3607.

(49)   Zhang, Z.; Wang, W.; Cheng, Z.; Zhu, J.; Zhou, N.; Yang, Y.; Tu, Y.; Zhu, X. *Macromolecules* **2010**, *43*, 7979.

(50)   Elsen, A. M.; Nicolay, R.; Matyjaszewski, K. *Macromolecules* **2011**, *44*, 1752.

(51)   Focarete, M. L.; Scandola, M.; Kumar, A.; Gross, R. A. *J. Polym. Sci., Part B: Polym. Phys.* **2001**, *39*, 1721.

(52)   Albertsson, A. C.; Varma, I. K. *Biomacromolecules* **2003**, *4*, 1466.

(53)   Place, E. S.; George, J. H.; Williams, C. K.; Stevens, M. M. *Chem. Soc. Rev.* **2009**, *38*, 1139.

(54)   Uhrich, K. E.; Cannizzaro, S. M.; Langer, R. S.; Shakesheff, K. M. *Chem. Rev.* **1999**, *99*, 3181.

(55)   Williams, C. K. *Chem. Soc. Rev.* **2007**, *36*, 1573.

(56)   *Handbook of Ring-Opening Polymerization*; Dubois, P. C., O.; Raquez, Jean-Marie, Ed.; Wiley-VCH, 2009.

(57)   O'Keefe, B. J.; Hillmyer, M. A.; Tolman, W. B. *J. Chem. Soc., Dalton Trans.* **2001**, 2215.

(58)   Dechy-Cabaret, O.; Martin-Vaca, B.; Bourissou, D. *Chem. Rev.* **2004**, *104*, 6147.

(59)   Nederberg, F.; Connor, E. F.; Moller, M.; Glauser, T.; Hedrick, J. L. *Angew. Chem. Int. Ed.* **2001**, *40*, 2712.

(60)   Dove, A. P. *ACS Macro Letters* **2012**, *1*, 1409.

(61)   Pratt, R. C.; Lohmeijer, B. G. G.; Long, D. A.; Waymouth, R. M.; Hedrick, J. L. *JACS* **2006**, *128*, 4556.

(62)   Kobayashi, S.; Uyama, H.; Kimura, S. *Chem. Rev.* **2001**, *101*, 3793.

(63)   Gross, R. A.; Kumar, A.; Kalra, B. *Chem. Rev.* **2001**, *101*, 2097.

(64)   Albertsson, A. C.; Srivastava, R. K. *Adv. Drug Deliver. Rev.* **2008**, *60*, 1077.

(65)   Kobayashi, S. *P. Jpn. Acad. B - Phys.* **2010**, *86*, 338.

(66)   Uyama, H.; Kobayashi, S. *Chem. Lett.* **1993**, 1149.

(67)   Knani, D.; Gutman, A. L.; Kohn, D. H. *J. Polym. Sci., Part A: Polym. Chem.* **1993**, *31*, 1221.

(68)   Macdonald, R. T.; Pulapura, S. K.; Svirkin, Y. Y.; Gross, R. A.; Kaplan, D. L.; Akkara, J.; Swift, G.; Wolk, S. *Macromolecules* **1995**, *28*, 73.

(69)   Uyama, H.; Takeya, K.; Kobayashi, S. *P. Jpn. Acad. B - Phys.* **1993**, *69*, 203.

(70)   Uyama, H.; Takeya, K.; Kobayashi, S. *B. Chem. Soc. Jpn.* **1995**, *68*, 56.

(71)   Uyama, H.; Takeya, K.; Hoshi, N.; Kobayashi, S. *Macromolecules* **1995**, *28*, 7046.

(72)   Uyama, H.; Kikuchi, H.; Takeya, K.; Kobayashi, S. *Acta. Polym.* **1996**, *47*, 357.

(73)   Uyama, H.; Kikuchi, H.; Takeya, K.; Hoshi, N.; Kobayashi, S. *Chem. Lett.* **1996**, 107.

(74)   Noda, S.; Kamiya, N.; Goto, M.; Nakashio, F. *Biotechnol. Lett.* **1997**, *19*, 307.

(75)   Uyama, H.; Kuwabara, M.; Tsujimoto, T.; Kobayashi, S. *Polym. J.* **2002**, *34*, 970.

(76)   Bisht, K. S.; Henderson, L. A.; Gross, R. A.; Kaplan, D. L.; Swift, G. *Macromolecules* **1997**, *30*, 2705.

(77)   Hunsen, M.; Azim, A.; Mang, H.; Wallner, S. R.; Ronkvist, A.; Xie, W.; Gross, R. A. *Macromolecules* **2007**, *40*, 148.

(78)   Hunsen, M.; Abul, A.; Xie, W. C.; Gross, R. *Biomacromolecules* **2008**, *9*, 518.

(79)   van der Mee, L.; Helmich, F.; de Bruijn, R.; Vekemans, J. A. J. M.; Palmans, A. R. A.; Meijer, E. W. *Macromolecules* **2006**, *39*, 5021.

(80)   Matsumoto, M.; Odachi, D.; Kondo, K. *Biochem. Eng. J.* **1999**, *4*, 73.

(81)   Namekawa, S.; Suda, S.; Uyama, H.; Kobayashi, S. *Int. J. Biol. Macromol.* **1999**, *25*, 145.

(82)   Hedfors, C.; Hult, K.; Martinelle, M. *J. Mol. Catal. B: Enzym.* **2010**, *66*, 120.

(83)   Duda, A.; Kowalski, A.; Penczek, S.; Uyama, H.; Kobayashi, S. *Macromolecules* **2002**, *35*, 4266.

(84)   Kikuchi, H.; Uyama, H.; Kobayashi, S. *Polym. J.* **2002**, *34*, 835.

(85)   Malberg, S.; Finne-Wistrand, A.; Albertsson, A.-C. *Polymer* **2010**, *51*, 5318.

(86)   Taden, A.; Antonietti, M.; Landfester, K. *Macromol. Rapid Commun.* **2003**, *24*, 512.

(87)   Wosnick, J. H.; Faucher, S.; Pereira, L. *Abstr. Pap. Am. Chem. S.* **2010**, *240*.

(88)   Kumar, A.; Gross, R. A.; Wang, Y. B.; Hillmyer, M. A. *Macromolecules* **2002**, *35*, 7606.

(89)   He, F.; Li, S. M.; Vert, M.; Zhuo, R. X. *Polymer* **2003**, *44*, 5145.

(90)   Srivastava, R. K.; Albertsson, A. C. *Macromolecules* **2006**, *39*, 46.

(91)   Kumar, A.; Garg, K.; Gross, R. A. *Macromolecules* **2001**, *34*, 3527.

(92)   Xiao, Y.; Coulembier, O.; Koning, C. E.; Heise, A.; Dubois, P. *Chem. Commun.* **2009**, 2472.

(93)   Hunley, M. T.; Sari, N.; Beers, K. L. *ACS Macro Letters* **2013**, *2*, 375.

(94)   Kumar, A.; Kalra, B.; Dekhterman, A.; Gross, R. A. *Macromolecules* **2000**, *33*, 6303.

(95)   Kumar, A.; Gross, R. A. *JACS* **2000**, *122*, 11767.

(96)   Namekawa, S.; Uyama, H.; Kobayashi, S. *Macromol. Chem. Phys.* **2001**, *202*, 801.

(97)   Srivastava, R. K.; Albertsson, A. C. *Macromolecules* **2007**, *40*, 4464.

(98)   Jiang, Z. Z.; Azim, H.; Gross, R. A.; Focarete, M. L.; Scandola, M. *Biomacromolecules* **2007**, *8*, 2262.

(99)   Vaida, C.; Keul, H.; Moeller, M. *Green Chem.* **2011**, *13*, 889.

(100)   Gualandi, C.; White, L. J.; Chen, L.; Gross, R. A.; Shakesheff, K. M.; Howdle, S. M.; Scandola, M. *Acta Biomater.* **2010**, *6*, 130.

(101)   Zotzmann, J.; Behl, M.; Feng, Y.; Lendlein, A. *Adv. Funct. Mater.* **2010**, *20*, 3583.

(102)   Zotzmann, J.; Ziegler, H. J.; Behl, M.; Zierke, M.; Radke, W.; Lendlein, A. *J. Mater. Sci. - Mater. Med.* **2011**, *22*, 2147.

(103)   Kratz, K.; Voigt, U.; Lendlein, A. *Adv. Funct. Mater.* **2012**, *22*, 3057.

(104)   Matsumoto, H.; Ishiguro, T.; Konosu, Y.; Minagawa, M.; Tanioka, A.; Richau, K.; Kratz, K.; Lendlein, A. *Eur. Polym. J.* **2012**, *48*, 1866.

(105)   Behl, M.; Zotzmann, J.; Lendlein, A. *Int. J. Artif. Organs* **2011**, *34*, 231.

(106)   Razzaq, M. Y.; Behl, M.; Kratz, K.; Lendlein, A. *Adv. Mater.* **2013**, *25*, 5730.

(107)   Razzaq, M. Y.; Behl, M.; Frank, U.; Koetz, J.; Szczerba, W.; Lendlein, A. *J. Mater. Chem.* **2012**, *22*, 9237.

(108)   Balk, M.; Behl, M.; Noechel, U.; Lendlein, A. *Macromol. Mater. Eng.* **2012**, *297*, 1184.

(109)   Wisse, E.; Renken, R. A. E.; Roosma, J. R.; Palmans, A. R. A.; Meijer, E. W. *Biomacromolecules* **2007**, *8*, 2739.

(110)   Magusin, P. C. M. M.; Mezari, B.; van der Mee, L.; Palmans, A. R. A.; Meijer, E. W. *Macromol. Symp.* **2005**, *230*, 126.

(111)   Jerome, C.; Lecomte, P. *Adv. Drug Deliver. Rev.* **2008**, *60*, 1056.

(112)   van der Meulen, I.; Li, Y. Y.; Deumens, R.; Joosten, E. A. J.; Koning, C. E.; Heise, A. *Biomacromolecules* **2011**, *12*, 837.

(113)   Claudino, M.; van der Meulen, I.; Trey, S.; Jonsson, M.; Heise, A.; Johansson, M. *J. Polym. Sci., Part A: Polym. Chem.* **2012**, *50*, 16.

(114)   Habaue, S.; Asai, M.; Morita, M.; Okamoto, Y.; Uyama, H.; Kobayashi, S. *Polymer* **2003**, *44*, 5195.

(115)   Namekawa, S.; Uyama, H.; Kobayashi, S. *Biomacromolecules* **2000**, *1*, 335.

(116)   Jiang, Z. *Biomacromolecules* **2008**, *9*, 3246.

(117)   Mazzocchetti, L.; Scandola, M.; Jiang, Z. Z. *Macromolecules* **2009**, *42*, 7811.

(118)   Jiang, Z. *Biomacromolecules* **2011**, *12*, 1912.

(119)   Martino, L.; Scandola, M.; Jiang, Z. *Polymer* **2012**, *53*, 1839.

(120) Focarete, M. L.; Gualandi, C.; Scandola, M.; Govoni, M.; Giordano, E.; Foroni, L.; Valente, S.; Pasquinelli, G.; Gao, W.; Gross, R. A. *J. Biomater. Sci., Polym. Ed.* **2010**, *21*, 1283.

(121) Thompson, C. J.; Hansford, D.; Higgins, S.; Rostron, C.; Hutcheon, G. A.; Munday, D. L. *Int. J. Pharm.* **2007**, *329*, 53.

(122) Liu, J.; Jiang, Z.; Zhang, S.; Liu, C.; Gross, R. A.; Kyriakides, T. R.; Saltzman, W. M. *Biomaterials* **2011**, *32*, 6646.

(123) Tawfeek, H. M.; Evans, A. R.; Iftikhar, A.; Mohammed, A. R.; Shabir, A.; Somavarapu, S.; Hutcheon, G. A.; Saleem, I. Y. *Int. J. Pharm.* **2013**, *441*, 611.

(124) Liu, J.; Jiang, Z. Z.; Zhang, S. M.; Saltzman, W. M. *Biomaterials* **2009**, *30*, 5707.

(125) Skaria, S.; Smet, M.; Frey, H. *Macromol. Rapid Commun.* **2002**, *23*, 292.

(126) Kumar, R.; Gross, R. A. *JACS* **2002**, *124*, 1850.

(127) Kobayashi, S.; Uyama, H.; Namekawa, S. *Polym. Degrad. Stab.* **1998**, *59*, 195.

(128) Takwa, M.; Hult, K.; Martinelle, M. *Macromolecules* **2008**, *41*, 5230.

(129) Uyama, H.; Kikuchi, H.; Kobayashi, S. *Chem. Lett.* **1995**, 1047.

(130) Kalra, B.; Kumar, A.; Gross, R. A.; Baiardo, M.; Scandola, M. *Macromolecules* **2004**, *37*, 1243.

(131) Srivastava, R. K.; Kumar, K.; Varma, I. K.; Albertsson, A.-C. *Eur. Polym. J.* **2007**, *43*, 808.

(132) Takwa, M.; Xiao, Y.; Simpson, N.; Malmstrom, E.; Hult, K.; Koning, C. E.; Heise, A.; Martinelle, M. *Biomacromolecules* **2008**, *9*, 704.

(133) Xiao, Y.; Takwa, M.; Hult, K.; Koning, C. E.; Heise, A.; Martinelle, M. *Macromol. Biosci.* **2009**, *9*, 713.

(134) Hedfors, C.; Ostmark, E.; Malmstrom, E.; Hult, K.; Martinelle, M. *Macromolecules* **2005**, *38*, 647.

(135) Kerep, P.; Ritter, H. *Macromol. Rapid Commun.* **2007**, *28*, 759.

(136) Takwa, M.; Simpson, N.; Malmstrom, E.; Hult, K.; Martinelle, M. *Macromol. Rapid Commun.* **2006**, *27*, 1932.

(137) Simpson, N.; Takwa, M.; Hult, K.; Johansson, M.; Martinelle, M.; Malmstrom, E. *Macromolecules* **2008**, *41*, 3613.

(138) Eriksson, M.; Fogelstrom, L.; Hult, K.; Malmstrom, E.; Johansson, M.; Trey, S.; Martinelle, M. *Biomacromolecules* **2009**, *10*, 3108.

(139) van As, B. A. C.; Thomassen, P.; Kalra, B.; Gross, R. A.; Meijer, E. W.; Palmans, A. R. A.; Heise, A. *Macromolecules* **2004**, *37*, 8973.

(140) Meyer, U.; Palmans, A. R. A.; Loontjens, T.; Heise, A. *Macromolecules* **2002**, *35*, 2873.

(141) De Geus, M.; Schormans, L.; Palmans, A. A.; Koning, C. E.; Heise, A. *J. Polym. Sci., Part A: Polym. Chem.* **2006**, *44*, 4290.

(142) Peeters, J. W.; Palmans, A. R. A.; Meijer, E. W.; Koning, C. E.; Heise, A. *Macromol. Rapid Commun.* **2005**, *26*, 684.

(143) Duxbury, C. J.; Wang, W. X.; de Geus, M.; Heise, A.; Howdle, S. M. *JACS* **2005**, *127*, 2384.

(144) Zhou, J.; Villarroya, S.; Wang, W.; Wyatt, M. F.; Duxbury, C. J.; Thurecht, K. J.; Howdle, S. M. *Macromolecules* **2006**, *39*, 5352.

(145) Villarroya, S.; Zhou, J. X.; Duxbury, C. J.; Heise, A.; Howdle, S. M. *Macromolecules* **2006**, *39*, 633.

(146) Thurecht, K. J.; Gregory, A. M.; Villarroya, S.; Zhou, J.; Heise, A.; Howdle, S. M. *Chem. Commun.* **2006**, 4383.

(147) Villarroya, S.; Thurecht, K. J.; Heise, A.; Howdle, S. M. *Chem. Commun.* **2007**, 3805.

(148) Hans, M.; Gasteier, P.; Keul, H.; Moeller, M. *Macromolecules* **2006**, *39*, 3184.

(149) Duxbury, C. J.; Cummins, D.; Heise, A. *Macromol. Rapid Commun.* **2007**, *28*, 235.

(150) Yoon, K. R.; Lee, K. B.; Chi, Y. S.; Yun, W. S.; Joo, S. W.; Choi, I. S. *Adv. Mater.* **2003**, *15*, 2063.

(151) Li, J.; Xie, W. H.; Cheng, H. N.; Nickol, R. G.; Wang, P. G. *Macromolecules* **1999**, *32*, 2789.

(152) Duxbury, C. J.; Hilker, I.; de Wildeman, S. M. A.; Heise, A. *Angew. Chem. Int. Ed.* **2007**, *46*, 8452.

(153) Yeniad, B.; Koklukaya, N. O.; Naik, H.; Fijten, M. W. M.; Koning, C. E.; Heise, A. *J. Polym. Sci., Part A: Polym.Chem.* **2013**, *51*, 84.

(154) Villarroya, S.; Zhou, J.; Thurecht, K. J.; Howdle, S. M. *Macromolecules* **2006**, *39*, 9080.

(155) Villarroya, S.; Dudek, K.; Zhou, J.; Irvine, D. J.; Howdle, S. M. *J. Mater. Chem.* **2008**, *18*, 989.

(156) Popescu, D.; Keul, H.; Moeller, M. *Macromol. Rapid Commun.* **2011**, *32*, 559.

(157) Wang, S.; Fu, C.; Zhang, Y.; Tao, L.; Li, S.; Wei, Y. *ACS Macro Letters* **2012**, *1*, 1224.

(158) Fu, C.; Zhu, C.; Wang, S.; Liu, H.; Zhang, Y.; Guo, H.; Tao, L.; Wei, Y. *Polym. Chem.* 2**2013**, *4*, 264.

(159) Skoglund, P.; Fransson, A. *Polymer* **1998**, *39*, 1899.

(160) Skoglund, P.; Fransson, A. *Polymer* **1998**, *39*, 3143.

(161) Zhong, Z. Y.; Dijkstra, P. J.; Feijen, J. *Macromol. Chem. Phys.* **2000**, *201*, 1329.

(162) Gazzano, M.; Malta, V.; Focarete, M. L.; Scandola, M.; Gross, R. A. *J. Polym. Sci., Part B: Polym. Phys.* **2003**, *41*, 1009.

(163) Ren, J. D.; Adachi, K. *Macromolecules* **2003**, *36*, 4659.

(164) Cai, J.; Hsiao, B. S.; Gross, R. A. *Polym. Int.* **2009**, *58*, 944.

(165) de Geus, M.; van der Meulen, I.; Goderis, B.; van Hecke, K.; Dorschu, M.; van der Werff, H.; Koning, C. E.; Heise, A. *Polym. Chem.* **2010**, *1*, 525.

(166) Cai, J.; Liu, C.; Cai, M.; Zhu, J.; Zuo, F.; Hsiao, B. S.; Gross, R. A. *Polymer* **2010**, *51*, 1088.

(167) Cai, J.; Hsiao, B. S.; Gross, R. A. *Macromolecules* **2011**, *44*, 3874.

(168) Ceccorulli, G.; Scandola, M.; Kumar, A.; Kalra, L.; Gross, R. A. *Biomacromolecules* **2005**, *6*, 902.

(169) Mazzocchetti, L.; Scandola, M.; Jiang, Z. *Eur. Polym. J.* **2012**, *48*, 1883.

(170) Focarete, M. L.; Gazzano, M.; Scandola, M.; Kumar, A.; Gross, R. A. *Macromolecules* **2002**, *35*, 8066.

(171) van der Meulen, I.; de Geus, M.; Antheunis, H.; Deumens, R.; Joosten, E. A. J.; Koning, C. E.; Heise, A. *Biomacromolecules* **2008**, *9*, 3404.

(172) Scandola, M. F., M. L.; Gross, R. A. *Polym. Prepr. (Am. Chem. Soc., Div. Polym. Chem.)* **2009**, *50*.

(173) Zotzmann, J.; Behl, M.; Hofmann, D.; Lendlein, A. *Adv. Mater.* **2010**, *22*, 3424.

(174) Nakane, K.; Tamaki, C.; Hata, Y.; Ogihara, T.; Ogata, N. *J. App. Polym. Sci.* **2008**, *108*, 2139.

(175)   Sonnenschein, M. F.; Lysenko, Z.; Brune, D. A.; Wendt, B. L.; Schrock, A. K. *Polymer* **2005**, *46*, 10158.

(176)   Nomura, R.; Ueno, A.; Endo, T. *Macromolecules* **1994**, *27*, 620.

(177)   Jedlinski, Z.; Juzwa, M.; Adamus, G.; Kowalczuk, M.; Montaudo, M. *Macromol. Chem. Phys.* **1996**, *197*, 2923.

(178)   Nakayama, Y.; Watanabe, N.; Kusaba, K.; Sasaki, K.; Cai, Z.; Shiono, T.; Tsutsumi, C. *J. App. Polym. Sci.* **2011**, *121*, 2098.

(179)   Pascual, A.; Leiza, J. R.; Mecerreyes, D. *Eur. Polym. J.* **2013**, *49*, 1601.

(180)   Kunioka, M.; Wang, Y.; Onozawa, S. *Polym. J.* **2003**, *35*, 422.

(181)   Wang, Y.; Kunioka, M. *Macromol. Symp.* **2005**, *224*, 193.

(182)   van der Meulen, I.; Gubbels, E.; Huijser, S.; Sablong, R.; Koning, C. E.; Heise, A.; Duchateau, R. *Macromolecules* **2011**, *44*, 4301.

(183)   Pepels, M. P. F.; Bouyahyi, M.; Heise, A.; Duchateau, R. *Macromolecules* **2013**, *46*, 4324.

(184)   Bouyahyi, M.; Pepels, M. P. F.; Heise, A.; Duchateau, R. *Macromolecules* **2012**, *45*, 3356.

(185)   Wilson, J. A.; Hopkins, S. A.; Wright, P. M.; Dove, A. P. *Polym. Chem.* **2014**, *5*, 2691.

Chapter 2

Synthesis of Poly(ω-pentadecalactone)-b-Poly(acrylate) Copolymers via a Combination of Ring-Opening and RAFT Polymerization Techniques

2.1 Introduction

Reports that PPDL maintains similar properties to LDPE[1] and potentially high density polyethylene (HDPE) at higher molecular weights motivated our interest in PPDL as a "green" alternative to PE following its hydrolysable ester linkages. Furthermore, since PPDL can be prepared *via* eROP techniques, which enables α-chain-end functionalization *via* choice of initiator, we envisaged that the preparation of a PPDL macro-CTA utilizing a bifunctional initiator could enable facile preparation of RAFT-functional polymers with PE-like properties. Ultimately, this strategy could, in some circumstances, be a suitable, simple solution to the difficult problem of preparing block copolymers of PE *via* controlled radical polymerization techniques.

Preparation of block copolymers of CL *via* eROP has been demonstrated using bifunctional initiators with appropriate CRP techniques including NMP,[2] ATRP,[3-8] and RAFT[9] polymerization. Although block copolymers are typically prepared in two steps when combining ROP and CRP techniques, many of these strategies concern the one-pot preparation of block copolymers *via* eROP and ATRP which, remarkably proceed in scCO$_2$ 1) without the metal catalyst impairing enzyme activity, and 2) in the absence of transesterification reactions on methacrylic monomers.[6-8] To our knowledge, block copolymers of PPDL have not been prepared *via* eROP using a bifunctional initiator appropriate for CRP.

Our research group has previously demonstrated that the hydroxy-functional RAFT agent **1** (Figure 2.1) can be prepared in good yield and utilized for the preparation of block copolymers *via* ROP and RAFT polymerization techniques.[10-12] Specifically, it has been employed in the preparation of block copolymers of polylactide. As a trithioester absent of ester functionality, we envisaged that **1** is a suitable bifunctional initiator for the eROP of PPDL. However, since this CTA is appropriate for the CRP of acrylic and styrenic monomers, the PPDL block must be prepared first since the solution eROP of an acrylic macroinitiator would result in a mixture of products instead of defined block copolymers following transesterification of both the acrylic and PPDL block by the enzyme.
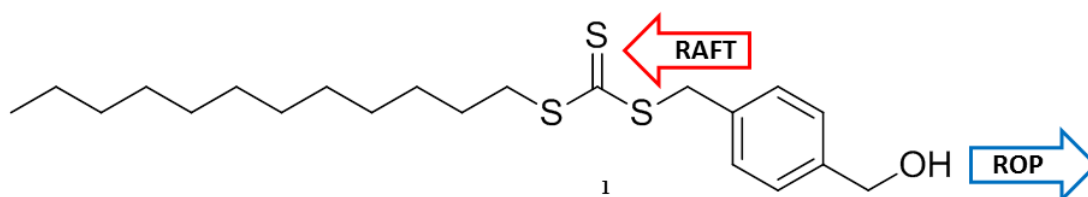
Figure 2.1: Structure of dodecyl 4-(hydroxymethyl) benzyl carbonotrithioate (**1**), which has been previously demonstrated as a bifunctional initiator for the preparation of block copolymers *via* ROP and RAFT polymerization techniques.[10-12]

Our initial interest concerning the preparation of RAFT-functional PPDL is to prepare acrylic or methacrylic block copolymers of PPDL for fuels applications, specifically as a potential cold-flow additive for diesel and biofuels. Many cold-flow additives are traditionally polyethylene-based copolymers and therefore PPDL-based polymers may present a novel paradigm for cold-flow technology. Herein the preparation of PPDL *via* eROP and the chain extension of a PPDL macro-CTA to prepare block copolymers of PPDL are investigated. The scaled up synthesis and fuels testing of selected block copolymers of PPDL is described in Chapter 3.

2.2 Results and Discussion

2.2.1 Enzymatic Ring-Opening Polymerization of ω-Pentadecalactone

2.2.1.1 Enzymatic Ring-Opening Polymerization of ω-Pentadecalactone Initiating from Benzyl Alcohol

PPDL was successfully prepared *via* the eROP of PDL adapted from literature methods.[13] Specifically, PDL was polymerized using Novozyme 435 as a catalyst and benzyl alcohol (BnOH) as an initiator in toluene at 60 °C (Scheme 2.1). The amount of lipase utilized, specifically 1 wt.%, was selected to obtain good control over the polymerization within a practical time frame.
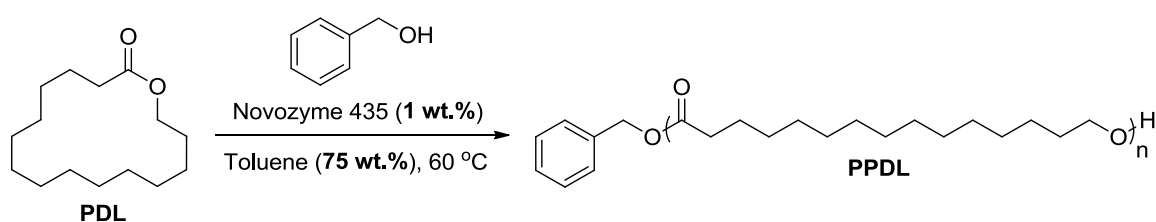
Scheme 2.1: Enzymatic ring-opening polymerization (eROP) of PDL using Novozyme-435 as a catalyst and benzyl alcohol as an initiator.

The polymerization was monitored by comparing the integral of the methylene protons adjacent to the ester in the cyclic monomer (δ = 4.13 ppm) and polymer (δ = 4.05 ppm) in ^{1}H NMR spectra (Figure 2.2). Furthermore, the degree of polymerization was evaluated by comparing the integral of the benzyl methylene protons (δ = 5.11 ppm) to that of the methylene protons adjacent to the ester in the polymer (δ = 4.05 ppm). By altering the ratio of monomer to initiator, the target degree of polymerization was varied.
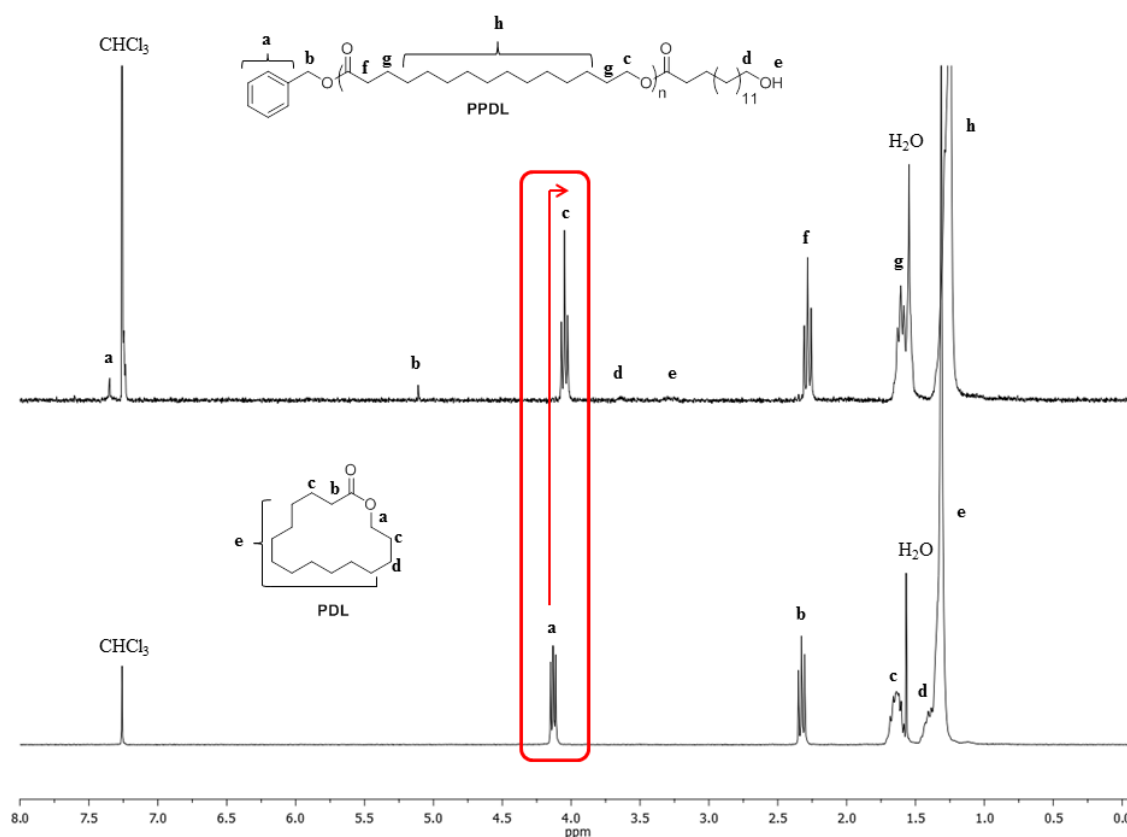
Figure 2.2: ^{1}H NMR spectral overlay of PDL and DP 32 PPDL prepared *via* eROP, initiated from benzyl alcohol ([M]/[I] = 35), and recrystallized from ethyl acetate, illustrating the chemical shift between the methylene protons adjacent to the ester in the monomer and polymer (300 MHz; CDCl$_3$).

Good control was demonstrated for the eROP of PDL initiating from benzyl alcohol across a range of targeted DPs, specifically DP 20, 35, 50, 75, and 100. This was evidenced by linear semi-logarithmic plots (Figure 2.3), a linear correlation between the M_n and monomer conversion, and a decrease in the $Đ_M$ of the polymer with increasing degrees of polymerization (Figure 2.4). Interestingly, the dispersity is significantly higher than that observed with conventional ROP techniques since eROP is a transesterification process that does not discriminate between ester bonds in the monomer or polymer product, resulting in chain scission, and consequently cannot be considered a living polymerization technique.[14] Overall, however, a good correlation between the M_n and DP was observed across all degrees of polymerization performed, and follow theoretical values (Figure 2.5). Finally, MALDI-ToF mass spectral analysis of PPDL revealed two distributions with regular repeat units equal to the molecular weight of PDL (Figure 2.6). One distribution, centered on m/z = 2052.91 corresponds to sodium charged linear polymer initiated from benzyl alcohol, and the other corresponds to sodium charged cyclic polymer. The observation of cyclic polymers is consistent with the observations of other authors and arises following chain scission followed by cyclization during the

polymerization.[15] Importantly, a distribution corresponding to the polymer initiated from water was not observed.
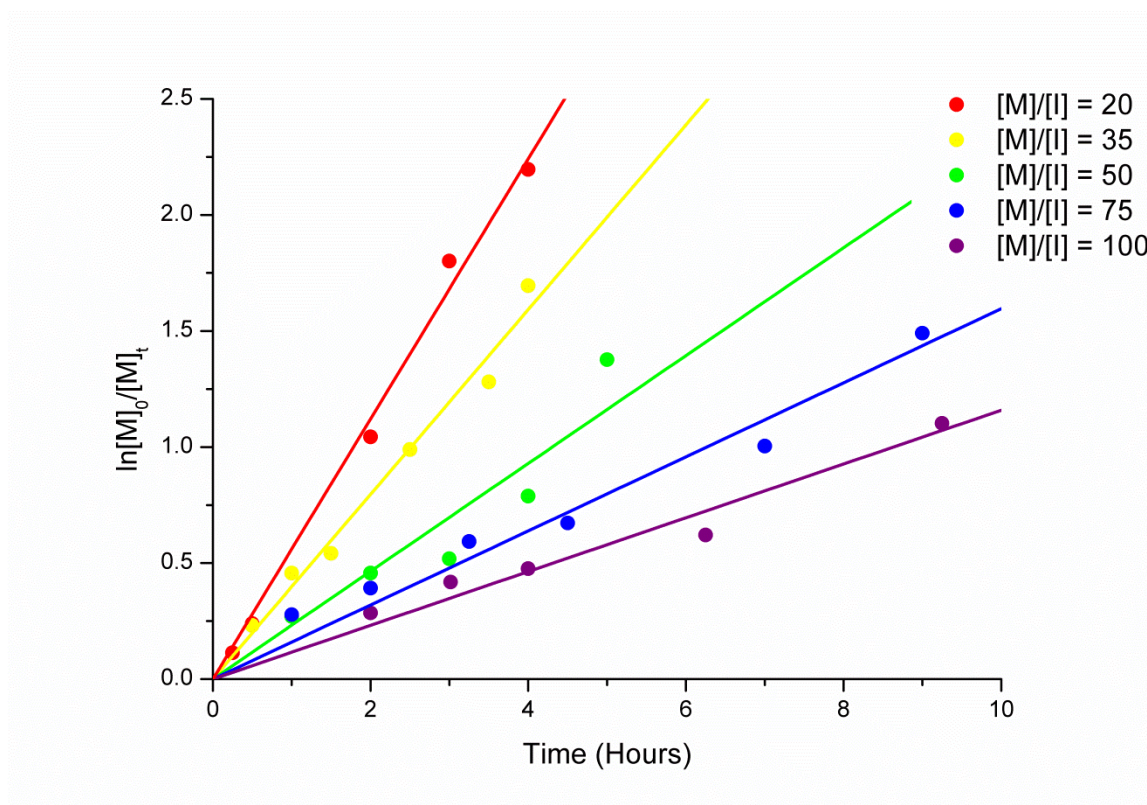
Figure 2.3: Semi-logarithmic plots for the eROP of PDL, initiating from benzyl alcohol.
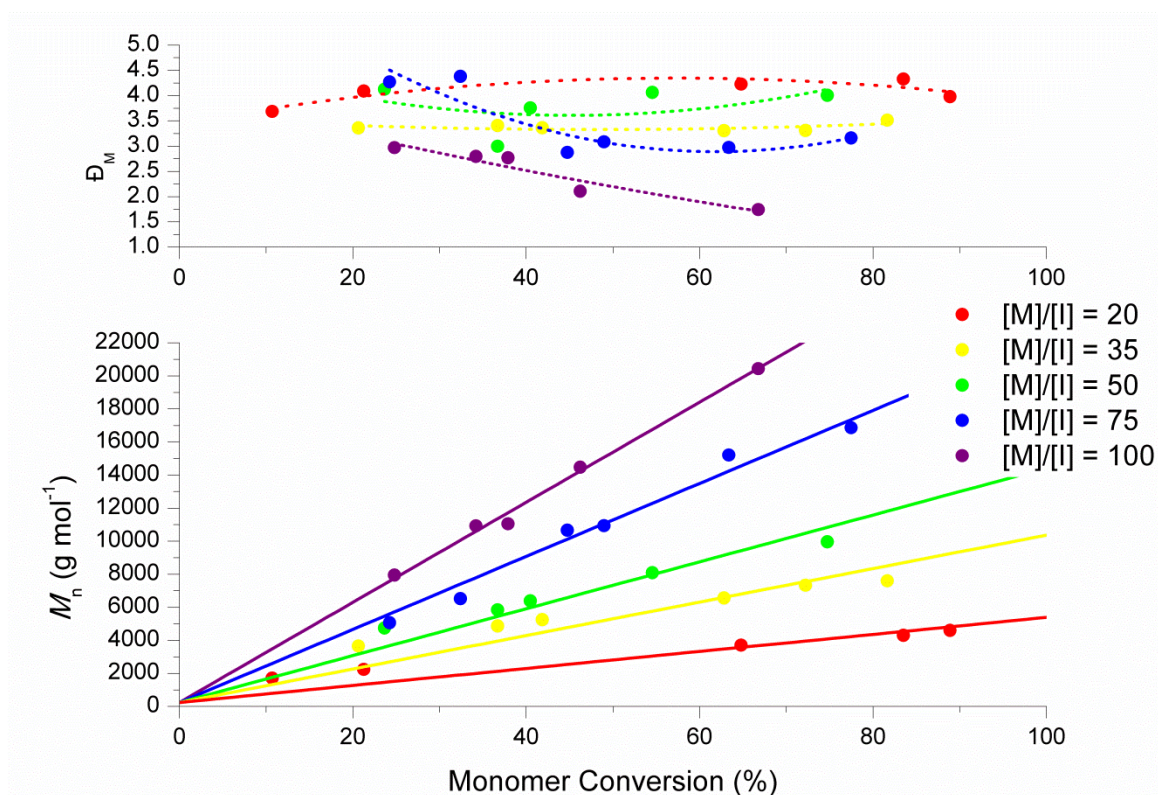
Figure 2.4: Plot of M_n and $Đ_M$ *versus* monomer conversion for the eROP of PDL, initiating from benzyl alcohol. Please note that trend lines fitted to $Đ_M$ *versus* percent monomer conversion plots are provided solely to guide the eye.
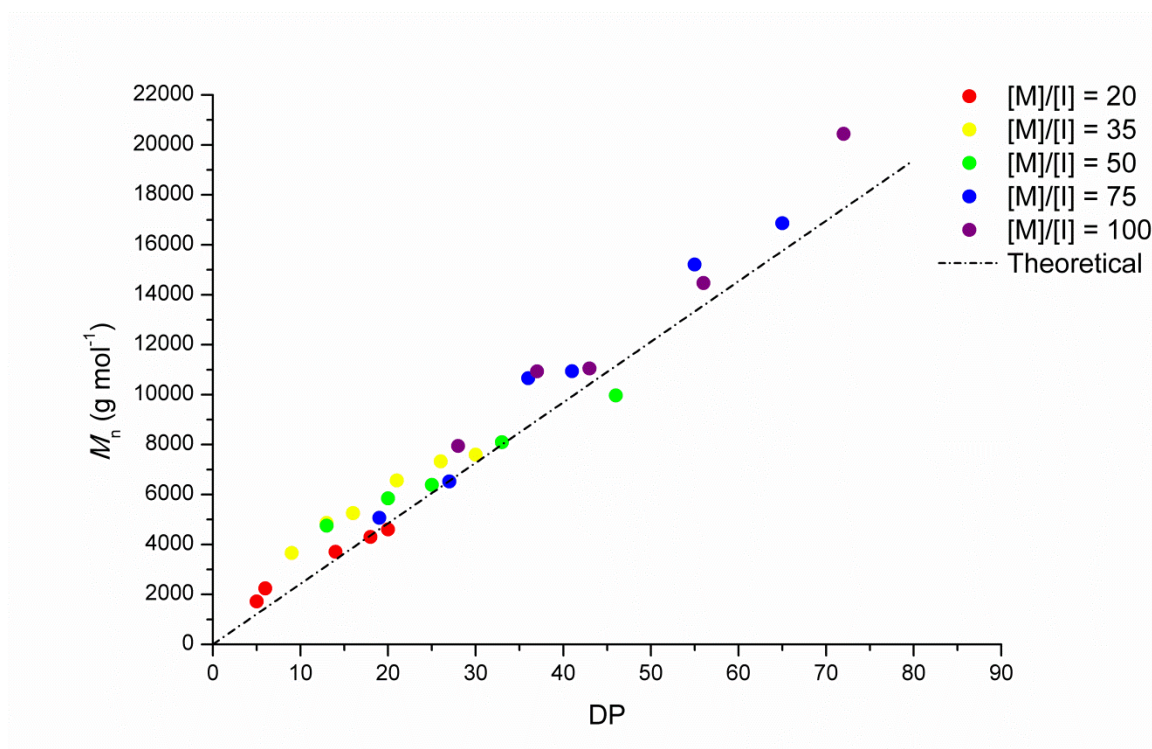
Figure 2.5: Plot of M_n *versus* DP for the eROP of PDL, initiating from benzyl alcohol.
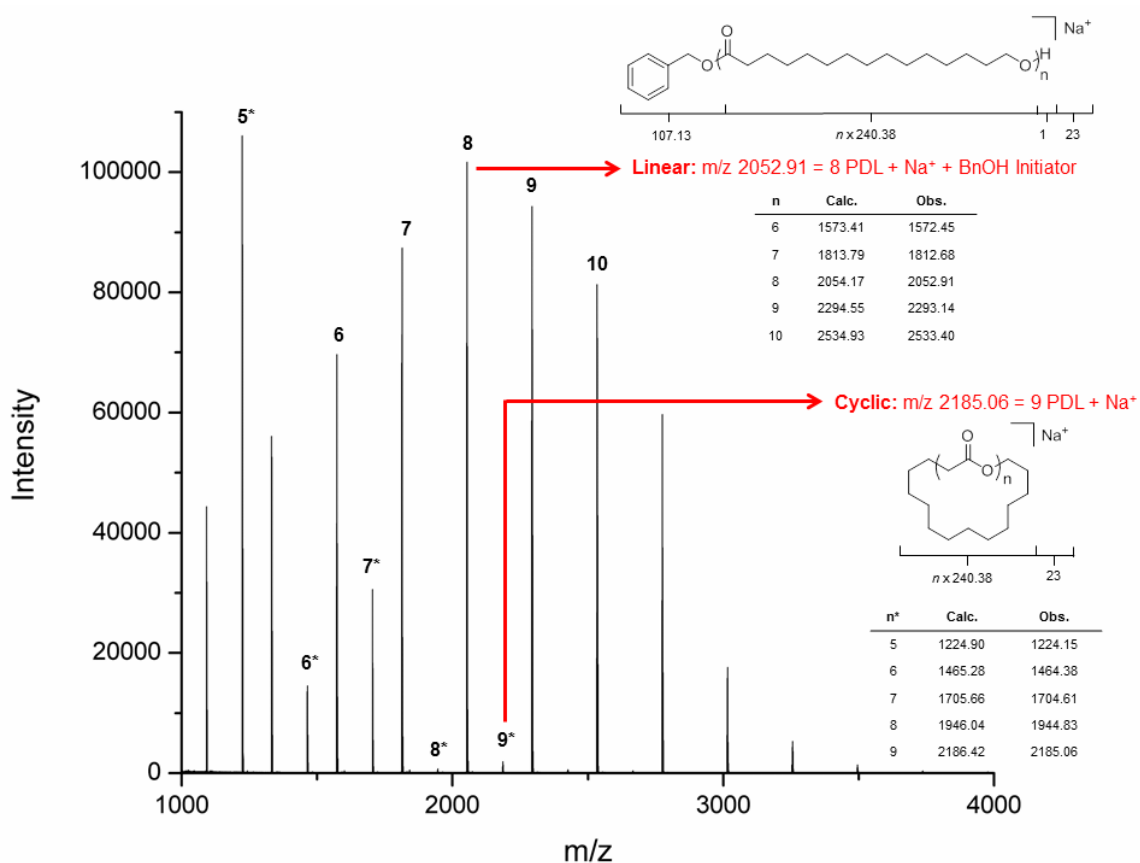
Figure 2.6: MALDI-ToF mass spectrum analysis of crude DP 10 PPDL prepared *via* eROP and initiated from benzyl alcohol ([M]/[I] = 20).

2.2.1.2 Enzymatic Ring-Opening Polymerization of ω-Pentadecalactone Initiating from Dodecyl 4-(hydroxymethyl) benzyl carbonotrithioate (1)

In order to prepare RAFT-functional PPDL, the bifunctional initiator dodecyl 4-(hydroxymethyl) benzyl carbonotrithioate (**1**) was synthesized according to literature methods (Scheme 2.2).[10] Specifically, all in one pot, dodecane thiol was deprotonated using potassium phosphate in acetone, and the resulting anion underwent a nucleophilic addition to an excess of carbon disulfide. Thereafter, the resulting dithiocarboxylate anion underwent a nucleophilic addition to 4-(chloromethyl)benzyl alcohol, driven by the formation of potassium chloride, to yield **1** in good yield (94%), exceeding reported yields (81%[10] and 90%[11]). Since the reaction was performed in acetone, the reaction time, however, could have been significantly reduced by performing an *in situ* Finkelstein reaction[16,17] on 4-(chloromethyl)benzyl alcohol during the final step *via* the addition of NaI to generate the corresponding iodo- compound (Scheme 2.3), which is more reactive towards the dithiocarboxylate anion than the chloro- derivative. The ^{1}H and ^{13}C distortionless enhancement by polarization transfer (DEPT) NMR spectra obtained for **1** match reported values (Figure 2.7).[10]
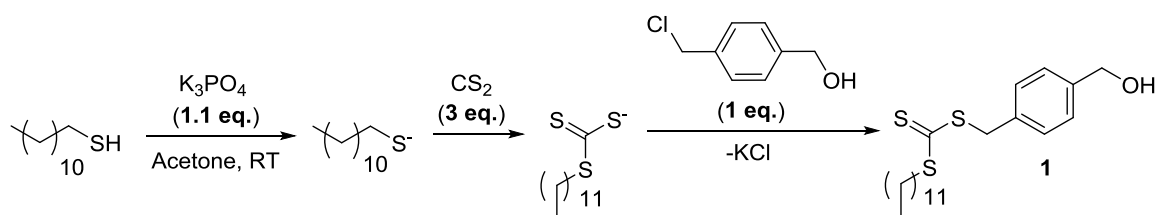
Scheme 2.2: Synthesis of dodecyl 4-(hydroxymethyl) benzyl carbonotrithioate (**1**).
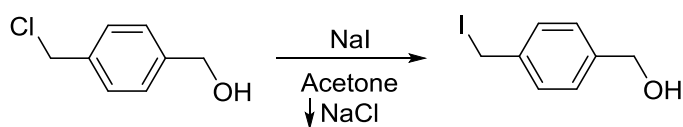
Scheme 2.3: Finkelstein reaction of 4-(chloromethyl)benzyl alcohol to generate 4-(iodomethyl)benzyl alcohol.
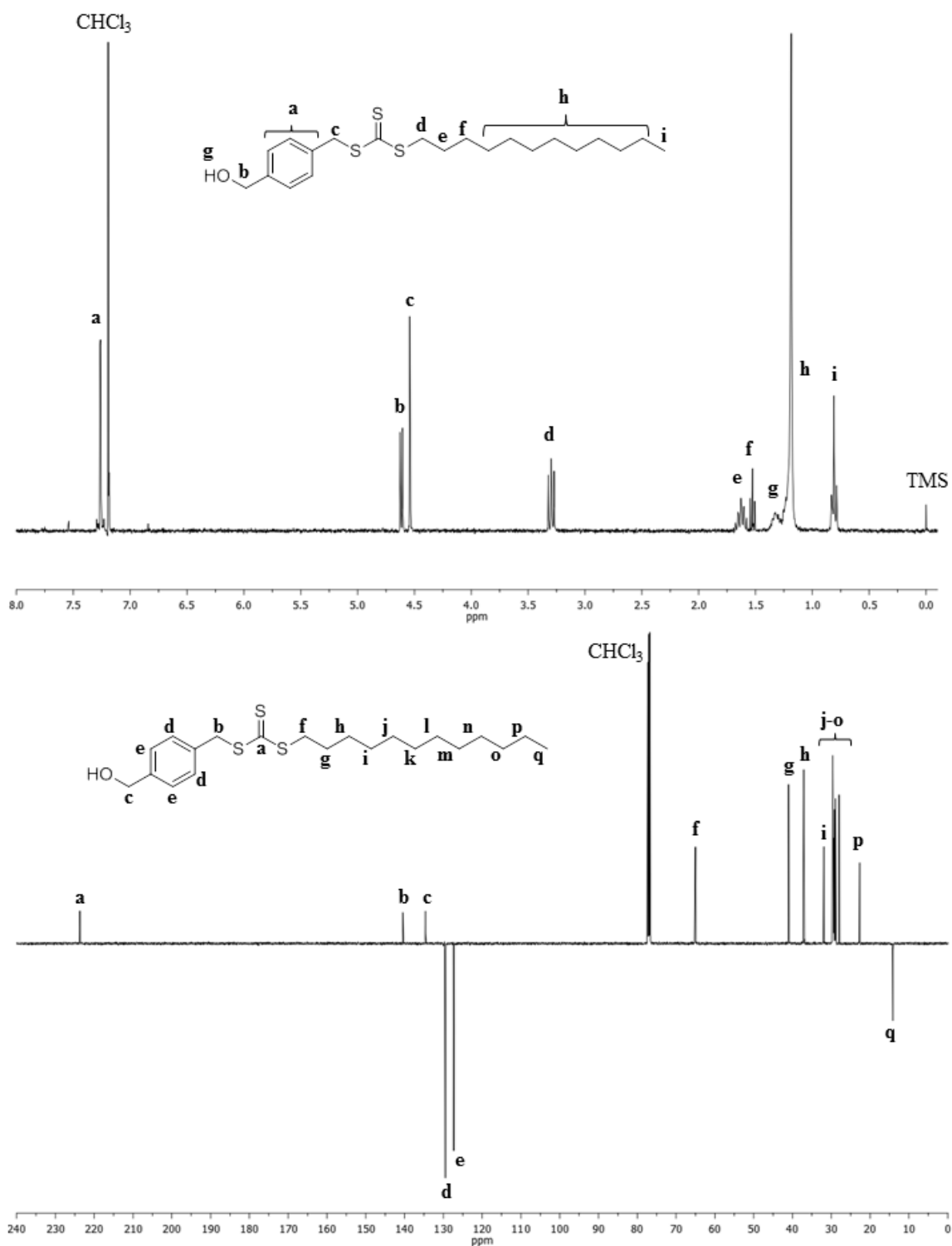
Figure 2.7: ^{1}H and ^{13}C DEPT NMR spectra of **1** (400 MHz, CHCl$_3$).

The polymerization of PDL *via* eROP using Novozyme-435 as a catalyst and **1** as an initiator (Scheme 2.4) was monitored as previously described (Figure 2.2). Similarly, the DP was evaluated by comparing the integral of the benzyl methylene protons (b) of **1** (δ = 5.08 ppm) to that of the methylene protons adjacent to the ester in the polymer (δ = 4.05 ppm) (Figure 2.8).
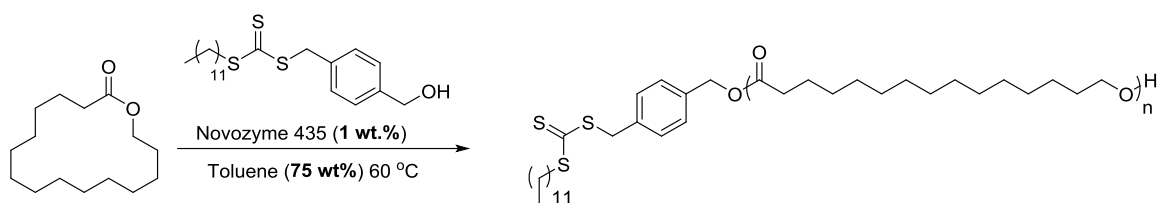
Scheme 2.4: Enzymatic ring-opening polymerization (eROP) of PDL using Novozyme-435 as a catalyst and **1** as an initiator.
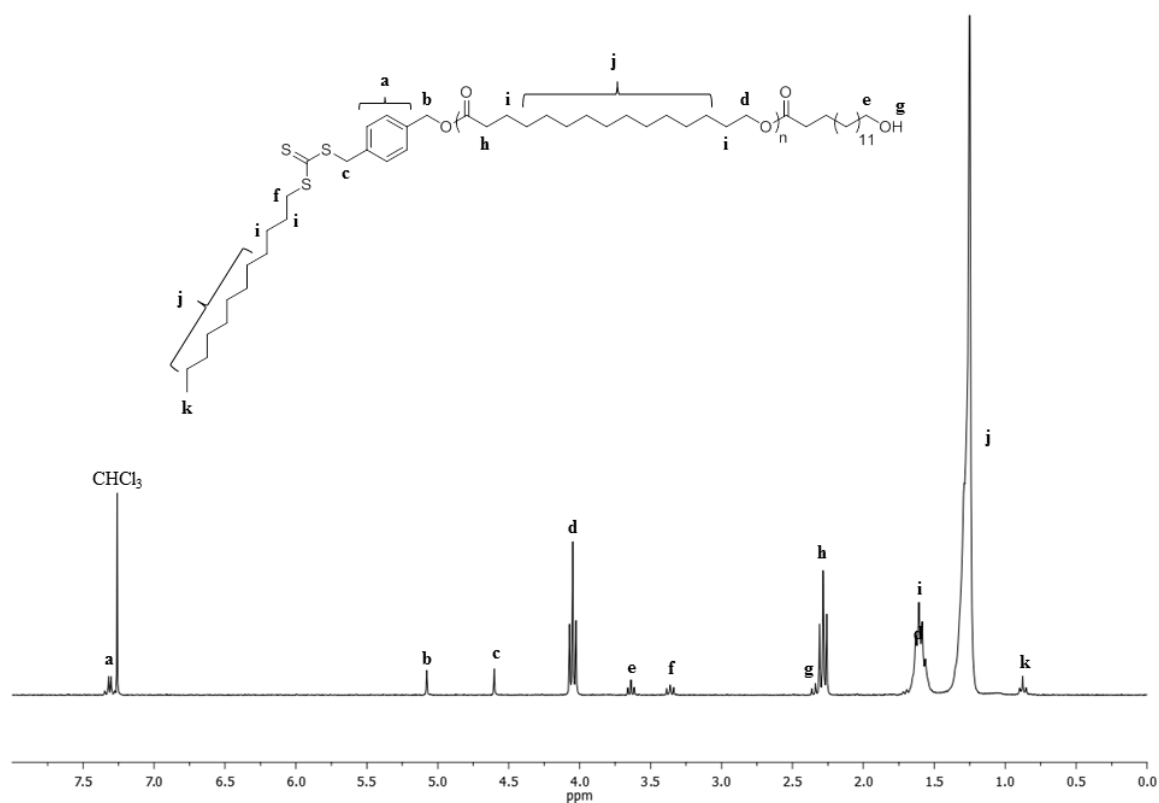
Figure 2.8: ^{1}H NMR spectrum of DP 11 PPDL prepared *via* eROP, initiating from **1** ([M]/[I] = 20) and recrystallized from ethyl acetate (300 MHz; CDCl$_3$).

As with the eROP of PDL initiated from BnOH, good control was demonstrated for the eROP of PDL initiated from **1** when targeting a range of DPs, specifically DP 20, 50, and 100. This was evidenced by linear semi-logarithmic plots (Figure 2.9), a linear correlation between the M_n and monomer conversion, and a decrease in the $Đ_M$ of the polymer with increasing degrees of polymerization (Figure 2.10). Overall, a good correlation between the M_n and DP was observed across all degrees of polymerization performed, and follow theoretical values (Figure 2.11). Finally, MALDI-ToF mass spectral analysis of PPDL revealed two distributions with regular repeat units equal to the molecular weight of PDL (Figure 2.12). One distribution, centered around m/z = 2583.75 corresponds to sodium charged linear polymer initiated from **1**, and the other distribution to sodium charged cyclic polymer. As with the eROP of PDL initiated from BnOH, cyclic polymers were observed following chain scission reactions followed by cyclization,

50

both catalysed by the enzyme, and importantly, no distribution corresponding to PDL initiated from water was observed.
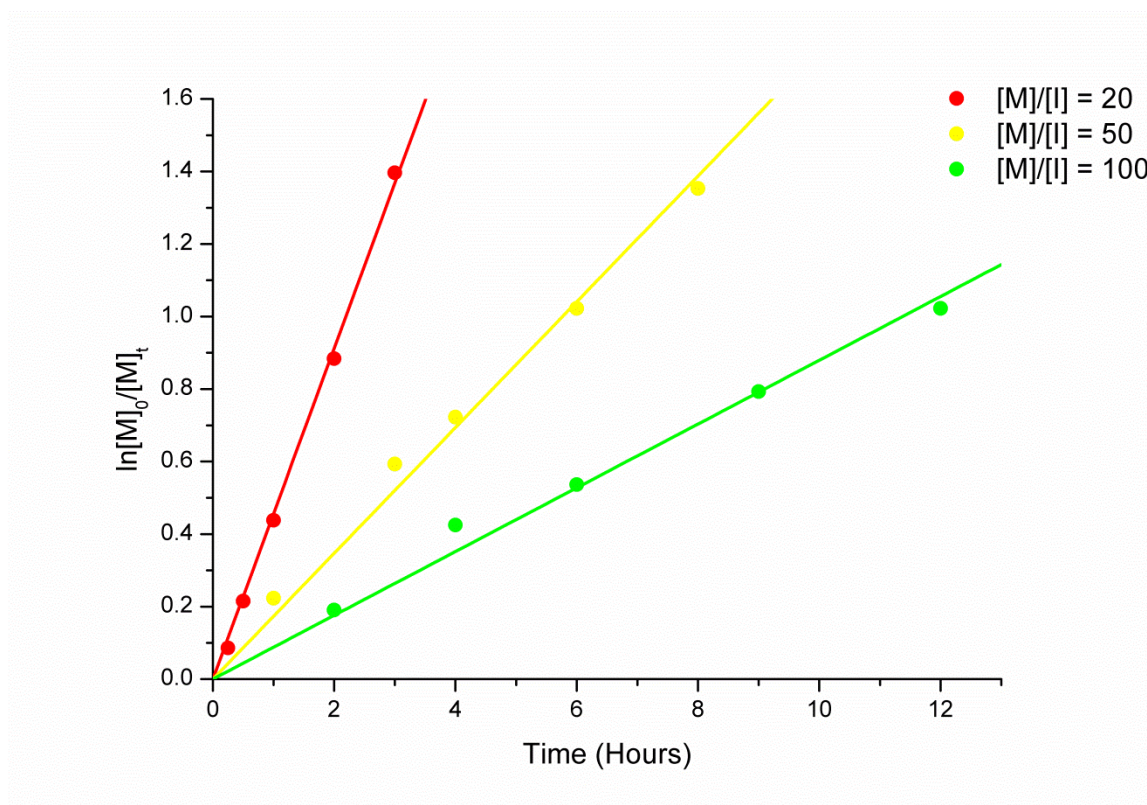
Figure 2.9: Semi-logarithmic plots for the eROP of PDL initiating from **1**.
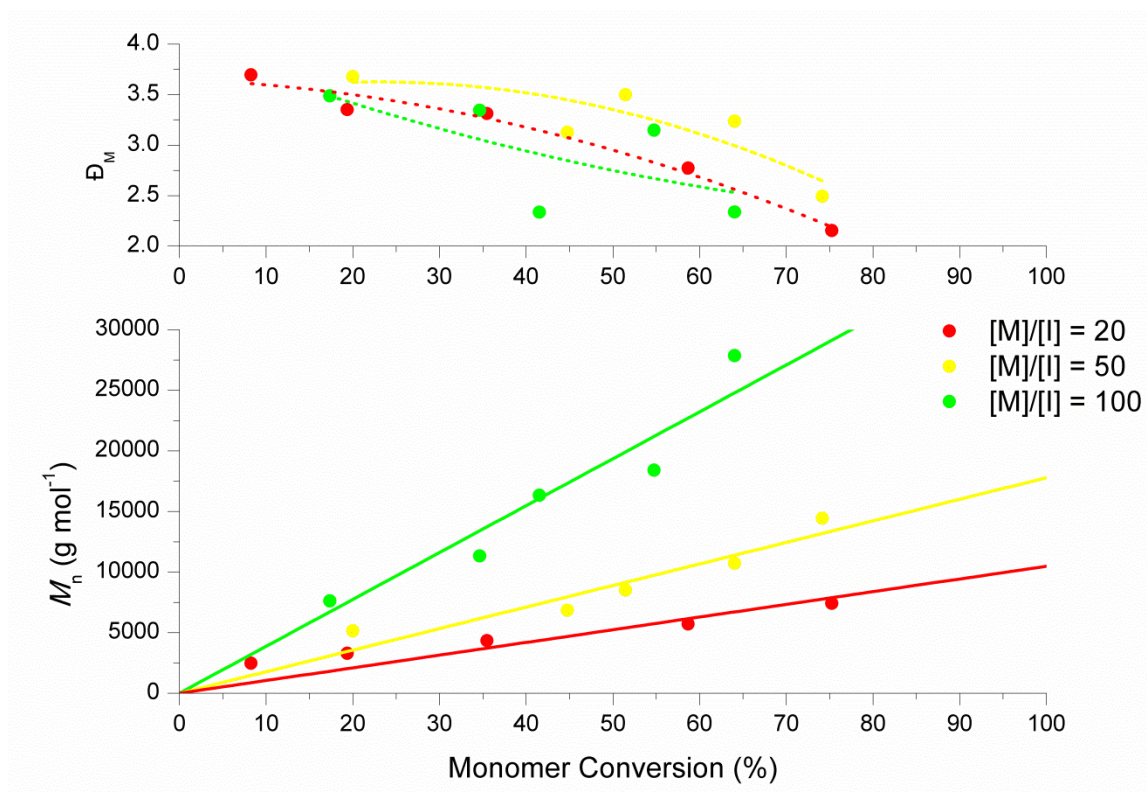
Figure 2.10: Plot of M_n and $Đ_M$ *versus* monomer conversion for the eROP of PDL, initiating from **1** ([M]/[I] = 20). Please note that trend lines fitted to $Đ_M$ *versus* percent monomer conversion plots are provided solely to guide the eye.
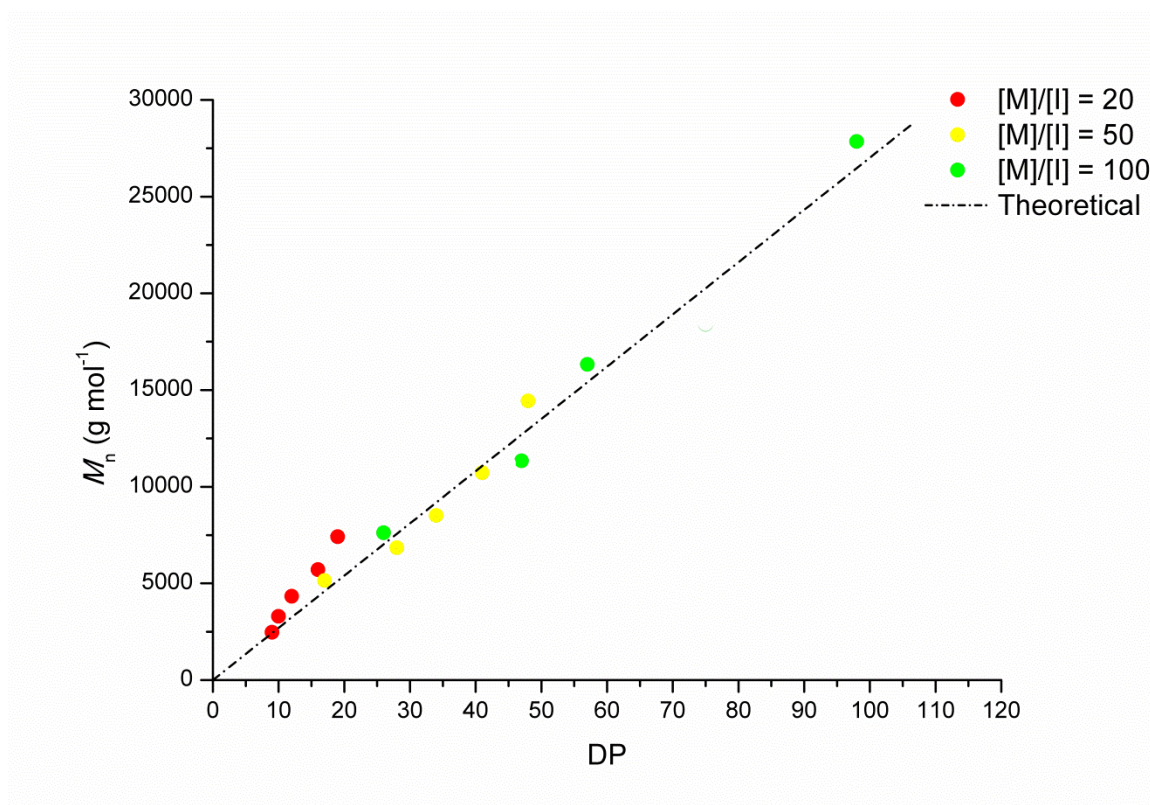
Figure 2.11: Plot of *Mn versus* DP for the eROP of PDL, initiating from **1** ([M]/[I] = 20).
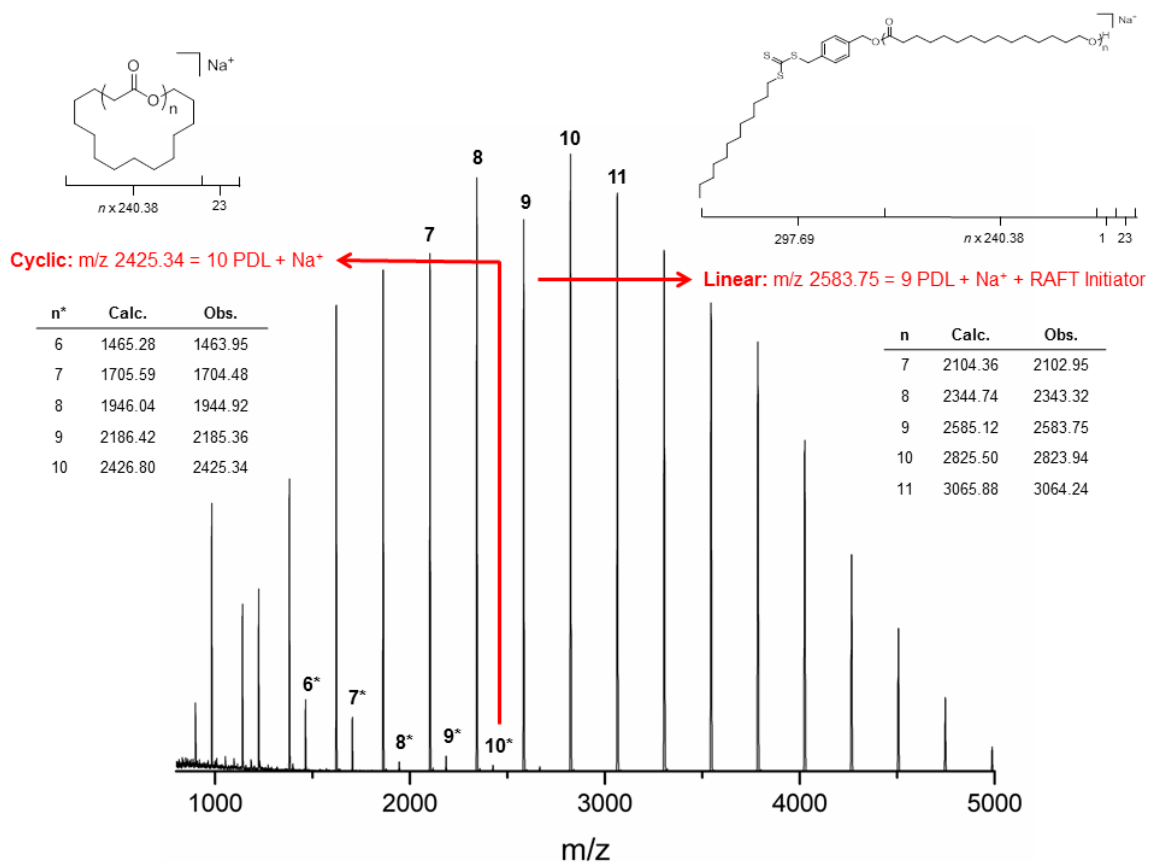
Figure 2.12: MALDI-ToF mass spectrum of crude DP 16 PPDL (**2**) prepared *via* eROP initiated from **1** ([M]/[I] = 20).

2.2.1.3 Synthesis and Purification of DP 16 Poly(ω-Pentadecalactone) macro-CTA 2

In order to synthesize block copolymers of PPDL, a large batch of PPDL macro-CTA (**2**) was prepared *via* eROP initiating from **1** (Scheme 2.5 and Table 2.1). A DP of 17 was targeted since an M_n approximating to 4000 g mol^{-1} was desired for block copolymers of PPDL for fuels applications.
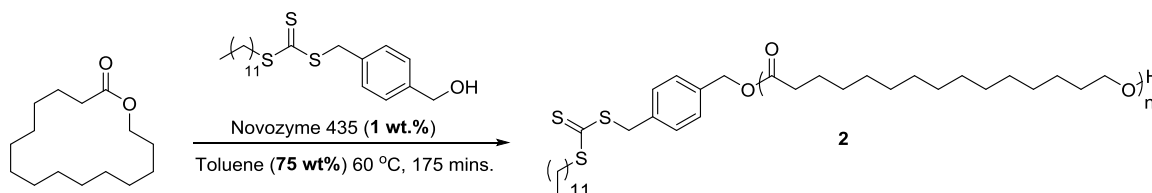
Scheme 2.5: Synthesis of DP 16 PPDL macro-CTA **2**.

Table 2.1: Characterization of crude PPDL macro-CTA **2** prepared according to Scheme 2.5.

[M]/[I]	[M]$_t$/[M]$_t$[a]	M_n (g mol^{-1})[b]	M_n (g mol^{-1})[a]	$Đ_M$[b]	DP[a]
20	0.72	4600	4200	3.65	16

[a]Determined by ^{1}H NMR spectral analysis in CDCl$_3$; [b]Determined by GPC analysis in CHCl$_3$.

Purification of **2** from PDL and cyclic PPDL oligomers was performed *via* precipitation in methanol from chloroform, as reported in the literature,[1,13] or recrystallization from ethyl acetate. Unfortunately, all attempts at purification resulted in significant fractionation of the polymer mixture, specifically the removal of the majority of material below 1000 g mol^{-1} (Figure 2.13). Since this low molecular weight material likely contains both cyclic oligomers and RAFT-functional linear oligomers, chain extension of **2** was performed utilizing the crude material in order to preserve the integrity of the macro-CTA mixture. This strategy was supported by the observation that acrylic block copolymers of **2** could be readily purified from trace PDL and cyclic PPDL oligomers *via* precipitation in methanol.
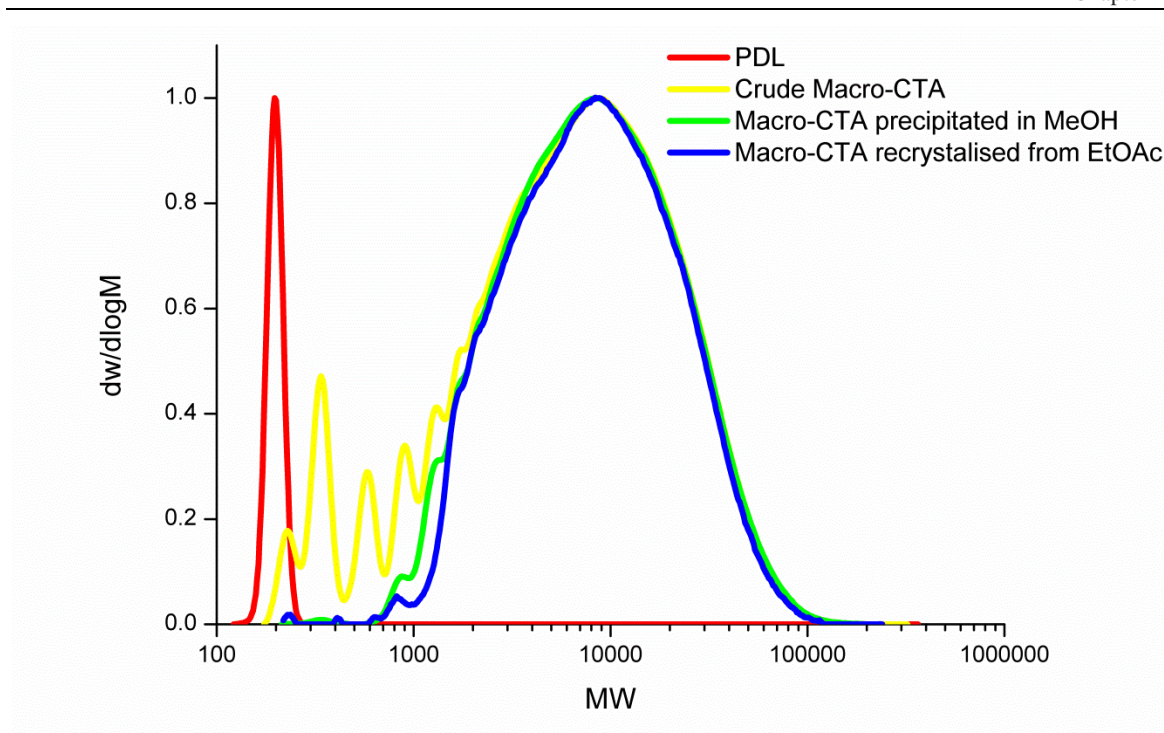
Figure 2:13: Overlay of GPC (CHCl$_3$) chromatograms of PDL and macro-CTA **2** (crude, precipitated in methanol (MeOH), and recrystallized from ethyl acetate (EtOAc)).

2.2.2 RAFT Polymerization of Selected Acrylates Using 1 as a CTA

The homopolymerization of selected acrylates, including those suitable for fuels applications, specifically 2-ethylhexyl acrylate (EHA), isodecyl acrylate (IDA), lauryl acrylate (LA), and stearyl acrylate (SA) was performed to verify that **1** controls the radical polymerization of acrylates (Scheme 2.6). The reaction temperature and solvent were selected to ensure dissolution of the PPDL macro-CTA during chain extension. The polymerization of methyl acrylate was monitored by comparing the integral of the methyl ester protons adjacent to the ester in the monomer ($\delta = 3.76$ ppm) and polymer ($\delta = 3.65$ ppm) in ^{1}H NMR spectra (Figure 2.14), whereas the polymerization of long chain acrylates was monitored by comparing the integral of acrylic protons in the monomer ($\delta = 6.45\text{-}5.75$ ppm) and methylene protons adjacent to the ester in the polymer ($\delta \approx 4.40\text{-}3.50$ ppm) (Figure 2.15). Further, the DP was evaluated by comparing the integral of the benzyl methylene protons of **1** ($\delta = 5.08$ ppm) to that of the methyl ester in MA or methylene protons adjacent to the ester in the polymer of long chain acrylates.
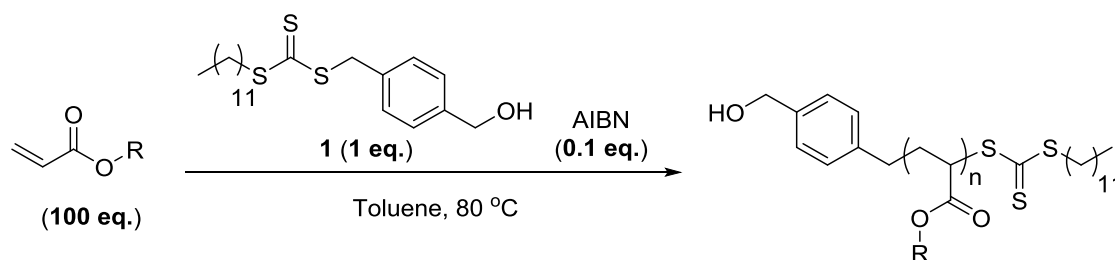
Scheme 2.6: Synthesis of polyacrylates *via* the RAFT process using **1** as a CTA.

54
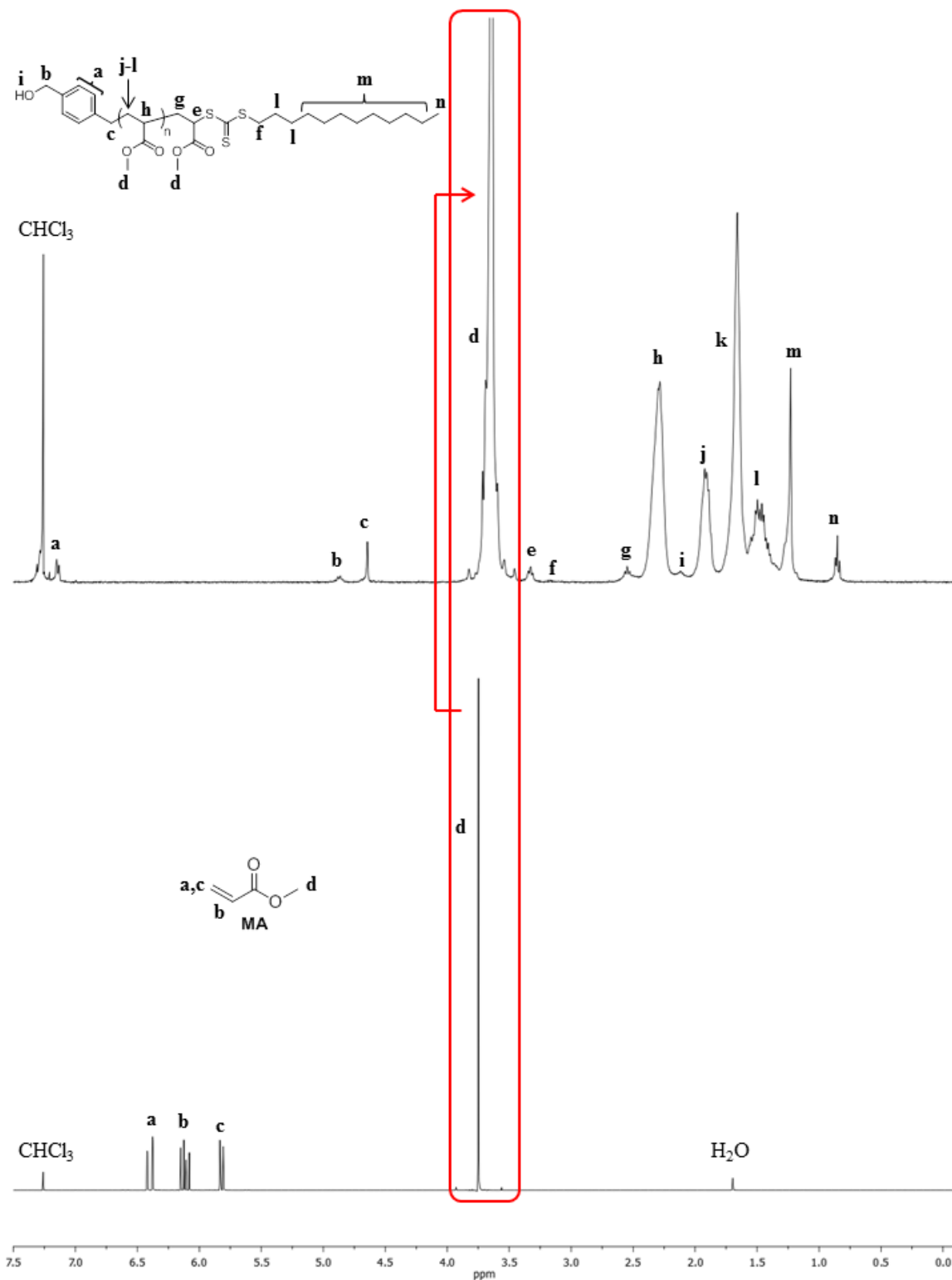
Figure 2.14: ^{1}H NMR spectral overlay of methyl acrylate and DP 59 poly(methyl acrylate) prepared *via* the RAFT process using **1** as a CTA and AIBN at 80 °C ([M]:[CTA]:[I] = 100:1:0.1) in toluene (50 wt.%) (300 MHz; CDCl$_3$).
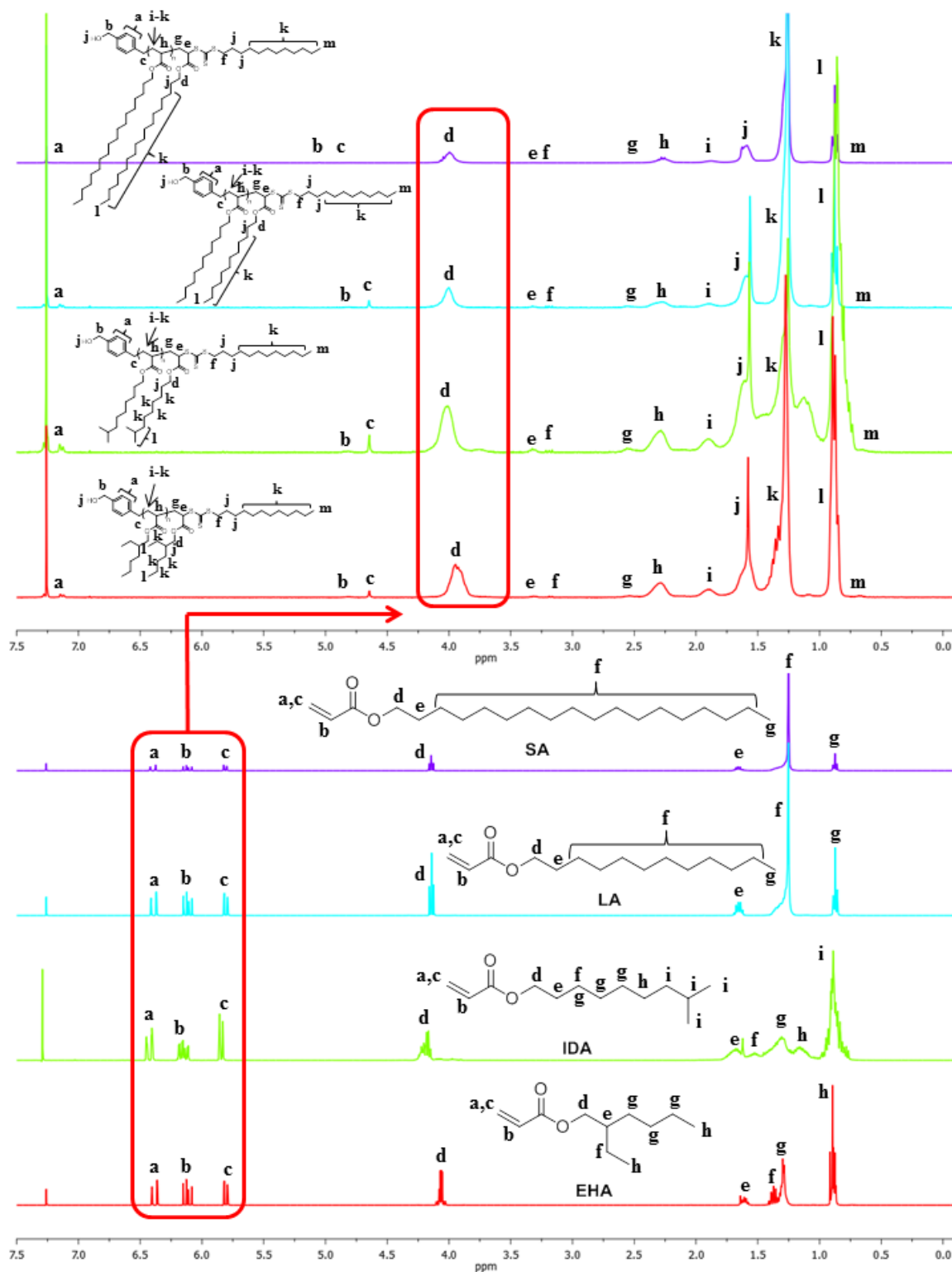
Figure 2.15: ^{1}H NMR spectral overlay of acrylic monomers and DP 48 poly(2-ethylhexyl acrylate), DP 25 poly(isodecyl acrylate), DP 20 poly(lauryl acrylate), and DP 327 poly(stearyl acrylate) prepared *via* the RAFT process using **1** as a CTA AIBN at 80 °C ([M]:[CTA]:[I] = 100:1:0.1) in toluene (50 wt.%) (300 MHz; CDCl$_3$).

The semi-logarithmic plots for RAFT polymerizations performed in toluene (50 wt.%) are linear, indicating a constant concentration of propagating radicals, for the first 25 minutes of the polymerization for all monomers with the exception of SA, which exhibits an induction period

(Figure 2.16). Potential causes of an induction period include slow fragmentation, slow re-initiation, the presence of impurities, and the occurrence of side reactions.[18] Although slow fragmentation of the CTA benzylic R group is expected with acrylates, it is well known that propagating acrylic monomer radicals undergo backbiting β-scission reactions which complicate the polymerization of these monomers (Scheme 2.7).[19] The incidence of backbiting increases with increasing monomer side chain length and, in the case of stearyl acrylate, these reactions compete with propagation and therefore likely account for the observed induction period.[20] Importantly, backbiting β-scission reactions result in branching, which is especially pronounced at high monomer conversions and molecular weights.[20] At t = 25 minutes, rate retardation is observed and control of the polymerization is lost, as evidenced by an increase in $Đ_M$, a loss in linearity between M_n and monomer conversion, and a decrease in M_n with increasing monomer conversions (Figure 2.17). These observations are consistent with an increased incidence of backbiting β-scission reactions at higher monomer conversions. Interestingly, although MA, EHA, and IDA exhibit similar rates of polymerization under these reaction conditions, the rate of polymerization of LA and SA is noticeably slower predominantly since the reaction conditions selected result in more dilute conditions for larger monomers. Regardless, monomer conversions between 35% (SA) and 65% (IDA) can be achieved within the first 25 minutes of the polymerization. Furthermore, MALDI-ToF mass spectral analysis of methyl acrylate (MA) revealed a single distribution with a regular repeat unit equal to the molecular weight of MA (Figure 2.18). A single distribution, centered around m/z = 2145.00 corresponds to sodium charged linear poly(methyl acrylate) polymerized from **1**, indicating good end-group fidelity.
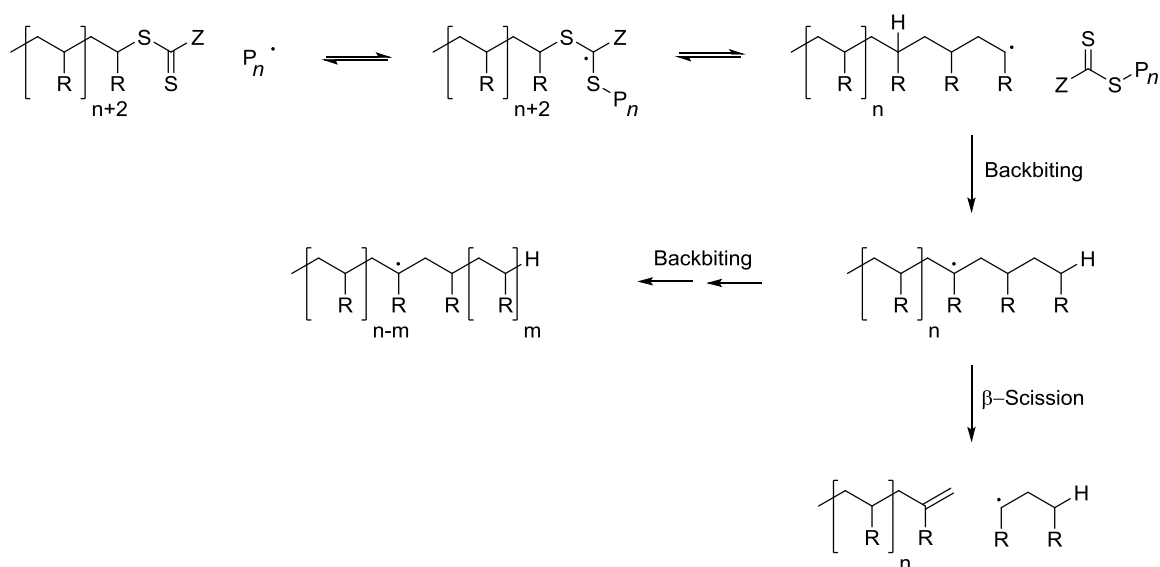
Scheme 2.7: Backbiting β-scission reactions in the RAFT polymerization of acrylates. Scheme adapted from Moad *et al.*[19]
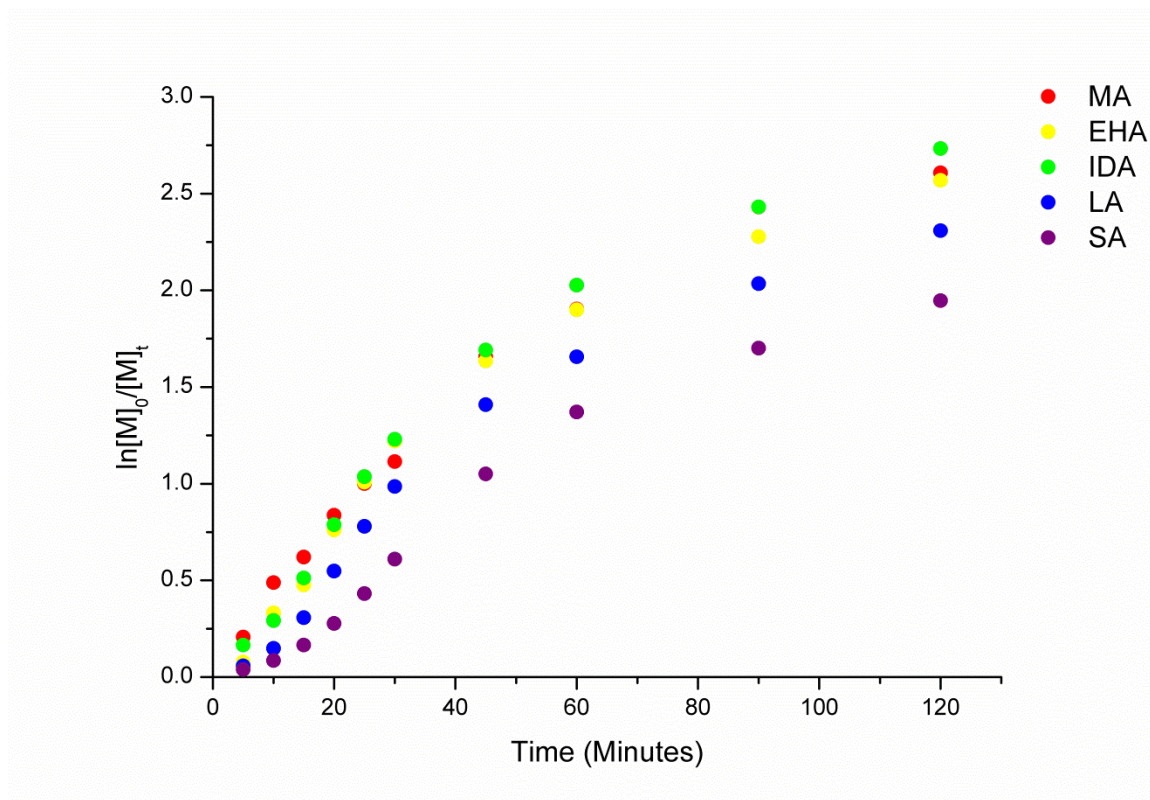
Figure 2.16: Semi-logarithmic plots for the RAFT polymerization of selected acrylates using **1** as a CTA and AIBN at 80 ℃ ([M]:[CTA]:[I] = 100:1:0.1) in toluene (50 wt.%).
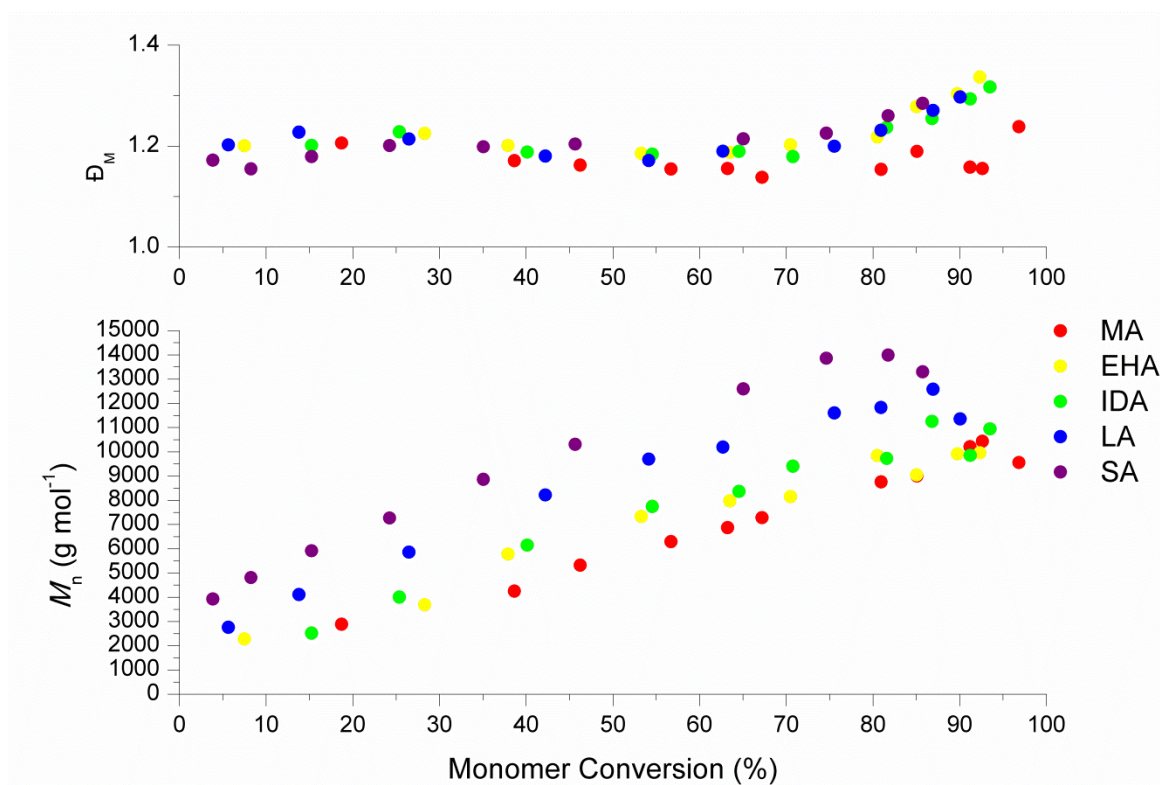
Figure 2.17: Plot of M_n and $Đ_M$ *versus* monomer conversion for the RAFT polymerization of selected acrylates using **1** as a CTA and AIBN at 80 ℃ ([M]:[CTA]:[I] = 100:1:0.1) in toluene (50 wt.%).
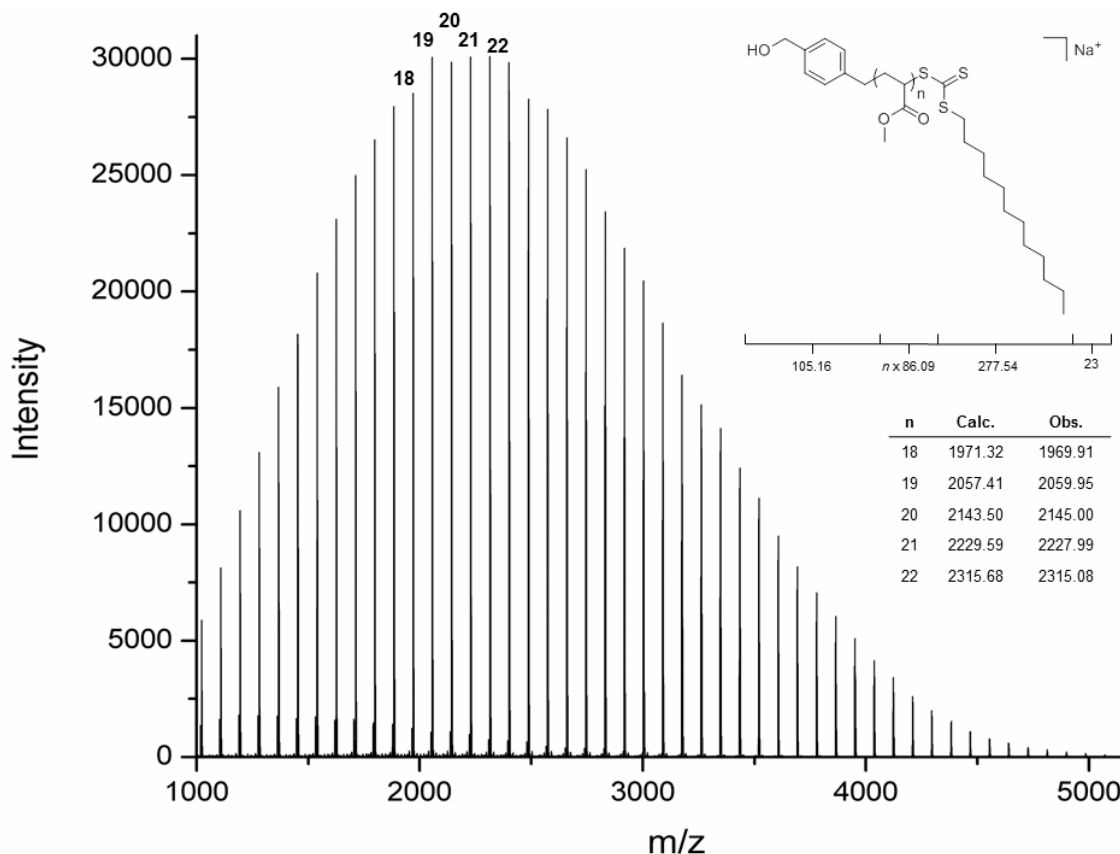
Figure 2.18: MALDI-ToF mass spectrum of poly(methyl acrylate) ($[M]_t/[M]_0 = 0.39$) prepared *via* the RAFT process using **1** as a CTA and AIBN at 80 ºC ([M]:[CTA]:[I] = 100:1:0.1) in toluene (50 wt.%).

In order to verify that the discrepancy observed in the rates of polymerization between shorter and longer chain acrylates for reactions performed in toluene (50 wt.%) result from varied monomer concentration, the RAFT polymerizations were performed at a fixed concentration (2.55 M) in toluene. The rates of polymerization were similar between monomers as evidenced by the semi-logarithmic plots (Figure 2.19). Since the monomer concentration was decreased for all monomers except stearyl acrylate, a decreased rate of polymerization was observed relative to those presented in Figure 2.16, which pronounced induction periods arising from slow fragmentation of the CTA benzylic R group during the addition-fragmentation stage of the RAFT process and backbiting β-scission reactions. Control of the polymerization, however, was achieved between approximately 15% and 50% monomer conversion for all monomers as evidenced by favorable disperities and a linear relationship between M_n and monomer conversion (Figure 2.20).
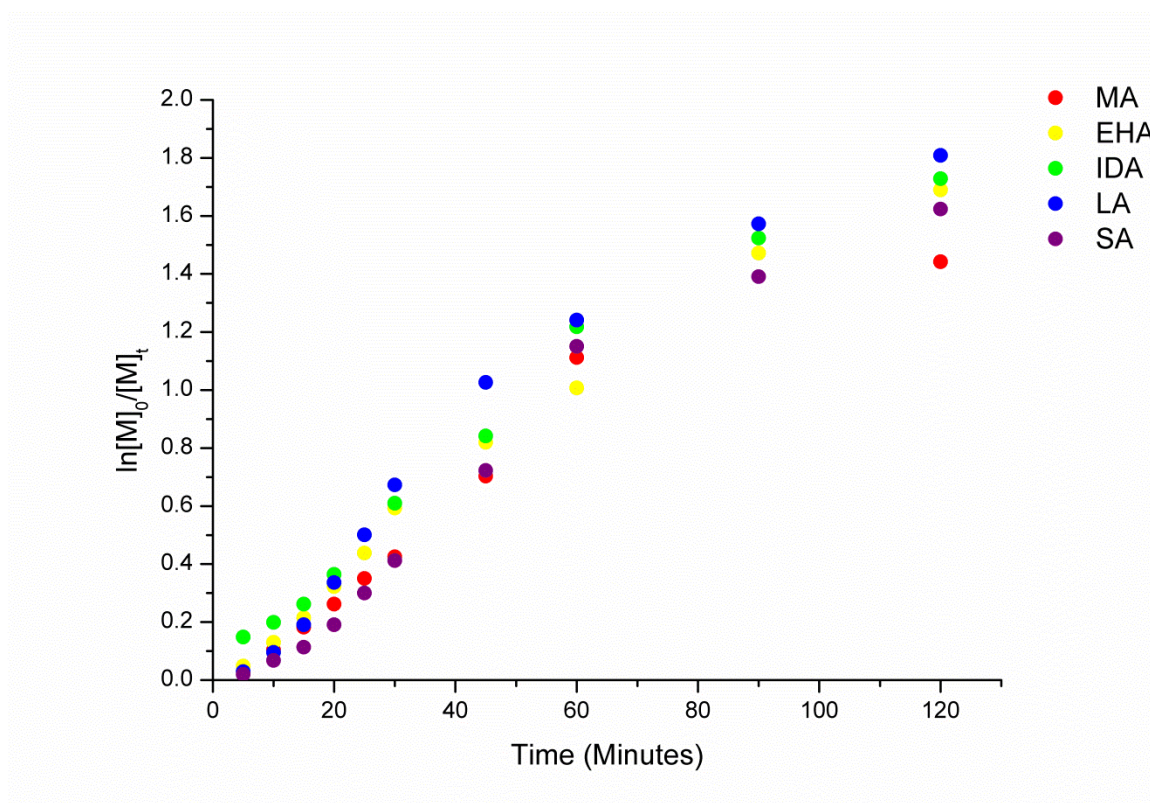
Figure 2.19: Semi-logarithmic plots for the RAFT polymerization of selected acrylates using **1** as a CTA and AIBN at 80 °C ([M]:[CTA]:[I] = 100:1:0.1) in toluene (2.55 M).
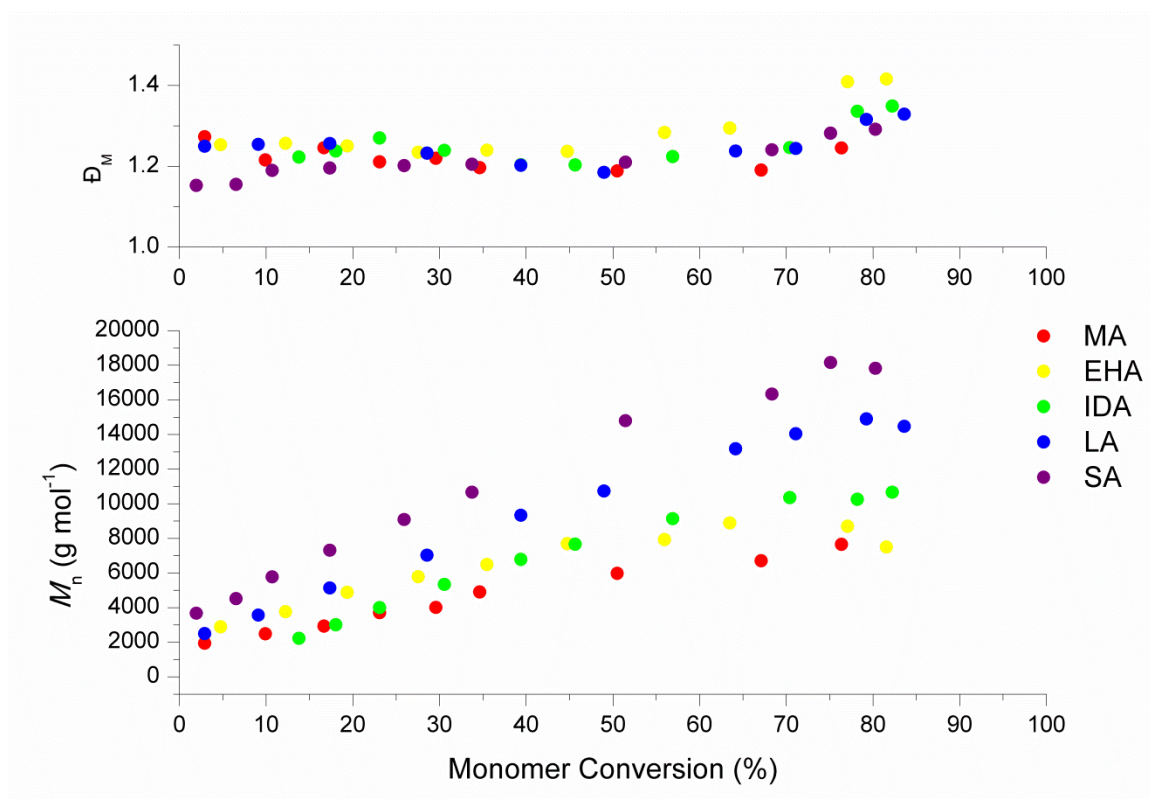
Figure 2.20: Plot of M_n and $Đ_M$ *versus* monomer conversion for the RAFT polymerization of selected acrylates using **1** as a CTA and AIBN at 80 °C ([M]:[CTA]:[I] = 100:1:0.1) in toluene (2.55 M).

2.2.3 Chain Extension of PPDL macro-CTA 2 *via* the RAFT Process

Standard reaction conditions employed in the homopolymerization of acrylates using **1** as a CTA (Scheme 2.6) were applied in the chain extension of PPDL macro-CTA **2** using 2-ethylhexyl acrylate (Scheme 2.8). The polymerization was monitored by comparing the integral of the acrylic protons in the monomer (δ = 6.45-5.75 ppm) and the methylene protons adjacent to the ester in the polymer (δ = 4.01-3.70 ppm) in ^{1}H NMR spectra (Figure 2.21). Furthermore, the DP was evaluated by comparing the integral of the methylene protons of **2** (δ = 5.05 ppm) to that of the methylene protons adjacent to the ester in the polymer (δ = 4.01-3.70 ppm).
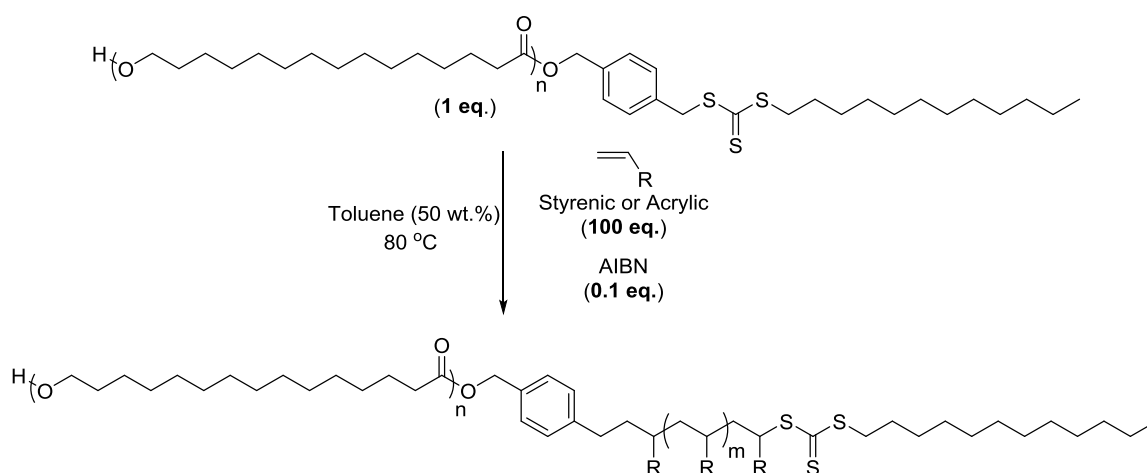
Scheme 2.8: General reaction scheme for the chain extension of macro-CTA **2** using acrylic or styrenic monomers.
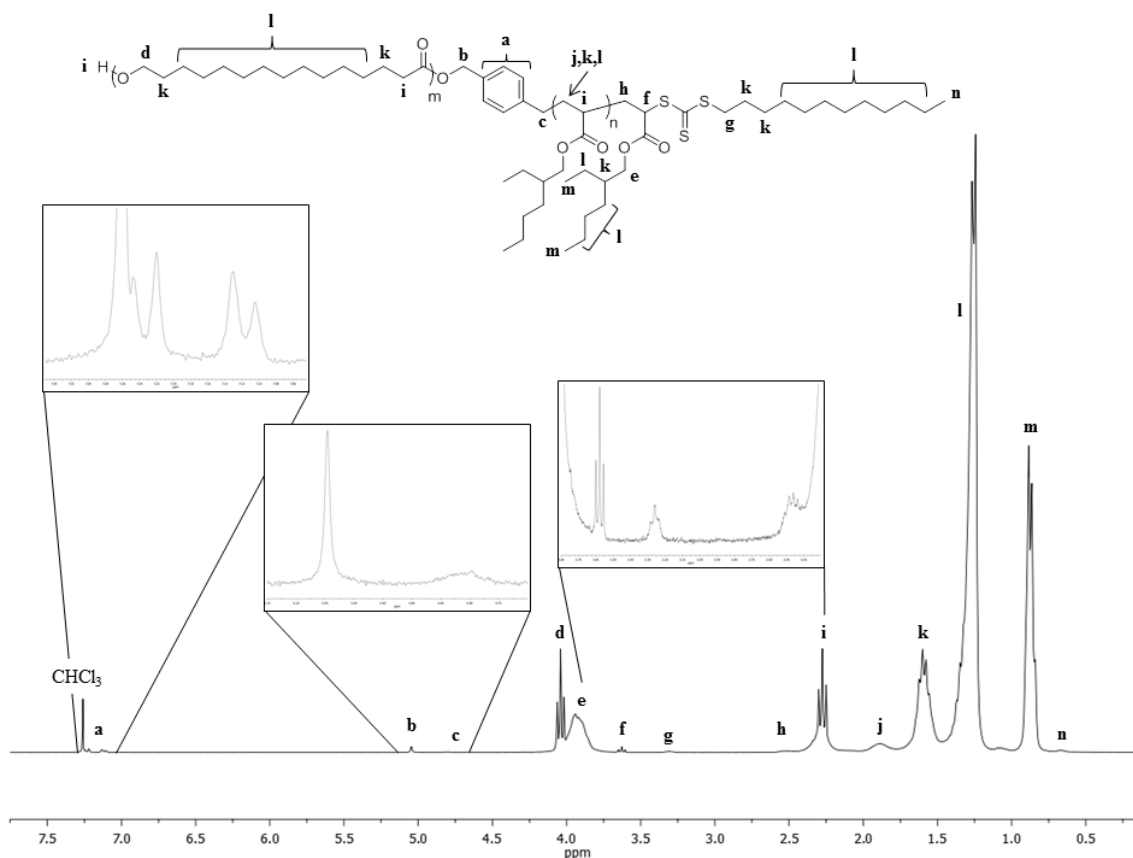
Figure 2.21: ^{1}H NMR spectrum of PPDL-*b*-(DP 32 PEHA) prepared *via* the chain extension of **2** ([M]:[CTA]:[I] = 100:1:0.1) with 2-ethylhexyl acrylate using AIBN at 80 ºC in toluene (50 wt.%), and precipitated in methanol from ethyl acetate (300 MHz; CDCl$_3$).

Good control was achieved up to 56% monomer conversion as evidenced by a linear semi-logarithmic plot (Figure 2.22), a linear correlation between the M_n and monomer conversion, and a decrease in the $Đ_M$ of the polymer with increasing degrees of polymerization (Figure 2.23). Importantly, an induction period was observed following slow fragmentation of the macro-CTA benzylic R group during the addition-fragmentation stage of the RAFT process. Beyond 56% monomer conversion, however, loss of control followed significant backbiting β-scission reactions as evidenced by an increase in $Đ_M$, a loss in linearity between M_n and monomer conversion, and a decrease in M_n with increasing monomer conversions. Ultimately, control of the chain extension reaction can be achieved across various target DPs, specifically DP 50, 75, 100, and 300 where monomer conversions are limited to approximately 50% (Figures 2.24 and 2.25).
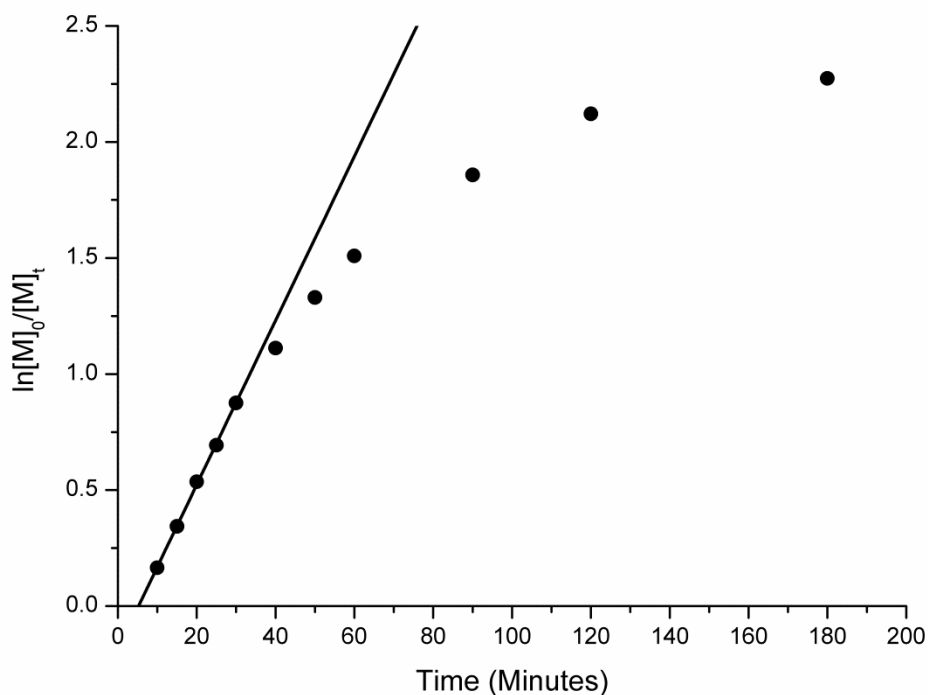
Figure 2.22: Semi-logarithmic plot for the chain extension of **2** with 2-ethylhexyl acrylate using AIBN at 80 °C ([M]:[CTA]:[I] = 100:1:0.1) in toluene (50 wt.%).
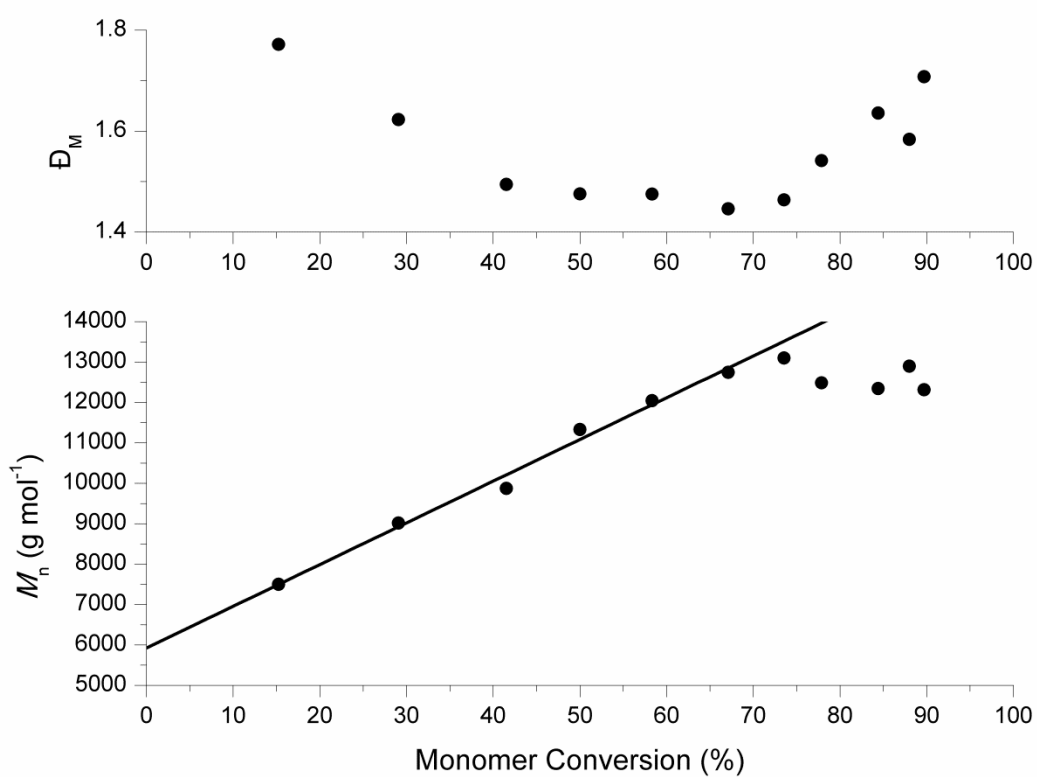
Figure 2.23: Plot of M_n and $Đ_M$ *versus* monomer conversion for the chain extension of **2** with 2-ethylhexyl acrylate using AIBN at 80 °C ([M]:[CTA]:[I] = 100:1:0.1) in toluene (50 wt.%).
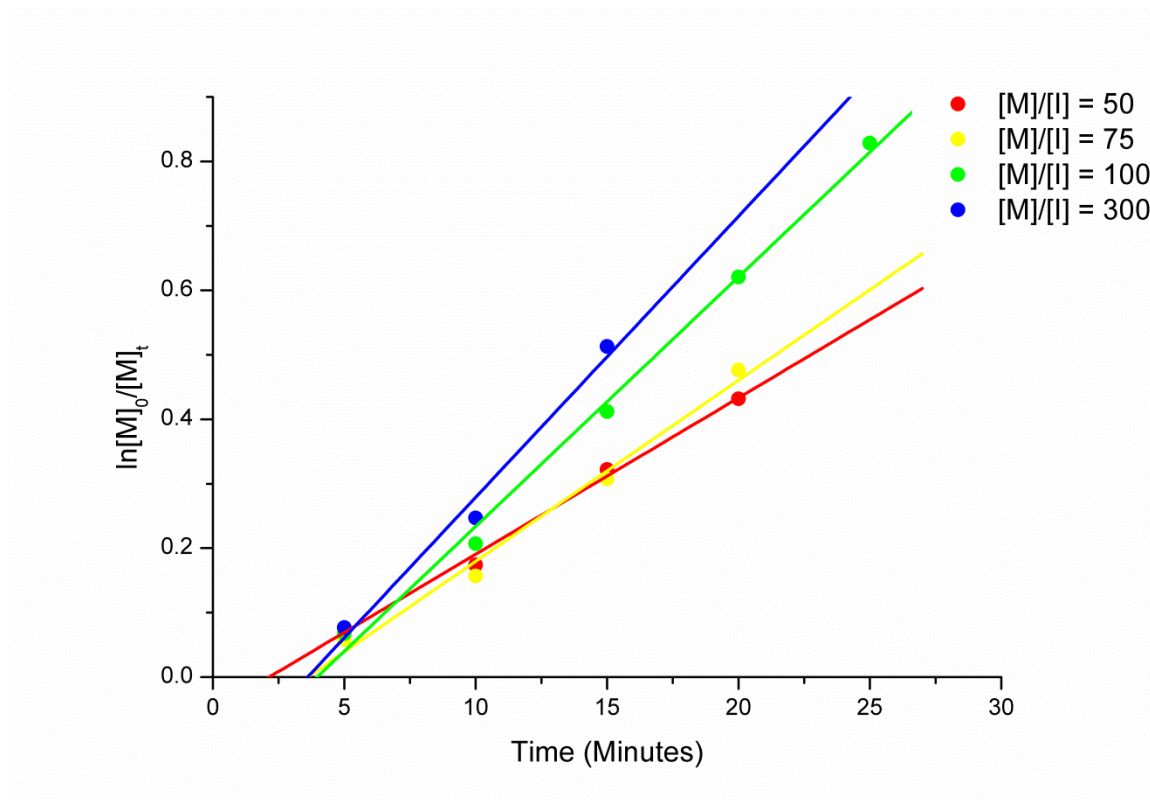
Figure 2.24: Semi-logarithmic plots for the chain extension of **2** with 2-ethylhexyl acrylate, varying [M]:[CTA] and using the reaction conditions outlined in Scheme 2.8.
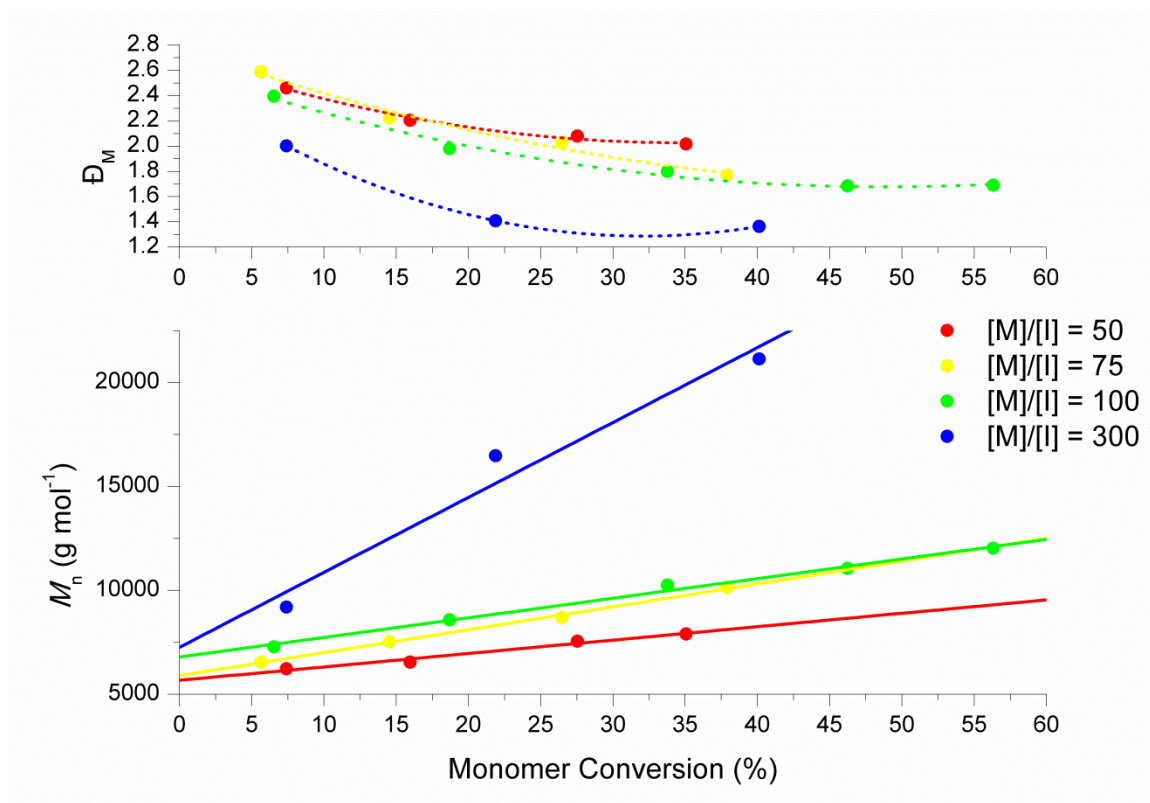
Figure 2.25: Plot of M_n and $Đ_M$ *versus* monomer conversion for the chain extension of **2** using 2-ethylhexyl acrylate, varying [M]:[CTA] and using the reaction conditions outlined in Scheme 2.8. Please note that trend lines fitted to $Đ_M$ *versus* percent monomer conversion plots are provided solely to guide the eye.

In order to purify block copolymer from PPDL homopolymer, in particular cyclic polymeric impurities obtained in the preparation of **2**, block copolymers were precipitated in methanol. GPC chromatograms of crude **2**, crude PPDL-*b*-PEHA, and purified PPDL-*b*-PEHA (Figure 2.26) suggest that a significant portion of macro-CTA **2** initiated from the bifunctional initiator **1** and was chain extended to prepare block copolymer *via* the RAFT process.
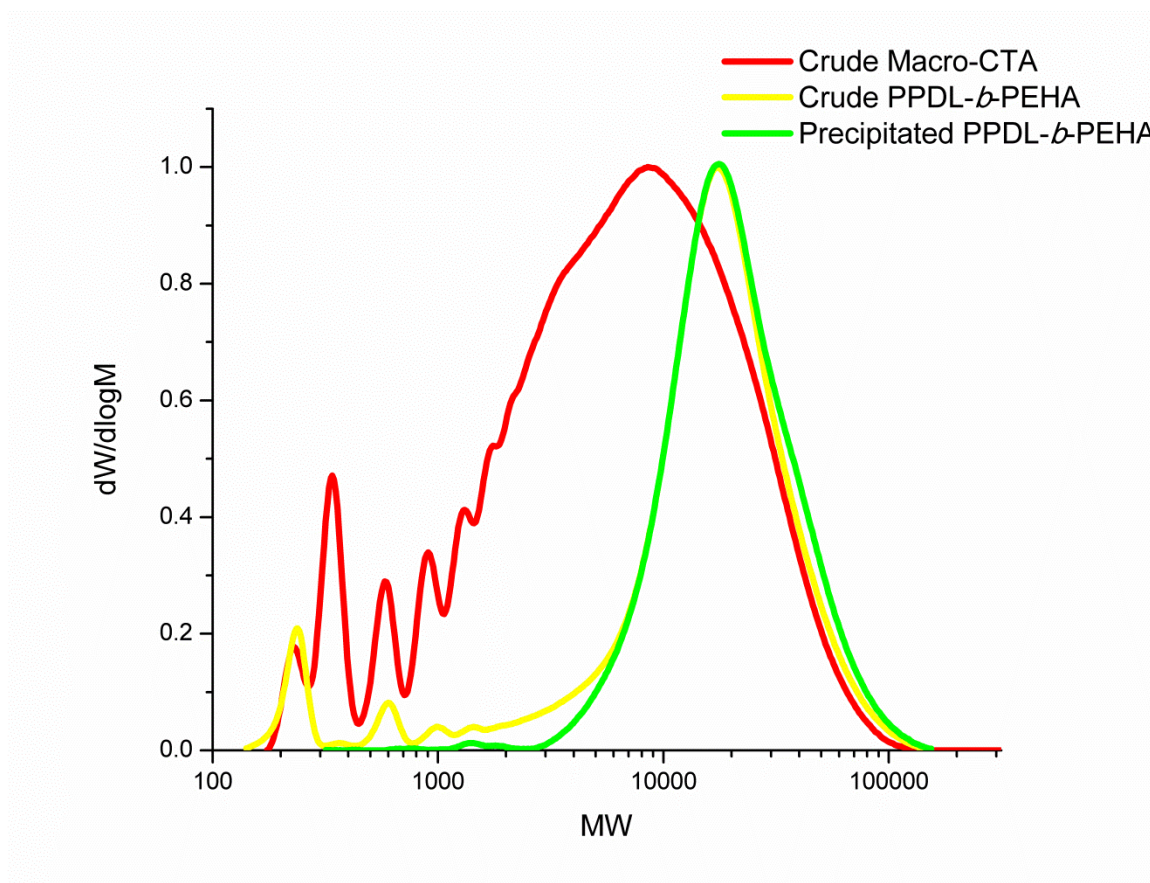
Figure 2.26: Overlay of GPC (CHCl$_3$) chromatograms for macro-CTA **2**, crude PPDL-*b*-PEHA, and PPDL-*b*-PEHA purified *via* precipitation in methanol.

In order to explore whether control of the chain extension process could be achieved up to higher conversions, the polymerization was repeated at 100 $^\circ$C using the azo initiator 1,1′-azobis(cyclohexanecarbonitrile) (AICN). In a subsequent reaction, a second charge of AICN was added 47 minutes into the reaction in an attempt to prolong control of the reaction. The semi-logarithmic plots for these polymerizations (Figure 2.27) indicate that the initial reaction temperature and initiator selected (Scheme 2.8) afforded the best control, as additionally evidenced by the correlation between the M_n and monomer conversion, and the $Đ_M$ and monomer conversion of the polymerizations (Figure 2.28). Furthermore, since Zhu *et al.*[21] report a dramatic increase in the dispersity of poly(stearyl acrylate) in RAFT polymerizations performed above 80 $^\circ$C, subsequent reactions were thus performed at 80 $^\circ$C.
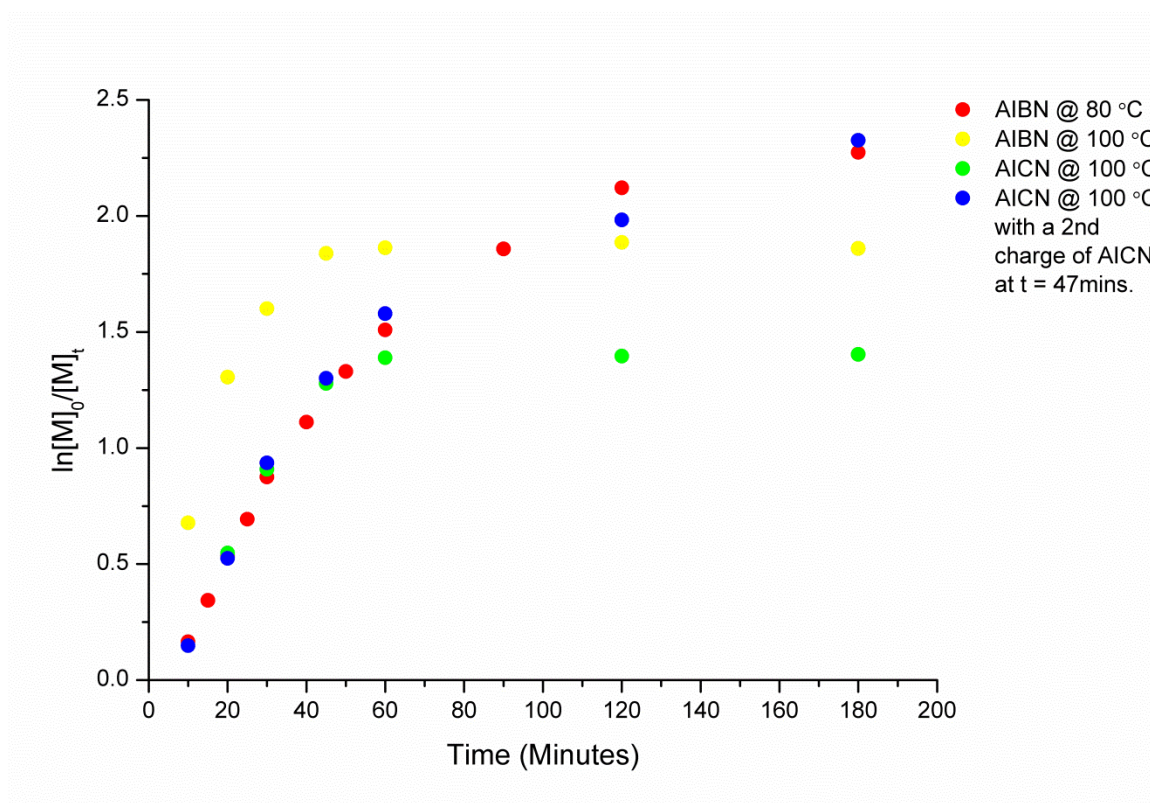
Figure 2.27: Semi-logarithmic plots for the chain extension of **2** with 2-ethylhexyl acrylate ([M]:[CTA]:[I] = 100:1:0.1) in toluene (50 wt.%), varying the initiator and reaction temperature.
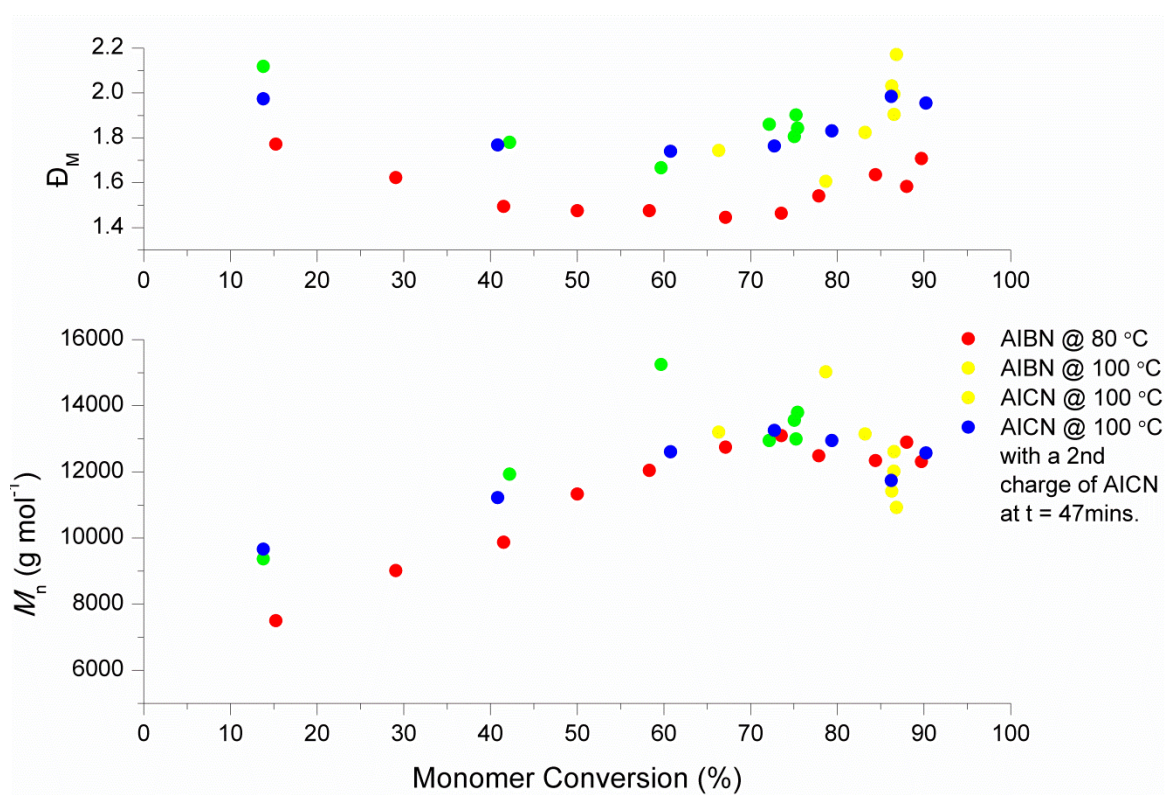
Figure 2.28: M_n and $Đ_M$ versus monomer conversion for the chain extension of **2** with 2-ethylhexyl acrylate ([M]:[CTA]:[I] = 100:1:0.1) in toluene (50 wt.%), varying the initiator and reaction temperature.

The effect of monomer concentration on the control of the RAFT polymerization of **2** was similarly explored by varying the solvent content. As expected, increasing and decreasing the monomer concentration increases and decreases the rate of the polymerization, respectively as evidenced by semi-logarithmic plots (Figure 2.29). Performing a polymerization in 25 wt.% toluene furthermore resulted in rapid increases in the M_n of polymer whereas dilute conditions (100 wt.% and 150 wt.% toluene) yielded marginal increases in M_n within an unpractical time frame as evidenced by the plot of M_n *versus* monomer conversion (Figure 2.30). Therefore, in order to achieve repeatable control over the M_n of the polymer product within a practical time frame, the original reaction conditions (Scheme 2.8) were adopted for subsequent reactions.
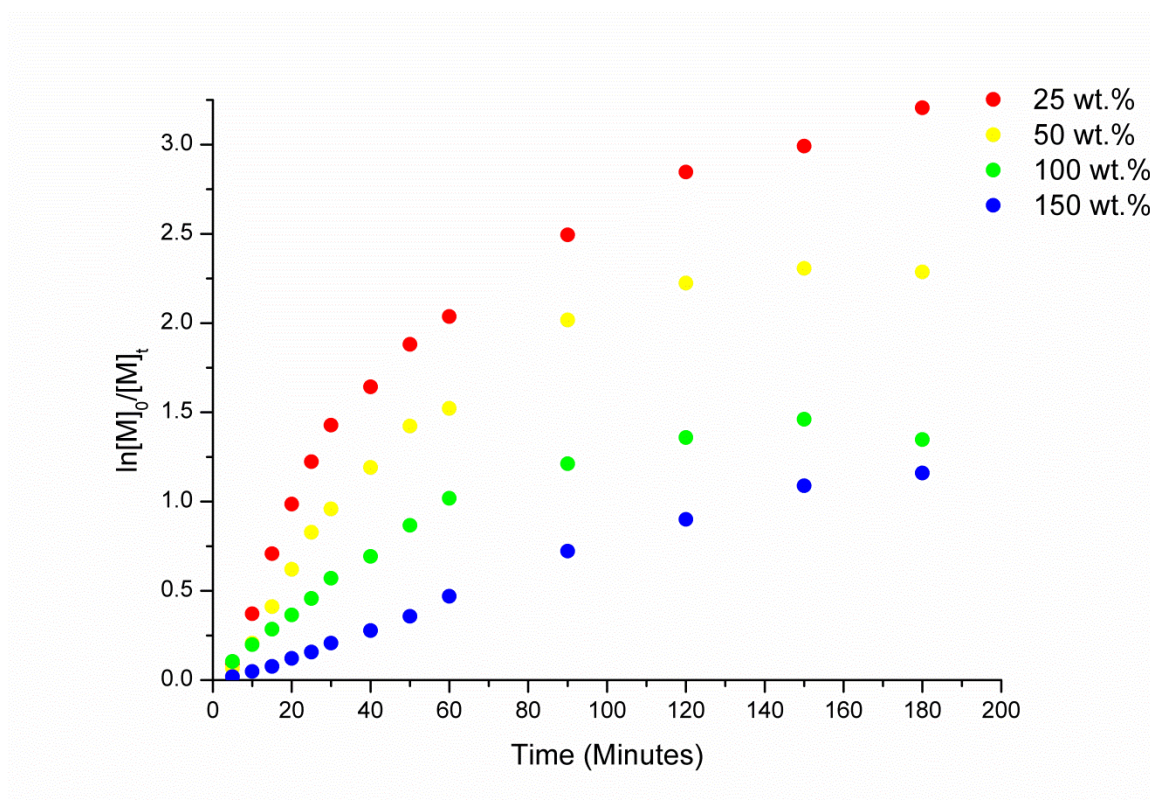
Figure 2.29: Semi-logarithmic plots for the chain extension of **2** with 2-ethylhexyl acrylate using AIBN at 80 °C ([M]:[CTA]:[I] = 100:1:0.1), varying [M] in toluene.
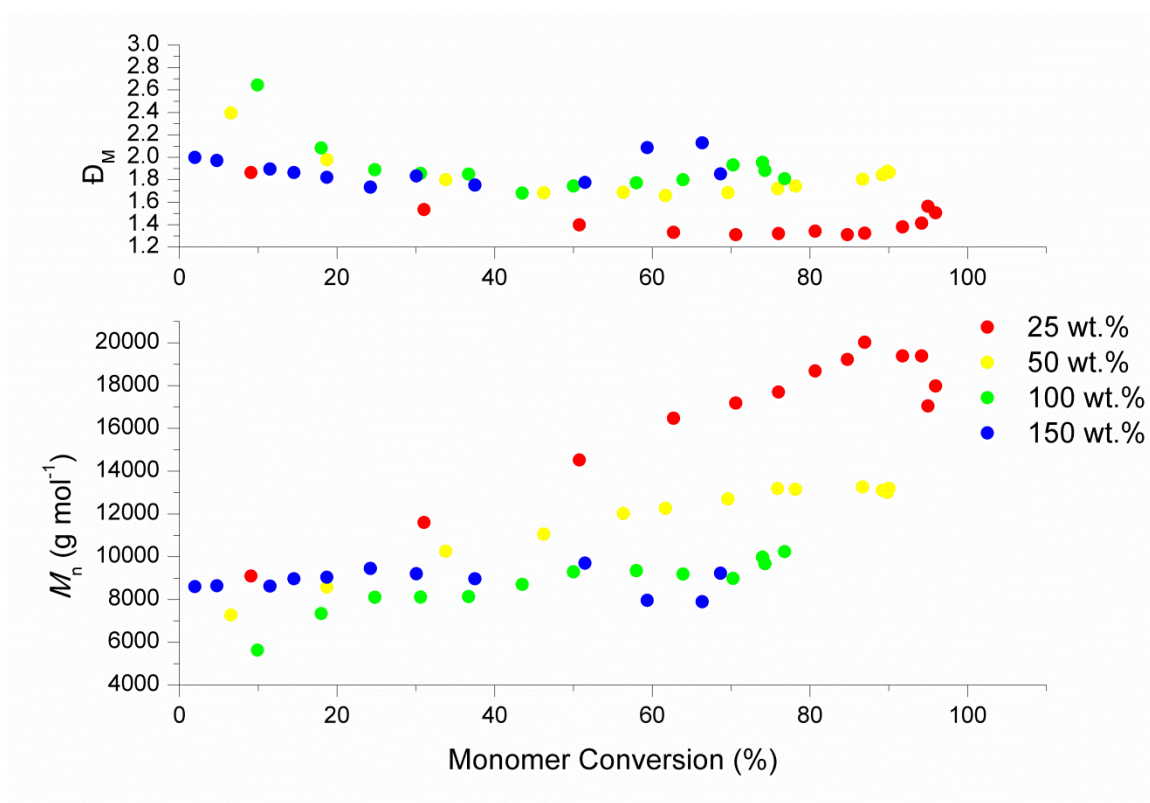
Figure 2.30: Plot of M_n and $Đ_M$ *versus* monomer conversion for the chain extension of **2** with 2-ethylhexyl acrylate using AIBN at 80 ºC ([M]:[CTA]:[I] = 100:1:0.1), varying [M] in toluene.

The chain extension of **2** targeting DP 100 and DP 300 was further demonstrated using the acrylic monomers IDA, LA, and SA. As with the chain extension of **2** with EHA (Figure 2.21), the polymerization was monitored by comparing the integral of the acrylic protons in the monomer ($δ$ = 6.45-5.75 ppm) and the methylene protons adjacent to the ester in the polymer ($δ ≈$ 4.40-3.50 ppm) in ^{1}H NMR spectra (Figure 2.31). Furthermore, the DP was evaluated by comparing the integral of the methylene protons of **2** ($δ$ = 5.05 ppm) to that of the methylene protons adjacent to the ester in the polymer ($δ ≈$ 4.40-3.50 ppm). The chain extension polymerizations proceeded with good control as evidenced by linear semi-logarithmic plots (Figure 2.32 and Figure 2.35), a linear correlation between the M_n and monomer conversion, and a decrease in the $Đ_M$ of the polymer with increasing degrees of polymerization (Figure 2.33 and Figure 2.36). The rate of chain extension was fastest for EHA and slowest for SA, as observed in the RAFT homopolymerizations in 50 wt.% toluene (Figure 2.16). In order to target specific acrylic block lengths in the large scale synthesis of acrylic block copolymers of PPDL, plots of DP *versus* time were prepared (Figure 2.34 and Figure 2.37). Furthermore, respectable end-group fidelity was achieved as evidenced by the overlay of RI and UV GPC chromatograms for crude PPDL-*b*-PLA (Figure 2.38). Although a minor amount of UV-inactive and therefore non-functional material was observed, it is suspected that this material is residual cyclic PPDL

homopolymer from the crude macro-CTA **2** that can be removed *via* precipitation of the copolymer in methanol.
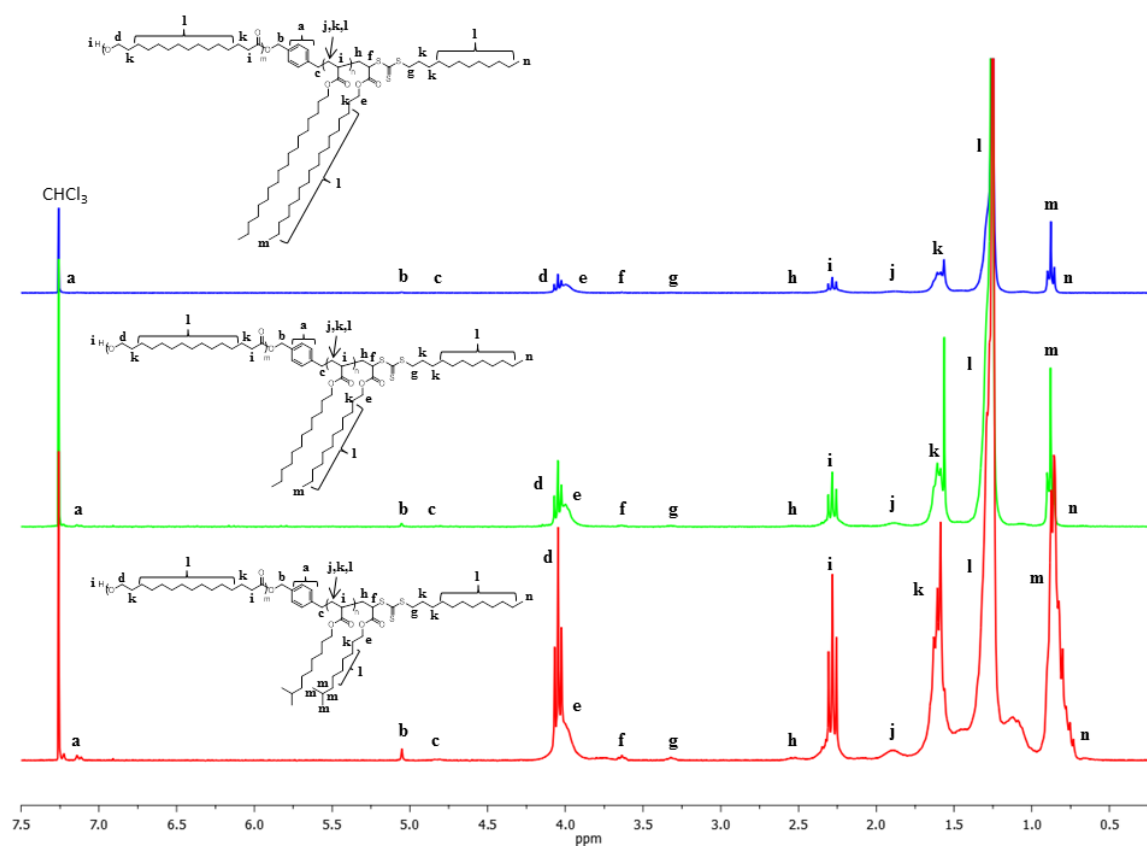
Figure 2.31: ^{1}H NMR spectra of PPDL-*b*-(DP 17 PIDA), PPDL-*b*-(DP 30 PLA), and PPDL-*b*-(DP 47 PSA) prepared *via* the chain extension of **2** ([M]:[CTA]:[I] = 100:1:0.1) with selected acrylates using AIBN at 80 ºC in toluene (50 wt.%), and precipitated in methanol from ethyl acetate (300 MHz; CDCl$_3$).

Figure 2.32: Semi-logarithmic plots for the chain extension of **2** with selected acrylates using AIBN at 80 °C ([M]:[CTA]:[I] = 100:1:0.1) in toluene (50 wt.%).
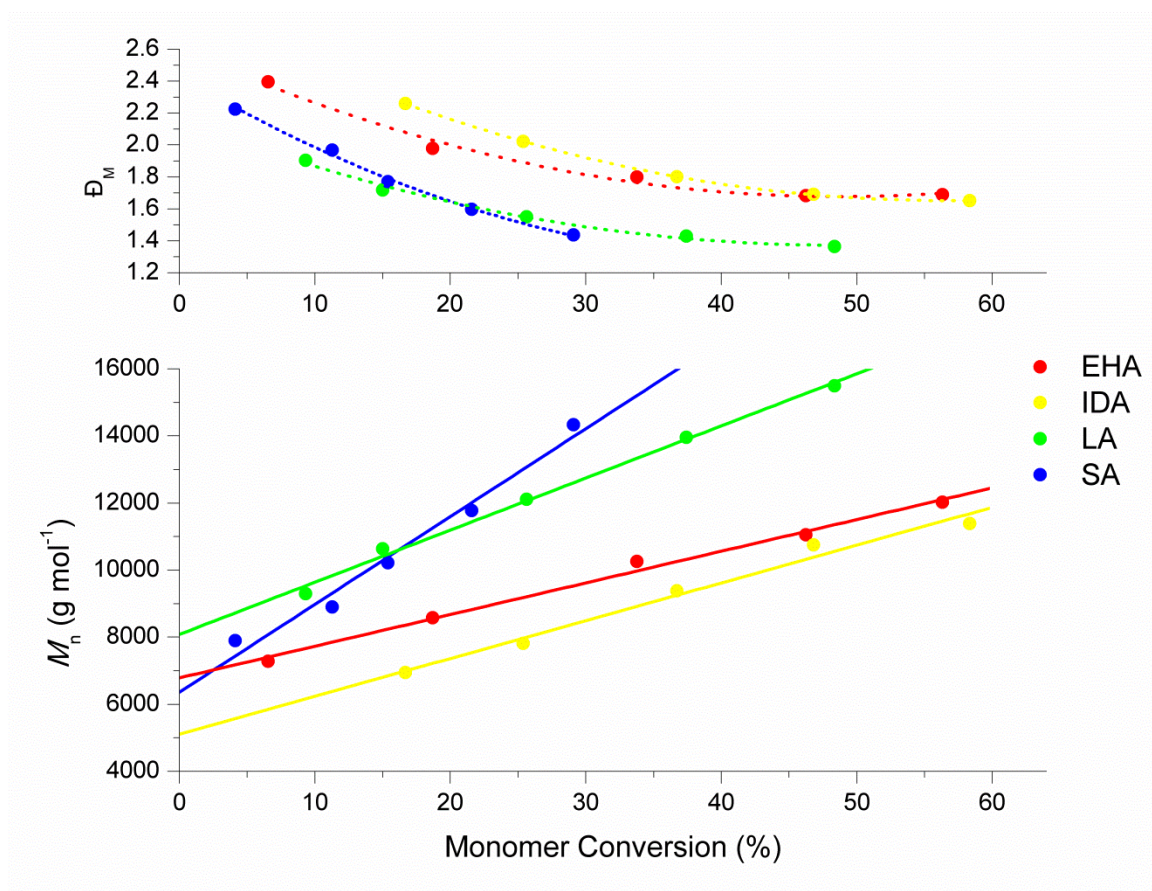
Figure 2.33: Plot of M_n and $Đ_M$ *versus* monomer conversion for the chain extension of **2** with selected acrylates ([M]:[CTA]:[I] = 100:1:0.1) using AIBN at 80 °C in toluene (50 wt.%). Please note that trend lines fitted to $Đ_M$ *versus* percent monomer conversion plots are provided solely to guide the eye.
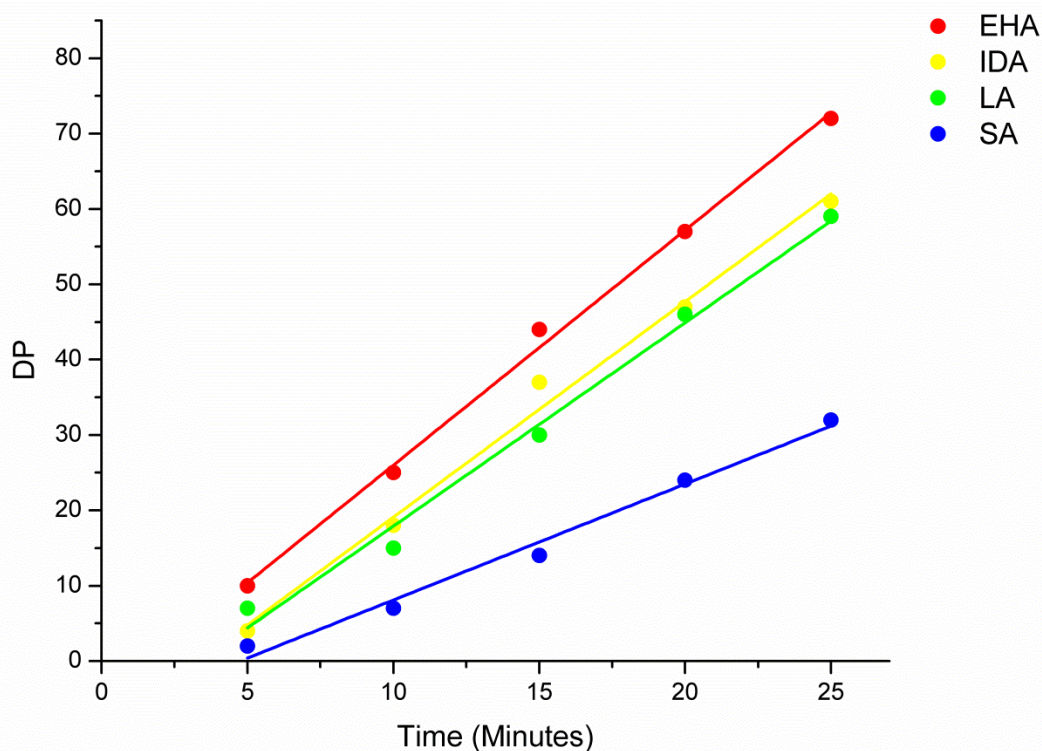
Figure 2.34: Plot of DP *versus* time for the chain extension of **2** with selected acrylates using AIBN at 80 ºC ([M]:[CTA]:[I] = 100:1:0.1) in toluene (50 wt.%).
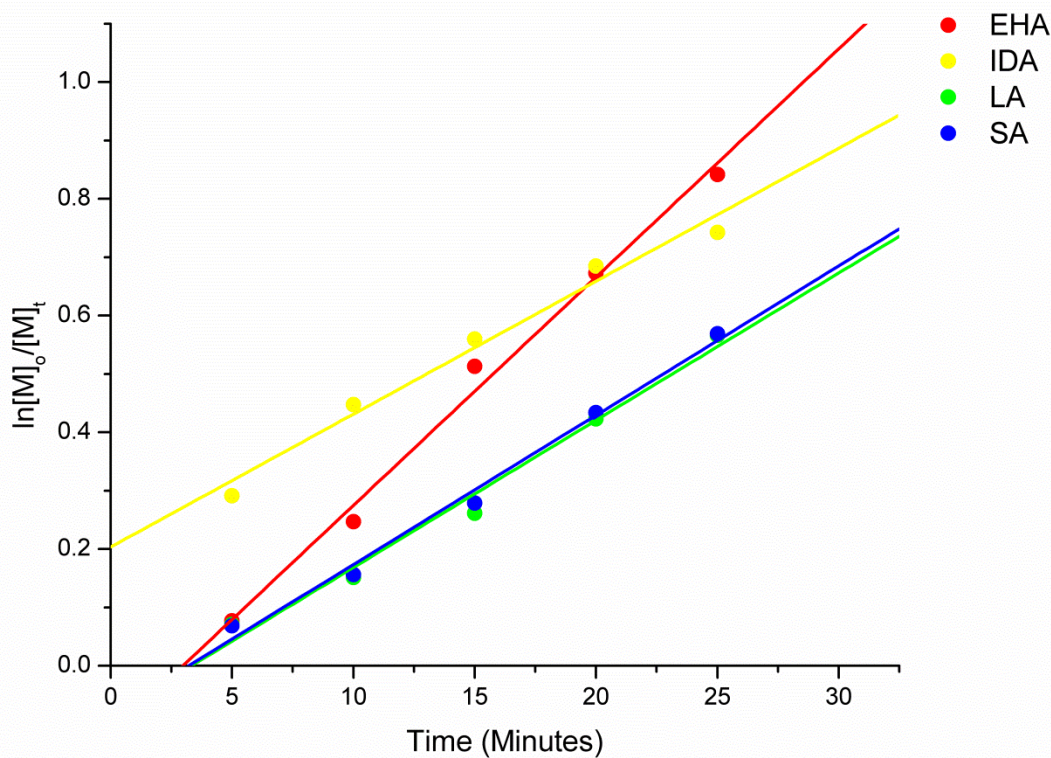
Figure 2.35: Semi-logarithmic plots for the chain extension of **2** with selected acrylates using AIBN at 80 ºC ([M]:[CTA]:[I] = 300:1:0.1) in toluene (50 wt.%).

Figure 2.36: Plot of M_n and $Đ_M$ *versus* monomer conversion for chain extension of **2** with acrylates using AIBN at 80 °C ([M]:[CTA]:[I] = 100:1:0.1) in toluene (50 wt.%). Please note that trend lines fitted to $Đ_M$ *versus* percent monomer conversion plots are provided solely to guide the eye.
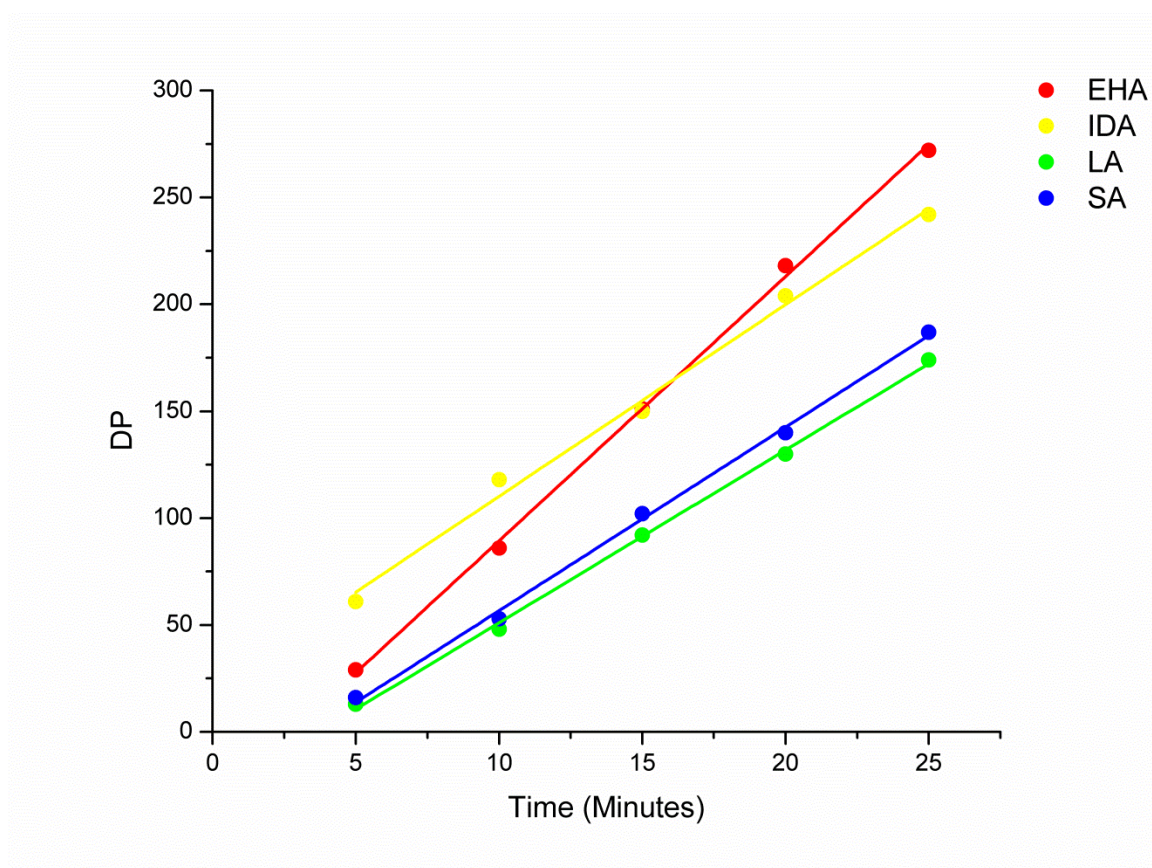
Figure 2.37: Plot of DP *versus* time for the chain extension of **2** with selected acrylates using AIBN at 80 °C ([M]:[CTA]:[I] = 300:1:0.1) in toluene (50 wt.%).
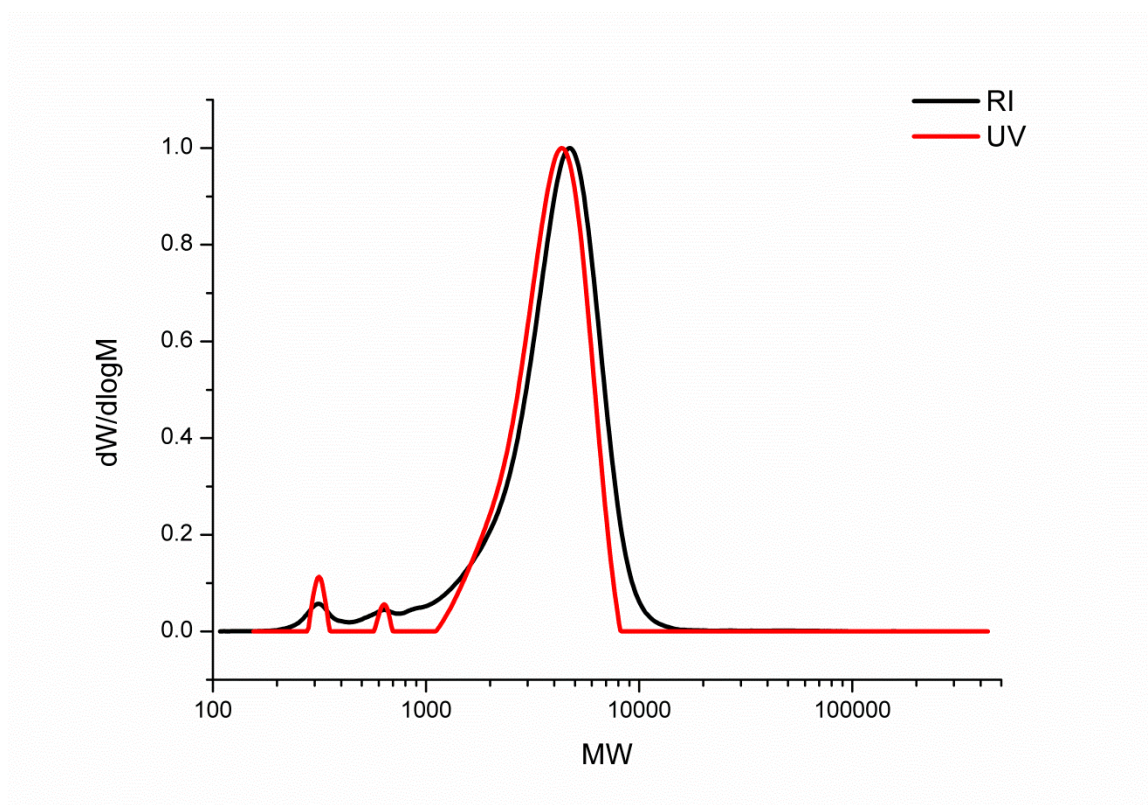
Figure 2.38: Overlay of RI and UV-GPC (CHCl$_3$, 309 nm) chromatograms of crude PPDL-*b*-PLA copolymer ([M]$_t$/[M]$_0$ = 0.48) prepared *via* the chain extension of **2** with lauryl acrylate using AIBN at 80 ℃ ([M]:[CTA]:[I] = 100:1:0.1) in toluene (50 wt.%).

Finally, the chain extension of **2** was performed with MA, S, and the thermoresponsive monomer *N*-isopropylacrylamide (NIPAM) according to reaction conditions outlined in Scheme 2.8, with the exception that the chain extension with NIPAM was performed in chloroform at 60 ℃. The polymerization was monitored by comparing the integral of the acrylic protons in the monomer ($\delta \approx$ 6.80-5.10 ppm) and the methyl ester protons in poly(MA) (δ = 3.65 ppm), the methyne proton in polystyrene (δ = 2.20-1.85 ppm), and the methyl protons in poly(NIPAM) (δ = 1.2–0.95 ppm). Furthermore, the DP was evaluated by comparing the integral of the methylene protons of **2** (δ = 5.05 ppm) with that for the specified polymer resonances. The chain extension polymerizations proceeded with good control as evidenced by linear semi-logarithmic plots (Figure 2.40), a linear correlation between the M_n and monomer conversion, and a decrease in the $Đ_M$ of the polymer with increasing degrees of polymerization (Figure 2.41). The rate of chain extension was fastest with MA and slowest with styrene following varied resonance stabilization of the radicals generated. Furthermore, a significant induction period was observed in the chain extension with NIPAM following slow fragmentation of the macro-CTA benzylic R group during the addition-fragmentation stage of the RAFT process.
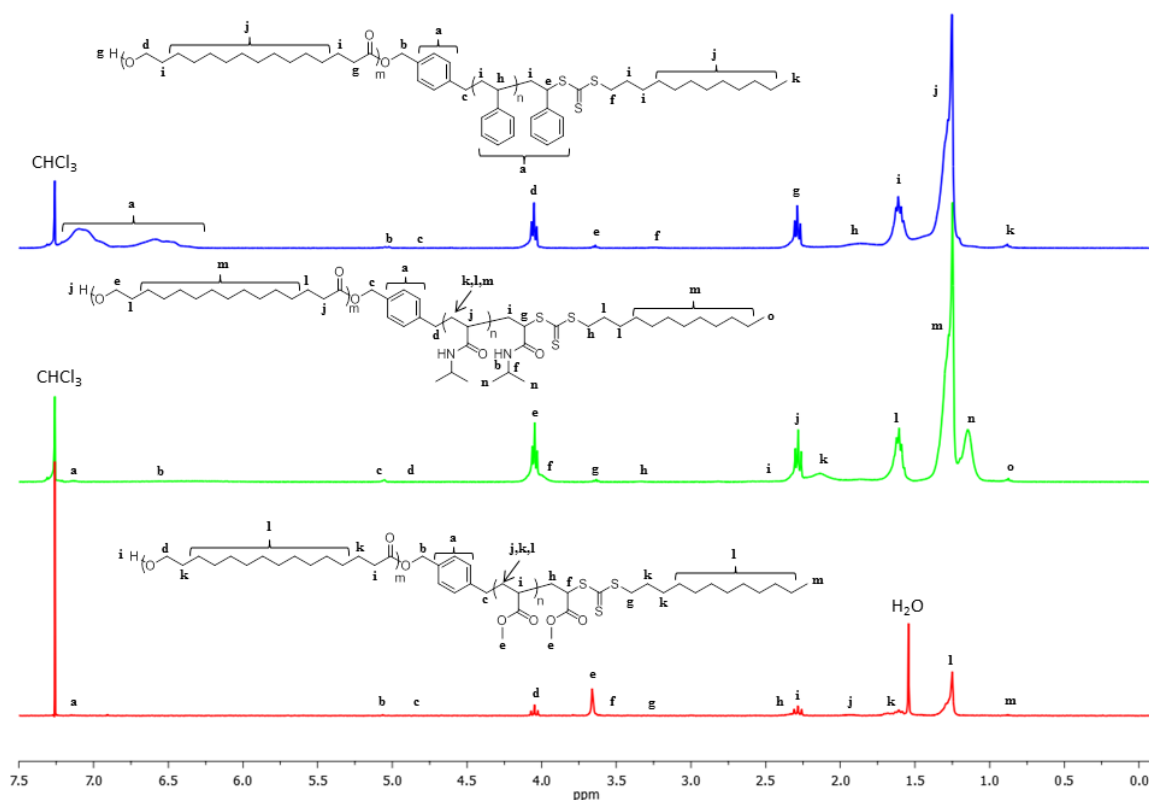
Figure 2.39: ^{1}H NMR spectra of PPDL-*b*-(DP 43 P(MA)), PPDL-*b*-(DP 27 P(NIPAM)), and PPDL-*b*-(DP 31 P(S)) prepared *via* the chain extension of **2** with MA, NIPAM, and S using AIBN ([M]:[CTA]:[I] = 100:1:0.1), and precipitated in methanol (P(MA) and P(S)) or diethyl ether (P(NIPAM)) (300 MHz; CDCl$_3$).
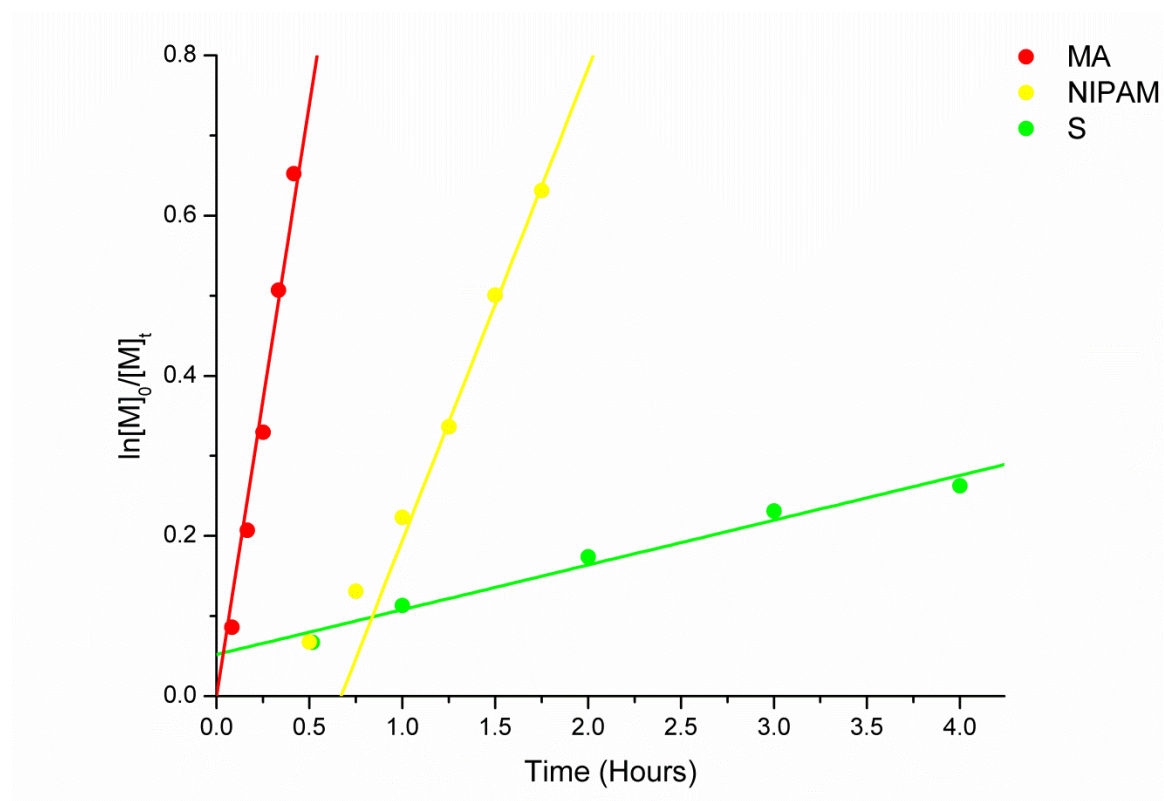
Figure 2.40: Semi-logarithmic plots for the chain extension of **2** with MA, NIPAM, and S using AIBN ([M]/[I] = 100) ([M]:[CTA]:[I] = 100:1:0.1).
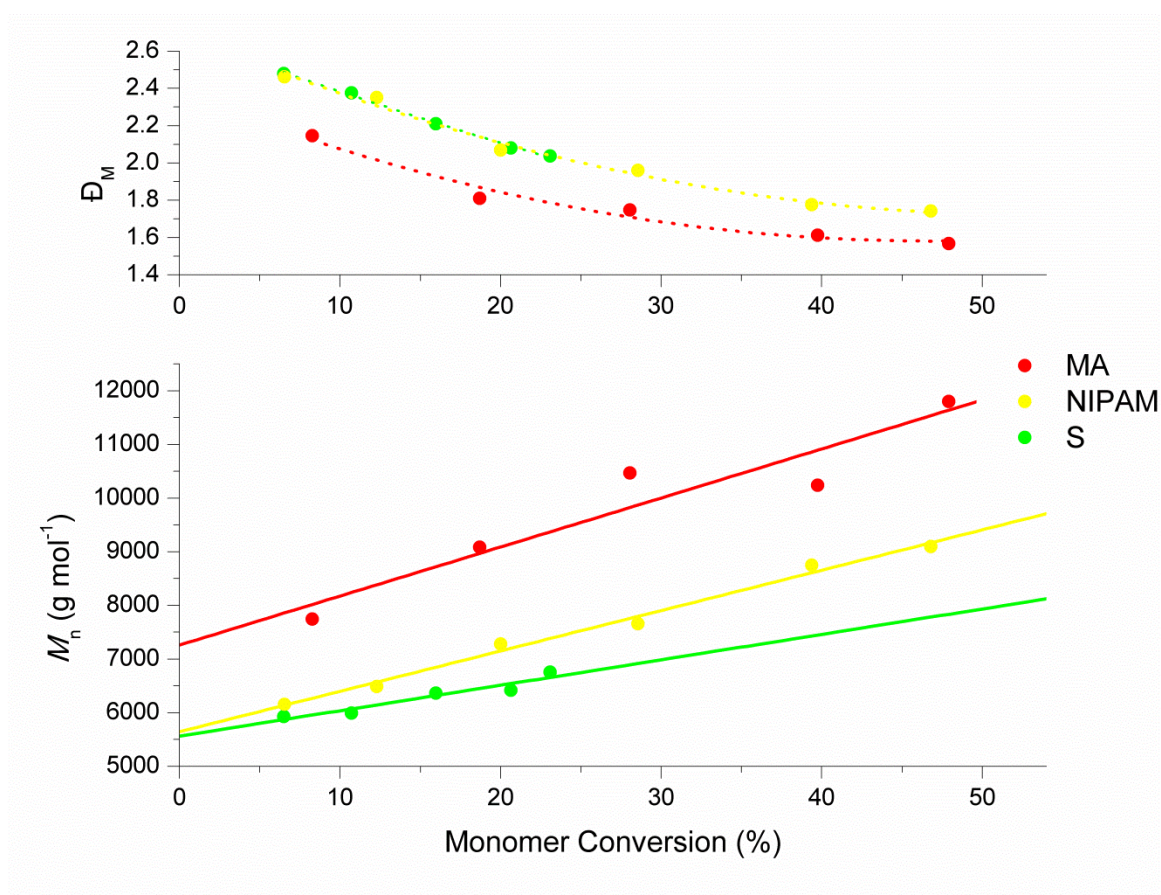
Figure 2.41: Plot of M_n and $Đ_M$ *versus* monomer conversion for the chain extension of **2** with MA, NIPAM, and S using AIBN ([M]/[I] = 100) ([M]:[CTA]:[I] = 100:1:0.1). Please note that trend lines fitted to $Đ_M$ *versus* percent monomer conversion plots are provided solely to guide the eye.

2.3 Conclusions

PPDL was successfully prepared *via* eROP, initiating from BnOH in a controlled fashion. Furthermore, controlled eROP of PPDL initiating from the bifunctional initiator dodecyl 4-(hydroxymethyl) benzyl carbonotrithioate, which is appropriate for RAFT polymerization, was also demonstrated. Using both initiators, however, the presence of cyclic PPDL was noted alongside the desired linear polymer with intended functionality. Cyclic PPDL results *via* chain scission and cyclization reactions catalysed by indiscriminate transesterification by lipases, and its presence is consistent with literature reports.[15,22,23]

Chain extension of a PPDL macro-CTA was successfully performed with a selection of acrylic monomers, in particular those relevant to fuels applications, namely EHA, IDA, LA, and SA, in addition to MA, styrene and NIPAM. Good control of the RAFT process was observed with all monomers investigated and respectable end-group fidelity was achieved as evidenced by an overlay of the RI and UV (309 nm) GPC ($CHCl_3$) chromatograms of crude PPDL-*b*-PLA. The kinetic data obtained herein informed the large scale synthesis and characterization of PPDL-*b*-poly(acrylate) copolymers prepared in Chapter 3 for fuels testing.

Demonstrating that RAFT-functional PE-like PPDL can be readily prepared with moderate end-group fidelity and that the RAFT functionality can be successfully employed for CRP, it is anticipated that interesting novel materials can be prepared. Future studies could include the preparation of RAFT-functional PPDL from bifunctional initiators maintaining different Z and/or R groups or *via* convergent synthetic strategies, the preparation of higher architectures of PPDL and copolymers thereof, and the investigation of high molecular weight material. Additional investigations could include the development of non-enzymatic catalysts capable of polymerizing macrocyclic lactones in the absence of significant chain scission reactions and initiation from water.

2.4 References

(1)   Focarete, M. L.; Scandola, M.; Kumar, A.; Gross, R. A. *J. Polym. Sci., Part B: Polym. Phys.* **2001**, *39*, 1721.

(2)   van As, B. A. C.; Thomassen, P.; Kalra, B.; Gross, R. A.; Meijer, E. W.; Palmans, A. R. A.; Heise, A. *Macromolecules* **2004**, *37*, 8973.

(3)   Meyer, U.; Palmans, A. R. A.; Loontjens, T.; Heise, A. *Macromolecules* **2002**, *35*, 2873.

(4)   De Geus, M.; Schormans, L.; Palmans, A. A.; Koning, C. E.; Heise, A. *J. Polym. Sci., Part A: Polym. Chem.* **2006**, *44*, 4290.

(5)   Peeters, J. W.; Palmans, A. R. A.; Meijer, E. W.; Koning, C. E.; Heise, A. *Macromol. Rapid Commun.* **2005**, *26*, 684.

(6)   Duxbury, C. J.; Wang, W. X.; de Geus, M.; Heise, A.; Howdle, S. M. *JACS* **2005**, *127*, 2384.

(7)   Zhou, J.; Villarroya, S.; Wang, W.; Wyatt, M. F.; Duxbury, C. J.; Thurecht, K. J.; Howdle, S. M. *Macromolecules* **2006**, *39*, 5352.

(8)   Villarroya, S.; Zhou, J. X.; Duxbury, C. J.; Heise, A.; Howdle, S. M. *Macromolecules* **2006**, *39*, 633.

(9)   Thurecht, K. J.; Gregory, A. M.; Villarroya, S.; Zhou, J.; Heise, A.; Howdle, S. M. *Chem. Commun.* **2006**, 4383.

(10)   Petzetakis, N.; Dove, A. P.; O'Reilly, R. K. *Chem. Sci.* **2011**, *2*, 955.

(11)   Petzetakis, N.; Robin, M. P.; Patterson, J. P.; Kelley, E. G.; Cotanda, P.; Bomans, P. H. H.; Sommerdijk, N. A. J. M.; Dove, A. P.; Epps, T. H., III; O'Reilly, R. K. *ACS Nano* **2013**, *7*, 1120.

(12)   Sun, L. P., N.; Pitto-Barry, A.; Schiller, T. L.; Kirby, N.; Keddie, D. J.;; Boyd, B. J., O'Reilly, R. K.; Dove, A. P. *Macromolecules* **2013**, *46*.

(13)   van der Meulen, I.; de Geus, M.; Antheunis, H.; Deumens, R.; Joosten, E. A. J.; Koning, C. E.; Heise, A. *Biomacromolecules* **2008**, *9*, 3404.

(14)   *Handbook of Ring-Opening Polymerization*; Dubois, P. C., O.; Raquez, Jean-Marie, Ed.; Wiley-VCH, 2009.

(15)   Bouyahyi, M.; Pepels, M. P. F.; Heise, A.; Duchateau, R. *Macromolecules* **2012**, *45*, 3356.

(16)   Finkelstein, H. *Ber. Dtsch. Chem. Ges.* **1910**, *43*, 1528.

(17)   Smith, M. B. M., J. *March's Advanced Organic Chemistry: Reactions, Mechanisms, and Structure*; 6th ed.; John Wiley & Sons, Inc.: Hoboken, New Jersey, 2007.

(18)   Yu, B.; Lowe, A. B. *J. Polym. Sci., Part A: Polym. Chem.* **2009**, *47*, 1877.

(19)   Moad, G.; Rizzardo, E.; Thang, S. H. *Aust. J. Chem.* **2006**, *59*, 669.

(20)   Boschmann, D.; Vana, P. *Macromolecules* **2007**, *40*, 2683.

(21)   Zhu, J.; Zhu, X. L.; Cheng, Z. P.; Lu, J. M.; Liu, F. *J. Macromol. Sci., Pure App. Chem.* **2003**, *A40*, 963.

(22)   de Geus, M.; Peters, R.; Koning, C. E.; Heise, A. *Biomacromolecules* **2008**, *9*, 752.

(23)   van der Meulen, I.; Gubbels, E.; Huijser, S.; Sablong, R.; Koning, C. E.; Heise, A.; Duchateau, R. *Macromolecules* **2011**, *44*, 4301.

Chapter 3

Synthesis and Fuels Testing of Block Copolymers of

Poly(ω-Pentadecalactone) as Cold Flow Additives for Diesel

3.1 Introduction

Although the popularity of diesel vehicles has fluctuated with the general public, especially within North America, the diesel engine remains the motor of choice within industry and the military for both transport and machinery. Advantages of the diesel engine include its superior efficiency, reliability, durability, and torque in addition to its minimal carbon monoxide emissions and ability to withstand turbo-charging, limited only by the strength of individual engine components. Advantages of diesel fuel include that diesel is significantly less flammable than petrol and, in principle, cheaper since diesel can be sourced from a broad range of feedstocks, from petroleum through to plant and animal fats and used without significant blending or processing following the robustness of diesel engine design. Despite these advantages, diesel engines suffer some disadvantages, in particular cold weather operability, which restrict their performance, reliability, and popularity for personal vehicle use. Not only are diesel engines significantly more difficult to start when cold, diesel fuel is prone to gelling at cold temperatures, blocking fuel lines, filters, and pumps, leading to fuel starvation and resulting in loss of power and even complete failure depending on the fuel, temperature, and engine design. Although fuel line and tank heaters can be installed to reduce fuel gelling, chemical additives have been developed, beginning in the 1960s, to significantly improve the cold flow properties of diesel at low treat rates and extend the operable temperature range of diesel engines. This strategy, however, suffers from the fact that additive performance is highly dependent on diesel fuel composition.

Diesel fuel sourced from petroleum is simply a middle distillate of crude oil with a typical boiling point range of 130 – 370 $^{\circ}$C[1] and is comprised predominantly of hydrocarbons including alkanes, cycloalkanes, and aromatics, some of which contain heteroatoms. Straight chain paraffins account for 15-30% of diesel content, with a distribution from C9 through to C36 that varies significantly depending on the regional source of the crude oil and the fractionation efficiency of the refinery at which it was processed (Figure 3.1).[2] Diesel cold flow properties are highly dependent on *n*-alkane content and distribution since, at low temperatures, larger paraffins precipitate from the fuel as rhomboid crystals that can grow up to 1 mm in diameter and block fuel lines and filters. Furthermore, in the presence of as little as 0.5% precipitated wax, a gel structure forms whereby bulk fuel is trapped in a "house of cards" of interlocking wax crystals following their strong edge-to-edge attractive forces.[3] Cold flow problems typically arise when overnight temperatures reach between -10 $^{\circ}$C and -15 $^{\circ}$C, and unfortunately, removal of paraffins from diesel altogether results in ignition failures.[4] Middle distillates can be generalized by both

their boiling point range and final boiling point temperature.[2] Narrow boiling distillates are significantly waxier and exhibit very poor cold flow performance relative to broader boiling distillates since, in broad boiling distillates, the lighter fraction solubilizes the heavier paraffin content to a significant extent. Furthermore, high final boiling point distillates also exhibit inferior cold flow performance following their greater heavy paraffin content. Therefore, extremely narrow or high boiling distillates can be very difficult to treat in order to achieve desirable cold flow performance. Indeed, the most difficult to treat fuels often require blending with other distillates, preferably those with high aromatic content.
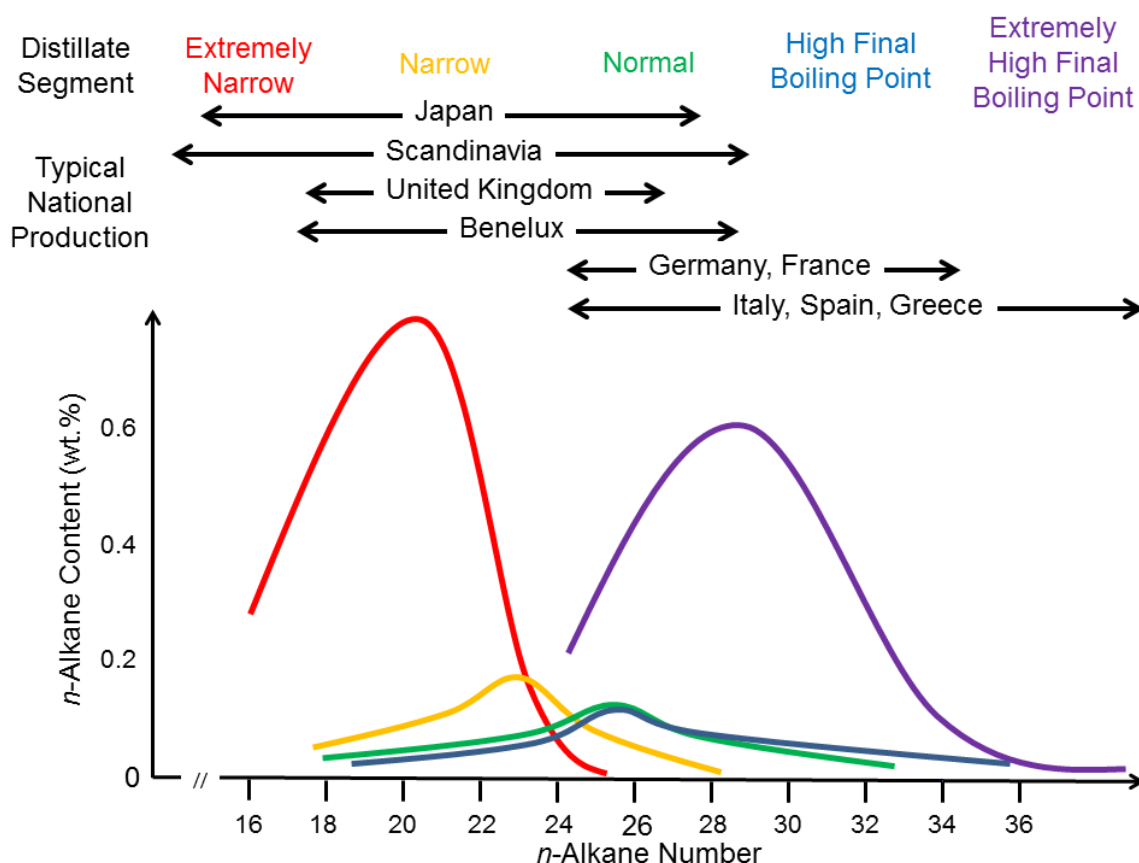
Figure 3.1: Characteristics of middle distillate fuels sourced from different national production sites, including the distribution of *n*-alkanes separating 10 °C below the cloud point. Figure adapted from Reference 2.[2]

In order to predict the field performance of various diesel fuels, two laboratory assessments were initially developed, namely the *Cloud Point* or temperature at which the first wax crystal precipitates from fuel, and the *Pour Point* or temperature at which fuel solidifies. These assessments, however, were determined to be too severe and too optimistic, respectively since most diesel engines running untreated fuel fail just below the cloud point.[2] In 1965, however, the *Cold Filter Plugging Point* (CFPP) test was developed and thereafter standardized and widely adopted following its good correlation in predicting the low temperature operability of

diesel fuel. Using a specialized apparatus, the CFPP is defined as the temperature at which diesel, when cooled under prescribed conditions, either fails to pass, under vacuum, through a standardized filtration device within a specified amount of time, or fails to flow back through the filter prior to the next vacuum cycle.[2] Ultimately, the CFPP evaluates the flow and filterability of diesel below its cloud point, and therefore in the presence of wax crystals, and remains the most precise and reliable cold flow performance test to date.

In order to improve CFPP performance, additives were developed to promote 1) *nucleation*, enabling the formation of a large number of smaller wax crystals that are less prone to blocking fuel lines, pumps, and filters by interacting with the first crystal nuclei formed several degrees above the cloud point, 2) *growth inhibition*, preventing large crystal growth and crystal-crystal interactions that cause fuels to gel by adsorbing onto growing crystal surfaces, preventing plate type growth, and forcing crystals to adopt more compact shapes such as needles, and 3) *wax anti-settling*, stabilizing wax dispersion through the fuel in order to prevent wax crystals from settling, enabling faster re-melting of wax as fuel warms up and ensuring uniform paraffin content in fuel for good ignition.[4] Importantly, these middle distillate flow improvers (MDFIs) do not alter the cloud point or quantity of wax that precipitates from diesel. Rather, they increase tolerance to wax by modifying the size and shape of the crystals generated since, where wax crystals no longer pass through filters, their modified shape ensures that a porous wax crystal cake is formed, permitting continued flow of liquid diesel, ultimately altering the CFPP and pour point of the fuel (Figure 3.2).[2] Interestingly, where cloud point depressants are employed, CFPP performance can be seriously impaired since cloud point depressants yield very large, although well-separated crystals.[5] Since MDFIs modify both the size and shape of wax crystals formed in diesel, they are also referred to as *wax crystal modifiers* (WCMs). It is additionally commonplace to visualize wax crystal morphology by microscopy and evaluate wax dispersion throughout a treated fuel at specified temperatures in the laboratory assessment of WCM performance. These observations assist in developing a fundamental understanding of the affect and mechanism of an additive as a WCM in a specific fuel.
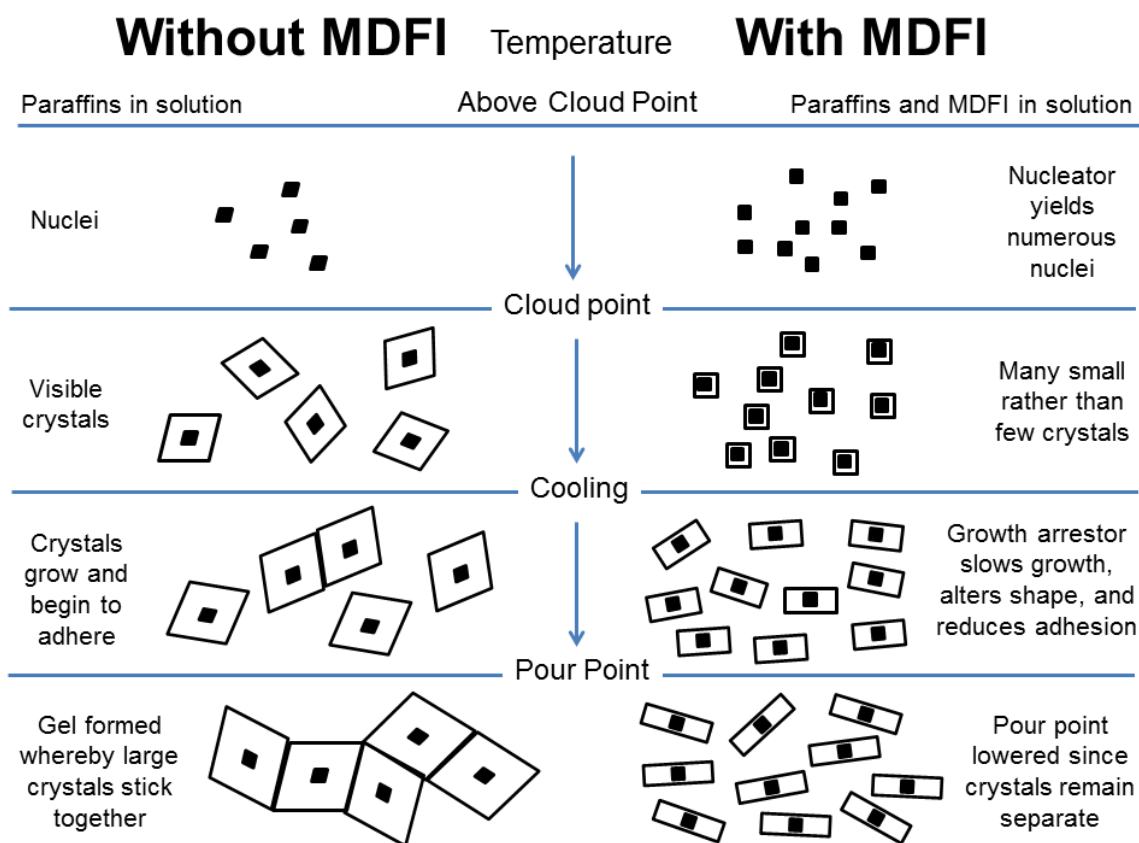
Figure 3.2: Comparison of wax crystal growth in diesel with and without MDFIs. Figure adapted from Reference 2.[2]

MDFIs are typically fuel-soluble, polymeric materials maintaining *n*-alkane- or polyethylene-like backbones. The most effective and widely used MDFIs are random ethylene-*co*-vinyl acetate copolymers (EVAs) prepared *via* high pressure, high temperature free radical polymerization. Interestingly, EVAs can function as both nucleators and growth arrestors depending on the middle distillate and the EVA vinyl acetate content.[4] For example, varying the vinyl acetate content tunes the function of the EVA.[6] Although very little is known about their structure and monomer distribution, it is widely accepted that EVAs function as growth arrestors by adsorbing onto the growing face of a wax crystal *via* the polyethylene backbone, and that the acetate groups extend into the fuel, inhibiting both further crystal growth and crystal-crystal interactions.[7] EVA performance is further improved where vinyl acetate branches are eliminated *via* hydrolysis and re-acetylation, and intrachain interactions are promoted by tuning the molecular weight and vinyl acetate content of the copolymer to the fuel.[8] Similarly, block copolymers maintaining a semi-crystalline polyethylene block coupled to an amorphous diblock copolymer such as poly(ethylene-*co*-propylene) or poly(ethylene-*co*-butene) behave as both nucleators and growth arrestors whereby the semi-crystalline polyethylene block promotes nucleation and the amorphous component serves as a steric barrier.[3] Wax anti-settling agents

(WASAs), which prevent wax crystal sedimentation by adsorbing onto wax crystal surfaces and enhancing their colloidal stability, are typically adducts of dialkylamines and cyclic anhydrides (Figure 3.3).[4] Additional MDFIs include comb polymers maintaining branch chain lengths between C12 and C18, which typically form assemblies in fuel and behave as cloud point depressants or WASAs depending on the polymer molecular weight.[9] Interestingly, fumarate vinyl acetate comb polymers have been found to specifically nucleate waxes of a given carbon chain length depending on the length of the alkyl side branches.[10]
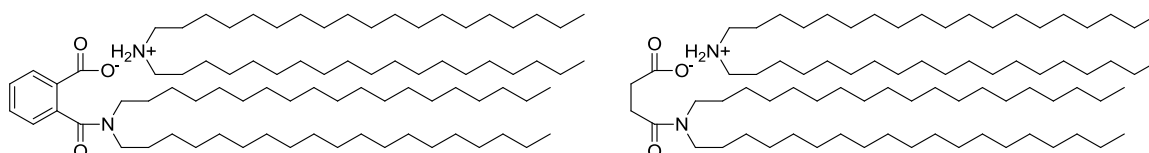
Figure 3.3: Dialkyl amine adducts of phthalic anhydride (left) and succinic anhydride (right) commonly employed as wax anti-settling agents (WASAs).[4]

Cold flow technology is similarly employed to increase the reliability of heating oil and marine fuel, and the pipeline transport of crude oil and heavy fuel. Furthermore, it is routinely used in refinery processing to increase capacity by reducing the amount of filters and heating facilities required for de-waxing, and to increase revenue through improved fractionation, increasing yields, upgrading less valuable, heavier streams to diesel, and liberating higher value fractions, such as kerosene.[2] The fuel additives industry has also realized the development of numerous additional products to increase engine power, economy, and overall performance including additives for detergency, which maintain fuel injector systems, lubricity, to reduce engine wear following the introduction of low-sulfur diesel, improved combustion, anti-corrosion, fuel stabilization, fuel demulsification, and the regeneration of diesel particulate filters.[11] Despite these achievements, however, there remains a demand for 1) an improved understanding of MDFI mechanisms, 2) more universal MDFI packages, reducing the need to tailor an additives package to each fuel processed at a refinery, and 3) improved cold flow performance since winterized diesel blends, or diesel treated to reduce low temperature fuel gelling, continue to require kerosene and, in some remote regions, heavy duty vehicles continue to be left running overnight in severe climates to prevent fuel gelling. Furthermore, it has been reported that conventional MDFIs are not as effective with biodiesel.[12]

Growing demand for energy security, especially following the energy crisis of the 1970s, in addition to environmental policies calling for a reduction in petroleum consumption have driven the legislated use of biodiesel as set out by EN 590 standards for diesel characteristics in

Europe. Biodiesel is typically composed of transesterified vegetable oils since unprocessed oils, specifically triglycerides of saturated or unsaturated fatty acids, suffer from high viscosity, poor atomization, and the tendency to cause engine coking. Fatty acid methyl esters (FAMEs) are suitable for direct-injection diesel engines and their superior cetane rating, lubricating properties, and reduced emissions relative to low sulfur petroleum diesel make them an attractive fuel choice.[13] Additional advantages of biodiesel include that it is safer to handle following its low toxicity and higher flash point, and that it is sourced from renewable feedstocks including edible vegetable oil, non-edible vegetable oil, waste or recycled oil, and animal fat. Unfortunately, waste oil and animal fats are highly saturated and consequently maintain very high cloud points, often exceeding 15 °C, and therefore must be blended for fuels applications.[13,14] Highly unsaturated vegetable oils exhibit superior biodiesel cold flow performance, however, their reduced cetane rating and oxidative stability relative to other biodiesels similarly often limits their use to blends with petroleum diesel.[14,15]

Currently, biodiesel is typically sold as a 5-20 % blend in conventional diesel, the amount of which is designated by a "B" factor - for example, blended diesel fuel consisting of 10% biodiesel is designated "B10" - since blended diesel is easier to treat than neat biodiesel and since biodiesel significantly improves the lubricating properties and cetane rating of low sulfur petroleum diesel, even in 1-2% blends.[12,14] Biodiesel however, suffers problems for which additives are required including water contamination, degradation, inconsistent fuel quality, biological growth, increased nitrogen oxide emissions, increased motor wear, hazing during storage, and critically, poor cold flow performance.[1,14] The very narrow *n*-alkane distribution in biodiesel results in biodiesel having a significantly higher cloud point than petroleum diesel, namely 0 °C compared to -16 °C, respectively, which is very difficult to treat with conventional MDFIs and suggests the requirement for biodiesel specific cold flow additives.[14] Therefore, biodiesel continues to be blended with petroleum diesel in order to satisfy performance requirements, although cold flow properties can also be improved using additives, blending with kerosene or alcohols, or *via* costly chemical modification.[12,16]

Advantages of the diesel engine have driven successive technological improvements that have been greatly supported by developments within the fuel additives industry, in particular cold flow technology (Figure 3.4). Furthermore, socio-economically driven changes including the legislated use of low-sulfur diesel, biodiesel, and diesel particulate filters, for example, have delivered additional challenges that have also been successfully managed by the additives industry. The enhanced operability and reliability of diesel vehicles has increased their popularity

to the extent that diesel engines currently account for nearly half of the vehicles in Western Europe. On-going developments in MDFI technology are expected to continue improving the reliability and cold weather operability of diesel vehicles; however, the overwhelming challenge remains to treat varied diesel quality from different sources.
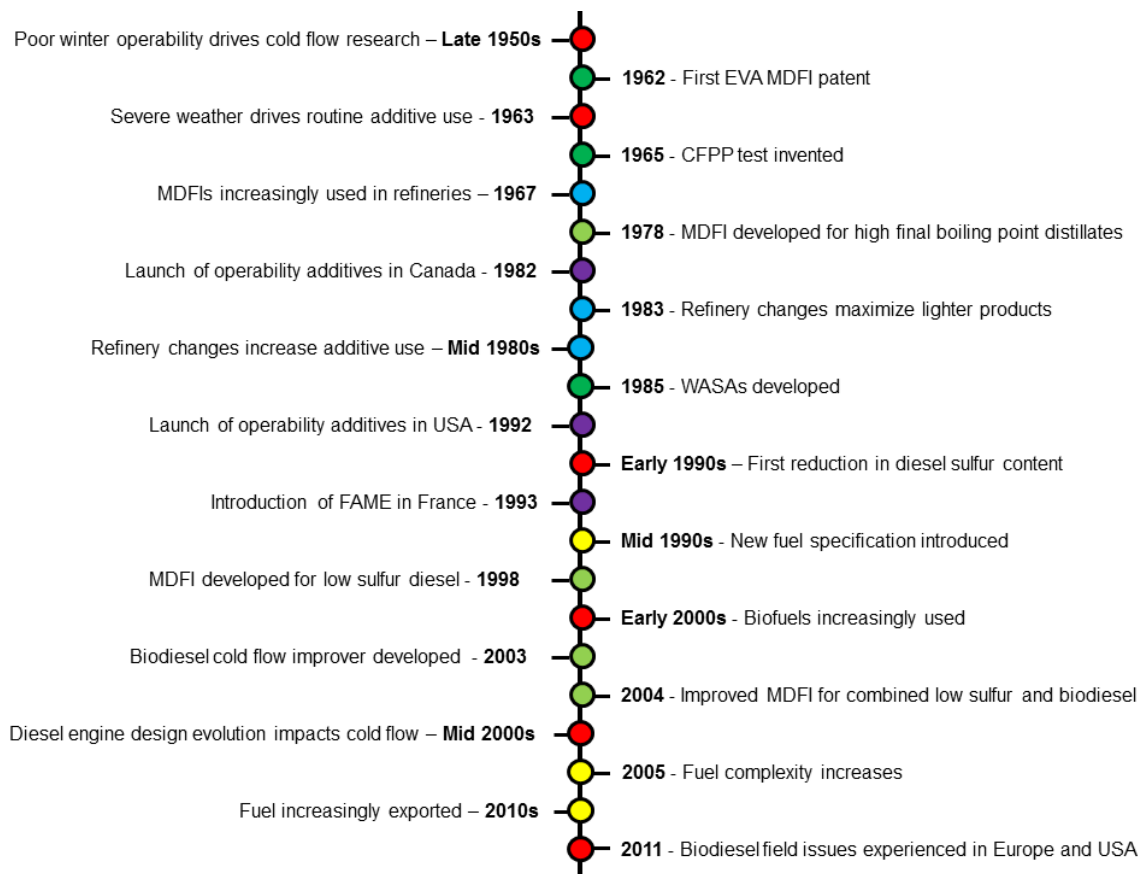
Figure 3.4: Timeline of the cold flow additives industry. Figure adapted from Reference 17.[17]

To date, alternate commercial MDFI products have not matched the umbrella success of EVAs. Therefore, new MDFI research initiatives are often polyolefin-based approaches. Recent reports that PPDL maintains polyethylene-like properties motivated our interest in PPDL for cold flow technology, particularly since its hydrolysable ester linkages, which uphold PPDL as a potential "green" alternative to PE, complements environmental incentives for legislated biodiesel production.[18] Therefore, chemistry developed in Chapter 2 was utilized to prepare PPDL copolymer samples for cold flow fuel testing, the results for which are discussed herein.

3.2 Results and Discussion

3.2.1 Synthesis and Fuels Testing of Poly(ω-Pentadecalactone)-*b*-Poly(2-Ethylhexyl acrylate) Block Copolymers

3.2.1.1 Polymer Synthesis

Analysis conducted on PPDL samples at Infineum UK Ltd determined that PPDL is insoluble in fuel, even with heating, which was expected since PPDL is insoluble in the majority of common laboratory solvents, with the exception of chloroform. In order for PPDL to be explored as a potential fuels additive, it must be soluble in fuel. Therefore, block copolymers of PPDL were proposed whereby the second block is highly soluble in fuel and therefore solubilizes the PPDL component of the copolymer. Since polyacrylates are well known to be soluble in fuel and since the bifunctional CTA **1** described in Chapter 2 is well known in our research group and suitable for both the initiation of ROP and the RAFT polymerization of acrylates, the chemistry described in Chapter 2 was developed. Poly(2-ethylhexyl acrylate) (PEHA) was selected for the second block for initial fuels testing since 1) it is known to be highly soluble in fuels, and 2) its branched nature will disrupt the linearity of the acrylic backbone and therefore reduce the ability of the acrylic block to promote nucleation. Therefore, whilst developing the chemistry in Chapter 2, an initial set of PPDL-*b*-PEHA copolymers with varied acrylic block length were prepared in two steps for fuels testing to evaluate the efficacy of this strategy for fuels applications.

First, a batch of purified DP 19 PPDL macro-CTA **3** was prepared on a 10 g scale (Scheme 3.1 and Table 3.1) *via* the eROP of PDL from the bifunctional initiator **1**. Thereafter, the PPDL macro-CTA was chain extended with 2-ethylhexyl acrylate (EHA) to prepare a selection of block copolymers with varying acrylic block lengths as described (Scheme 3.2, Table 3.2). Finally, the samples underwent fuels testing at Infineum UK Ltd.
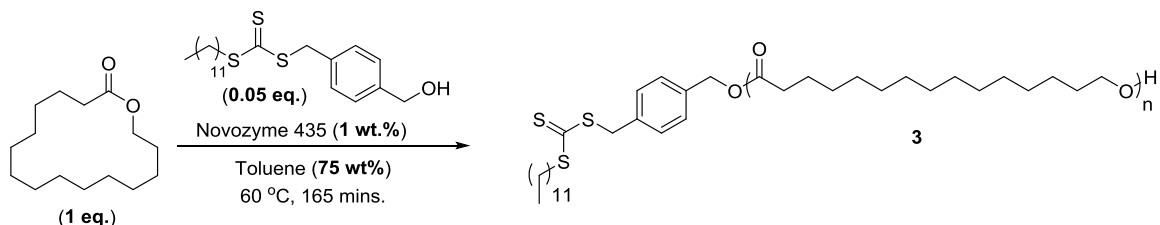
Scheme 3.1: Synthesis of PPDL macro-CTA **3** (target DP 17).

Table 3.1: Characterization of PPDL macro-CTA **3** prepared according to Scheme 3.1.

$[M]_0/[I]_0$	$[M]_t/[M]_0{}^a$	M_n (g mol^{-1})^b	M_n (g mol^{-1})^a	$Đ_M{}^b$	DP^a
20	0.67	7800	4600	2.15	19

[a]Determined by ^{1}H NMR spectroscopic analysis in CDCl$_3$; [b]Determined by GPC analysis in CHCl$_3$.
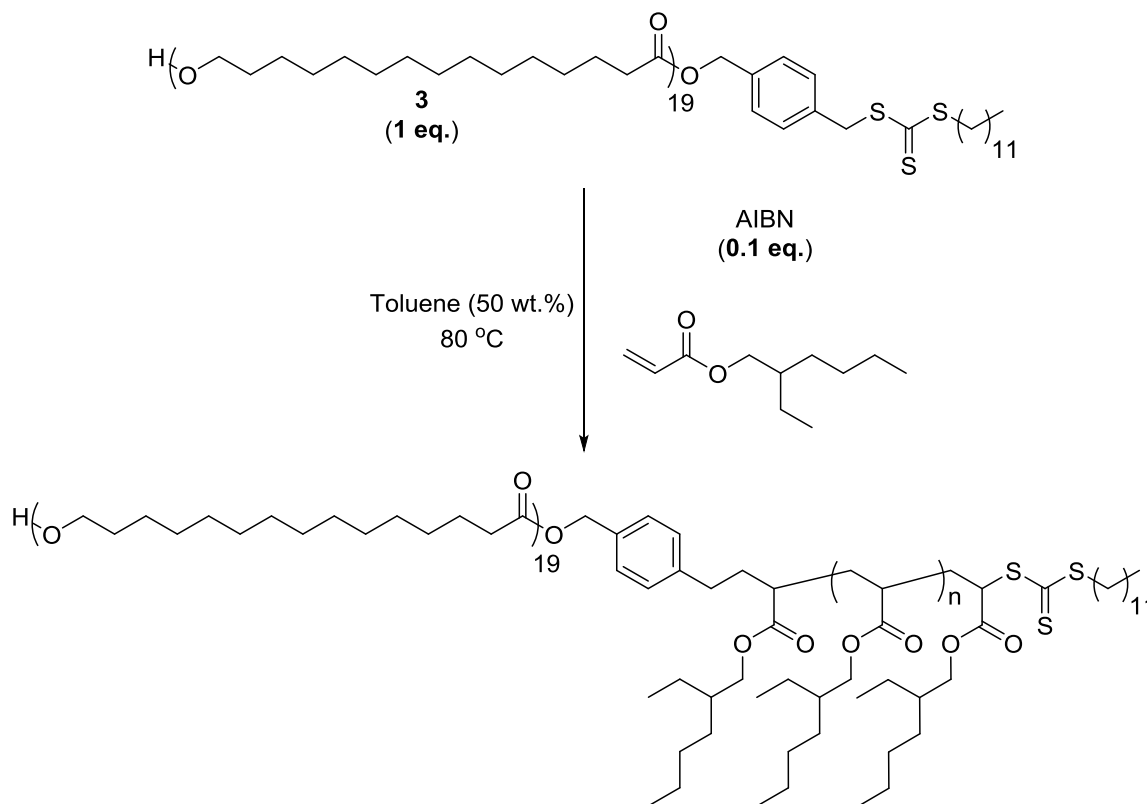
Scheme 3.2: Chain extension of DP 19 PPDL macro-CTA **3** to prepare PPDL-*b*-PEHA copolymers.

Table 3.2: Summary of PPDL-*b*-PEHA copolymers prepared according to Scheme 3.2.

Entry	$[M]_0/[I]_0$	Time (min)	M_p (g mol^{-1})^a	M_n (g mol^{-1})^a	M_n (g mol^{-1})^b	$Đ_M{}^a$	DP PEHA^b	Block Ratio^b
1	100	42	11000	8800	5700	1.88	6	0.3
2	100	82	12000	10800	8400	1.63	21	1.1
3	100	162	17600	14800	16200	1.38	63	3.3
4	100	1200	20900	12600	18600	1.69	76	4.0
5	200	75	25100	22100	37900	1.24	181	9.5
6	200	80	35400	13600	29800	2.43	137	7.2
7	200	370	40800	30100	45800	1.43	224	11.8

[a]Determined by GPC analysis in CHCl$_3$; [b]Determined by ^{1}H NMR spectroscopic analysis in CDCl$_3$.

All GPC chromatograms of the block copolymers (Figure 3.5), with the exception of those that correspond to entries 4 and 6 in Table 3.2, are monomodal and exhibit a good correlation between the M_p of the copolymer and the acrylic block length as evaluated by ^{1}H NMR spectroscopy, indicating good control of the polymerizations. Since polymer entry 4 (Table 3.2) was obtained from the end point of a lengthy polymerization and at a monomer conversion well beyond a controlled polymerization range, at which point significant backbiting β-scission reactions occur, it is likely that the low molecular weight shoulder present in this sample is PEHA homopolymer. It is also possible that PEHA homopolymer was obtained since the reaction mixture was not homogeneous at the start of the reaction. Similarly, the low molecular weight shoulder observed for the entry 6 (Table 3.2) may be PEHA homopolymer, however, is also possible that these low molecular weight shoulders are PPDL homopolymer resulting from initiation from water during eROP. These poorly defined polymers provided the opportunity to determine whether the presence of PPDL or PEHA homopolymer affects the fuels testing performance of the copolymers. Furthermore, these results informed future syntheses for defined copolymers of PPDL such that: 1) the bifunctional initiator was thereafter dried over 3 Å molecular sieves instead of P_2O_5 to reduce initiation from water, 2) chain extensions were thereafter performed within a controlled radical polymerization range, as evaluated by semi-logarithmic plots, and 3) the azo initiator was injected into reaction mixtures equilibrated to the desired reaction temperature in order to improve the repeatability and dispersity of the RAFT polymerizations, especially where reactions were performed on different scales.
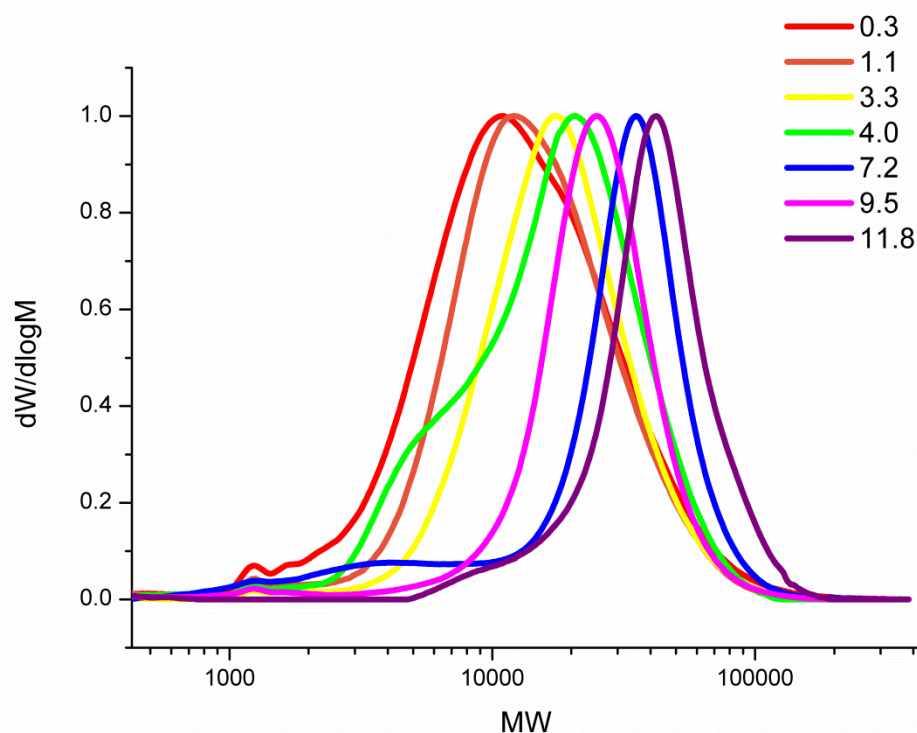
Figure 3.5: GPC (CHCl$_3$) chromatograms of PPDL-*b*-PEHA copolymers of various acrylic block ratios as described in Table 3.2 (DP PPDL:PEHA = 1:0.3, 1:1.1, 1:3.3, 1:4.0, 1:7.2, 1:9.5, and 1:11.8).

Differential scanning calorimetry (DSC) analysis of the copolymers (Figure 3.6) indicate that, in general, the onset crystallization temperature of the copolymers decreases as the size of the acrylic block is increased, substantiating the assertion that the copolymers are block copolymers. Entry 6 (Table 3.2) however does not fit this trend. This sample is suspected to contain a significant amount of PEHA homopolymer and therefore exhibits a higher acrylic block ratio than determined by ^{1}H NMR spectroscopy, as substantiated by the M_p of the predominant polymer product. A corrected acrylic block ratio, however, fits the onset crystallization temperature trend. Similarly, since entry 4 (Table 3.2) did not disrupt the trend, it is suspected that the low molecular weight shoulder observed in the GPC chromatogram for this sample is PEHA.
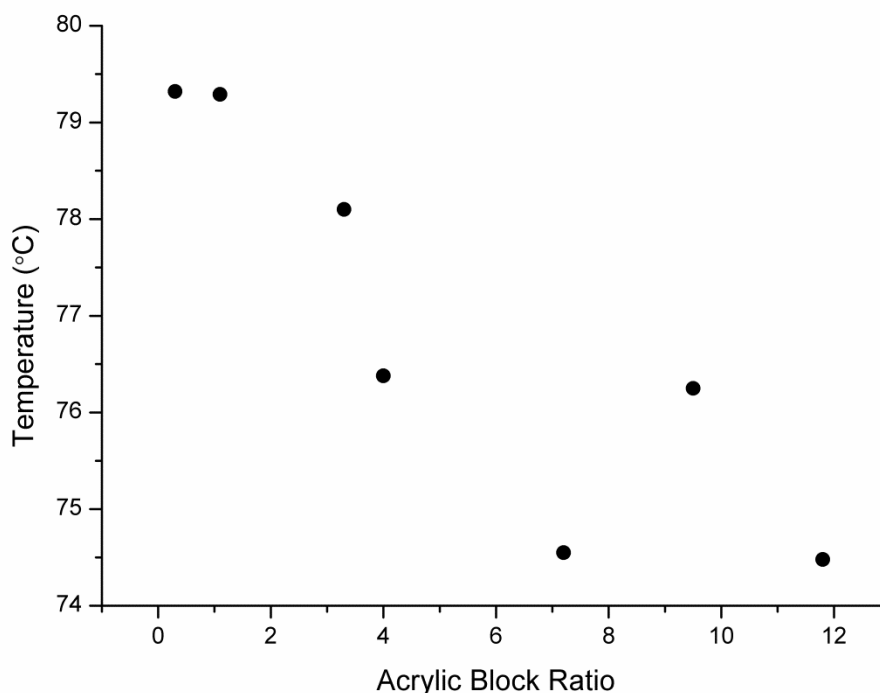
Figure 3.6: Onset crystallization temperatures for PPDL-*b*-PEHA copolymers described in Table 3.2, as determined by DSC analysis.

3.2.1.2 Fuels Testing

The block copolymers were used to treat Fuel A (Figure 3.7) and underwent CFPP testing (Figure 3.8). Fuel A contains 2% biodiesel and maintains a very narrow distribution of lower molecular weight paraffins, with the predominant *n*-alkane content being C15. It was determined that all of the polymer samples had a positive impact on CFPP performance at a treat rate of 200 ppm, reducing the temperature at which the test failed relative to untreated fuel. In general, most of the polymers reduced the CFPP temperature from -9 ^{0}C to between -16 ^{0}C and -18 ^{0}C, indicating that the size of the acrylic block length is not critical, although a block ratio greater than two and below ten achieves superior results. Anomalies were observed, however, particularly with the sample described in entry 4 (Table 3.2), the CFPP results for which suggest the presence of insoluble PPDL and not PEHA homopolymer.
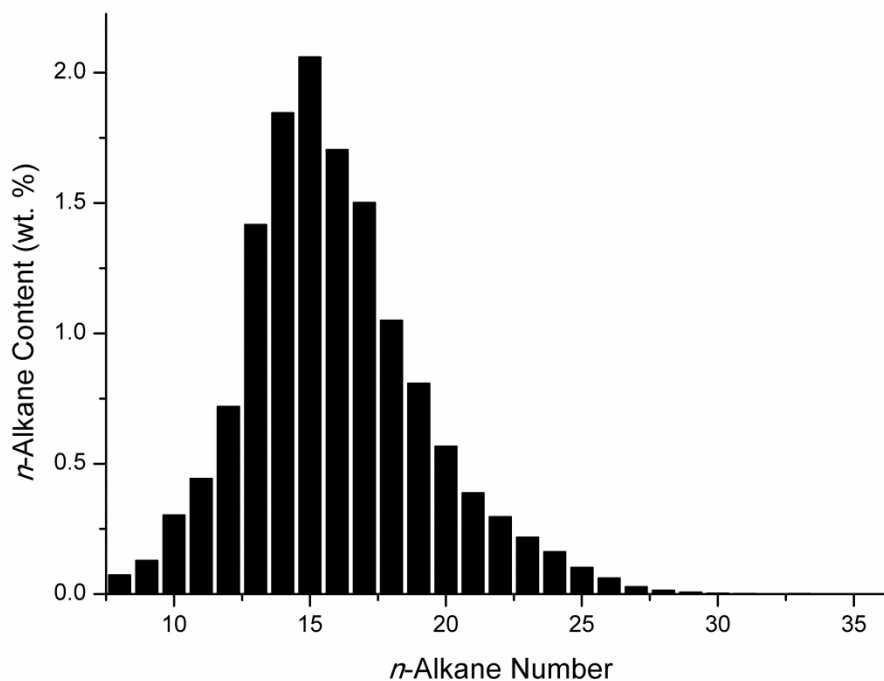
Figure 3.7: Distribution of *n*-alkanes separating from B2 Fuel A.
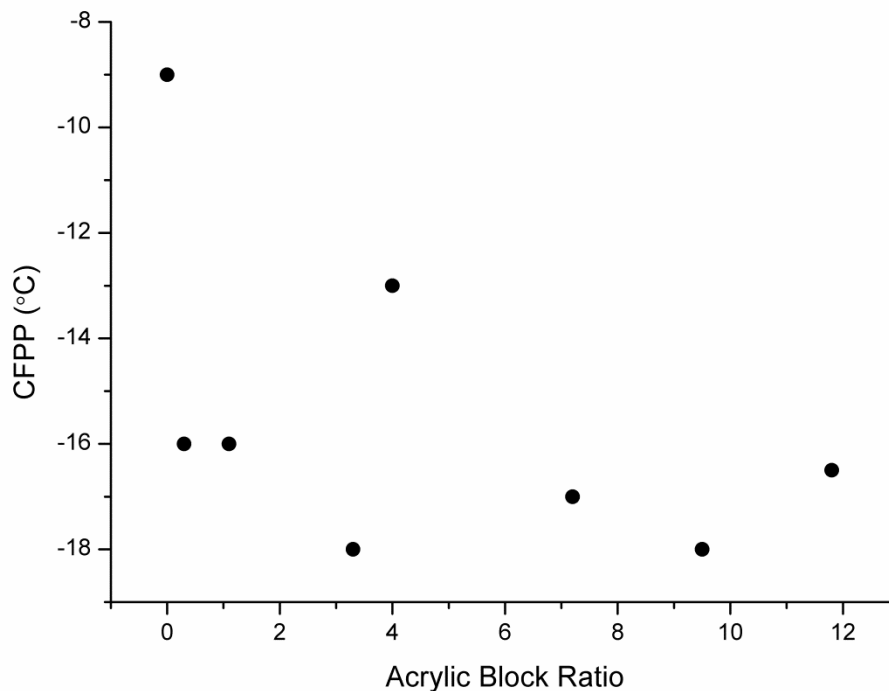
Figure 3.8: CFPP results for various acrylic block lengths of PPDL-*b*-PEHA (200 ppm treat rate in B2 Fuel A).

The polymers were further tested in Fuel B (Figure 3.9), which does not contain biodiesel and maintains a broad distribution of lower molecular weight *n*-alkanes, with the predominant *n*-alkane being C10. It was determined that, as with Fuel A, all of the block copolymers had a positive impact on CFPP performance, reducing the temperature at which the test failed relative to untreated fuel from -7.5 ^{0}C to as low as -17.5 ^{0}C at a treat rate of 300 ppm (Figure 3.10). As with Fuel A, the CFPP results obtained with Fuel B indicate that superior results are obtained where the size of the acrylic block ratio is between two and ten. Since the 1:0.3 PPDL-*b*-PEHA sample failed the CFPP test in Fuel B, it can be concluded that there is a minimum acrylic block ratio required to solubilize the block copolymer in a range of fuels. As with Fuel A, some anomalies in CFPP performance were observed with Fuel B, notably with the polymer described in entry 4 (Table 3.2). This anomaly, however, can similarly be attributed to the presence of PPDL homopolymer in the copolymer sample, as indicated by low molecular weight shoulders present in the GPC chromatogram for this sample.
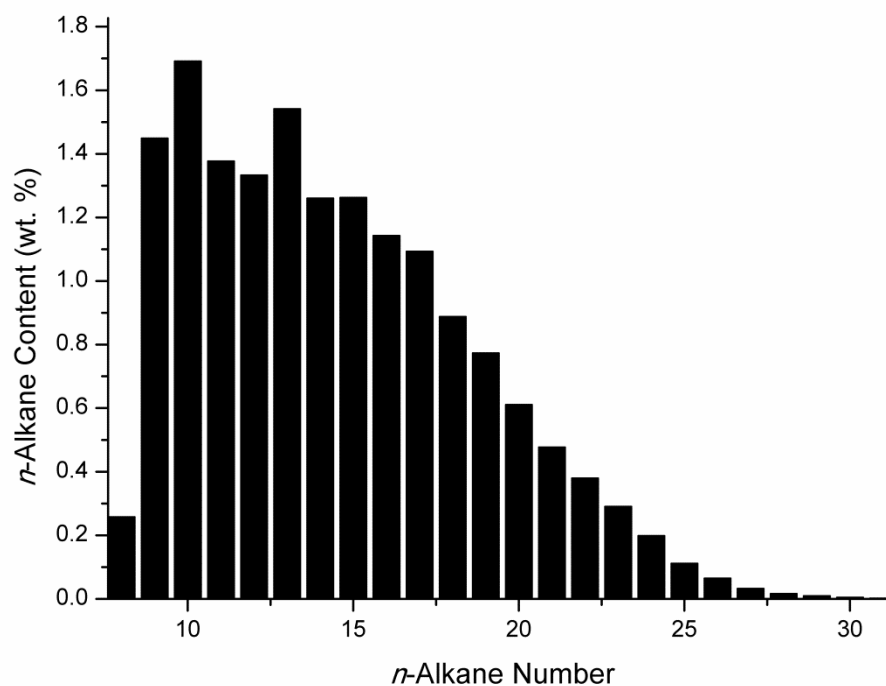
Figure 3.9: Distribution of *n*-alkanes separating from B0 Fuel B.
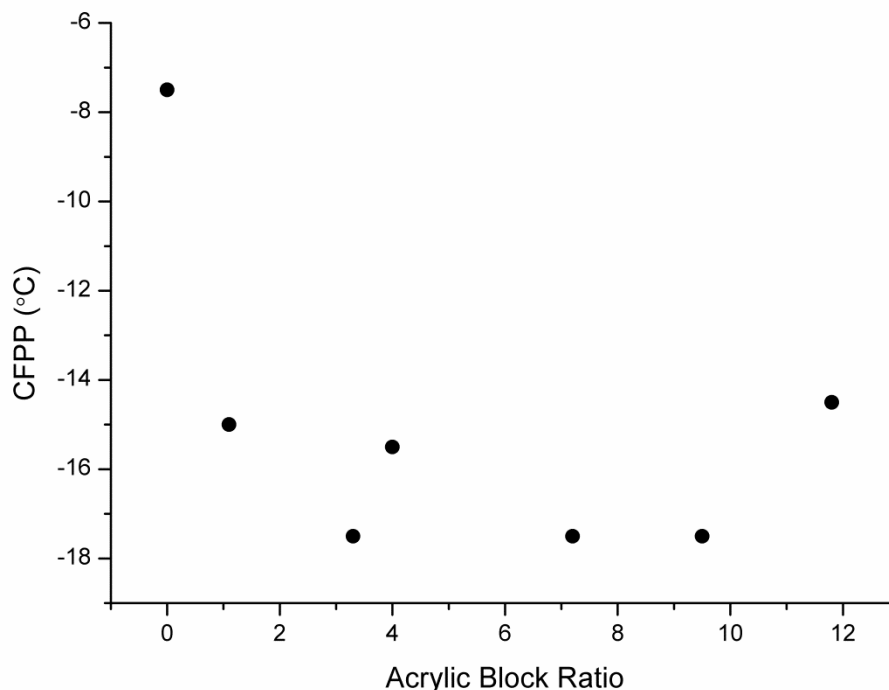
Figure 3.10: CFPP results for various acrylic block lengths of PPDL-*b*-PEHA (300 ppm treat rate in B0 Fuel B). Please note that 1:0.3 PPDL-*b*-PEHA failed the test.

Overall, initial CFPP results indicate that block copolymers of PPDL merit further investigation as WCMs in fuels. Importantly, it was determined that the presence of PPDL homopolymer could potentially hinder CFPP performance whereas the presence of PEHA homopolymer may not where a corrected acrylic block ratio is taken into account. Furthermore, since testing was performed on unoptimized samples in the absence of any additional additives, it is anticipated that further improvements in performance could be observed, especially since WCMs can often perform in combination with other additives. Finally, the observation that the change in CFPP is greater in Fuel B than Fuel A suggests that Fuel A is more difficult to treat as a result of its narrower *n*-alkane distribution.

3.2.2 Synthesis and Fuels Testing of a Selection of Acrylic Block Copolymers of Poly(ω-Pentadecalactone)

3.2.2.1 Polymer Synthesis

The promising results obtained with the PPDL-*b*-PEHA copolymers inspired the synthesis of a more extensive range of acrylic block copolymers of PPDL for further fuels testing. Ultimately, the chemistry developed in Chapter 2 was utilized to prepare 18 different PPDL block

copolymer samples using acrylates, namely 2-ethylhexyl acrylate, isodecyl acrylate (IDA), lauryl acrylate (LA), and stearyl acrylate (SA) as the solubilizing block in various acrylic block lengths. The block copolymers were prepared by first preparing a batch of DP 19 PPDL macro-CTA (**4**) (Scheme 3.3 and Table 3.3), the crude material of which was thereafter chain extended with acrylic monomers *via* RAFT polymerization to prepare various block copolymers as described (Scheme 3.4 and Tables 3.4-3.7). Semi-logarithmic plots (Figure 2.31 and Figure 2.34) and plots of DP *versus* time (Figure 2.33 and Figure 2.36) for the chain extension of **2** using various acrylates determined in Chapter 2 were utilized to select appropriate reaction conditions and times for the preparation of desired range of block copolymer ratios described in Tables 3.4-3.7. Importantly, the M_p increased whilst the dispersity of the block copolymers obtained decreased with increasing acrylic block length, and there is a good correlation between the M_n evaluated by GPC and ^1H NMR spectroscopic analysis.
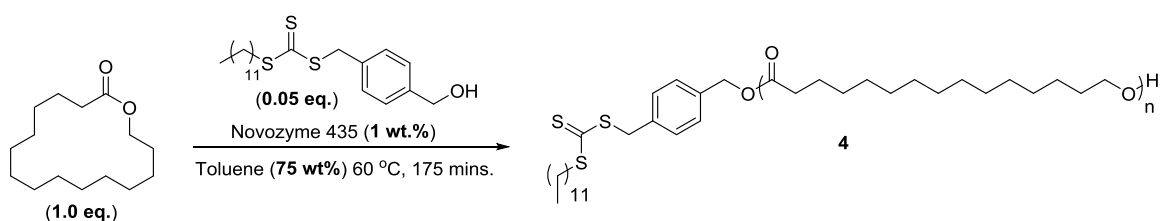
Scheme 3.3: Synthesis of DP 19 PPDL macro-CTA **4** (target DP 17).

Table 3.3: Characterization of crude PPDL macro-CTA **4** prepared according to Scheme 3.3.

$[M]_0/[I]_0$	$[M]_t/[M]_0^a$	M_n (g mol^{-1})^b	M_n (g mol^{-1})^a	$Đ_M^b$	DP^a
20	0.70	4100	4600	3.81	19

^{a}Determined by ^1H NMR spectroscopic analysis in CDCl$_3$; ^{b}Determined by GPC analysis in CHCl$_3$.
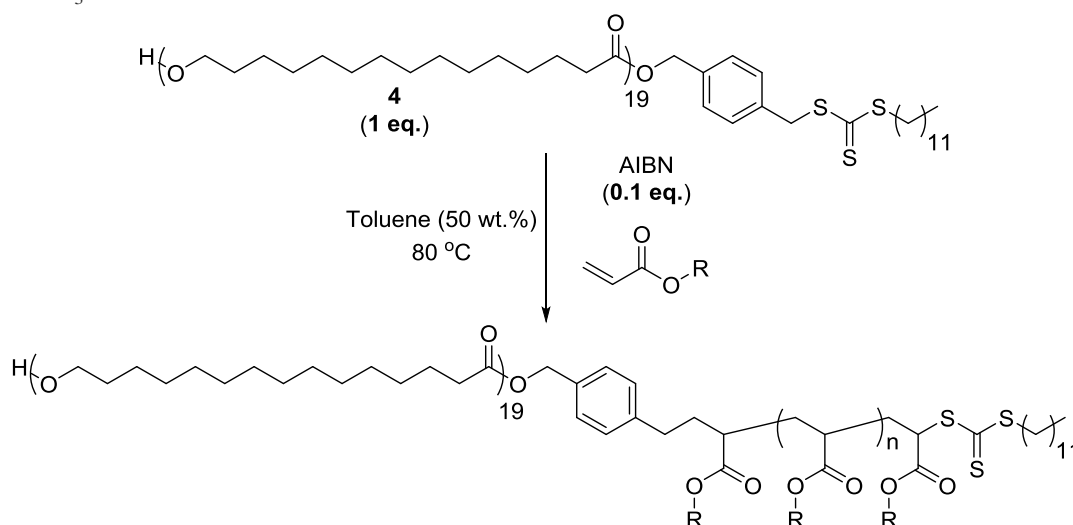
Scheme 3.4: Chain extension of crude DP 19 PPDL macro-CTA **4** to prepare PPDL-*b*-poly(acrylate) copolymers.

Table 3.4: Summary of PPDL-*b*-PEHA copolymers.

Entry	$[M]_0/[I]_0$	Time (min)	$[M]_t/[M]_0$ [a]	M_p (g mol^{-1}) [a]	M_n (g mol^{-1}) [a]	M_n (g mol^{-1}) [b]	$Đ_M$ [a]	DP PEHA [b]	Block Ratio [b]
1	100	8	0.15	10600	9900	8100	1.95	19	1:1
2	100	11	0.56	11400	11200	11600	1.69	38	1:2
3	100	28	0.45	13400	14400	18600	1.45	76	1:4
4	300	15	0.31	22200	19100	31000	1.38	143	1:7.5
5	300	29	0.62	35000	25600	50100	1.46	247	1:13

[a]Determined by ^{1}H NMR spectroscopic analysis in CDCl$_3$; [b]Determined by GPC analysis in CHCl$_3$.

Table 3.5: Summary of PPDL-*b*-PIDA copolymers.

Entry	$[M]_0/[I]_0$	Time (min)	$[M]_t/[M]_0$ [a]	M_p (g mol^{-1}) [a]	M_n (g mol^{-1}) [a]	M_n (g mol^{-1}) [b]	$Đ_M$ [a]	DP PEHA [b]	Block Ratio [b]
1	100	10	0.33	11000	11200	8800	1.83	20	1:1
2	100	17	0.43	12000	12500	12600	1.68	38	1:2
3	100	31	0.62	16000	15400	22000	1.45	82	1:4.3
4	300	15	0.38	24000	18600	28800	1.45	114	1:6

[a]Determined by ^{1}H NMR spectroscopic analysis in CDCl$_3$; [b]Determined by GPC analysis in CHCl$_3$.

Table 3.6 Summary of PPDL-*b*-PLA copolymers.

Entry	$[M]_0/[I]_0$	Time (min)	$[M]_t/[M]_0$ [a]	M_p (g mol^{-1}) [a]	M_n (g mol^{-1}) [a]	M_n (g mol^{-1}) [b]	$Đ_M$ [a]	DP PEHA [b]	Block Ratio [b]
1	100	10	0.25	10900	10100	9100	1.95	19	1:1
2	100	17	0.42	14400	12800	15400	1.63	45	1:2.4
3	100	31	0.55	18500	17400	22800	1.40	76	1:4
4	300	23	0.46	34400	27300	48600	1.35	183	1:9.6
5	300	23	0.59	37300	28900	59900	1.36	230	1:12

[a]Determined by ^{1}H NMR spectroscopic analysis in CDCl$_3$; [b]Determined by GPC analysis in CHCl$_3$.

Table 3.7: Summary of PPDL-*b*-PSA copolymers.

Entry	$[M]_0/[I]_0$	Time (min)	$[M]_t/[M]_0$ [a]	M_p (g mol^{-1}) [a]	M_n (g mol^{-1}) [a]	M_n (g mol^{-1}) [b]	$Đ_M$ [a]	DP PEHA [b]	Block Ratio [b]
1	100	9	0.18	10700	12000	10700	1.64	19	1:1
2	100	17	0.37	17100	16200	19800	1.40	47	1:2.5
3	100	27	0.50	20000	18000	29600	1.37	77	1:4
4	300	21	0.51	40300	29100	70100	1.43	202	1:10.6

[a]Determined by ^{1}H NMR spectroscopic analysis in CDCl$_3$; [b]Determined by GPC analysis in CHCl$_3$.

All of the polymers exhibit a good correlation between an increase in the M_n and M_p evaluated by GPC, and an increase in acrylic block ratio as evaluated by ^{1}H NMR spectroscopy. Furthermore, a good correlation exists between increasing acrylic block length and decreasing polymer dispersity, indicating good control of the chain extension polymerization reaction. GPC chromatograms of the polymers precipitated to remove monomer and cyclic PPDL oligomers (Figures 3.11-3.14) are predominantly monomodal, noting that the low molecular weight shoulders observed, particularly in low molecular weight copolymers, are resolved oligomers.
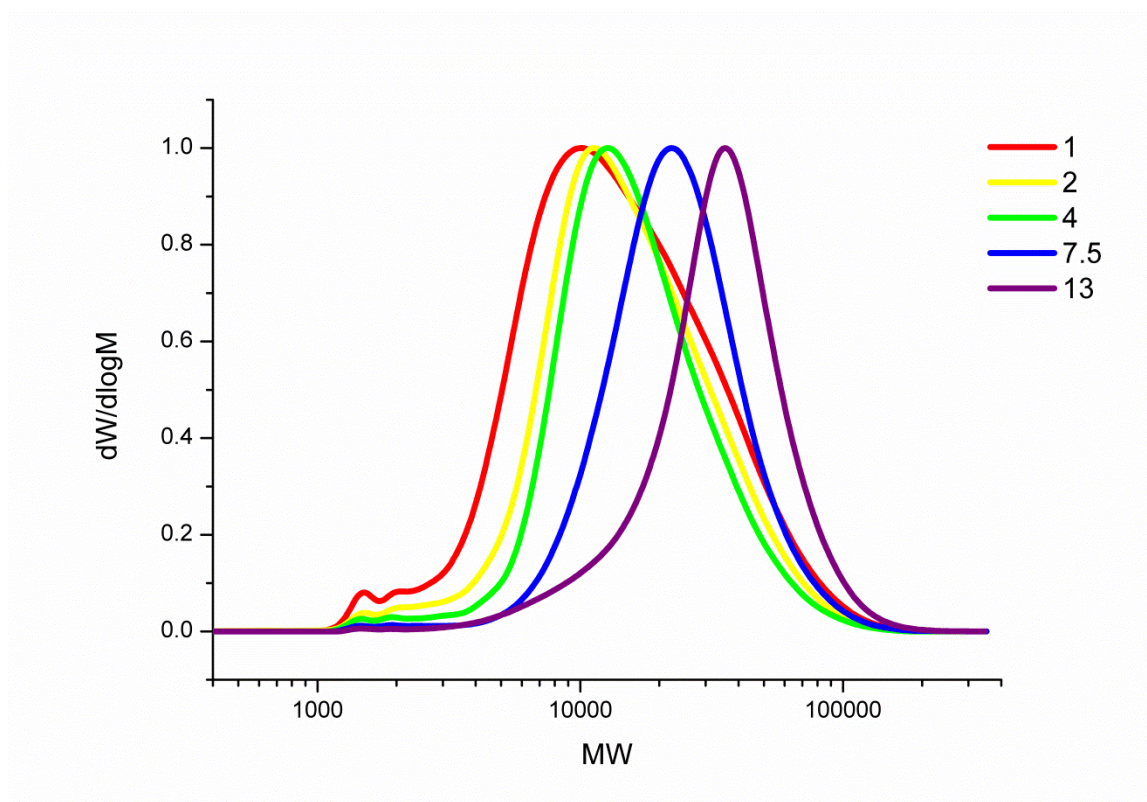
Figure 3.11: GPC (CHCl$_3$) chromatograms of PPDL-*b*-PEHA copolymers described in Table 3.4 (DP PPDL:PEHA = 1:1, 1:2, 1:4, 1:7.5, and 1:13).
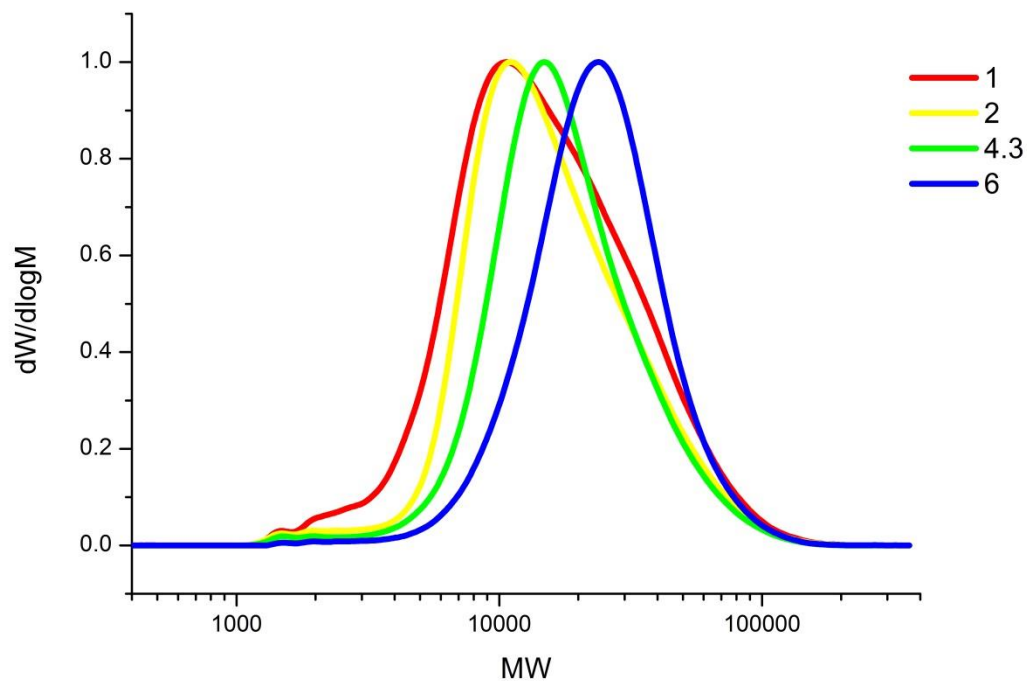
Figure 3.12: GPC (CHCl$_3$) chromatograms of PPDL-*b*-PIDA copolymers described in Table 3.5 (DP PPDL:PIDA = 1:1, 1:2, 1:4.3, and 1:6).
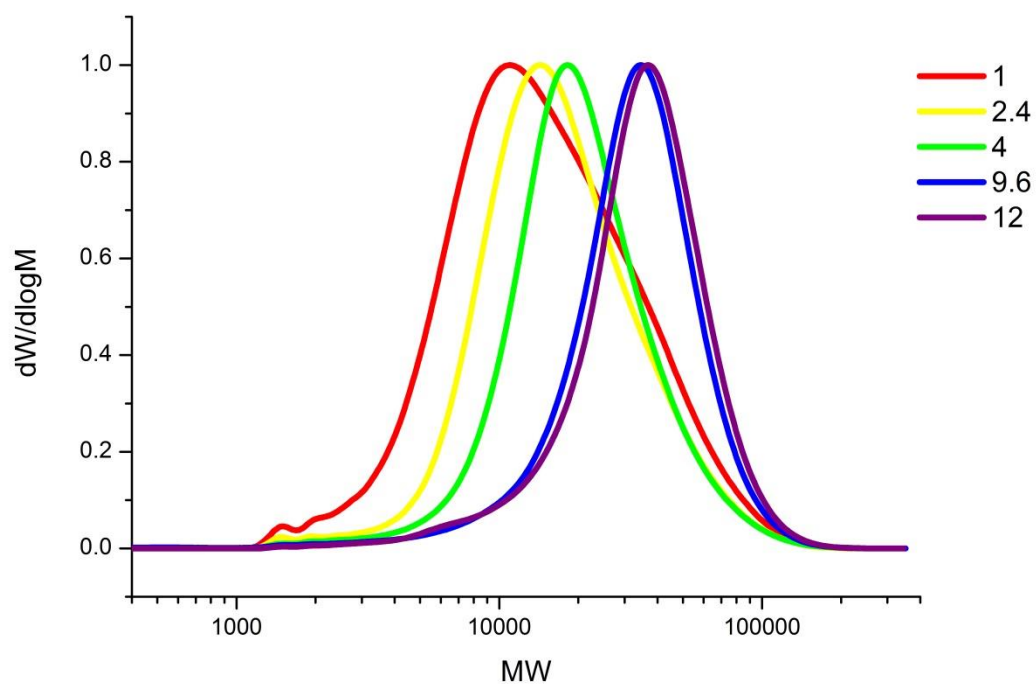
Figure 3.13: GPC (CHCl$_3$) chromatograms of PPDL-*b*-PLA copolymers described in Table 3.6 (DP PPDL:PLA = 1:1, 1:2.4, 1:4, 1:9.6, and 1:12).
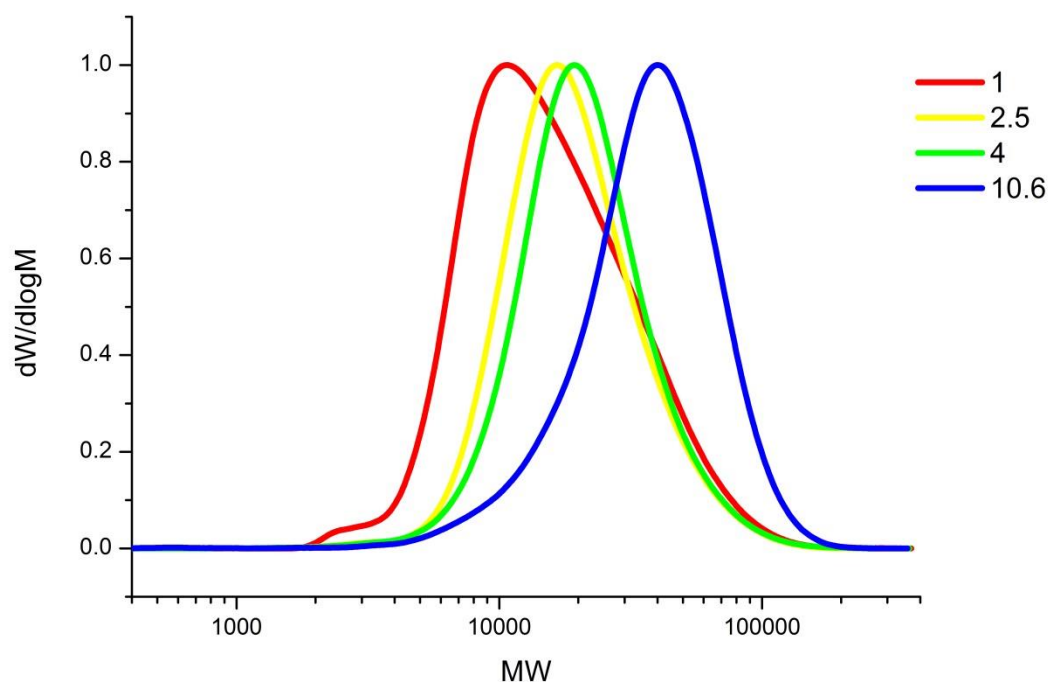
Figure 3.14: GPC (CHCl$_3$) chromatograms of PPDL-*b*-PSA copolymers described in Table 3.7 (DP PPDL:PSA = 1:1, 1:2.5, 1:4, and 1:10.6).

In order to evaluate the end group fidelity of the precipitated copolymers, RI and UV-GPC (CHCl$_3$, 309 nm) data was acquired (Figure 3.15). Importantly, it was determined that all 1:1 block copolymers were UV inactive in the high molecular weight range, indicating the presence of PPDL homopolymer that is not functionalized with initiator **1**, as similarly observed in the overlay of the RI and UV-GPC chromatograms of macro-CTA **4** (Figure 3.16). This observation is consistent with de Geus *et al.*'s[19] conclusion that water initiation dominates the initial eROP process. Specifically, initiation in eROP predominates from trace water present for the enzyme to function, however as the reaction progresses, the intended initiator becomes incorporated into the polymer *via* the transesterification mechanism of the enzyme. Therefore, the longer the reaction takes place, the greater the probability of the intended initiator functionalizing the polymer product. Importantly, the structure of the initiator must be carefully considered to ensure that it cannot be further transesterified in order to ensure that it does not become incorporated into the polymer main chain.

Preparation of a larger second block, however, facilitated purification of the block copolymer from PPDL homopolymer. In general, the mid-length block copolymers exhibit similar RI and UV GPC chromatograms, indicating good end-group fidelity and substantiating the preparation of block copolymer architecture. Importantly, the larger acrylic ratio block copolymer

samples 1:13 PPDL-*b*-PEHA and 1:10.6 PPDL-*b*-PSA exhibit bimodal UV-GPC chromatograms, indicating significant branching *via* backbiting β-scission reactions at the monomer conversions obtained, specifically 62% and 51%, respectively.
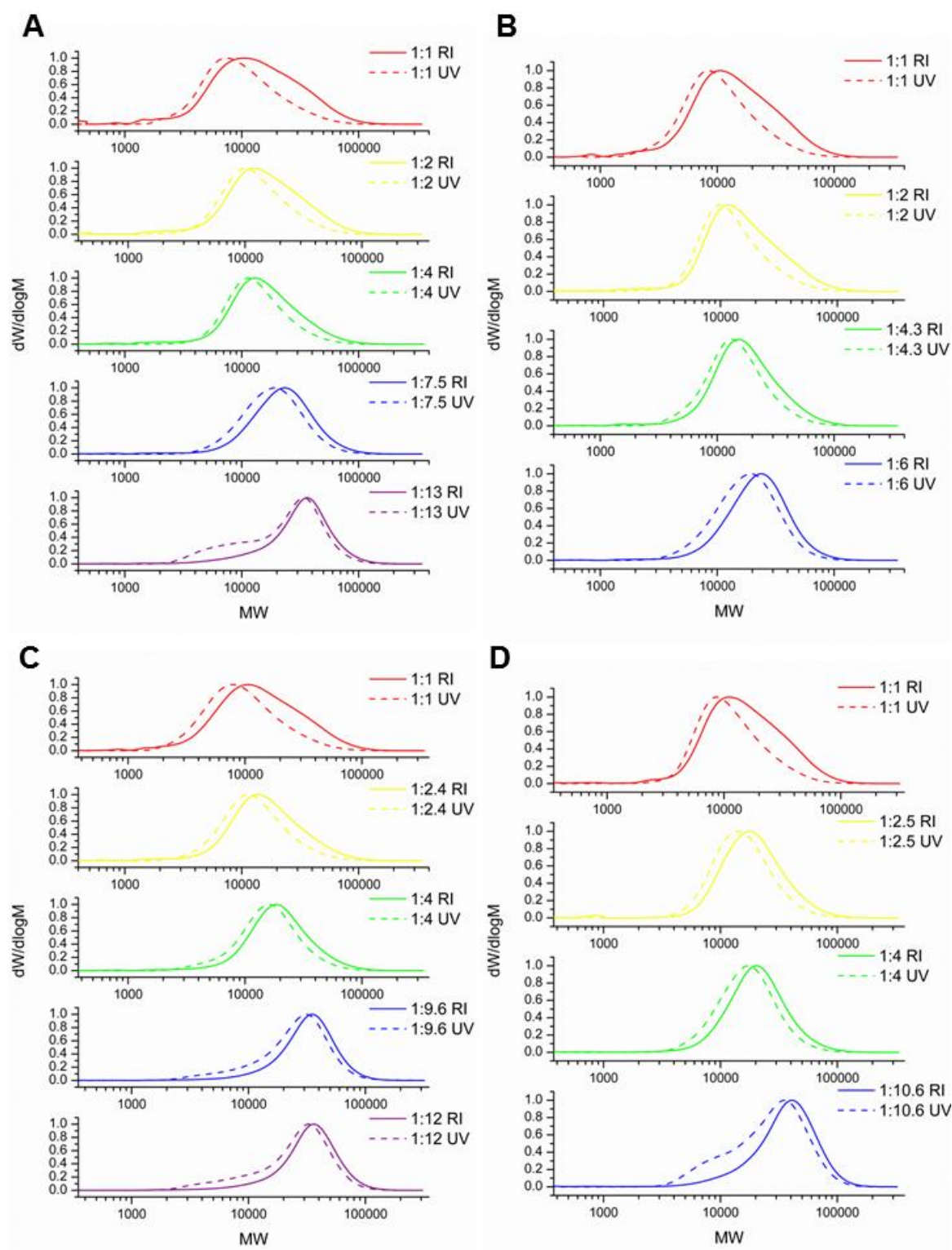
Figure 3.15: Overlay of RI and UV-GPC (CHCl$_3$, 309 nm) chromatograms of PPDL-*b*-poly(acrylate) copolymers described in Tables 3.4-3.7: A) DP PPDL:PEHA = 1:1, 1:2, 1:4, 1:7.5, 1:13, B) DP PPDL:PIDA = 1:1, 1:2, 1:4.3, 1:6, C) DP PPDL:PLA = 1:1, 1:2.4, 1:4, 1:9.6, 1:12, D) DP PPDL:PSA = 1:1, 1:2.5, 1:4, 1:10.6.
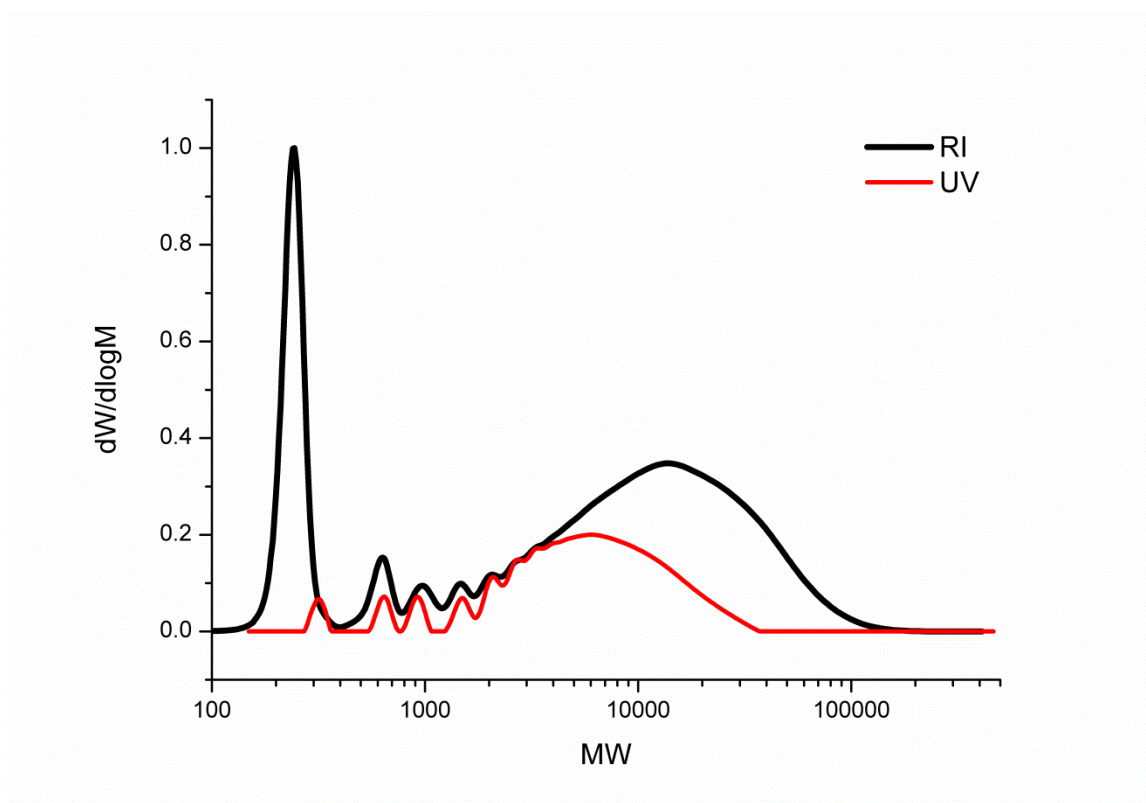
Figure 3.16: Overlay of RI and UV-GPC (CHCl$_3$, 309 nm) chromatogram of crude DP 19 PPDL macro-CTA **4**.

DSC analysis of the copolymers (Figure 3.17) indicate that the onset crystallization temperature decreases as the size of the acrylic block increases, which substantiates the assertion that the copolymers are block copolymers. Furthermore, the polymers exhibit markedly different physical appearances (Figures 3.18-3.21). Specifically, they dramatically decrease in crystallinity with increasing acrylic block length, with the exception of PPDL-*b*-PSA copolymers, all of which appear crystalline following side chain intermolecular aggregation.[20]
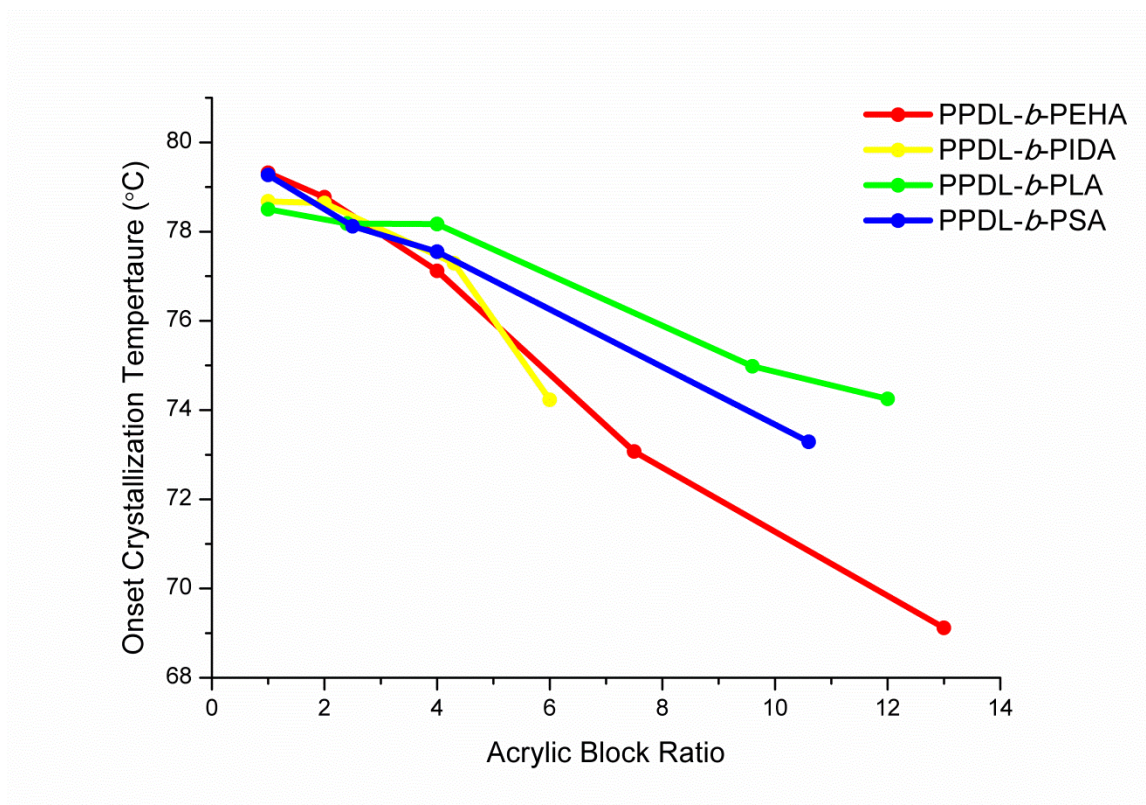
Figure 3.17: Onset crystallization temperatures for PPDL-*b*-poly(acrylate) copolymers described in Tables 3.4 – 3.7, as determined by DSC analysis.

Figure 3.18: Image of PPDL-*b*-PEHA copolymers described in Table 3.4 (Left to right: DP PPDL:PEHA = 1:1, 1:2, 1:4, 1:7.5, and 1:13).

Figure 3.19: Image of PPDL-*b*-PIDA copolymers described in Table 3.5 (Left to right: DP PPDL:PIDA = 1:1, 1:2, 1:4.3, 1:6).

Figure 3.20: Image of PPDL-*b*-PLA copolymers described in Table 3.6 (Left to right: DP PPDL:PLA = 1:1, 1:2.4, 1:4, 1:9.6, 1:12).

Figure 3.21: Image of PPDL-*b*-PSA copolymers described in Table 3.7 (Left to right: DP PPDL:PSA = 1:1, 1:2.5, 1:4, 1:10.6).

MALDI-ToF mass spectrometry is not routinely utilized to characterize copolymers since a complex mixture of distribution patterns is generally observed (Figure 3.22). However, since the molecular weight of PDL and LA are exactly the same, namely 240.38 g mol^{-1}, a single distribution pattern is expected in the MALDI-ToF mass spectrum of these copolymers. MALDI-ToF mass spectra were therefore acquired for several PPDL-*b*-PLA copolymer samples and exhibit both a single distribution pattern (neglecting the presence of cyclic PPDL) and increases in the average mass to charge ratio of the copolymer with increasing acrylic block length, substantiating block copolymer architecture (Figures 3.23 and 3.24). It should be noted, however, that MALDI-ToF mass spectroscopy is not a quantitative technique and since higher molecular weight polymers are less susceptible to ionization, low molecular weight cyclic PPDL homopolymers present in trace quantities are more readily observed when analysing larger molecular weight polymers (Figure 3.24). Importantly, high molecular weight PPDL initiated from water, hypothesized from the overlay of RI and UV-GPC chromatograms (Figures 3.15 and 3.16) was not observed.
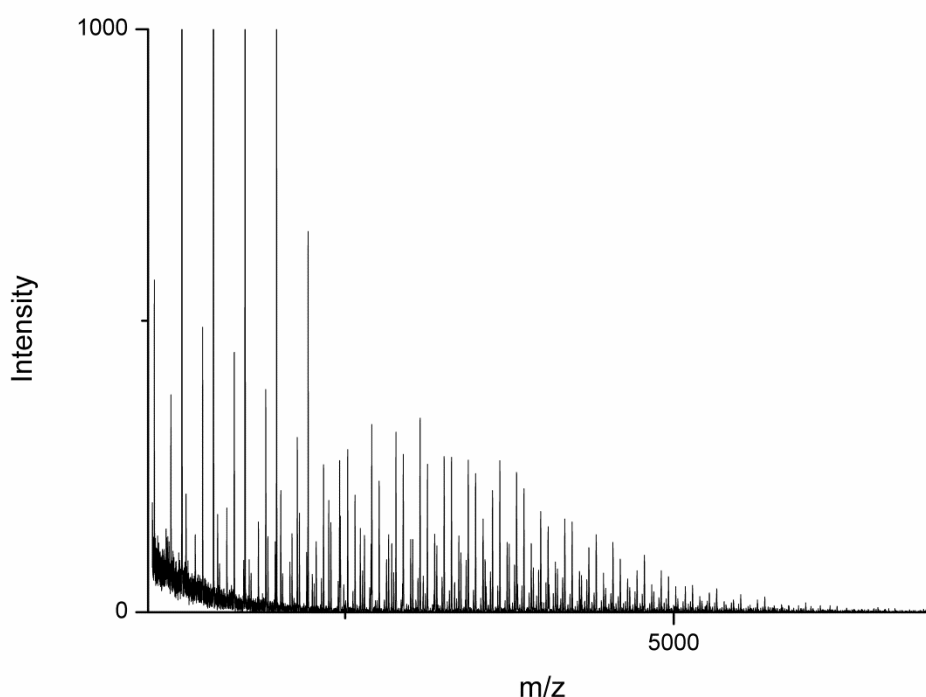
Figure 3.22: MALDI-ToF mass spectrum of PPDL-*b*-PEHA prepared *via* the chain extension of crude PPDL macro-CTA **4** ([M]:[CTA]:[I] = 100:1:0.1) in toluene (50 wt.%).
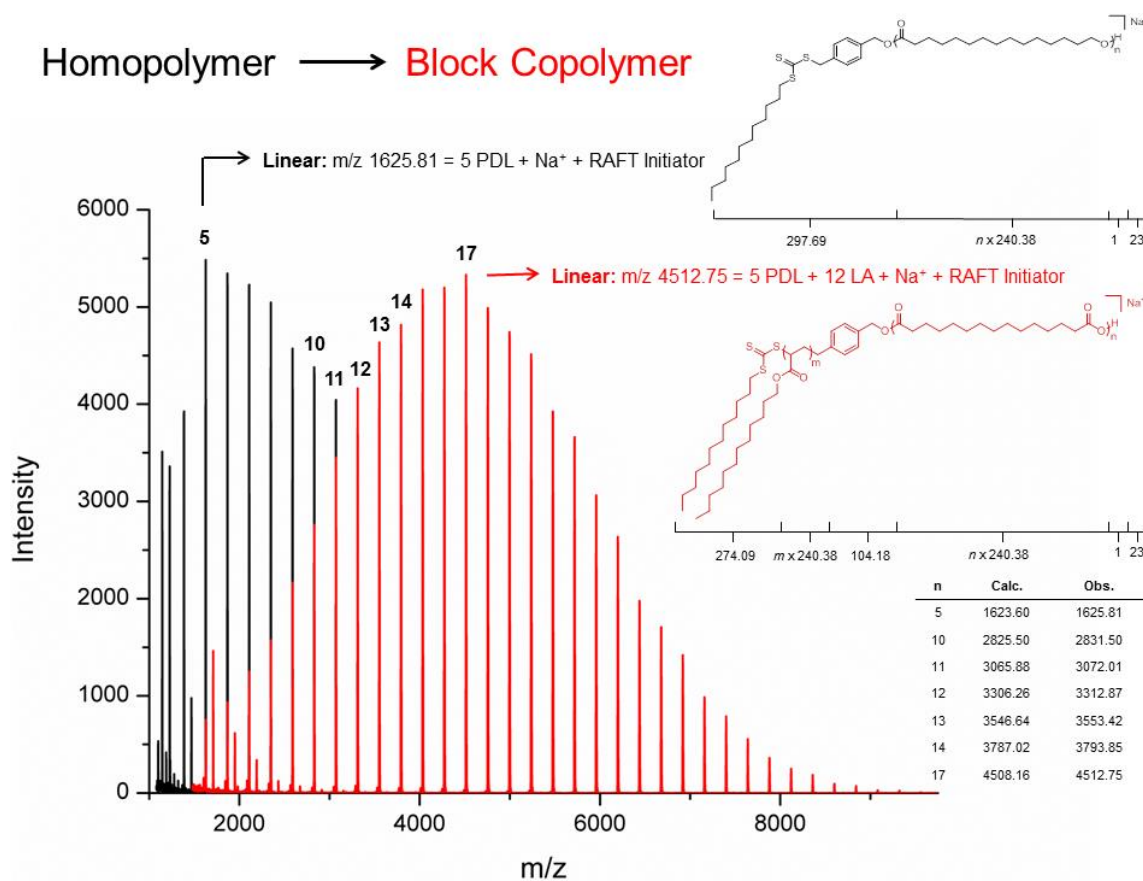
Figure 3.23: Overlay of the MALDI-ToF mass spectra of crude PPDL macro-CTA **4** with 1:1 PPDL-*b*-PLA.
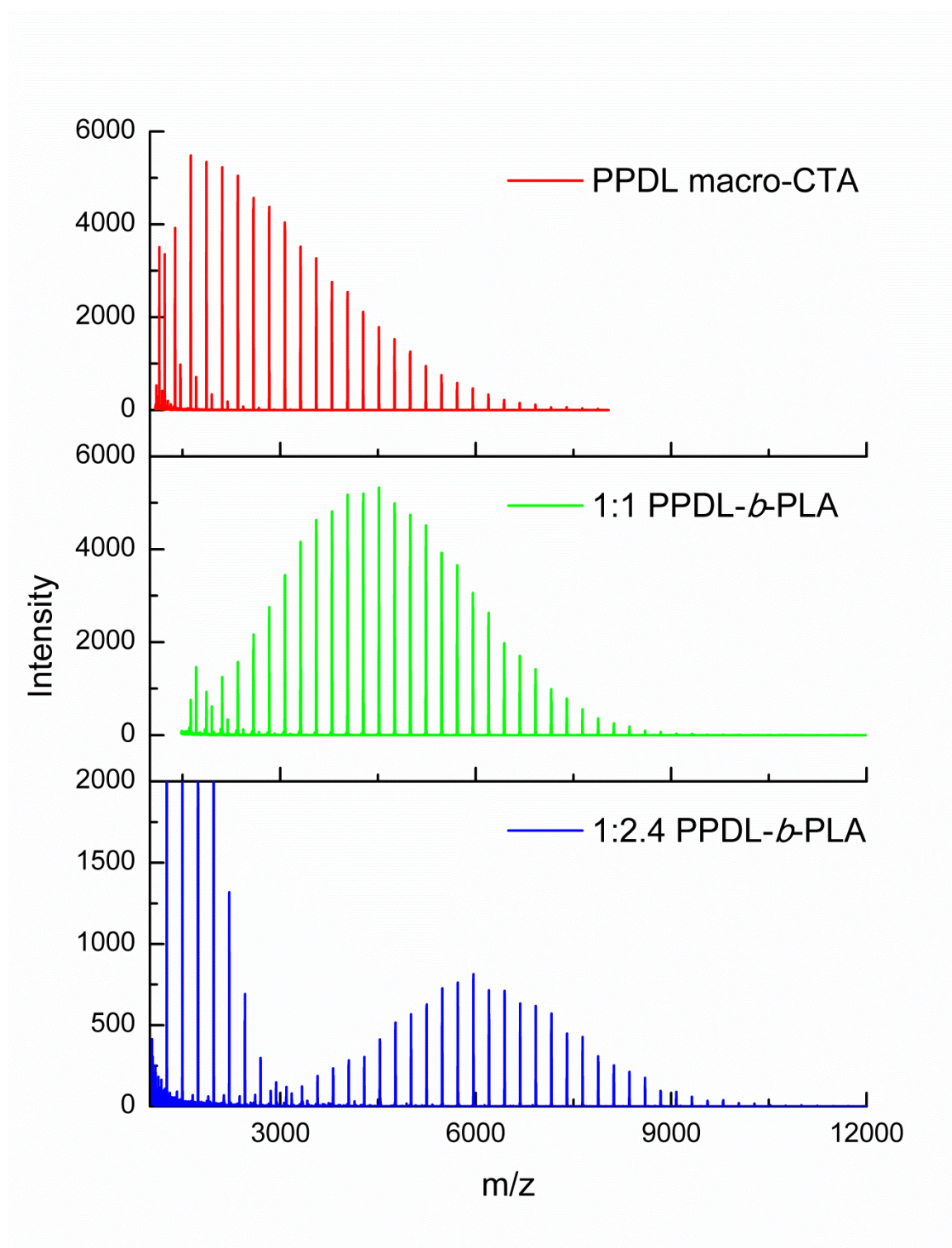
Figure 3.24: MALDI-ToF mass spectra of crude PPDL macro-CTA **4**, 1:1 PPDL-*b*-PLA, and 1:2.4 PPDL-*b*-PLA.

In conclusion, 18 acrylic block copolymers of DP 19 PPDL were prepared with good control of the RAFT chain extension polymerization process, as indicated by good correlations between an increase in M_n and M_p and increasing acrylic block length, and decreasing polymer dispersity. UV-GPC analyses indicate that the precipitated polymers exhibit good end-group fidelity where the acrylic block length is between a ratio of 2 and 10. Below 2, it is suspected that

a significant amount of high molecular weight unfunctionalized PPDL homopolymer exists, which is difficult to remove by precipitation. Above 10, significant branching was observed since the chain extensions were performed to monomer conversions beyond a range of controlled radical polymerization. Finally, the decrease in onset crystallization temperatures as evaluated by DSC, increase in mass to charge ratio in MALDI-ToF mass spectroscopic analyses, and visible decrease in crystallinity of the copolymers with increasing acrylic block length confirm the preparation of block copolymer architecture.

3.2.2.2 Fuels Testing

3.2.2.2.1 Wax Anti-Settling and Crystal Morphology

Stock solutions of the block copolymers (Tables 3.4-3.7) were prepared in Solvesso 150, an aromatic distillate, and left overnight. All of the 1:1 PPDL-*b*-poly(acrylate) copolymers appeared hazy at room temperature and exhibited settling from solution overnight, indicating that the 1:1 PPDL-*b*-poly(acrylate) copolymers are not very soluble in fuel. All other PPDL-*b*-poly(acrylate) copolymers, however, remained in solution overnight. This observation, in combination with UV-GPC data obtained for the block copolymers (Figure 3.15) suggests that the 1:1 copolymers likely contain PPDL homopolymer, which is not soluble in fuel. Therefore, it can be concluded that the acrylic block ratio must be greater than 2 to prepare block copolymers of DP 19 PPDL that are sufficiently large to purify the block copolymer from residual PPDL.

The stock solutions were used to treat a variety of fuels, which were cooled to -18 $^{\circ}$C in a Clive Hurley Cold Room in order to evaluate wax settling and crystal morphology by optical microscopy. A selection of the PPDL-*b*-poly(acrylate) copolymers were used to treat B0 Fuel C (Figure 3.25) with up to 400 ppm of the block copolymers in the absence and presence of additional additives in order to investigate their effect as wax crystal modifiers. B0 Fuel C does not contain any biodiesel, however, contains two distributions of *n*-alkanes with C11-12 and C17 averages. First, B0 Fuel C was treated with 200 ppm of copolymer and the percent wax settling was noted (Table 3.8). In general, all of the polymers, with the exception of the polymers containing stearyl acrylate, exhibited 10% wax settling.
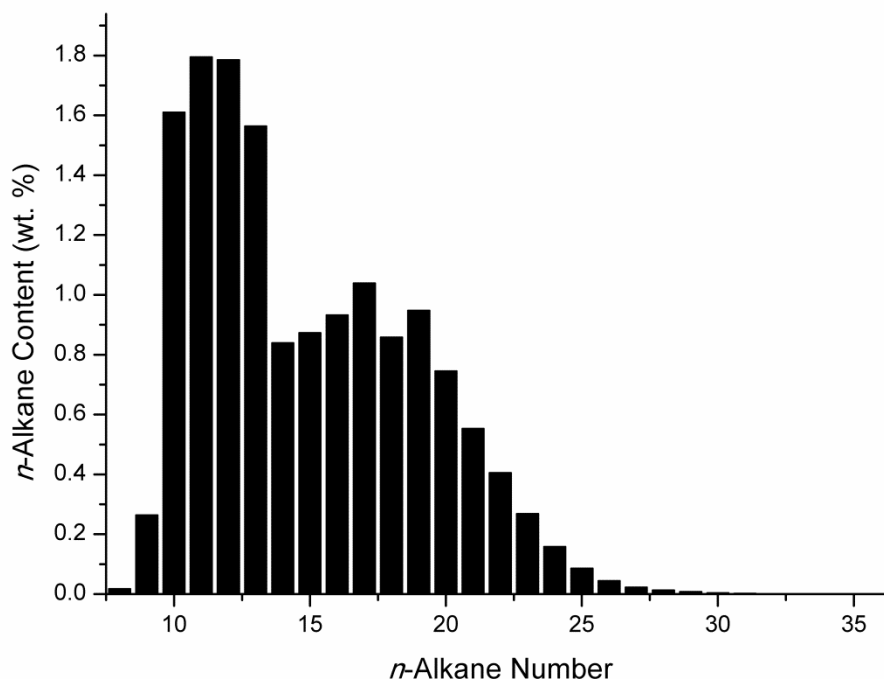
Figure 3.25: Distribution of *n*-alkanes separating from B0 Fuel C.

Table 3.8: Percent wax dispersed in B0 Fuel C treated with 200 ppm of PPDL-*b*-P(acrylates).

Polymer	Percent Wax	Fuel Appearance
1:1 PEHA	90	Hazy
1:13 PEHA	90	Hazy
1:1 PIDA	90	Hazy
1:6 PIDA	90	Hazy
1:1 PLA	90	Hazy
1:12 PLA	90	Hazy
1:1 PSA	100	Hazy
1:10.6 PSA	100	Hazy

The wax crystals were then visualized using an optical microscope. It was determined that, in general, the block copolymers did not decrease the size or morphology of wax crystals obtained – the wax crystals appeared similar to those observed in the base or untreated fuel (Figure 3.26). The copolymers 1:12 PPDL-*b*-PLA and 1:1 PPDL-*b*-PSA, however, appeared to reduce the size of the wax crystals obtained relative to the untreated base fuel (Figures 3.27 and

3.28). Interestingly, needle-like wax crystals were obtained using 1:1 PPDL-*b*-PSA in this fuel at this treat rate. Therefore, although most of the copolymers did not have a positive or negative effect on wax crystallization in this fuel at this treat rate, it can be concluded that 1:12 PPDL-*b*-PLA and 1:1 PPDL-*b*-PSA did have a positive effect on wax crystal morphology, reducing wax crystal size to less than 25 µm and 50 µm, respectively, with 1:1 PPDL-*b*-PSA additionally positively modifying the shape of the wax crystals formed.
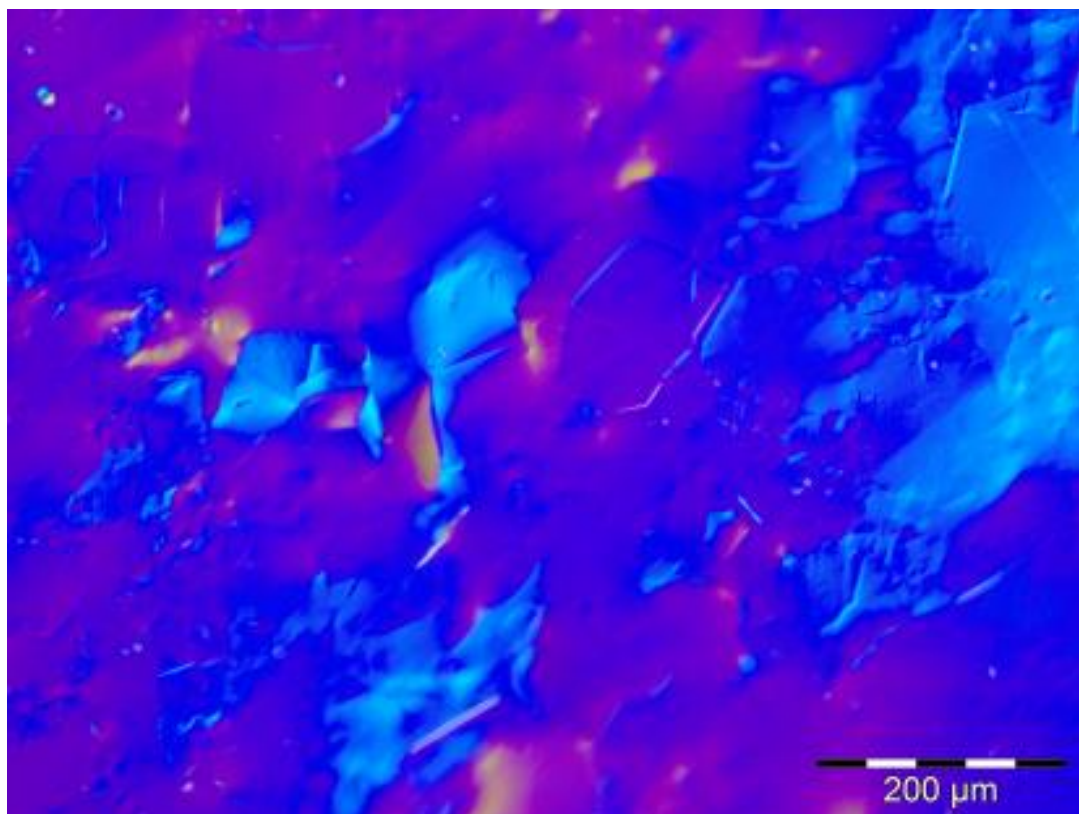
Figure 3.26: Wax crystals observed in untreated B0 Fuel C.
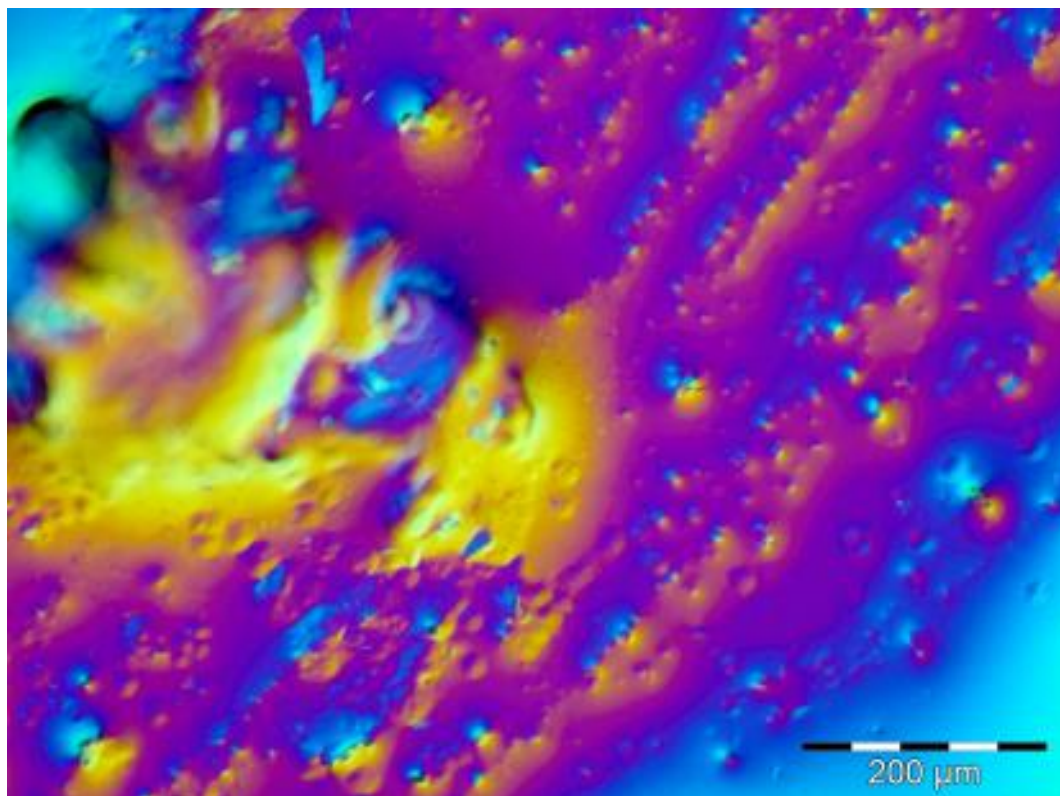
Figure 3.27: Wax crystals observed in B0 Fuel C treated with 200 ppm of 1:12 PPDL-*b*-PLA copolymer.
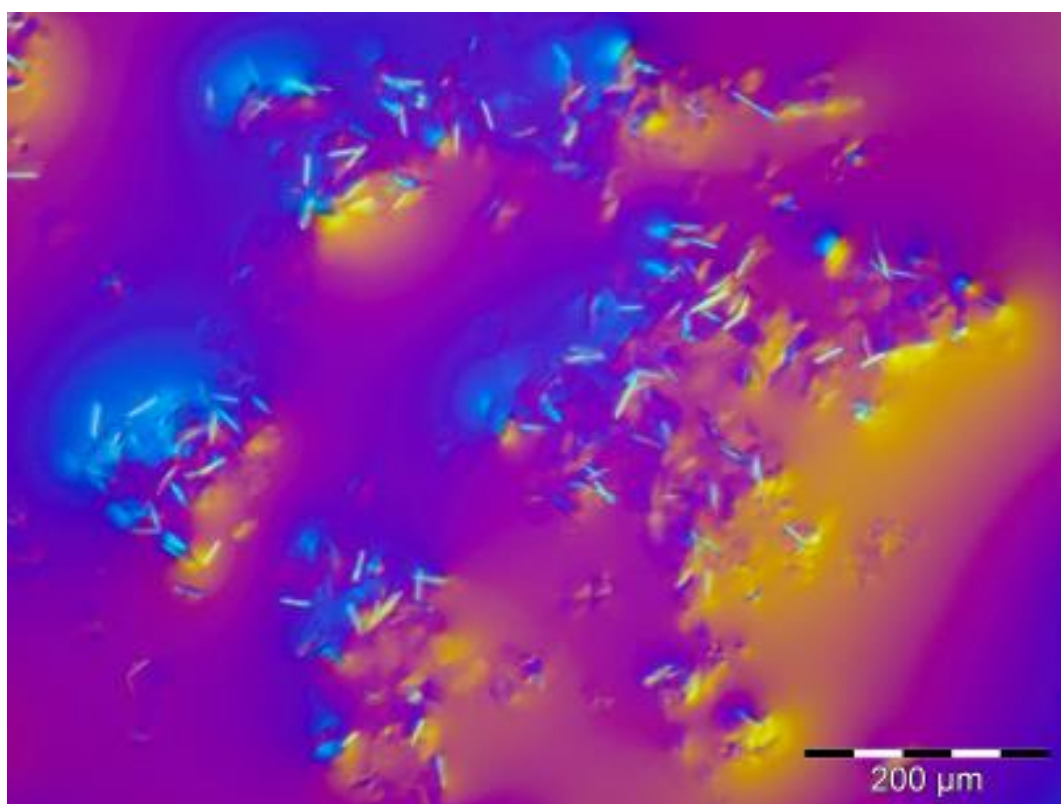
Figure 3.28: Wax crystals observed in B0 Fuel C treated with 200 ppm of 1:1 PPDL-*b*-PSA copolymer.

Thereafter the same fuel was treated with both the selected copolymers and a commercial wax crystal modifier to investigate the performance of the copolymers in combination with other additives since many WCMs exhibit enhanced performance in the presence of other additives. The percent wax settling was noted (Table 3.9) and the wax crystals were visualized using an optical microscope. It was determined that the commercial wax crystal modifier reduces the size of the wax crystals to below 50 μm and yields needle-like morphologies (Figure 3.29). Furthermore, some of the copolymers appeared to further reduce the size of the wax crystals to below 25 μm (Figures 3.30 and 3.31).

Table 3.9: Percent wax dispersed in B0 Fuel C treated with 190 ppm of PPDL copolymer and 10 ppm of a commercial wax crystal modifier.

Polymer	Percent Wax	Fuel Appearance
WCM A	20-30	Hazy
1:1 PEHA	20	Hazy
1:13 PEHA	20	Hazy
1:1 PIDA	20	Hazy
1:6 PIDA	20	Hazy
1:1 PLA	20-30	Hazy
1:12 PLA	20-30	Hazy
1:1 PSA	20-30	Hazy
1:10.6 PSA	20-30	Hazy
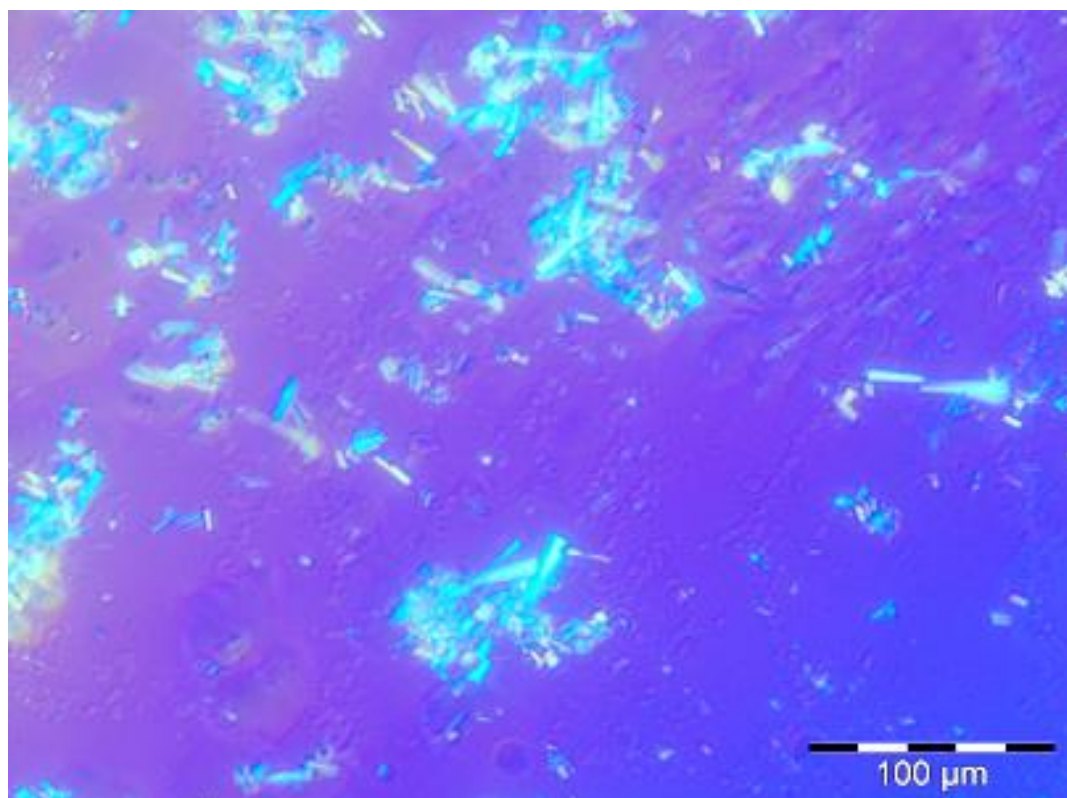
Figure 3.29: Wax crystals observed in B0 Fuel C treated with 200 ppm of commercial wax crystal modifier A.
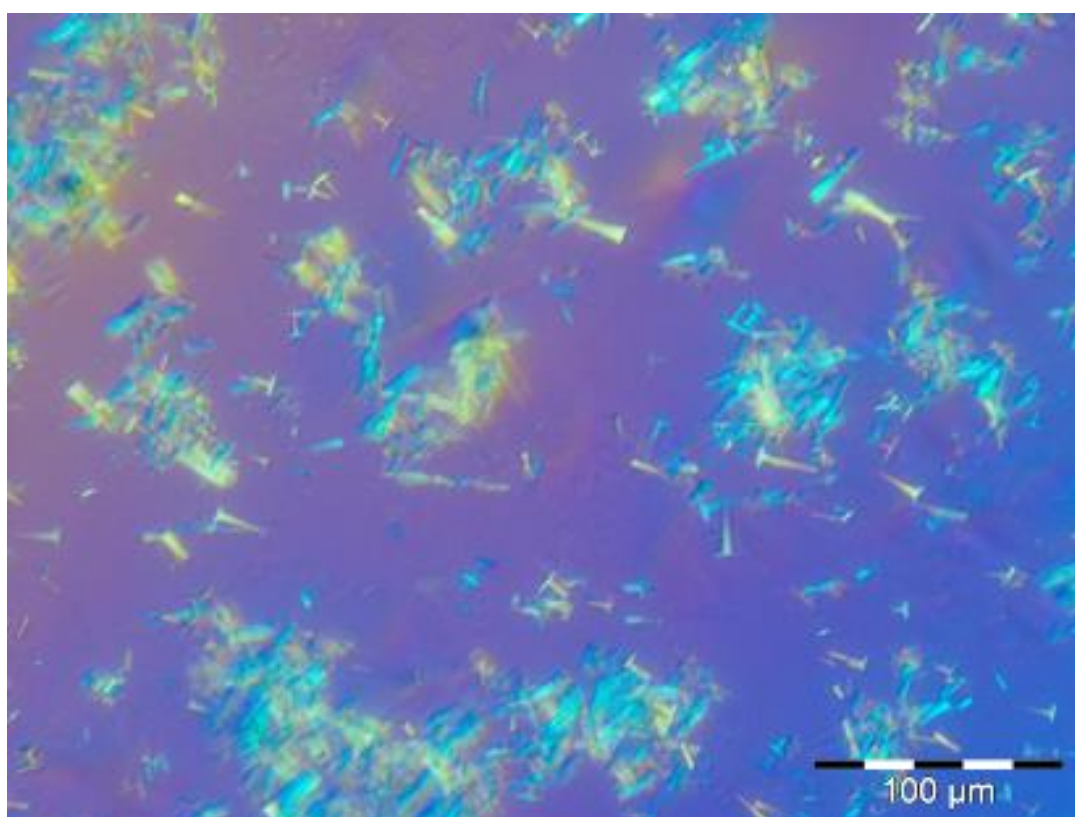
Figure 3.30: Wax crystals observed in B0 Fuel C treated with 190 ppm of 1:12 PPDL-*b*-PLA and 10 ppm of commercial wax crystal modifier A.
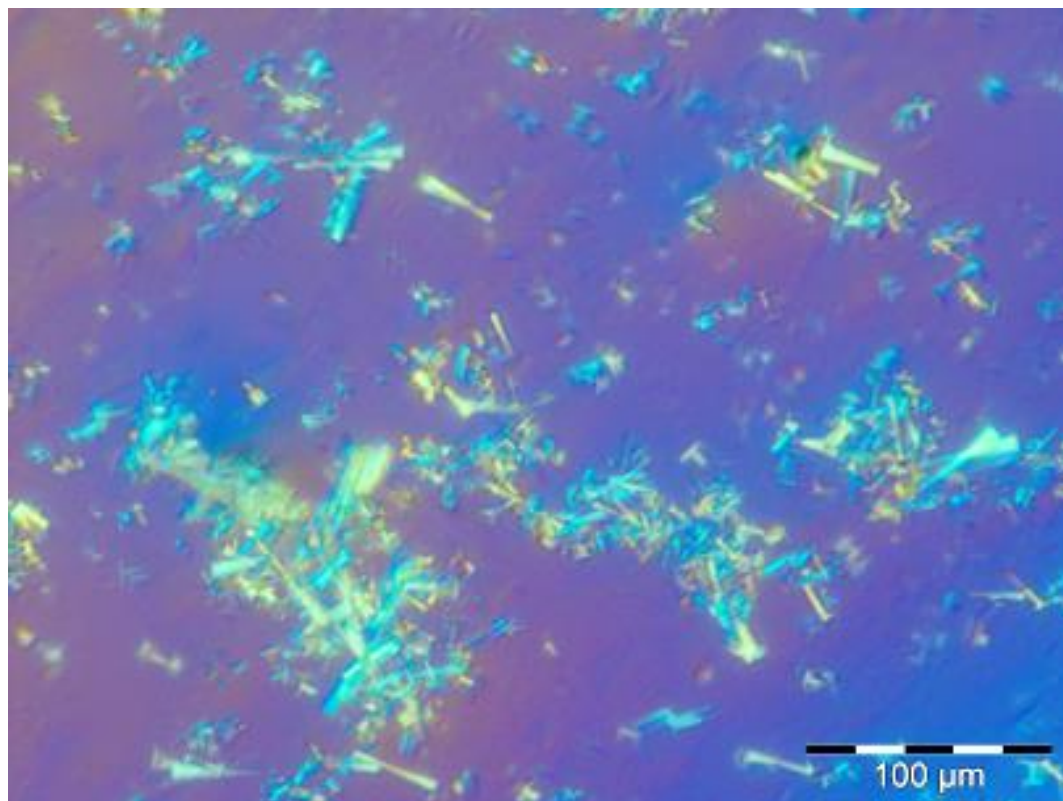
Figure 3.31: Wax crystals observed in B0 Fuel C treated with 190 ppm of 1:1 PPDL-*b*-PSA and 10 ppm of commercial wax crystal modifier A.

Finally, B0 Fuel C was treated with the selected block copolymers, commercial wax crystal modifier A, and a commercial WASA. Although large wax crystals were observed with most of the block copolymers tested, with the exception of 1:10.6 PPDL-*b*-PSA, 1:12 PPDL-*b*-PLA, and 1:4 PPDL-*b*-PLA, a difference in percent wax settling was noted (Table 3.10). The 1:12 and 1:4 PPDL-*b*-PLA copolymers dispersed wax through 90% of the fuel sample, which is superior to many observed commercial diesel additive packages. Significant wax dispersion (50-60%) was also observed with 1:1 PPDL-*b*-PLA, however this sample exhibited large crystals. All other block copolymers tested exhibited inferior wax dispersion relative to the commercial wax crystal modifier, and interestingly, very compact wax settling was observed with 1:10.6 PPDL-*b*-PSA.

Table 3.10: Percent wax dispersed in B0 Fuel C treated with 100 ppm of PPDL copolymer, and 300 ppm of a commercial wax crystal modifier and WASA.

Polymer	Percent Wax	Fuel Appearance
WCM A + WASA	100	No Wax Settling
1:1 PEHA	20-30	Hazy
1:4 PEHA	20-30	Hazy
1:13 PEHA	20-30	Hazy
1:1 PIDA	20-30	Hazy
1:4.3 PIDA	10-20	Hazy
1:6 PIDA	10	Hazy
1:1 PLA	50-60	Hazy
1:4 PLA	5	Hazy
1:12 PLA	5-10	Hazy
1:1 PSA	30	Hazy
1:4 PSA	20-30	Hazy
1:10.6 PSA	5-10	Hazy

Ultimately, it was determined that the PPDL-*b*-poly(acrylate) copolymers, with the exception of 1:12 PPDL-*b*-PLA and 1:1 PPDL-*b*-PSA, did not have a significant positive or negative effect on wax crystal morphology or wax dispersion. This is not necessary a negative finding since many commercial WCMs similarly do not influence wax crystal morphology or dispersion when used in the absence of other commercial fuel additives. Interestingly, varied wax dispersion was noted using the copolymers in combination with both a commercial wax crystal modifier and WASA. In order to evaluate the performance of the copolymers across multiple fuels with different *n*-alkane distribution and base CFPP performance, a number of fuels were treated with selected PPDL-*b*-poly(acrylate) polymers for CFPP testing.

3.2.2.2.2   CFPP Testing

PPDL-*b*-poly(acrylate) copolymers underwent CFPP testing at Infineum UK Ltd. Initial tests determined the CFPP of a selection of the copolymers in B0 Fuel C at various treat rates (Figure 3.32). It was determined that 300 ppm is a good treat rate to screen PPDL-*b*-poly(acrylate) copolymers since, although better performance is observed with some of the copolymers using higher treat rates, others exhibit reduced performance at 400 ppm. In general,

none of the copolymers hindered CFPP performance, with the exception of 1:1 PPDL-*b*-PLA, which increased the CFPP by 0.5 $^{\circ}$C relative to the base fuel, except at a treat rate of 400 ppm, where the CFPP was decreased by 3 $^{\circ}$C. Furthermore, it was determined that PPDL-*b*-poly(acrylate) copolymers maintaining branched acrylates generally exhibit superior CFPP performance in this fuel, specifically improving the CFPP by up to 7 $^{\circ}$C.
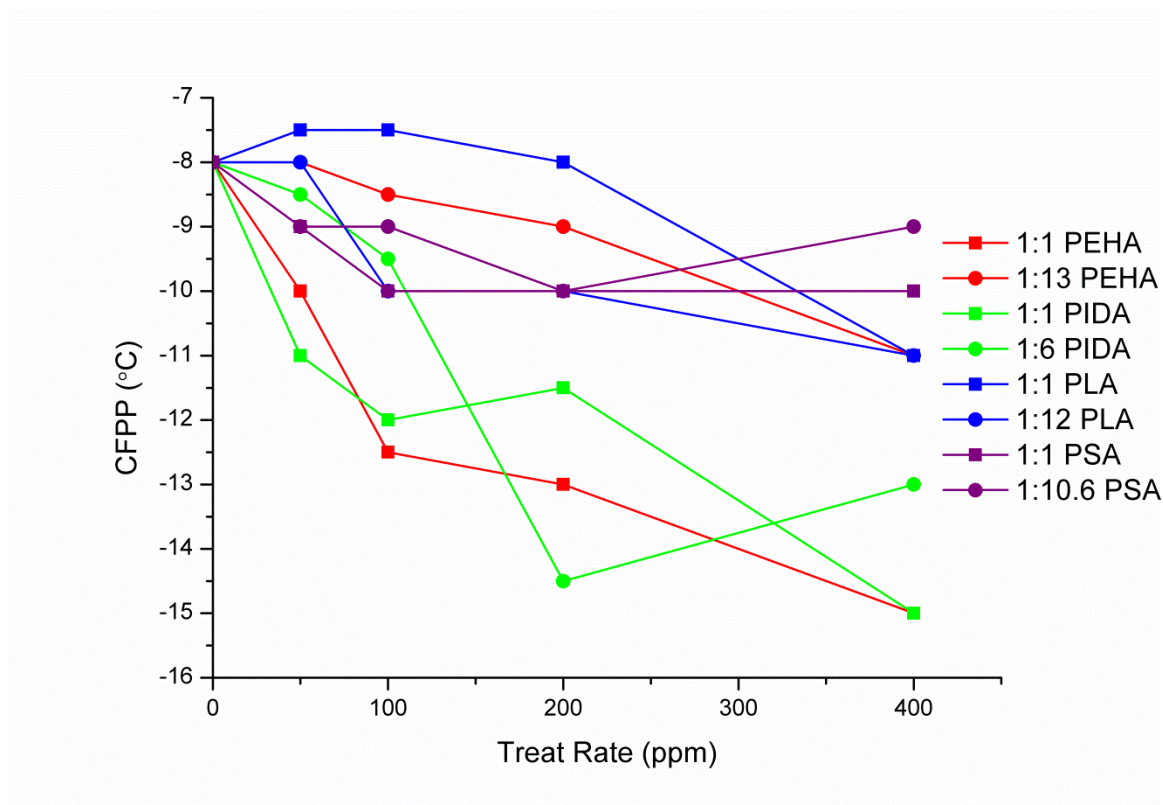
Figure 3.32: CFPP performance of selected PPDL-*b*-poly(acrylate) copolymers in B0 Fuel C at various treat rates.

The CFPP performance of selected copolymers was further evaluated in additional fuels, specifically B0 Fuel D, B0 Fuel E, and B0 Fuel B (Table 3.11). Fuel D does not contain any biodiesel and maintains significant C16-17 *n*-alkane content (Figure 3.33). Fuel E also does not contain any biodiesel and maintains a C17 average *n*-alkane content, although with a significant amount of C13 *n*-alkane (Figure 3.34). Finally, Fuel B does not contain any biodiesel and maintains a broad distribution of lower molecular weight *n*-alkanes, with the predominant *n*-alkane being C10 (Figure 3.9). At a treat rate of 300 ppm, the block copolymers did not improve the performance of B0 Fuel D. The copolymers did, however, exhibit a moderate (up to 4 ^{0}C) and significant (up to 11 ^{0}C) improvement in the CFPP performance in B0 Fuel E and B0 Fuel B, respectively, and importantly did not hinder the performance of the fuels, unlike with B0 Fuel D. It is possible that the copolymers did not significantly alter the CFPP performance of Fuel D since this fuel maintains a much lower CFPP relative to other fuels tested.
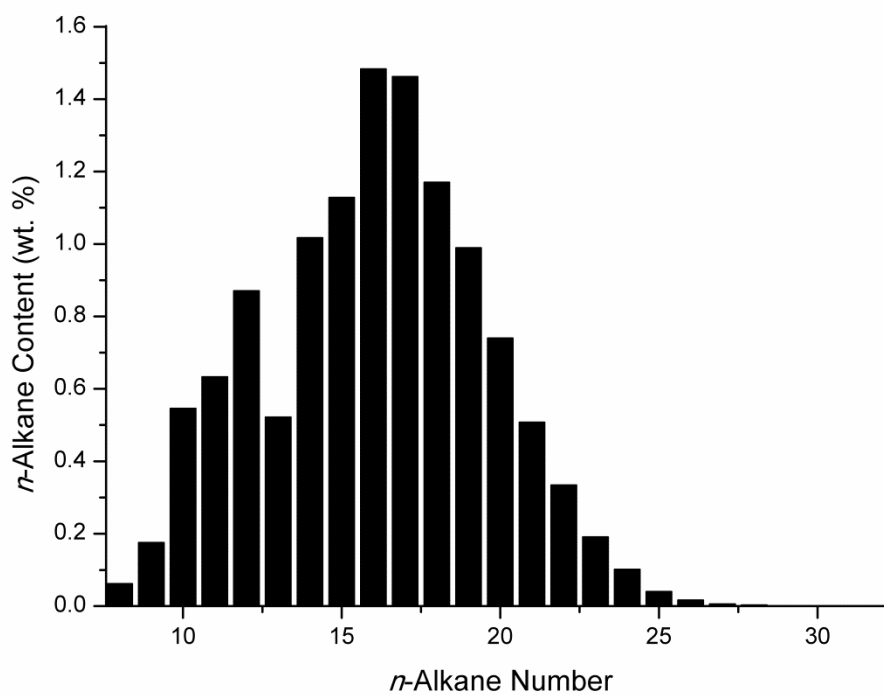
Figure 3.33: Distribution of *n*-alkanes separating from B0 Fuel D.
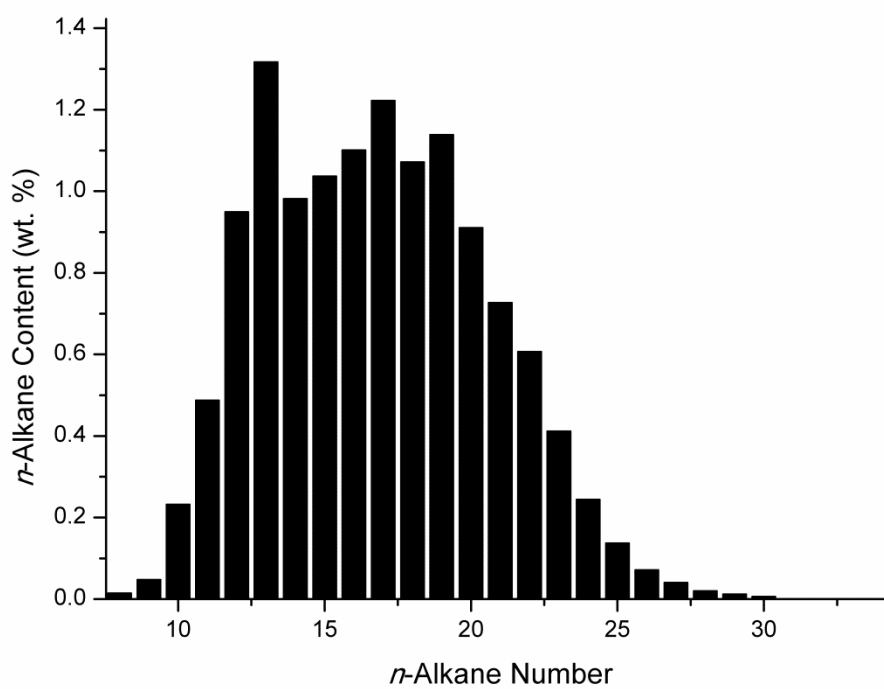
Figure 3.34: Distribution of *n*-alkanes separating from B0 Fuel E.

Table 3.11: CFPP performance of selected PPDL-*b*-poly(acrylate) block copolymers in various fuels at a treat rate of 300 ppm.

Polymer	CFPP (°C)		
	B0 Fuel D	**B0 Fuel E**	**B0 Fuel B**
Basefuel	-15	-3.5	-7.5
1:1 PEHA	-15	-7.5	-16
1:13 PEHA	-14.5	-3.5	-18.5
1:1 PIDA	-14	-6.5	-16.5
1:6 PIDA	-15	-5	-18
1:1 PLA	-14	-5	-9
1:12 PLA	-13	-6	-13.5
1:1 PSA	-14.5	-5	-9
1:10.6 PSA	-14	-5.5	-8
CFPP Δ_{max}	0	4	11

B0 Fuel B was therefore selected to perform CFPP testing with all 18 of block copolymer samples and it was determined that all polymers had a positive impact on the CFPP performance of this fuel at this treat rate (Table 3.12). Furthermore, copolymers maintaining branched acrylates, namely PPDL-*b*-PEHAs and PPDL-*b*-PIDAs, exhibited superior performance relative to copolymers maintaining linear acrylates, with PPDL-*b*-PSAs exhibiting the poorest performance.

Table 3.12: CFPP performance of PPDL-*b*-poly(acrylate) block copolymers in B0 Fuel B at a treat rate of 300 ppm.

Polymer	CFPP (°C)
	B0 Fuel B
Basefuel	-7.5
1:1 PEHA	-19
1:2 PEHA	-16
1:4 PEHA	-16.5
1:7.5 PEHA	-16.5
1:13 PEHA	-15.5
1:1 PIDA	-16
1:2 PIDA	-16
1:4.3 PIDA	-17.5
1:6 PIDA	-17
1:1 PLA	-16
1:2.4 PLA	-15.5
1:4 PLA	-14
1:9.6 PLA	-14.5
1:12 PLA	-14.25
1:1 PSA	-10
1:2.5 PSA	-9
1:4 PSA	-8.5
1:10.6 PSA	-9.5
CFPP Δ_{max}	11.5

The CFPP performance was thereafter evaluated in B10 Fuel F, which contains 10% biodiesel with high C10-13 *n*-alkane content (Figure 3.35). The CFPP performance was measured at various treat rates and all polymers, except 1:1 PPDL-*b*-PSA at a treat rate of 100 ppm, had a positive impact on the CFPP performance in this fuel (Figure 3.36). In general, significant improvements were observed with treat rates up to 300 ppm, after which only marginal improvements were observed. Furthermore, copolymers maintaining branched acrylates exhibited a superior performance relative to copolymers maintaining linear acrylates.
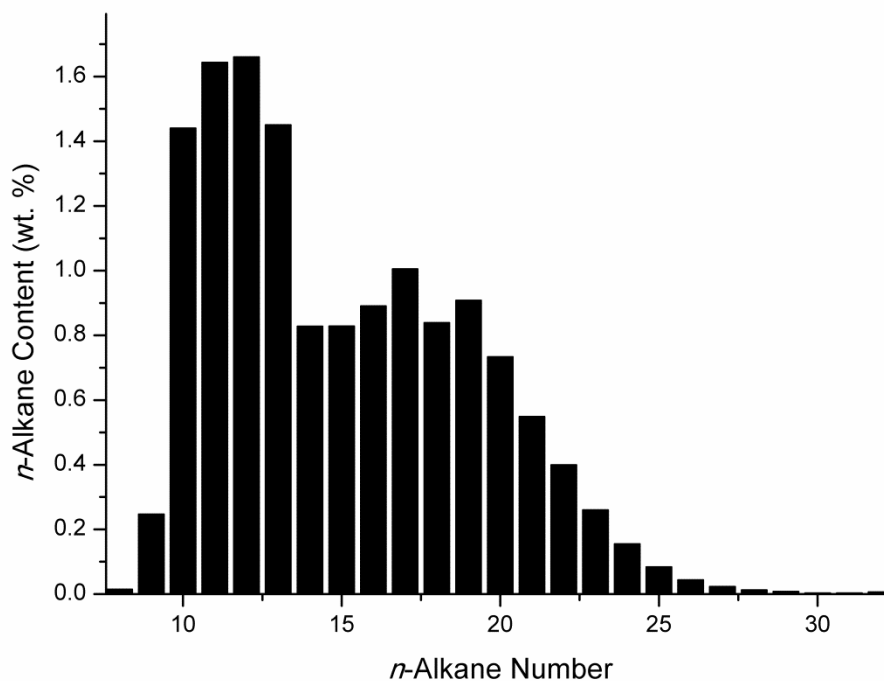
Figure 3.35: Distribution of *n*-alkanes separating from B10 Fuel F.
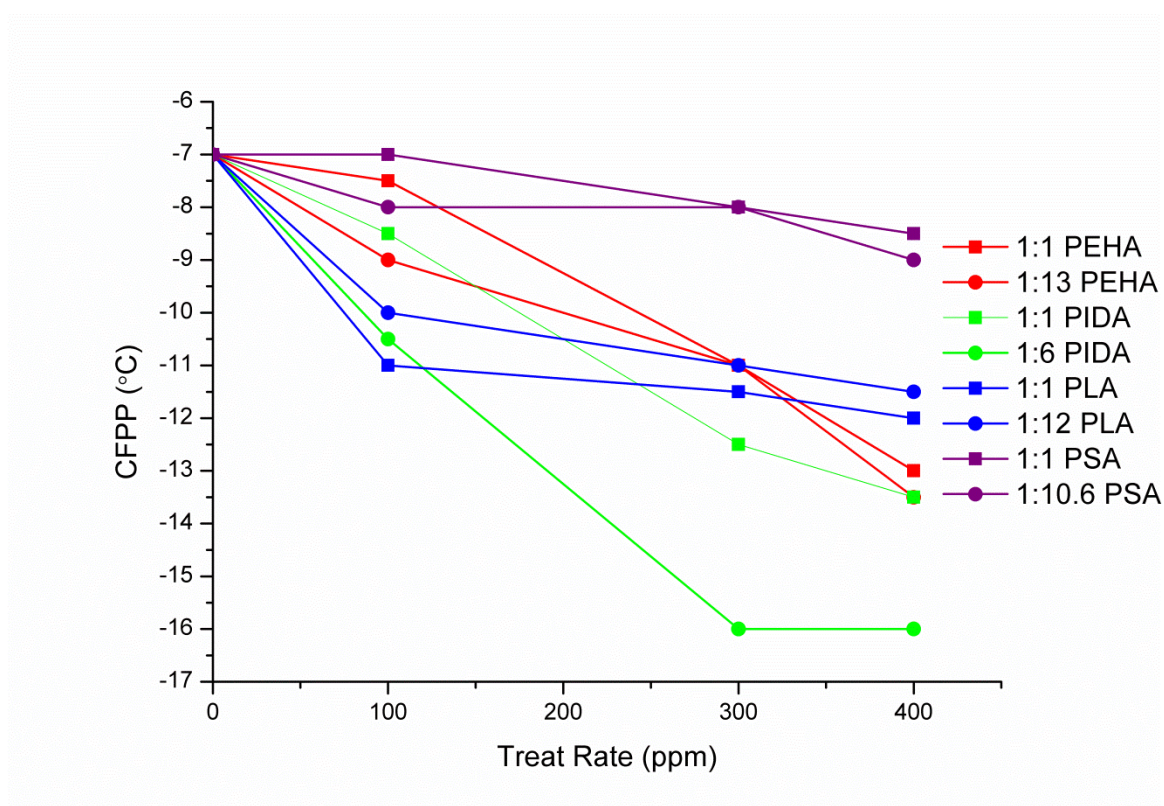
Figure 3.36: CFPP performance of selected PPDL-*b*-poly(acrylate) copolymers in B10 Fuel F at various treat rates.

The CFPP performance of the block copolymers was further evaluated in the narrow distillate B2 Fuel A (Figure 3.7). It was determined that all polymers had a positive impact on the CFPP performance in this fuel at this treat rate (Table 3.13). Exhibiting up to a 9.5 ^{o}C improvement in CFPP performance, it was similarly determined that copolymers maintaining branched acrylates exhibit superior CFPP performance relative to copolymers maintaining linear acrylates. The CFPP performance of the copolymers was thereafter evaluated in combination with commercial wax crystal modifier A in B0 Fuel C. The commercial wax crystal modifier improved the CFPP performance of this fuel by 14 ^{o}C (Table 3.14), however, it was determined that the polymers did not significantly alter the CFPP performance of this fuel at that treat rate relative to the commercial wax crystal modifier.

Table 3.13: CFPP performance of selected PPDL-*b*-poly(acrylate) block copolymers in B2 Fuel A at a treat rate of 100 ppm.

Polymer	CFPP (^{o}C)
	B2 Fuel A
Basefuel	-9
1:1 PEHA	-18.5
1:13 PEHA	-16
1:1 PIDA	-17.5
1:6 PIDA	-17
1:1 PLA	-11
1:12 PLA	-13
1:1 PSA	-10
1:10.6 PSA	-12
CFPP Δ_{max}	9.5

Table 3.14: CFPP performance of selected PPDL-*b*-poly(acrylate) block copolymers (20 ppm) in combination with commercial wax crystal modifier A (180 ppm) in B0 Fuel C.

Polymer	CFPP (°C)
	B0 Fuel C
Basefuel	-8
Basefuel + WCM A (200 ppm)	-22
1:1 PEHA	-20
1:13 PEHA	-23
1:1 PIDA	-22
1:6 PIDA	-23
1:1 PLA	-21.5
1:12 PLA	-20.5
1:1 PSA	-23
1:10.6 PSA	-23.5
CFPP Δ_{max}	1.5

The CFPP performance of selected copolymers was similarly evaluated in combination with commercial wax crystal modifier B in B0 Fuel C, although at different treat rates. It was determined that, in combination with commercial wax crystal modifier B, the copolymers generally improved the CFPP performance of this fuel relative to commercial wax crystal modifier B alone at these treat rates (Table 3.15). Since 1:6 PPDL-*b*-PIDA in combination with commercial wax crystal modifier B significantly improved CFPP performance by 11 °C, fuel samples treated with 1) commercial wax crystal modifier B, 2) 1:6 PPDL-*b*-PIDA and commercial wax crystal modifier B, and 3) 1:1 PPDL-*b*-PIDA and commercial wax crystal modifier B, which did not improve CFPP performance relative to commercial wax crystal modifier B alone, were visualized by optical microscopy (Figures 3.37 - 3.39). These images reveal that 1:6 PPDL-*b*-PIDA in combination with commercial wax crystal modifier B yielded smaller (<25 μm), more dispersed wax crystals than obtained with commercial wax crystal modifier B (<50 μm). Interestingly, 1:1 PPDL-*b*-PIDA in combination with commercial wax crystal modifier B yielded a mixture of large and small wax crystals, accounting for its poor CFPP performance. Therefore, it can be concluded that the poly(isodecyl acrylate) block length significantly influences the CFPP performance in combination with commercial wax crystal modifier B in this fuel, however this trend cannot be extended to all of the copolymers. For

example, 1:1 PPDL-*b*-PSA in combination with commercial wax crystal modifier B exhibits good CFPP performance, which is similar to that achieved in combination with 1:10.6 PPDL-*b*-PSA.

Table 3.15: CFPP performance of selected PPDL-*b*-poly(acrylate) block copolymers (150 ppm) in combination with commercial wax crystal modifier A (150 ppm) in B0 Fuel C.

Polymer	CFPP (°C)
	B0 Fuel C
Basefuel	-8.5
Basefuel + WCM B (300 ppm)	-12
1:1 PEHA	-17
1:13 PEHA	-21
1:1 PIDA	-11
1:6 PIDA	-23
1:1 PLA	-12
1:12 PLA	-11
1:1 PSA	-20
1:10.6 PSA	-19
CFPP Δ_{max}	11
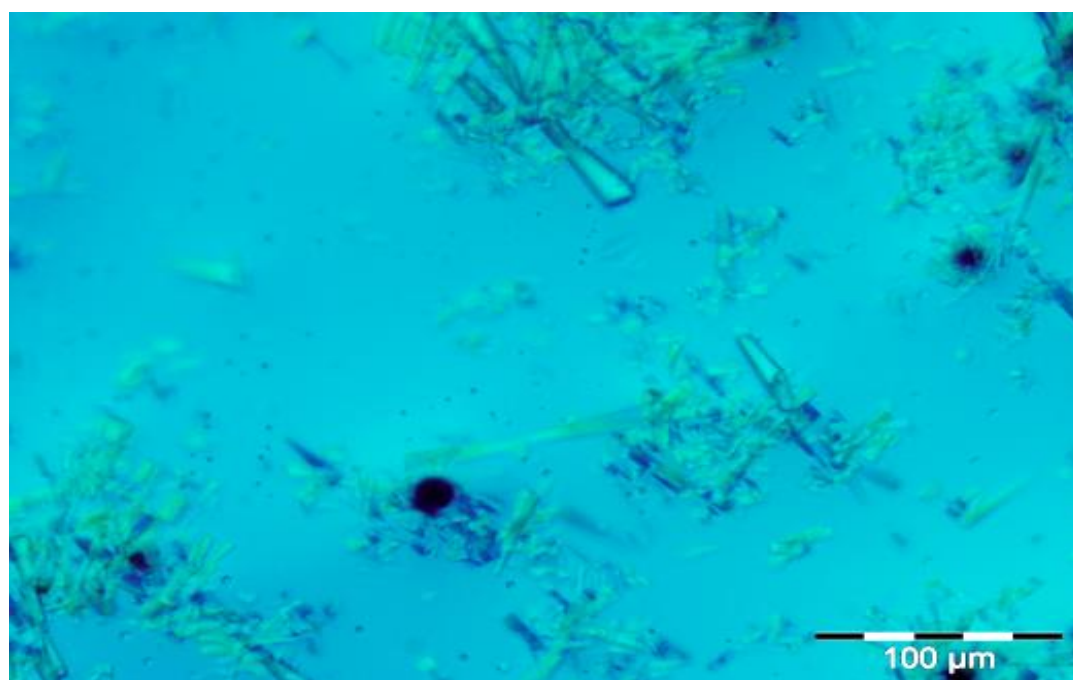
Figure 3.37: Wax crystals observed in B0 Fuel C treated with 300 ppm of commercial wax crystal modifier B (CFPP = -12 °C).
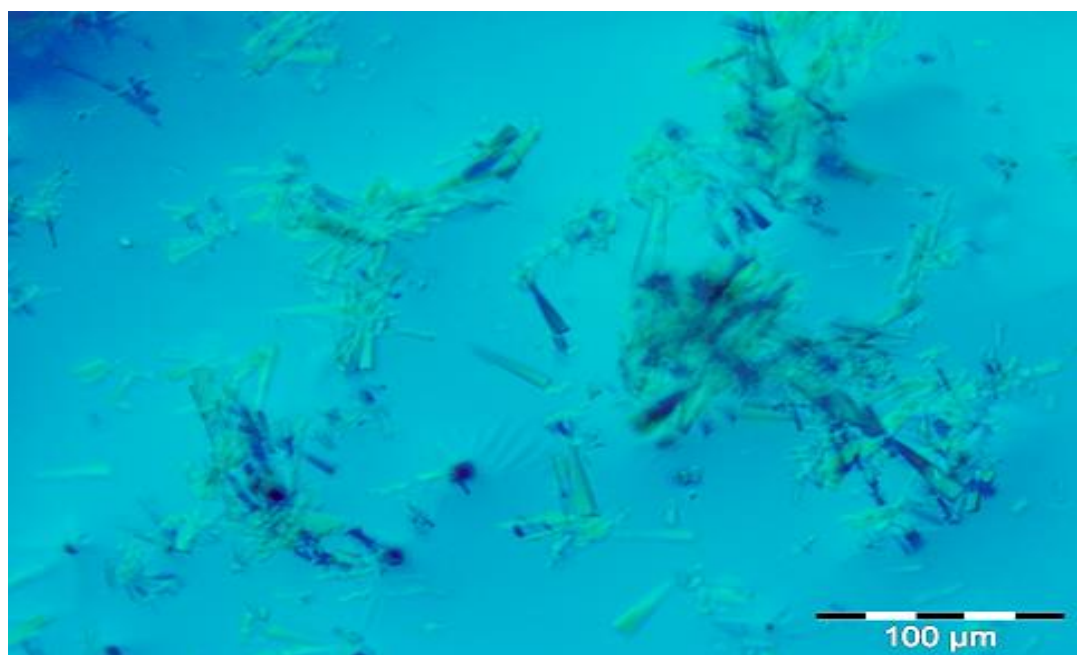
Figure 3.38: Wax crystals observed in B0 Fuel C treated with 150 ppm of commercial wax crystal modifier B and 150 ppm of 1:6 PPDL-*b*-PIDA (CFPP = -23 °C).
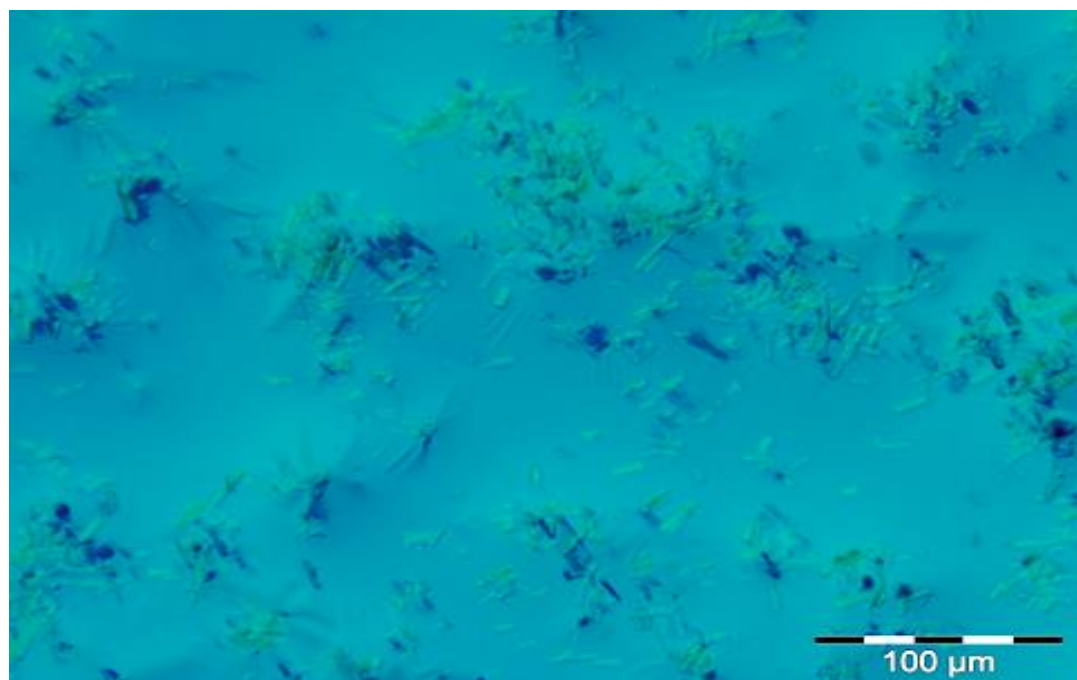
Figure 3.39: Wax crystals observed in B0 Fuel C treated with 150 ppm of commercial wax crystal modifier B and 150 ppm of 1:1 PPDL-*b*-PIDA (CFPP = -11 °C).

Finally, the CFPP performance of selected copolymers was evaluated in combination with commercial wax crystal modifier B in B10 Fuel F. In general, it was determined that all copolymers significantly improved CFPP performance, with the exception of 1:12 PPDL-*b*-PLA (Table 3.16).

Table 3.16: CFPP performance of selected PPDL-*b*-poly(acrylate) block copolymers (150 ppm) in combination with commercial wax crystal modifier B (150 ppm) in B10 Fuel F.

Polymer	CFPP ($^{\circ}$C)
	B10 Fuel F
Basefuel	-7
Basefuel + WCM B (300 ppm)	-13
1:1 PEHA	-19.5
1:13 PEHA	-20
1:1 PIDA	-20
1:6 PIDA	-19
1:1 PLA	-20
1:12 PLA	-13.5
1:1 PSA	-19
1:10.6 PSA	-19
CFPP Δ_{max}	7

Comparing crystal morphology, wax settling, and CFPP data obtained in B0 Fuel C, it can be concluded that good CFPP results can be achieved with wax crystal modifiers that do not exhibit dramatic wax crystal modification or wax anti-settling. Overall, it was determined that PPDL-*b*-poly(acrylate) copolymers exhibit promising CFPP performance that merits further investigation. PPDL-*b*-poly(acrylate) copolymers maintaining branched rather than linear acrylates generally exhibited superior CFPP, likely following their ability to disrupt the order of the acrylic backbone. Interestingly, CFPP results from a range of different fuels suggest that PPDL is more effective at improving the CFPP performance of fuels with significant <C12 *n*-alkane content, supported by a recent report that effective wax crystal modifiers maintain a similar melting point to the precipitated paraffins, which is approximately two carbons chain lengths longer than the average carbon number.[21] Finally, it was determined that, in combination with commercial wax crystal modifier B, PPDL-*b*-poly(acrylate) copolymers improve the CFPP performance relative to that observed with the commercial wax crystal modifier B alone.

3.3 Conclusions

A selection of acrylic block copolymers of DP 19 PPDL were prepared for fuels testing. Good control of the RAFT chain extension polymerization process used to prepare the acrylic block was achieved as indicated by the good correlation between an increase in M_n and M_p and increasing acrylic block length, and a decrease in polymer dispersity with increasing in acrylic block length. UV-GPC analysis indicated that the copolymers exhibited good end-group fidelity where the acrylic block length was between a ratio of 2 and 10. Below 2, a significant amount of high molecular weight PPDL homopolymer exists, which is not readily removed by precipitation. Furthermore, some higher acrylic ratio copolymers exhibited bimodal UV-GPC chromatograms, indicating significant branching since polymerizations were conducted to monomer conversions beyond a region of controlled radical polymerization. Finally, the physical appearance, DSC onset crystallization temperature data, and MALDI-ToF mass spectrometric analysis of the copolymers confirm block copolymer architecture.

It was determined that the PPDL-*b*-poly(acrylate) copolymers, with the exception of 1:12 PPDL-*b*-PLA and 1:1 PPDL-*b*-PSA, did not have any significant effect on wax crystal morphology or wax dispersion. Comparing crystal morphology, wax settling, and CFPP data obtained in B0 Fuel C revealed that good CFPP results can be achieved with wax crystal modifiers that do not dramatically alter wax crystal morphology or wax settling. Overall, it was determined that PPDL-*b*-poly(acrylate) copolymers, particularly those featuring branched rather than linear side chain acrylates exhibit promising CFPP performance that merits further investigation. Future investigations could include the preparation and fuels testing of PPDL-*b*-poly(methacrylate) copolymers in order to further disrupt the backbone of the solubilising block, in addition to block copolymers of varied PPDL molecular weights and/or mixed poly(ester)s, and alternate architectures of related polymers.

3.4 References

(1)   Ribeiro, N. M.; Pinto, A. C.; Quintella, C. M.; da Rocha, G. O.; Teixeira, L. S. G.; Guarieiro, L. L. N.; do Carmo Rangel, M.; Veloso, M. C. C.; Rezende, M. J. C.; da Cruz, R. S.; de Oliveira, A. M.; Torres, E. A.; de Andrade, J. B. *Energy Fuels* **2007**, *21*, 2433.

(2)   *Fuel Additives Manual, Wax Crystal Modifiers*; Paramins, 1988.

(3)   Ashbaugh, H. S.; Radulescu, A.; Prud'homme, R. K.; Schwahn, D.; Richter, D.; Fetters, L. J. *Macromolecules* **2002**, *35*, 7044.

(4)   Marie, E.; Chevalier, Y.; Brunel, S.; Eydoux, F.; Germanaud, L.; Flores, P. *J. Colloid Interface Sci.* **2004**, *269*, 117.

(5)   Letoffe, J. M.; Claudy, P.; Vassilakis, D.; Damin, B. *Fuel* **1995**, *74*, 1830.

(6)   Ashbaugh, H. S.; Guo, X. H.; Schwahn, D.; Prud'homme, R. K.; Richter, D.; Fetters, L. J. *Energy Fuels* **2005**, *19*, 138.

(7)   Marie, E.; Chevalier, Y.; Eydoux, F.; Germanaud, L.; Flores, P. *J. Colloid Interface Sci.* **2005**, *290*, 406.

(8)   Qian, J. W.; Li, J.; Zhou, G. H.; Qi, G. R. *J. Appl. Polym. Sci.* **2000**, *78*, 836.

(9)   Kern, R.; Dassonville, R. *J. Cryst. Growth* **1992**, *116*, 191.

(10)   Beiny, D. H. M.; Mullin, J. W.; Lewtas, K. *J. Cryst. Growth* **1990**, *102*, 801.

(11)   Infineum International Limited; Vol. 2013.

(12)   Misra, R. D.; Murthy, M. S. *Renew. Sust. Energ. Rev.* **2011**, *15*, 2413.

(13)   Kumar, N.; Varun; Chauhan, S. R. *Renew. Sust. Energ. Rev* **2013**, *21*, 633.

(14)   Smith, P. C.; Ngothai, Y.; Nguyen, Q. D.; O'Neill, B. K. *Renew. Energ.* **2010**, *35*, 1145.

(15)   Dunn, R. O.; Shockley, M. W.; Bagby, M. O. *J. Am. Oil Chem. Soc.* **1996**, *73*, 1719.

(16)   Chiu, C. W.; Schumacher, L. G.; Suppes, G. J. *Biomass Bioenerg.* **2004**, *27*, 485.

(17)   In *Insight: The Fuel and Lubricant Additives Industry Journal from Infineum International Limited*; Infineum International Limited: 2013; Vol. 58.

(18)   Focarete, M. L.; Scandola, M.; Kumar, A.; Gross, R. A. *J. Polym. Sci., Part B: Polym. Phys.* **2001**, *39*, 1721.

(19)   de Geus, M.; Peters, R.; Koning, C. E.; Heise, A. *Biomacromolecules* **2008**, *9*, 752.

(20)   He, X. W.; Oishi, Y.; Takahara, A.; Kajiyama, T. *Polym. J.* **1996**, *28*, 452.

(21)   Lue, Y.; Zhang, X.; Yao, G. *Energy Fuels* **2011**, *25*, 2115.

Chapter 4

Sn-RAFT Polymerization

4.1 Introduction

Development of F-RAFT agents in an attempt to control the radical polymerization of ethylene determined that the RAFT agent Z group must destabilize the polyethylene adduct by strongly withdrawing electrons along the thiocarbonyl carbon-Z group sigma bond. Furthermore, it was determined that this bond must not be able to form a pi bond, eliminating the possibility of forming the zwitterion form of the RAFT agent that stabilizes the radical adduct.[1-3] Although the RAFT process was developed predominantly to perform CRP in the absence of metals, complementing ATRP, we envisaged that RAFT agent reactivity could be significantly altered through the incorporation of metals into RAFT agent design. Considering numerous applications in which the presence of metals in the polymer product is acceptable, the development of metallo-RAFT chemistry is appropriate where novel functionality is demonstrated.

Many potential strategies to incorporate metals into RAFT agent design were considered, however, we envisaged that metallo-RAFT agents bearing a metal in the α-position of the thiocarbonyl could potentially dramatically modify the reactivity of RAFT agents towards ethylene, and that the reactivity could be further tuned by varying coordinated ligands. Furthermore, metals are unlikely to form a pi bond with the thiocarbonyl carbon or undergo a change in oxidation state upon addition of a radical to the thiocarbonyl. To our knowledge, triarylstannane dithioesters[4-13] (Figure 4.1) are the only reported examples of dithioalkylesters bearing a metal in the α-position relative to the thiocarbonyl carbon, with the exception of $Fe(CO)_2(C_5Me_5)(CS_2CH_3)$, which we suspect could rearrange in solution to adopt bidentate instead of monodentate coordination of the dithiomethylester (Figure 4.2).[14]

$R = CH_3, C_2H_5, C_3H_7, C_3H_7, C_3H_5, Bn$
$R' = o$-methyl, p-methyl
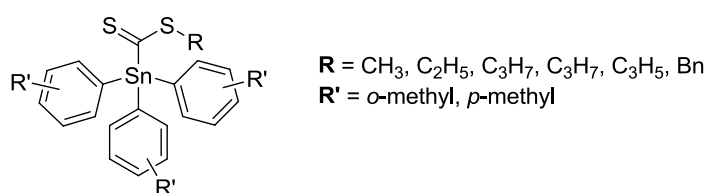
Figure 4.1: Structure of reported triarylstannane dithioesters.
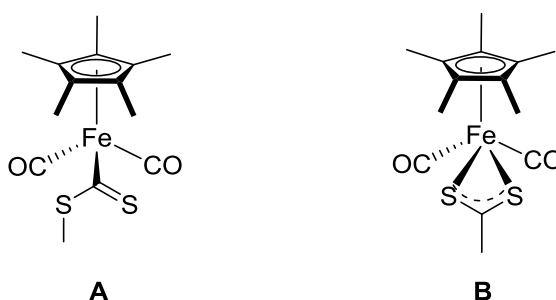
Figure 4.2: Structure of $Fe(CO)_2(C_5Me_5)(CS_2CH_3)$ with a) monodentate, and b) bidentate coordination of the dithiomethylester.

In pursuit of novel ligand systems for the preparation of dithiocarboxylato complexes, in particular ones incorporating main group elements, Bolz and co-workers[4] considered the addition of strong group 14 nucleophiles, namely Ph_3X^- where X = Si, Ge, Sn, or Pb, to heteroallenes including carbon dioxide, carbonyl sulfide, carbon disulfide, isocyanates, and isothiocyanates to form a metal-carbon bond which can be stabilized by the addition of a Lewis acid (Scheme 4.1). Almost all previous attempts to prepare such compounds, however, failed since formation of the stable di-element compounds (R_3X-XR_3) predominates.[15]

$$R_3X^- \quad + \quad A{=}B{=}C \quad \longrightarrow \quad \left[R_3X-B \begin{matrix} \diagup\!\!\!\diagup C \\ \diagdown A \end{matrix} \right]^- \quad \xrightarrow{\;+\,Y^+\;} \quad R_3X-B \begin{matrix} \diagup\!\!\!\diagup C \\ \diagdown A{-}Y \end{matrix}$$
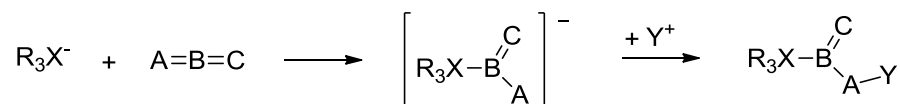
Scheme 4.1: Nucleophilic addition of group 14 nucleophiles to heteroallenes. Scheme reproduced from Bolz *et al.*[4]

Interestingly, known nucleophilic additions of group 14 nucleophiles to heteroallenes is limited. For example, organo-silicon and -germanium anions are known to react with carbon dioxide,[16-22] however, the analogous organo-tin and -lead compounds do not undergo addition to carbon dioxide or isocyanates,[15,23,24] and subsequent alkylation yields a mixture of tetraorganotin compounds.[10] Furthermore, the addition of organotin anions to carbon disulfide and sulfur dioxide often results in the formation of distannanes.[14,15,23,25] Despite the high nucleophilicity of organotin anions, the addition of organotin anions to heteroallenes to form a stable tin-carbon bond thus far appears to be limited to carbon disulfide (Figure 4.3). Of the reported triarylstannane dithioesters, triphenylstannane dithiobenzyl- and -dithioisopropylesters maintain suitable R groups for RAFT polymerization. Therefore, these compounds are explored herein as a potential novel class of RAFT agents. Interestingly, it has been reported that triphenylstannane dithioesters can undergo aminolysis (Scheme 4.2).[9]
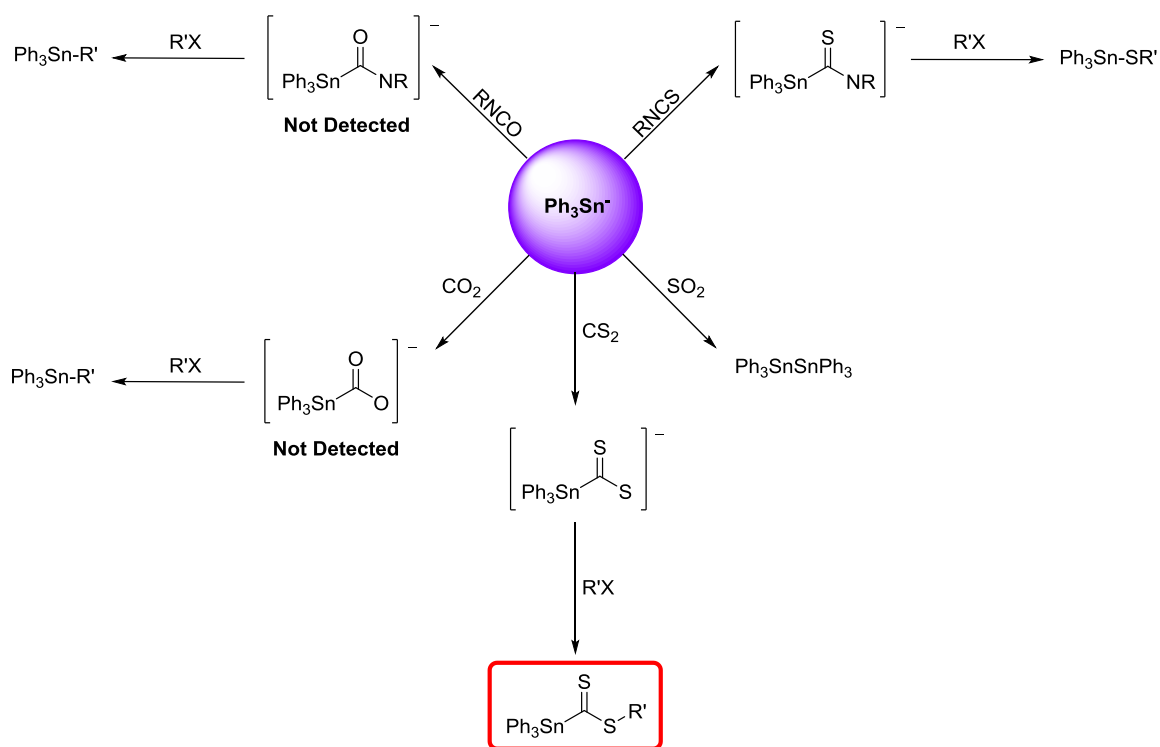
Figure 4.3: Nucleophilic addition of the triphenyltin anion to heteroallenes. Figure adapted from Kunze.[10]
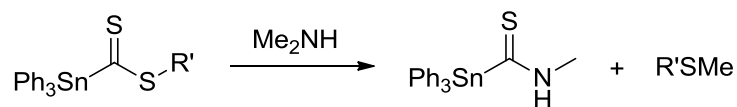
Scheme 4.2: Aminolysis of dithioesters to yield stannyl thioformamides.

4.2 Results and Discussion

4.2.1 Synthesis of Triphenylstannane dithioesters

Triphenylstannane dithioesters were prepared according to literature methods (Scheme 4.3).[7,9,26] Specifically, all in one pot, three equivalents of phenyllithium was added to stannous(II) chloride in anhydrous tetrahydrofuran. Thereafter, triphenyltin lithium underwent a nucleophilic addition to an excess of carbon disulfide. The resulting dithiocarboxylate anion, which was stabilized with dioxane, was reacted with an excess of either benzyl bromide or 2-iodopropane to yield triphenylstannane dithiobenzylester (**5**) (32%) and triphenylstannane dithioisopropylester (**6**) (13%), respectively. The ^{1}H and ^{13}C DEPT NMR spectra (Figure 4.4 and Figure 4.5), along with infra-red (IR), melting point (m.p.), and ultraviolet-visible (UV-vis) spectroscopy data are consistent with reported values.[7,9] The expected chemical shift for the quaternary carbon for **5** ($\delta = 264.6$ ppm) is exceptionally downfield and was not observed in the ^{13}C DEPT NMR spectroscopy experiment performed.[27] Furthermore, thermal gravimetric analysis confirmed that the compounds are thermally stable up to approximately 220 $^{\mathbf{o}}$C.
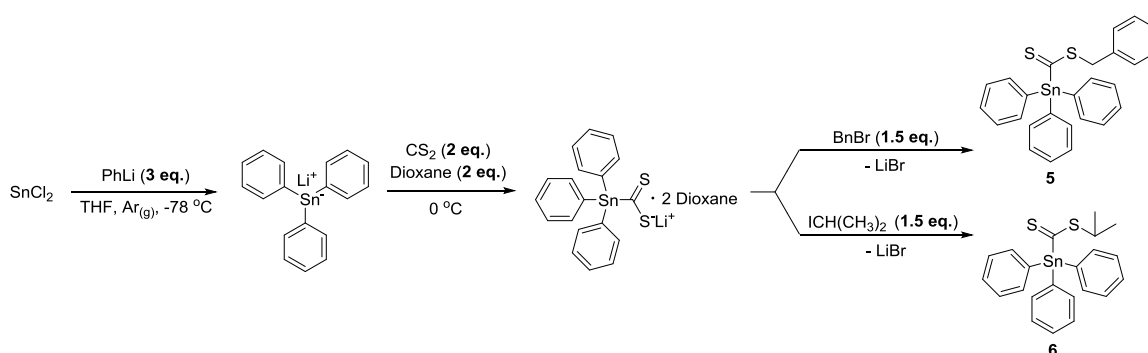
Scheme 4.3: Synthesis of triphenylstannane dithiobenzylester (**5**) and triphenylstannane dithioisopropylester (**6**).
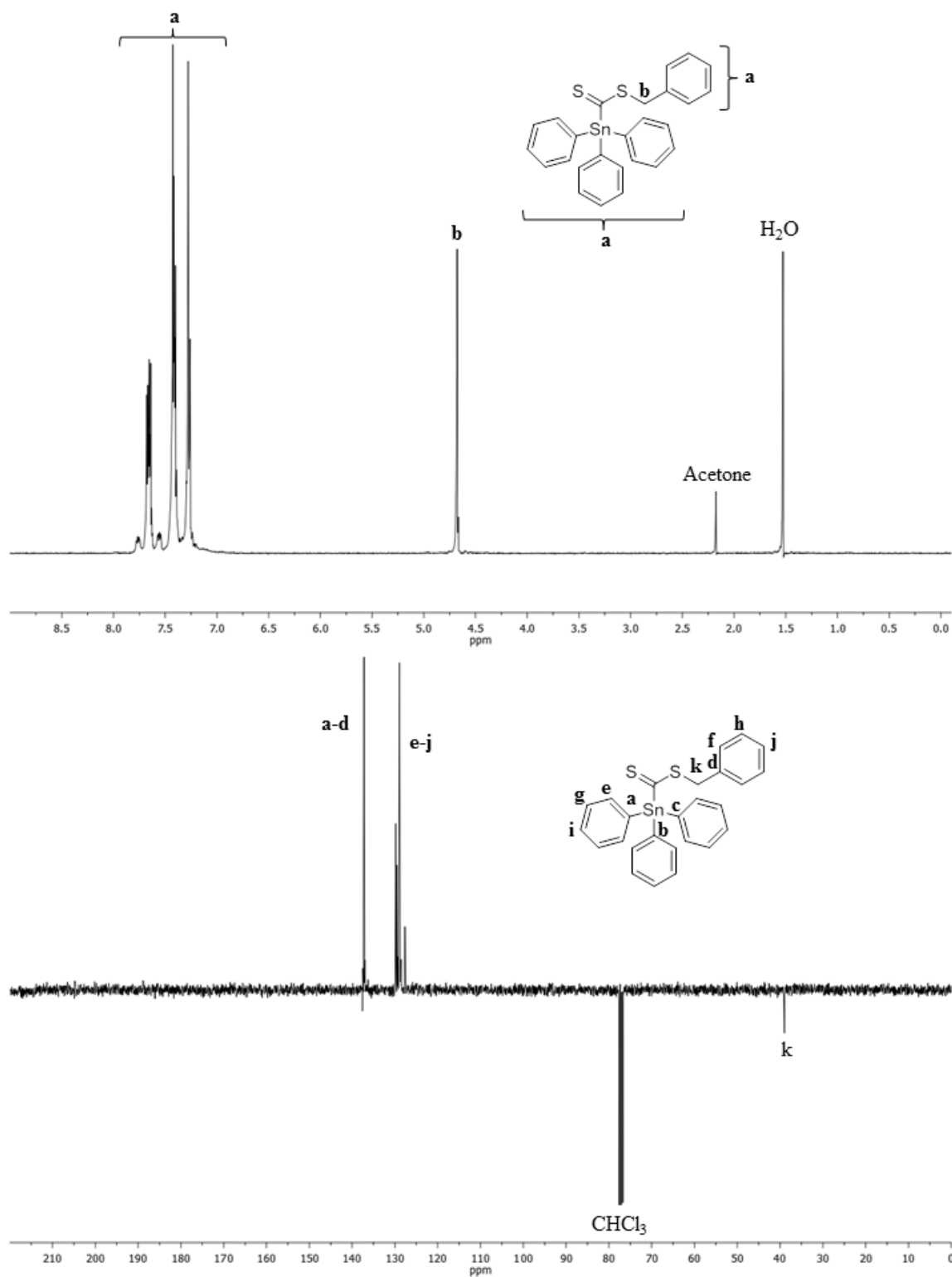
Figure 4.4: ^{1}H and ^{13}C DEPT NMR spectra of triphenylstannane dithiobenzylester (**5**) (400 MHz, CDCl$_3$).
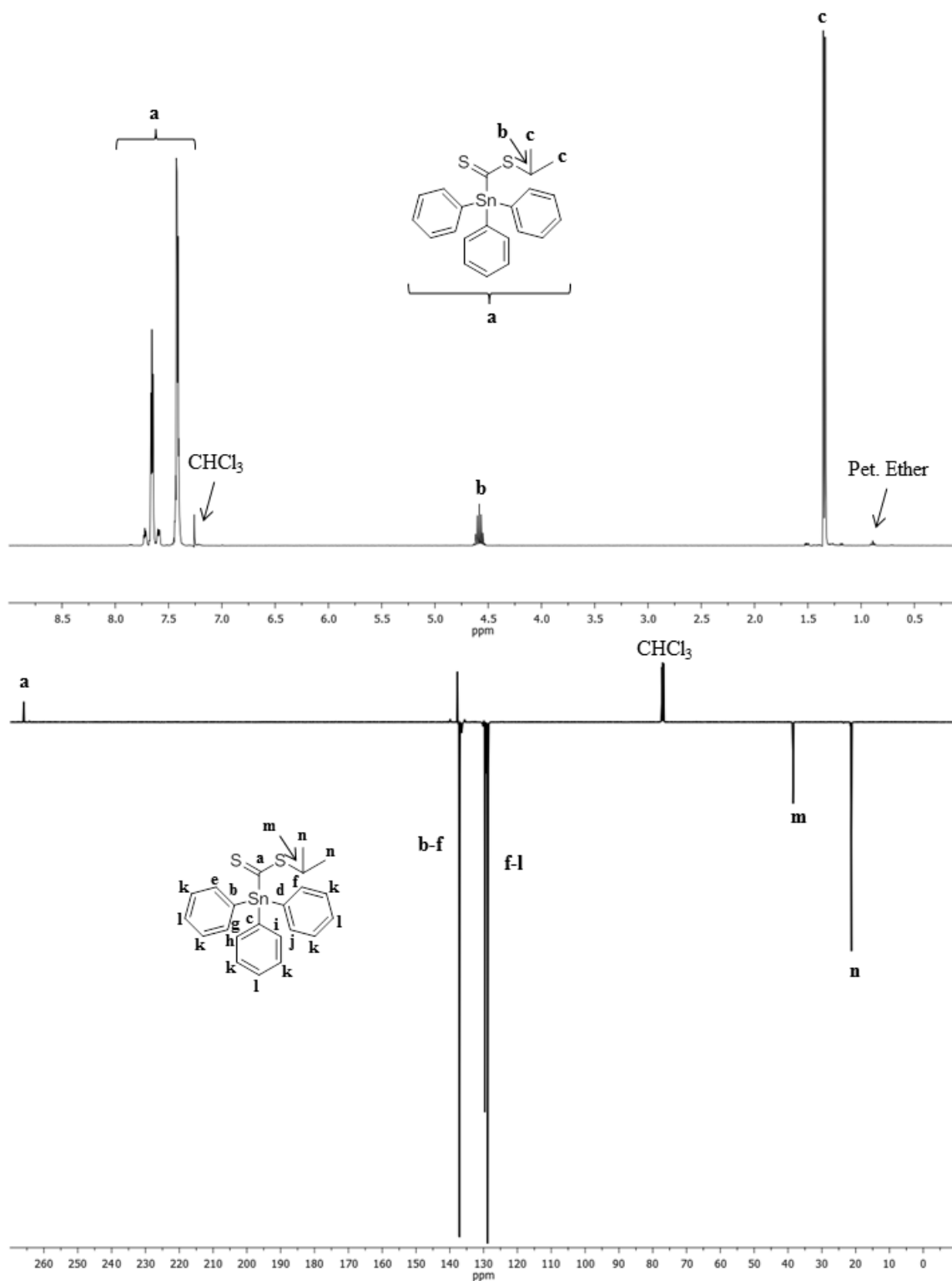
Figure 4.5: ^{1}H and ^{13}C DEPT NMR spectra of triphenylstannane dithioisopropyl (**6**) (300 and 500 MHz, CDCl$_3$).

4.2.2 Sn-RAFT Polymerization

4.2.2.1 Polymerizations using Triphenylstannane dithiobenzylester (5) as a CTA

Styrene was polymerized in bulk conditions using triphenylstannane dithiobenzylester (5) as a CTA and AIBN as a radical initiator at 60 °C (Scheme 4.4). The polymerization was monitored by comparing the integral of the vinylic methyne proton in the monomer (δ = 6.69-6.50 ppm) and the methyne proton in the polymer backbone (δ = 2.20-1.85 ppm) (Figure 4.6). Furthermore, the degree of polymerization was evaluated by comparing the integral of the polymer methyne proton adjacent to the dithioester (δ = 3.10-2.96 ppm) to that of the methyne proton in the polymer backbone (δ = 2.20-1.85 ppm). Good control was demonstrated as evidenced by a linear semi-logarithmic plot (Figure 4.7), indicating a constant concentration of propagating radicals, a linear correlation between the M_n and monomer conversion, and a narrow $Đ_M$ of the polymer product (Figure 4.8).
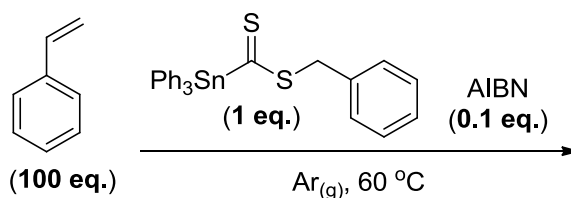
Scheme 4.4: Polymerization of styrene using **5** as a CTA and AIBN as an initiator.
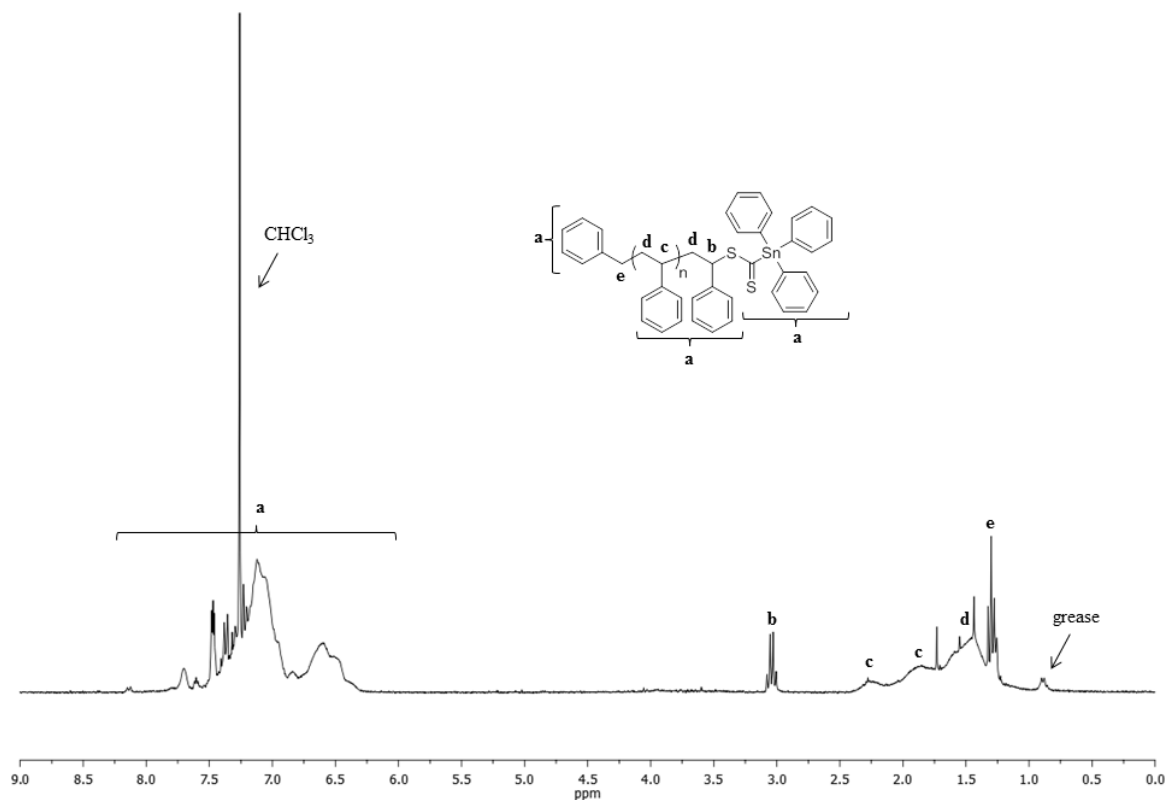
Figure 4.6: ^{1}H NMR spectrum of poly(styrene) (DP 6, $[M]_0/[M]_t$ = 0.04) prepared using **5** as a CTA and AIBN as a radical initiator at 60 °C in bulk conditions ([M]:[CTA]:[I] = 100:1:0.1) (300 MHz; CDCl$_3$).
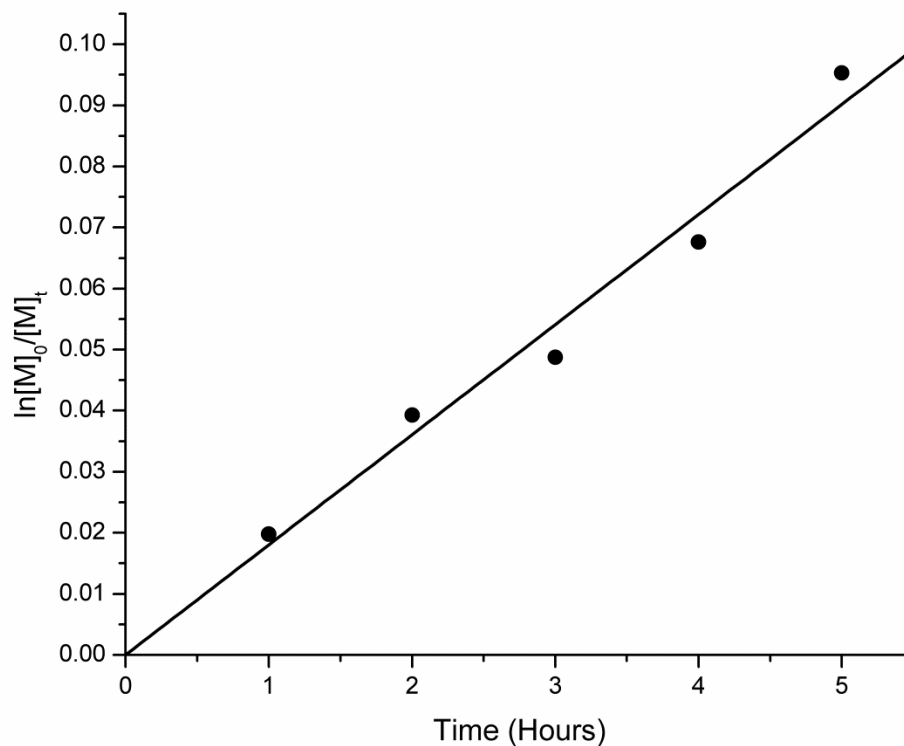
Figure 4.7: Semi-logarithmic plot for the bulk polymerization of styrene using **5** as a CTA and AIBN as a radical initiator at 60 ºC ([M]:[CTA]:[I] = 100:1:0.1).
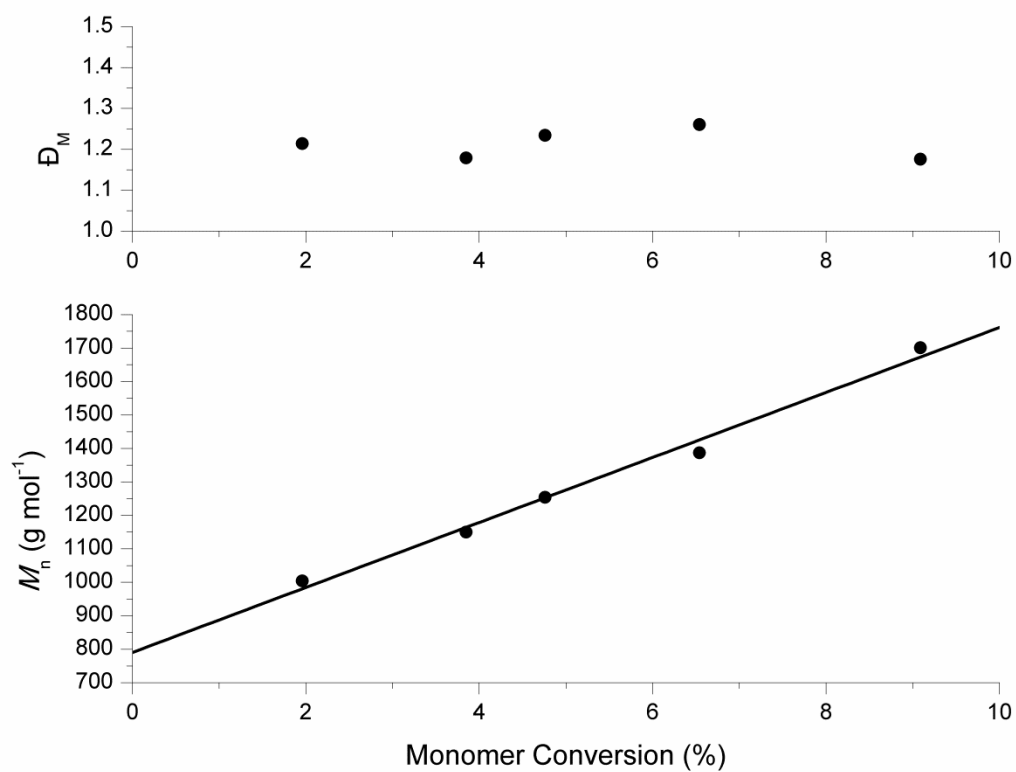
Figure 4.8: Plot of *Mn* and $Đ_M$ *versus* monomer conversion for the bulk polymerization of styrene using **5** as a CTA and AIBN as a radical initiator at 60 ºC ([M]:[CTA]:[I] = 100:1:0.1).

Furthermore, methyl acrylate was polymerized in bulk conditions using **5** as a CTA and AIBN as a radical initiator at 60 °C (Scheme 4.5). The polymerization was monitored by comparing the integral of the methyl protons in the monomer (δ = 3.72 ppm) and polymer (δ = 3.66 ppm) (Figure 4.9). Furthermore, the degree of polymerization was evaluated by comparing the integral of the polymer methyne proton adjacent to the dithioester (δ = 3.22-3.02 ppm) to that of the methyl ester protons in the polymer (δ = 3.95-3.35 ppm). Good control was demonstrated as evidenced by a linear semi-logarithmic plot (Figure 4.10), indicating a constant concentration of propagating radicals, a linear correlation between the M_n and monomer conversion, and a narrow dispersity of the polymer product (Figure 4.11). An induction period was observed, as frequently reported in low temperature RAFT polymerizations of methyl acrylate, particularly with non-aliphatic CTAs. This induction period is attributed to slow consumption of the RAFT agent and therefore can be eliminated by performing the reaction at a higher temperature.[28]

Scheme 4.5: Polymerization of methyl acrylate using **5** as a CTA and AIBN as an initiator.
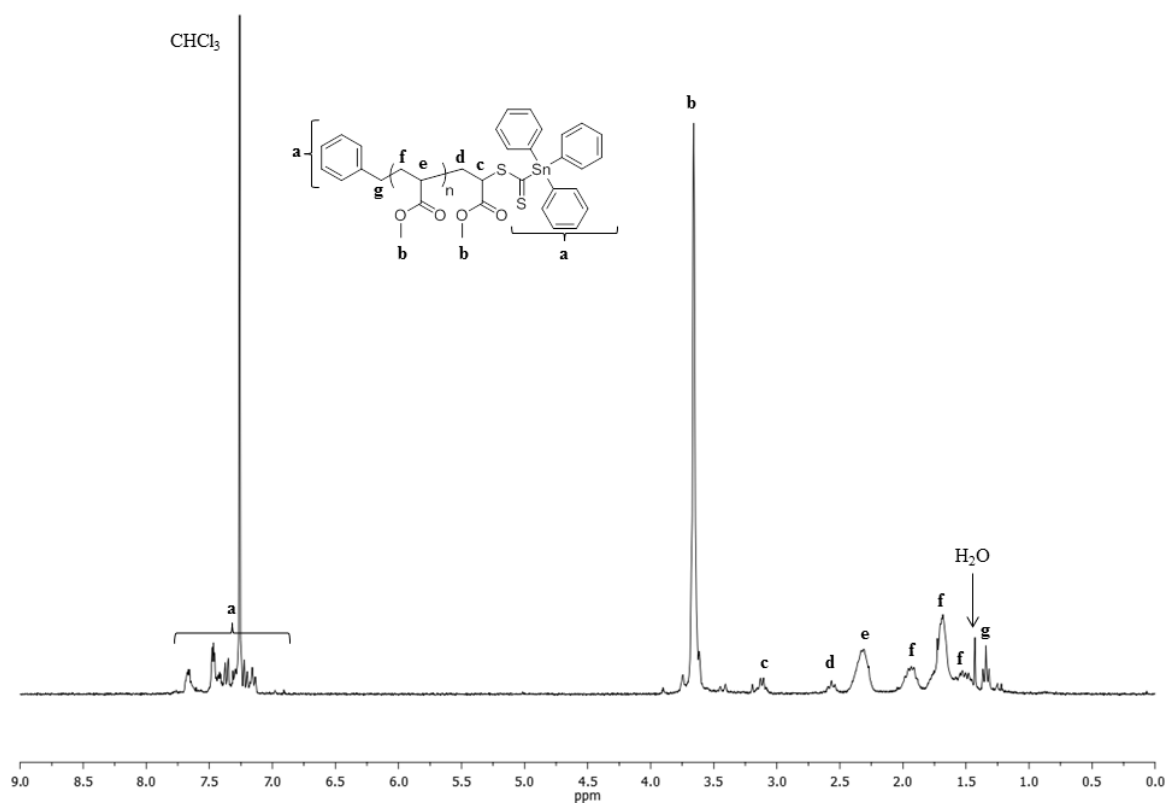
Figure 4.9: ^{1}H NMR spectrum of poly(methyl acrylate) (DP 11, $[M]_0/[M]_t$ = 0.13) prepared using **5** as a CTA and AIBN as a radical initiator at 60 °C in bulk conditions ([M]:[CTA]:[I] = 100:1:0.1) (300 MHz; CDCl$_3$).

Figure 4.10: Semi-logarithmic plot for the bulk polymerization of methyl acrylate using **5** as a CTA and AIBN as a radical initiator at 60 ºC ([M]:[CTA]:[I] = 100:1:0.1).

Figure 4.11: Plot of *Mn* and *Đ*$_M$ *versus* monomer conversion for the bulk polymerization of methyl acrylate using **5** as a CTA and AIBN as a radical initiator at 60 ºC ([M]:[CTA]:[I] = 100:1:0.1).

Data obtained for the polymerization of styrene and methyl acrylate using triphenylstannane dithiobenzylester (**5**) as a CTA indicate that triphenylstannane dithioesters may constitute a novel class of RAFT agents. Direct comparisons with other conventional RAFT agents were not completed, however, Chong and co-workers[29] report the bulk polymerizations of both styrene and methyl acrylate at 60 ºC using benzyl benzenecarbodithioate (Figure 4.12) and AIBN. Although their ratio of monomer to CTA to AIBN (1:0.00107:0.00019, respectively) was significantly different than that reported herein and consequently, rates cannot be compared, promising similarities in data obtained are observed, indicating that **5** may perform as a RAFT agent. For example, at t = 4 hours, an M_n 3630 polystyrene was obtained at 3.5% monomer conversion, and the dispersity of the polymerization was ≤ 1.36 throughout, which is similar to the M_n 1387 polystyrene obtained at 6.5% monomer conversion *via* Sn-RAFT polymerization ($Đ_M$ ≤ 1.26). Direct comparison of conventional CTAs, such as benzyl benzenecarbodithioate, and **5** under identical reaction conditions is required in order to evaluate the performance of triphenyltin as a Z group. It is anticipated that the reactivity of the thiocarbonyl is high in **5** relative to other CTAs following increased bond polarity, as evidenced by a significant downfield chemical shift for the thiocarbonyl carbon ($\delta \sim 265$ ppm). Comparison of rates of polymerization between CTAs will elucidate this alongside additional information, including the stability of the Sn-RAFT agent adduct radical generated. Finally, in additon to comparison with conventional RAFT agents, the end-group fidelity of polymerizations performed using **5** as a CTA must be evaluated. Considering that triphenylstannane dithioesters are highly coloured, UV-active compounds, end-group analysis should be performed *via* UV-GPC. Furthermore, ^{119}Sn NMR spectroscopy could be performed.
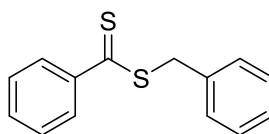
Figure 4.12: Structure of benzyl benzenecarbodithioate.

4.2.2.2 Polymerizations using Triphenylstannane dithioisopropylester (6) as a CTA

In order to explore the Sn-RAFT polymerization of primary radicals on a laboratory scale, the ketene acetal 2-methylene-1,3-dioxepane (MDO) was considered a potentially suitable monomer since it undergoes radical ring-opening to generate a primary radical, identical to that generated by ε-caprolactone, which propagates to yield a poly(ester) (Scheme 4.6).[30,31] MDO was synthesized in two steps according to literature methods (Scheme 4.7).[32] Specifically, 1,4-butane diol undergoes an acid catalysed condensation reaction with chloroacetaldehyde dimethyl acetal to yield 2-methylene-1,3-dioxepane (78%), which when treated with base generates the desired ketene acetal (**7**) (82%). The ^{1}H and ^{13}C DEPT NMR spectroscopy data match reported values (Figure 4.13).[31,32]
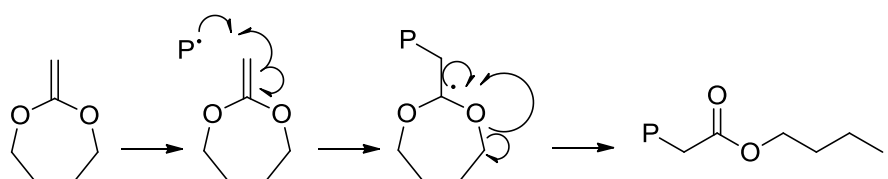
Scheme 4.6: Radical ring-opening mechanism of 2-methylene-1,3-dioxepane (MDO).
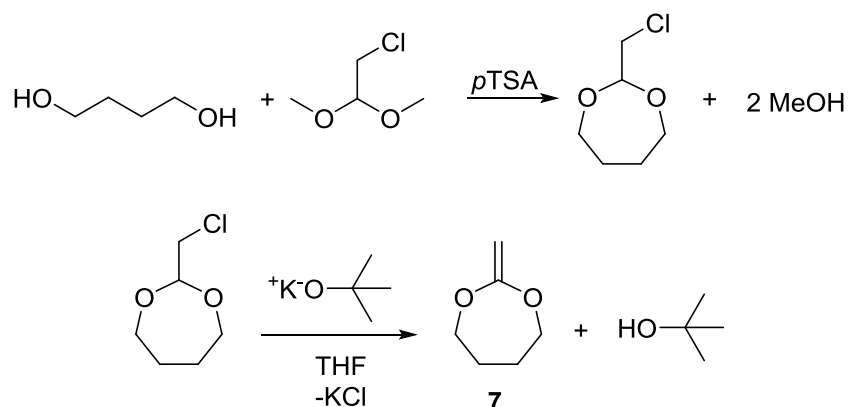
Scheme 4.7: Synthesis of 2-methylene-1,3-dioxepane (MDO) (**7**).
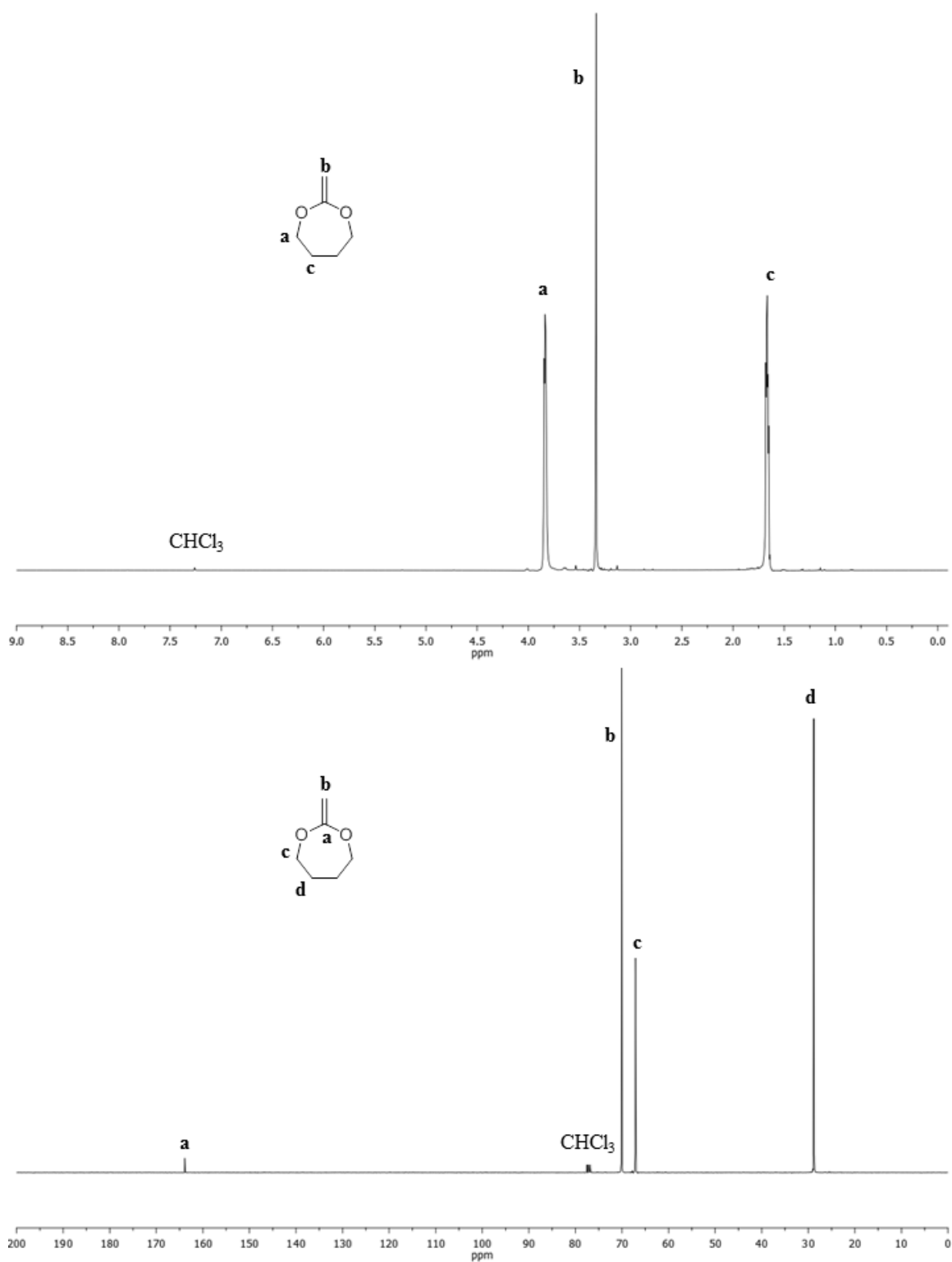
Figure 4.13: ^{1}H and ^{13}C DEPT NMR spectra of 2-methylene-1,3-dioxepane (MDO) (**7**) (400 MHz; CDCl$_3$).

MDO was polymerized in bulk, free radical conditions using AIBN as a radical initiator, and in bulk conditions using **6** as a CTA and AIBN as a radical initiator (Scheme 4.8). Various reaction temperatures were selected according to a previous report of MDO polymerization[33] in order to ensure high monomer conversion in the free radical case and highlight potential differences in polymerizations performed in the presence and absence of **6**. In the free radical polymerizations performed, an increase in the M_n and dispersity of the polymer product was observed with increasing reaction temperatures (Table 4.1). At increased temperatures, less control of the polymerization was achieved following decreased initiator half-lives and therefore shorter periods of radical flux. Although the monomer conversions obtained in the free radical polymerizations were not as high as those previously reported, predominantly linear polymer was obtained, with 8.5-12.8% branched product observed. Interestingly, Plikk *et al*.[33] report that the five-membered cyclic ester 3-vinyl-1,4-butyrolactone predominates at 150 °C, however this product was not observed. Since minimal monomer conversion was observed where MDO was polymerized in the presence of **6**, an inhibiting effect of the CTA was noted and therefore further kinetic studies were not undertaken. The triphenylstannane dithioester presumably inhibits the polymerization of MDO since the monomer adduct does not readily fragment from the chain transfer adduct radical following the poor homolytic leaving group ability of the primary radical.
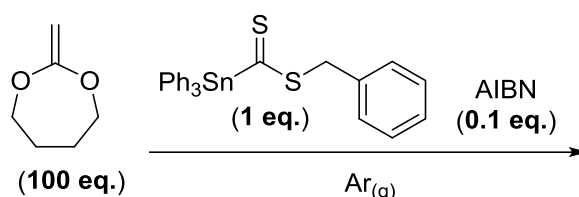
Scheme 4.8: Polymerization of MDO (**7**) using triphenylstannane dithioisopropylester (**6**) as a CTA and AIBN as an initiator.

Table 4.1: Comparison of free radical (FR) and Sn-RAFT polymerizations of MDO (**7**) at 60, 100, and 150 °C using **6** as a CTA and AIBN as a radical initiator.

Entry	Technique	T °C	Time (hours)	$[M]_0/[I]_0$	$[M]_t/[M]_0$[a]	M_n (g mol^{-1})[b]	$Đ_M$[b]
1	FR	60	78	100	0.78	15900	4.80
2	Sn-RAFT	60	78	100	0.01	400	1.23
3	FR	100	48	100	0.66	18000	2.50
4	Sn-RAFT	100	48	100	0.02	500	1.26
5	FR	150	24	100	0.42	8500	1.90
6	Sn-RAFT	150	24	100	0.05	600	2.60

[a]Determined by ^{1}H NMR spectroscopic analysis in CDCl$_3$; [b]Determined by GPC analysis in CHCl$_3$.

Beyond the CRP of monomers generating primary radicals, controlled radical polymerization of isoprene is also challenging, however, has been reported, including *via* the RAFT process.[34-48] Isoprene was polymerized in bulk conditions using **6** as a CTA and AIBN as a radical initiator at 60 °C (Scheme 4.9). The polymerization was monitored by gravimetry and the degree of polymerization was evaluated by comparing the integral of the polymer alkyne protons (δ = 6.00-4.50 ppm) to that of the aromatic protons of **6** (δ = 7.70-7.10 ppm) (Figure 4.14). Moderate control was demonstrated as evidenced by a linear semi-logarithmic plot (Figure 4.15), indicating a constant concentration of propagating radicals, a linear correlation between the M_n and monomer conversion, and a narrow dispersity of the polymer product (Figure 4.16). Importantly, very low molecular weights and dispersities were observed relative to the free radical case ($Đ_M \geq 8.7$). Interestingly, a high proportion of 1,4-*cis* polymer was obtained early on in the reaction, however, the 1,4-*trans* product predominated at later stages of the polymerization (Figure 4.17). Under all Sn-RAFT reaction conditions attempted, including reactions times of up to 96 hours, however, monomer conversion beyond approximately 50% was not observed.
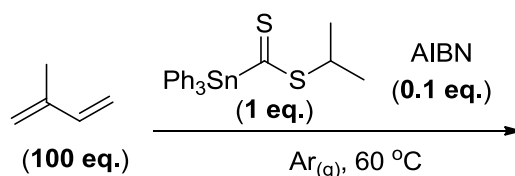
Scheme 4.9: Polymerization of isoprene at using triphenylstannane dithioisopropylester (**6**) as a CTA and AIBN as an initiator.
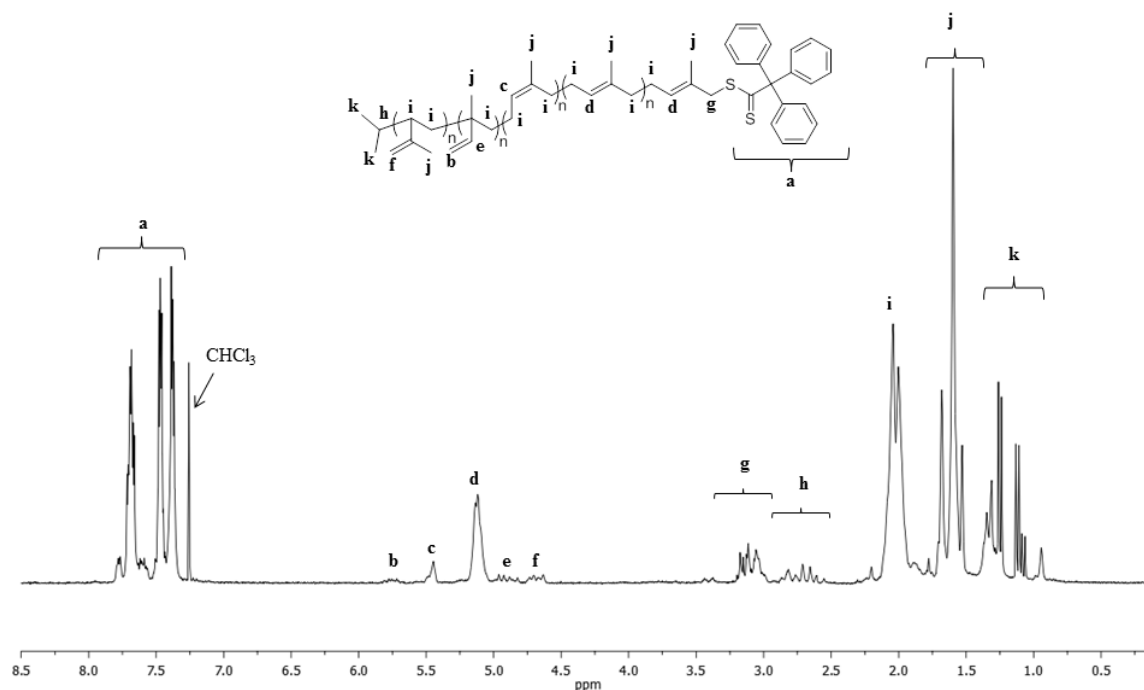
Figure 4.14: ^{1}H NMR spectrum of poly(isoprene) (DP 6, $[M]_0/[M]_t$ = 0.21) prepared using **6** as a CTA and AIBN as a radical initiator at 60 °C in bulk conditions ([M]:[CTA]:[I] = 100:1:0.1) (300 MHz; CDCl$_3$).
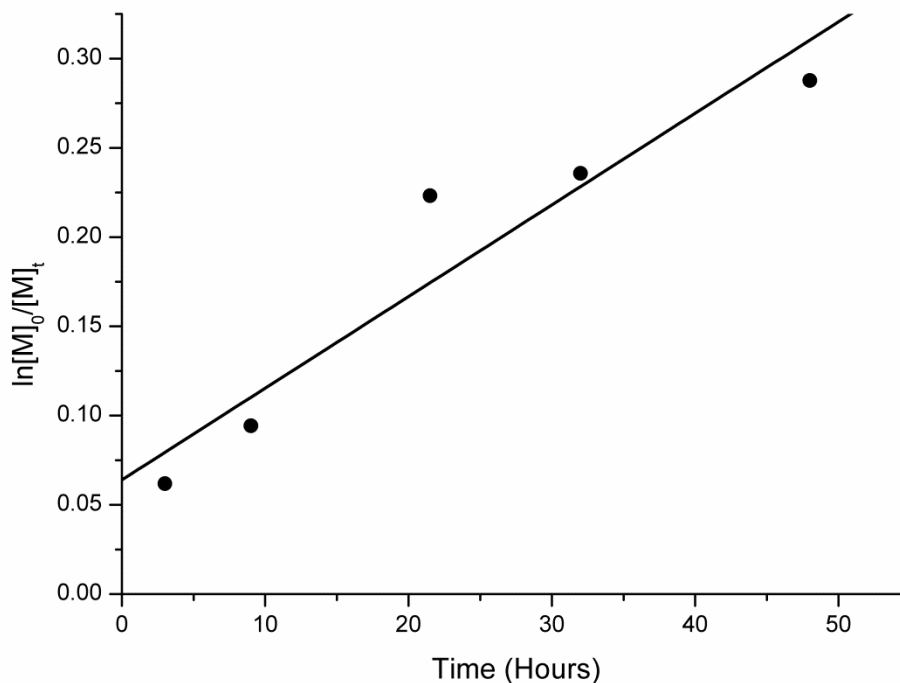
Figure 4.15: Semi-logarithmic plot for the bulk polymerization of isoprene using **6** as a CTA and AIBN as a radical initiator at 60 °C ([M]:[CTA]:[I] = 100:1:0.1).
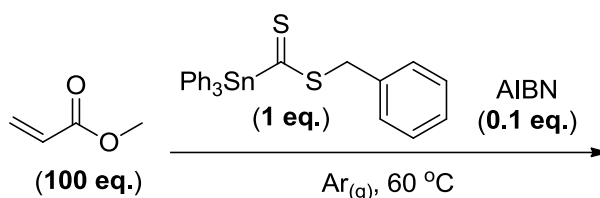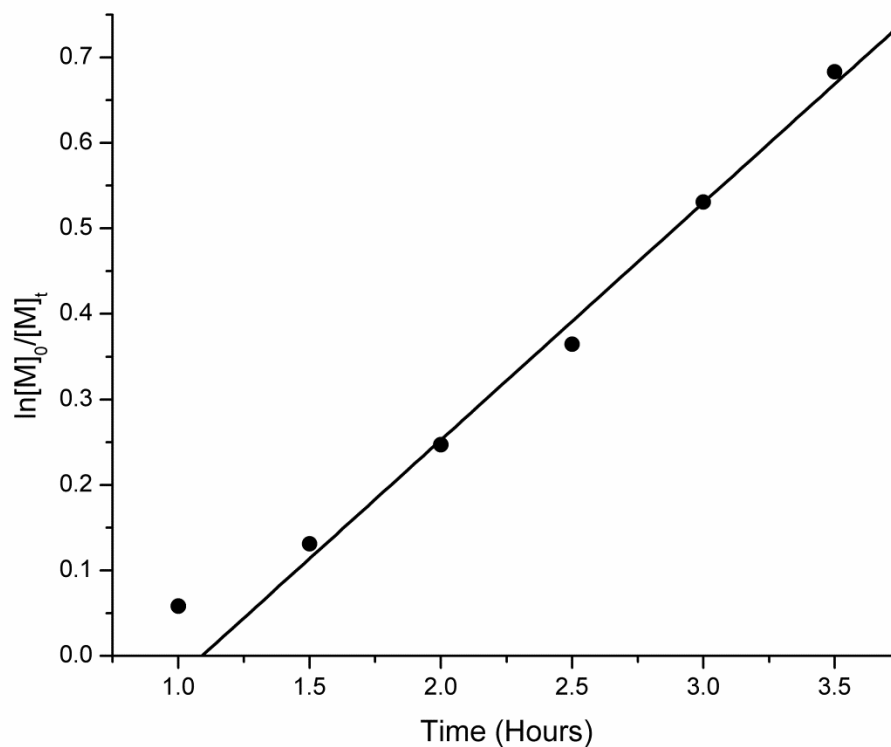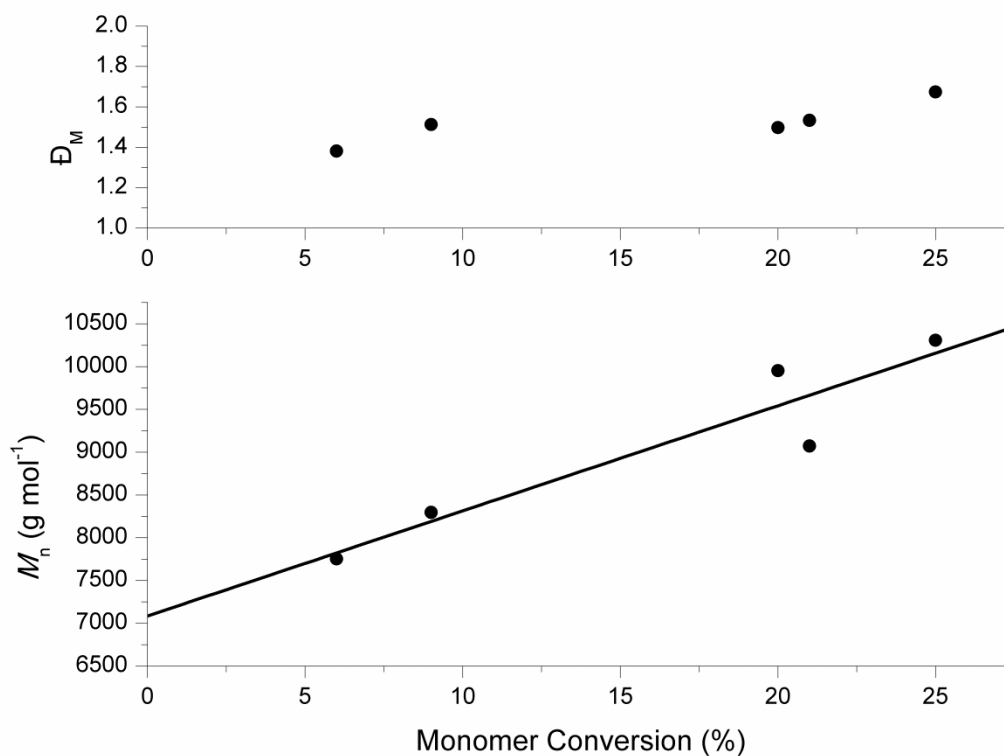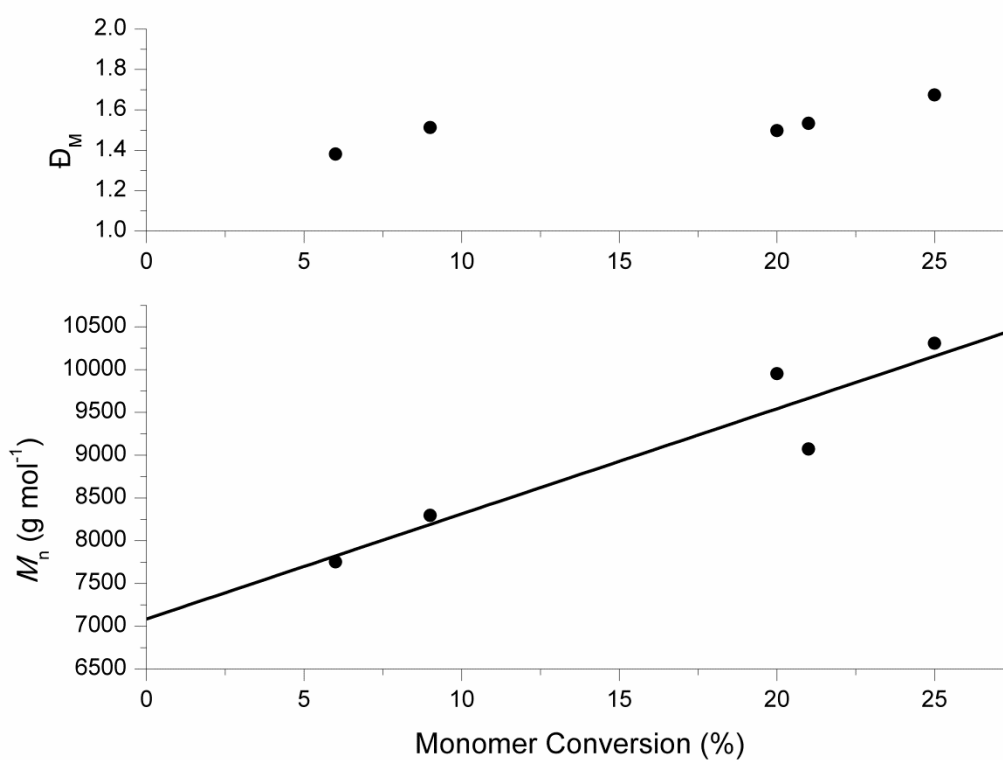

Figure 4.16: Plot of *Mn* and $Đ_M$ *versus* monomer conversion for the bulk polymerization of isoprene using **6** as a CTA and AIBN as a radical initiator at 60 °C ([M]:[CTA]:[I] = 100:1:0.1).
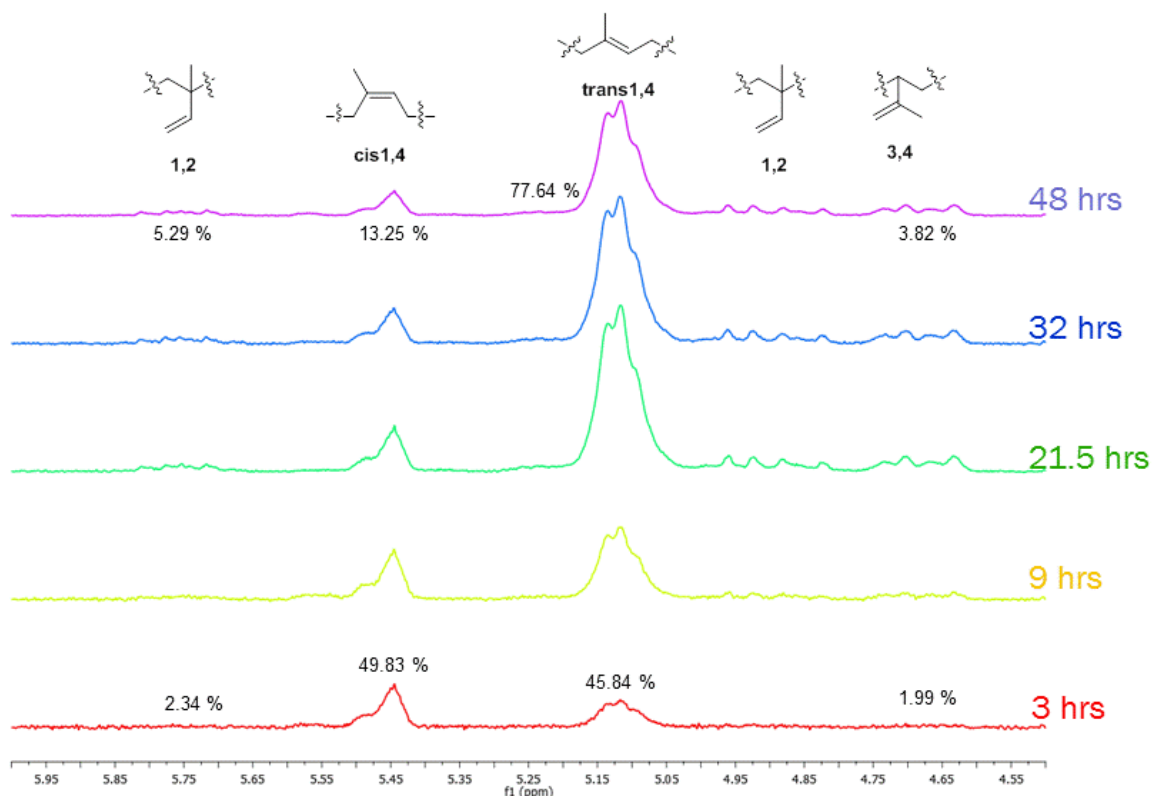
Figure 4.17: Overlay of ^{1}H NMR spectra of isoprene obtained at various kinetic points throughout a bulk polymerization using **6** as a CTA and AIBN as an initiator at 60 ºC, illustrating how the 1,4-*cis* product predominates during the initial stages of the polymerization and the 1,4-*trans* product predominates throughout the later stages of the polymerization ([M]:[CTA]:[I] = 100:1:0.1) (300 MHz; CDCl$_3$).

In order to ensure that triphenylstannane dithioester mediated polymerizations proceed *via* a chain-transfer process and not coordination insertion *via* the tin centre, a control polymerization was performed in the absence of a radical source (Scheme 4.10). Importantly, no polymer product was obtained in this control experiment, suggesting that triphenylstannane dithioester mediated polymerizations proceed *via* the RAFT process.
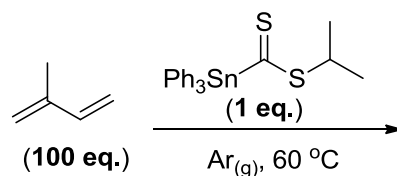
Scheme 4.10: Polymerization of isoprene at 60 ºC using triphenylstannane dithioisopropylester (**6**) as a CTA.

143

4.3 Conclusions

Triphenylstannane dithioesters were synthesized according to literature methods and tested as CTAs in the polymerization of styrene, methyl acrylate, and isoprene. It was determined that triphenylstannane dithiobenzylester controlled the polymerization of styrene and methyl acrylate, however the end-group fidelity of the polymer products was not evaluated. Furthermore, triphenylstannane dithioisopropylester mediated the polymerization of isoprene. These results alongside the observation that triphenylstannane dithioisopropylester (**6**) did not polymerize isoprene in the absence of a radical initiator, suggesting that **6** acts as a chain-transfer agent, encourage further development of Sn-RAFT agents. Future work on the development of Sn-RAFT agents must include analysis of end-group fidelity and direct performance comparisons with conventional CTAs. If end-group fidelity is confirmed and triphenylstannane dithioesters are determined to proceed *via* the RAFT mechanism, then future research could be expanded to include novel stannane dithioesters maintaining alternate substituents on the metal. Furthermore, the performance of triarylstannane dithioisopropylesters could be compared with that of the F-RAFT agent isopropylfluorodithioformate (IFDF) in the polymerization of ethylene. Ultimately, however, the toxicity of tin will significantly limit potential end-uses of polymers prepared *via* this method, and in many instances require removal of the tin end-group *via* post-polymerization modification of the polymer product.

4.4 References

(1) Theis, A.; Stenzel, M. H.; Davis, T. P.; Coote, M. L.; Barner-Kowollik, C. *Aust. J. Chem.* **2005**, *58*, 437.

(2) Coote, M. L.; Izgorodina, E. I.; Cavigliasso, G. E.; Roth, M.; Busch, M.; Barner-Kowollik, C. *Macromolecules* **2006**, *39*, 4585.

(3) Busch, M.; Roth, M.; Stenzel, M. H.; Davis, T. P.; Barner-Kowollik, C. *Aust. J. Chem.* **2007**, *60*, 788.

(4) Bolz, P. R.; Kunze, U.; Winter, W. *Angew. Chem. Int. Ed.* **1980**, *19*, 220.

(5) Kunze, U.; Bolz, P. R.; Winter, W. *Chem. Ber. Recl.* **1981**, *114*, 2744.

(6) Kunze, U.; Hattich, T. *Chem. Ber. Recl.* **1982**, *115*, 3663.

(7) Hattich, T.; Kunze, U. *Angew. Chem. Int. Ed.* **1982**, *21*, 364.

(8) Kunze, U.; Hattich, T. *Chem. Ber. Recl.* **1983**, *116*, 3071.

(9) Carr, S. W.; Colton, R.; Dakterniek, D.; Hoskins, B. F.; Steen, R. *J. Inorg. Chem.* **1983**, *22*, 3700.

(10) Kunze, U. R. *J. Organomet. Chem.* **1985**, *281*, 79.

(11) Hiller, W.; Kunze, U.; Tischer, R. *Inorg. Chim. Acta* **1987**, *133*, 51.

(12) Kunze, U.; Tischer, R. *Chem. Ber. Recl.* **1987**, *120*, 1099.

(13) Mathiasch, B.; Kunze, U. *Inorg. Chim. Acta* **1983**, *75*, 209.

(14) Ellis, J. E.; Fennell, R. W.; Flom, E. A. *Inorg. Chem.* **1976**, *15*, 2031.

(15) Tamborski, C.; Ford, F. E.; Soloski, E. J. *J. Org. Chem.* **1963**, *28*, 237.

(16) Benkeser, R. A.; Severson, R. G. *JACS* **1951**, *73*, 1424.

(17) Brook, A. G.; Gilman, H. *JACS* **1954**, *76*, 77.

(18) Brook, A. G.; Gilman, H. *JACS* **1954**, *76*, 2338.

(19) Brook, A. G.; Gilman, H. *JACS* **1955**, *77*, 2322.

(20) Neumann, G.; Neumann, W. P. *J. Organomet. Chem.* **1972**, *42*, 293.

(21) Steward, O. W.; Heider, G. L; Johnson, J. S. *J. Organomet. Chem.* **1979**, *168*, 33.

(22) Graziani, R.; Caseleato, U. *J. Organomet. Chem.* **1980**, *187*, 381.

(23) Blake, D.; Coates, G. E.; Tate, J. M. *J. Chem. Soc.* **1961**, 618.

(24) Gilman, H.; Marrs, O. L.; Sim, S.-Y. *J. Org. Chem.* **1962**, *27*, 4232.

(25) Ellis, J. E.; Flom, E. A. *J. Organomet. Chem.* **1975**, *99*, 263.

(26) Gilman, H.; Rosenberg, S. D. *JACS* **1952**, *74*, 531.

(27) Bisht, K. S.; Al-Azemi, T. F. *ACS Symp. Ser.* **2010**, *1043*, 175.

(28) *Handbook of RAFT Polymerization*; Barner-Kowollik, C., Ed.; Wiley-VCH: Weinheim, 2008.

(29) Chong, Y. K.; Krstina, J.; Le, T. P. T.; Moad, G.; Postma, A.; Rizzardo, E.; Thang, S. H. *Macromolecules* **2003**, *36*, 2256.

(30) Bailey, W. J.; Ni, Z.; Wu, S. R. *J. Polym. Sci., Part A: Polym. Chem.* **1982**, *20*, 3021.

(31) Undin, J.; Plikk, P.; Finne-Wistrand, A.; Albertsson, A.-C. *J. Polym. Sci., Part A: Polym. Chem.* **2010**, *48*, 4965.

(32) Taskinen, E.; Pentikäinen, M.-L. *Tetrahedron* **1978**, *34*, 2365.

(33)   Plikk, P.; Tyson, T.; Finne-Wistrand, A.; Albertsson, A.-C. *J. Polym. Sci., Part A: Polym. Chem.* **2009**, *47*, 4587.

(34)   Bar-Nes, G.; Hall, R.; Sharma, V.; Gaborieau, M.; Lucas, D.; Castignolles, P.; Gilbert, R. G. *Eur. Polym. J.* **2009**, *45*, 3149.

(35)   Bartels, J. W.; Billings, P. L.; Ghosh, B.; Urban, M. W.; Greenlief, C. M.; Wooley, K. L. *Langmuir* **2009**, *25*, 9535.

(36)   Bartels, J. W.; Cauet, S. I.; Billings, P. L.; Lin, L. Y.; Zhu, J.; Fidge, C.; Pochan, D. J.; Wooley, K. L. *Macromolecules* **2010**, *43*, 7128.

(37)   Chen, S.; Bertrand, A.; Chang, X.; Alcouffe, P.; Ladaviere, C.; Gerard, J.-F.; Lortie, F.; Bernard, J. *Macromolecules* **2010**, *43*, 5981.

(38)   Germack, D. S.; Wooley, K. L. *Macromol. Chem. Phys.* **2007**, *208*, 2481.

(39)   Germack, D. S.; Wooley, K. L. *J. Polym. Sci., Part A: Polym. Chem.* **2007**, *45*, 4100.

(40)   Gramlich, W. M.; Theryo, G.; Hillmyer, M. A. *Polym. Chem.* **2012**, *3*, 1510.

(41)   Jiang, T.; Hu, P. *Polym. J.* **2001**, *33*, 647.

(42)   Jitchum, V.; Perrier, S. *Macromolecules* **2007**, *40*, 1408.

(43)   Li, J.; El Harfi, J.; Howdle, S. M.; Carmichael, K.; Irvine, D. J. *Polym. Chem.* **2012**, *3*, 1495.

(44)   Li, Y. G.; Wang, Y. M.; Pan, C. Y. *J. Polym. Sci., Part A: Polym. Chem.* **2003**, *41*, 1243.

(45)   Miura, Y.; Dairoku, M. *J. Polym. Sci., Part A: Polym. Chem.* **2007**, *45*, 4364.

(46)   Miura, Y.; Miyake, K. *J. Polym. Sci., Part A: Polym. Chem.* **2005**, *43*, 6153.

(47)   Nakamura, Y.; Kitada, Y.; Kobayashi, Y.; Ray, B.; Yamago, S. *Macromolecules* **2011**, *44*, 8388.

(48)   Saetung, N.; Campistron, I.; Pascual, S.; Pilard, J.-F.; Fontaine, L. *Macromolecules* **2011**, *44*, 784.

Chapter 5

Conclusions

Poly(ω-pentadecalactone) was prepared *via* eROP, initiating from benzyl alcohol and the bifunctional initiator dodecyl 4-(hydroxymethyl) benzyl carbonotrithioate. Using both initiators, good control of the polymerization process was observed, however, the presence of cyclic PPDL oligomers was noted alongside the desired linear polymer product as a consequence of chain scission and cyclisation reactions catalysed by indiscriminate transesterification reactions by the lipase catalyst. This observation, however, is consistent with literature reports. Good end-group fidelity was achieved, enabling controlled chain extension of crude PPDL macro-CTA *via* the RAFT process using a selection of acrylic monomers, in particular those relevant to fuels applications, namely 2-ethylhexyl acrylate, isodecyl acrylate, lauryl acrylate, and stearyl acrylate, in addition to styrene, methyl acrylate, and *N*-isopropylacrylamide. To our knowledge, this is the first preparation of block copolymers of the "green" polyethylene-like material PPDL *via* a combination of eROP and RAFT polymerization techniques. Considering the potential for the preparation of novel materials *via* this technique, future studies could include the preparation of RAFT-functional PPDL from bifunctional initiators maintaining different Z and/or R groups or *via* convergent synthetic strategies, the preparation of higher architectures of PPDL and copolymers thereof, and the investigation of high molecular weight material. Additional investigations could include the development of non-enzymatic catalysts capable of polymerizing macrocyclic lactones in the absence of both significant chain scission reactions and initiation from water.

A selection of acrylic block copolymers of DP 19 PPDL were prepared on a large scale *via* a combination of eROP and RAFT polymerization techniques, characterized, and subsequently tested in various diesel fuels for cold-flow applications. Good control of the chain extension of the PPDL macro-CTA was demonstrated by the preparation of a selection of defined copolymers with good end-group fidelity, as evidenced by analysis of MALDI-ToF mass spectra for PPDL-*b*-poly(lauryl acrylate) copolymers and UV-GPC chromatograms. It was determined that all PPDL-*b*-poly(acrylate) copolymers tested, with the exception of 1:12 PPDL-*b*-poly(lauryl acrylate) and 1:1 PPDL-*b*-poly(stearyl acrylate), did not have any significant effect on wax crystal morphology or wax dispersion in diesel fuel. However, all PPDL-*b*-poly(acrylate) copolymers, particularly those featuring branched rather than linear side chains, improved the Cold Filter Plugging Point (CFPP) of most diesel fuels tested. Therefore, copolymers of PPDL merit further investigation as a novel class of cold-flow additives, and future investigations could include the preparation and fuels testing of PPDL-*b*-poly(methacrylate) copolymers in order to further disrupt the backbone of the solubilising block, in addition to block copolymers of varied PPDL molecular weights and/or mixed poly(ester)s, and finally alternate architectures of related polymers.

Finally, triphenylstannane dithioesters were prepared and explored as a novel class of RAFT agents. Although the toxicity of tin significantly limits potential end-uses of polymers prepared *via* this method, it was determined that triphenylstannane dithioisopropylester afforded moderate control of the polymerization of isoprene, comparable to that reported in the literature. Furthermore, triphenylstannane dithiobenzylester was shown to control the polymerization of methyl acrylate and styrene, however, end-group fidelity was not evaluated. Future work on the development of Sn-RAFT agents should include analysis of end-group fidelity and direct comparisons with conventional CTAs, including the F-RAFT agent isopropylfluorodithioformate (IFDF). If triphenylstannane dithioesters are confirmed to proceed *via* the RAFT mechanism, then future research could be expanded to include novel stannane dithioesters maintaining alternate substituents on the metal in order to tune the reactivity of the thiocarbonyl.

Chapter 6

Experimental

6.1 Materials

Chemicals were used as received from Alfa Aesar, SAFC, and Sigma-Aldrich, and solvents were purchased from Fisher Scientific. Anhydrous stannous chloride and Novozyme 435 were dried over P_2O_5 and stored in a nitrogen filled glovebox, with the *lipase* being stored at -20 ºC. Phenyllithium in dibutyl ether was titrated thrice against sublimed diphenylacetic acid to evaluate its molarity and 2,2′-Azobis(2-methylpropionitrile) and 1,1′-azobis(cyclohexanecarbonitrile) were recrystallized twice from methanol. Carbon disulfide, benzyl alcohol, 2-iodopropane, styrene, and isoprene were distilled from CaH_2 and stored in an ampoule under an inert atmosphere. Benzyl bromide was dried over 3 Å molecular sieves. Stock solutions of ω-pentadecalatone in anhydrous toluene were dried over 4 Å molecular sieves at 40 ºC and filtered prior to use. Anhydrous 1,4-dioxane was obtained by refluxing 1,4-dioxane over stannous chloride, followed by CaH_2, and storing the distilled solvent over 4 Å molecular sieves. Methyl acrylate, 2-ethylhexyl acrylate, lauryl acrylate, isodecyl acrylate, and stearyl acrylate were passed through a column of basic alumina prior to use. Anhydrous tetrahydrofuran and toluene were obtained by passing the solvent through a column of activated alumina using an Innovative Technologies Inc. Pure Solv MD-4-EN solvent purification system.

6.2 General Considerations

All moisture and oxygen sensitive manipulations were performed in either a nitrogen-filled glovebox or by standard Schlenk techniques.

NMR Spectroscopy: ^{1}H NMR and ^{13}C DEPT NMR spectra were recorded on a Bruker DPX-400, DPX 300, AC-400, or AV-250 spectrometer in $CDCl_3$ at 293 K unless otherwise stated. Chemical shifts are reported as δ in parts per million (ppm) and referenced to the chemical shift of residual solvent resonances ($CDCl_3$ ^{1}H: $\delta = 7.26$ ppm; ^{13}C: $\delta = 77.16$ ppm, or trimethylsilane ^{1}H: $\delta = 0.0$ ppm). Data are presented as follows: chemical shift, integration, peak multiplicity (s = singlet, d = doublet, dd = doublet of doublets, t = triplet, q = quartet, sept = septet, m = multiplet, dm = doublet of multiplets, bs = broad singlet), coupling constants (J/Hz), and assignment. Assignments were determined either on the basis of unambiguous chemical shift or coupling patterns, by analysis of 2D NMR spectroscopy (COSY, HMQC, HMBC), or by analogy to fully interpreted spectra for structurally related compounds.

Size exclusion chromatography (SEC)/Gel Permeation chromatography (GPC):
Measurements in THF were conducted on a system comprised of a Varian 390-LC-Multi detector suite fitted with differential refractive index (DRI), light scattering (LS) and ultra-violet (UV) detectors equipped with a guard column (Varian Polymer Laboratories PLGel 5 μM, 50 × 7.5 mm) and two mixed D columns (Varian Polymer Laboratories PLGel 5 μM, 300 × 7.5 mm). The mobile phase was tetrahydrofuran with 5% triethylamine at a flow rate of 1.0 mL min^{-1}, and samples were calibrated against Varian Polymer Laboratories Easi-Vials linear poly(styrene) standards (162 - 240,000 g mol^{-1}) using Cirrus v3.3 software.

Measurements in CHCl$_3$ were performed on a Polymer Laboratories modular GPC system comprising of a Polymer Laboratories Midas autosampler and LC1120 HPLC pump equipped with a guard column (Polymer Laboratories PLGel 5 mM, 50-7.5 mm), two mixed D columns (Polymer Laboratories PLGel 5 mM, 300-7.5 mm) and a Polymer Laboratories ERC-7515A differential refractive index (DRI) detector. The mobile phase was chloroform with 5% triethylamine at a flow rate of 1.0 mL min^{-1}, and samples were calibrated against linear poly(styrene) standards obtained from Polymer Laboratories using Cirrus v3.0 software; elution time was standardized against that for toluene.

Measurements in CHCl$_3$ for UV detection were conducted on a system composed of a Varian 390-LC-Multi detector suite fitted with differential refractive index, light scattering, and ultraviolet detectors equipped with a guard column (Varian Polymer Laboratories PLGel 5 μM, 50 × 7.5 mm) and two mixed D columns (Varian Polymer Laboratories PLGel 5 μM, 300 × 7.5 mm). The mobile phase was chloroform with 2% triethylamine at a flow rate of 1.0 mL min^{-1}, and samples were calibrated against Varian Polymer Laboratories Easi-Vials linear poly(styrene) standards (162 - 240,000 g mol^{-1}) using Cirrus v3.2 software.

MALDI-ToF Mass Spectrometry: Spectra were acquired by matrix-assisted laser desorption and ionisation time-of-flight (MALDI ToF) mass spectrometry using a Bruker Daltonics Ultraflex II MALDI ToF mass spectrometer equipped with a nitrogen laser delivering 2 ns laser pulses at 337 nm, and with positive ion detection performed using an accelerating voltage of 25 kV. Solutions of *trans*-2-[3-(4-*tert*-butylphenyl)-2-methyl-2-propyl-lidene]malonitrile (DCTB) as matrix (40 μL of a 40 g L^{-1} solution in THF), sodium trifluoroacetate as cationisation salt (10 μL of a 10 g L^{-1} solution in THF) and analyte (10 μL of a 10 g L^{-1} solution in CHCl$_3$) were combined and applied to the target, after which the solvent was evaporated to prepare a thin matrix/analyte film. The samples were measured in reflectron ion mode, unless otherwise stated, and calibrated by comparison to 2000 or 5000 g mol^{-1} monomethylether poly(ethylene oxide) standards.

Thermal Analysis: Samples were analysed by DSC on a Mettler Toledo instrument and a TA instruments DSC Q20 autosampler. Using the Mettler Toledo instrument and a 40 μL aluminium crucible under a nitrogen atmosphere, DSC heating and cooling cycles were run in triplicate in series between -70 ^{o}C and 120 ^{o}C at a heating rate of +/- 10 ^{o}C min^{-1}. Using the TA instruments DSC Q20 autosampler and a 40 μL aluminium crucible under a nitrogen atmosphere, DSC heating and cooling cycles were run in triplicate in series between -70 ^{o}C and 120 ^{o}C at a heating rate of +/- 10 ^{o}C min^{-1}. TGA analysis was conducted on a Universal TA Instruments TGA Q5000 using a 40 μL aluminium crucible between 50 ^{o}C and 600 ^{o}C at a heating rate of 10 ^{o}C min^{-1}.

Optical Microscopy: Fuel samples were visualized using an Olympus BX51 optical microscope and captured using an Olympus DP25 digital camera.

Infra-red Spectroscopy: FT-IR spectra were recorded on a Perkin Elmer Spectrum 100 FT-IR spectrometer using a diamond press.

UV-vis Spectroscopy: UV-vis spectra were recorded on a PerkinElmer LAMBDA 35 UV/Vis spectrometer.

Melting Point Determinations: Melting points were recorded on a Stanford Research Systems MPA100 Optimelt with a heating rate of 1.0 °C min^{-1} and are uncorrected.

Other Techniques: Reactions were monitored by thin layer chromatography (TLC) conducted on pre-coated aluminium-backed plates (Merck Kieselgel 60 with fluorescent indicator UV254). Spots were visualized either by quenching of UV fluorescence (254 nm) or by staining with basic potassium permanganate dip. Flash column chromatography was performed manually according to the method described by Still *et al.*[1] with ZEOprep 60 (25-40 μm) silica gel or neutral alumina, applying head pressure by means of compressed air.

6.3 Experimental Details for Chapter 2

Preparation of Dodecyl 4-(hydroxymethyl) benzyl carbonotrithioate (1)

Dodecane thiol (8.50 mL, 34.77 mmol) was injected into a suspension of potassium phosphate (7.53 g, 34.77 mmol) in acetone (600 mL) and permitted to stir at room temperature for approximately 20 minutes. Carbon disulfide (5.70 mL, 94.82 mmol) was added to the reaction mixture drop wise and the resulting mixture, which slowly turned yellow, was permitted to stir for approximately two hours. Thereafter 4-(chloromethyl)benzyl alcohol (5.0 g, 31.61 mmol) was

added to the reaction mixture and permitted to stir at room temperature for 8 days. The resulting bright yellow mixture was filtered, the filter cake washed with acetone and dichloromethane, and the filtrate concentrated by rotoevaporation. The residue was taken up in dichloromethane and washed with 500 mL of 0.1M hydrochloric acid, thrice with 500 mL of deionized water, and finally 500 mL of brine. The resulting organic layer was dried over magnesium sulfate, filtered, and concentrated by rotoevaporation to yield yellow solid, which was washed with chilled hexanes and methanol, and dried *in vacuo* (11.64 g, 94 %). ^{1}H and ^{13}C DEPT NMR spectroscopy data match reported values:[2] δ_H (300 MHz, CDCl$_3$) = 7.38-7.28 (4H, m, ArH), 4.68 (2H, d, $^3J_{H-H}$ = 6.0 Hz Ar-CH_2OH), 4.61 (2H, s, -SCH_2PhCH$_2$OH), 3.36 (2H, t, $^3J_{H-H}$ = 6.0 Hz, -SCH_2(CH$_2$)$_{10}$CH$_3$), 1.75-1.65 (2H, q, $^3J_{H-H}$ = 6.0 Hz, -SCH$_2$CH_2(CH$_2$)$_9$CH$_3$), 1.64-1.58 (1H, t, $^3J_{H-H}$ = 6.0 Hz, PhCH$_2$OH), 1.46-1.15 (18H, m, -SCH$_2$CH$_2$(CH_2)$_9$CH$_3$), 0.94-0.82 (3H, t, $^3J_{H-H}$ = 6.0 Hz, -S(CH$_2$)$_{11}$CH_3); δ_C (500 MHz, CDCl$_3$) = 223.7, 140.4, 134.6, 129.5, 127.3, 65.0, 41.0, 37.1, 31.9, 29.6, 29.5, 29.4, 29.3, 29.1, 28.9, 27.9, 22.7, 14.1.

General Protocol for the eROP of PDL

Working in a glovebox, *lipase* (10 mg, 1 wt.%), initiator (0.208 mmol, [M]/[I] = 20), and PDL in toluene (4.16 mmol, 4.6 mL of a 25 wt.% PDL stock solution in anhydrous toluene) were combined in an ampoule equipped with magnetic stirring. Additional ampoules were similarly prepared for individual kinetic points. The ampoules were immersed in a 60 °C oil bath with stirring and stopped at various time intervals. Aliquots were removed for direct ^{1}H NMR spectroscopy (CDCl$_3$) and GPC (CHCl$_3$) analysis, after which the remainder of the reaction mixtures were diluted in cold chloroform, filtered to remove the enzyme, and concentrated *in vacuo*. Crude products were purified *via* precipitation in methanol from chloroform and further analysed by MALDI-ToF mass spectrometry and DSC. Reactions were performed in triplicate and varying [M]/[I].

DP 32 PPDL initiated from BnOH: ^{1}H NMR: δ_H (300 MHz, CDCl$_3$) = ^{1}H NMR: δ_H (300 MHz, CDCl$_3$) = 7.35 (4H, s, ArH), 5.11 (2H, s, ArCH_2O-), 4.05 (62H, t, $^3J_{H-H}$ = 6.0 Hz, -C(O)OCH_2-), 3.75-3.45 (2H, bs, -CH$_2$CH_2OH), 3.35-3.15 (1H, bs, -CH$_2$OH), 2.28 (64H, t, $^3J_{H-H}$ = 6.0 Hz, -CH_2C(O)OCH$_2$-), 1.70-1.55 (128H, t, $^3J_{H-H}$ = 6.0 Hz, -C(O)OCH$_2$CH_2-; -OC(O)CH$_2$CH_2-), 1.40-1.15 (640H, m, -CH_2-).

DP 11 PPDL initiated from 1: ^{1}H NMR: δ_H (300 MHz, CDCl$_3$) = 7.31 (4H, dd, $^3J_{H-H}$ = 6.0 Hz, ArH), 5.08 (2H, s, ArCH_2OC(O)-), 4.60 (2H, s, ArCH_2S-), 4.05 (20H, t, $^3J_{H-H}$ = 6.0 Hz, -C(O)OCH_2-), 3.64 (2H, t, $^3J_{H-H}$ = 6.0 Hz, -CH$_2$CH_2OH), 3.36 (2H, t, $^3J_{H-H}$ = 6.0 Hz, -SCH_2CH$_2$-), 2.34 (1H, t, $^3J_{H-H}$ = 6.0 Hz, -CH$_2$CH$_2$OH), 2.28 (22H, t, $^3J_{H-H}$ = 6.0 Hz, -CH_2C(O)OCH$_2$-), 1.75-

1.45 (48H, m, -C(O)OCH$_2$CH$_2$-; -OC(O)CH$_2$CH$_2$-; -SCH$_2$CH$_2$(CH$_2$)$_9$CH$_3$; -SCH$_2$CH$_2$CH$_2$(CH$_2$)$_8$CH$_3$,), 1.25 (236H, m, -CH$_2$-; -S(CH$_2$)$_3$(CH$_2$)$_8$CH$_3$), 0.95-0.75 (3H, t, $^3J_{H-H}$ = 6.0 Hz, -CH$_2$CH$_3$).

Preparation of PPDL macro-CTA 2

Working in a glovebox, *lipase* (1.21 g, 1 wt.%) and dodecyl 4-(hydroxymethyl) benzyl carbonotrithioate (**1**) (10.0 g, 25.08 mmol, [M]/[I] = 20) were combined in a Schlenk flask equipped with magnetic stirring. PDL in toluene (501.64 mmol, 554.69 mL of a 25 wt.% PDL stock solution in anhydrous toluene) was transferred into the reaction flask using a cannula, and the resulting mixture was stirred until homogeneous. The flask was immersed in a 60 ℃ oil bath with stirring for 175 minutes and the resulting mixture was diluted with cold chloroform, filtered to remove the enzyme, concentrated by rotoevaporation, and dried *in vacuo*. The product was analysed by ^{1}H NMR spectroscopy (CDCl$_3$), GPC (CHCl$_3$), MALDI-ToF mass spectrometry, and DSC. Although the crude product was utilized for further experiments, it was however purified *via* precipitation in methanol from chloroform for DSC analysis.

General Protocol for RAFT Polymerizations using Dodecyl 4-(hydroxymethyl) benzyl carbonotrithioate (1) as a CTA ([M]:[CTA]:[I] = 100:1:0.1)

Methyl acrylate (1.14 mL, 12.54 mmol), dodecyl 4-(hydroxymethyl) benzyl carbonotrithioate (**1**) (50 mg, 12.54 x 10^{-3} mmol), and anhydrous toluene (4.70 mL ([M] = 2.55 M), or as otherwise stated (i.e.: 1.11 mL, 50 wt.%)) were combined in an ampoule equipped with magnetic stirring, degassed *via* three freeze-pump-thaw cycles, and refilled with argon. The ampoule was immersed in an 80 ℃ oil bath with stirring for approximately 1 hour. Thereafter AIBN (0.212 mL of a degassed 10 mg ml^{-1} AIBN stock solution in toluene, 12.54 x 10^{-4} mmol) was injected into the reaction mixture and aliquots removed at regular time intervals for ^{1}H NMR spectroscopy (CDCl$_3$), GPC (CHCl$_3$/THF), MALDI-ToF mass spectrometry, and DSC analysis. Additional polymerizations were similarly performed with other acrylic or styrenic monomers, and at varied [M].

DP 59 Poly(Methyl acrylate): ^{1}H NMR: δ_H (300 MHz, CDCl$_3$) = 7.36-7.10 (4H, dd, $^3J_{H-H}$ = 6.0 Hz, Ar*H*), 4.95-4.80 (2H, m, HOC*H*$_2$Ar), 4.65 (2H, s, ArC*H*$_2$CH$_2$R), 3.66 (177H, s, -OC*H*$_3$), 3.34 (1H, t, $^3J_{H-H}$ = 6.0 Hz, RSC(S)S-C*H*RCH$_2$-), 3.25-2.95 (2H, m, CH$_3$(CH$_2$)$_{10}$C*H*$_2$SC(S)S-), 2.56 (2H, t, $^3J_{H-H}$ = 6.0 Hz, RSC(S)S-CHRC*H*$_2$CHR-), 2.30 (58H, m, -CH$_2$C*H*RCH$_2$-), 2.13 (1H, bs, ArCH$_2$O*H*), 2.05-1.83 (24H, m, -CHRC*H*$_2$CHR- *meso*), 1.83-1.60 (58H, m, -CHRC*H*$_2$CHR-*racemo*), 1.60-1.25 (28H, m, -CHRC*H*$_2$CHR- *meso*; -SCH$_2$C*H*$_2$(CH$_2$)$_9$CH$_3$; -

SCH$_2$CH$_2$C*H*$_2$(CH$_2$)$_8$CH$_3$), 1.16 (16H, m, -S(CH$_2$)$_3$(C*H*$_2$)$_8$CH$_3$), 0.87 (3H, t, $^3J_{H-H}$ = 6.0 Hz, -CH$_2$C*H*$_3$).

DP 48 Poly(2-Ethylhexyl acrylate): ^{1}H NMR: δ_H (300 MHz, CDCl$_3$) = 7.36-7.10 (4H, dd, $^3J_{H-H}$ = 6.0 Hz, Ar*H*), 4.90-4.75 (2H, m, HOC*H*$_2$Ar), 4.65 (2H, s, ArC*H*$_2$CH$_2$R), 4.4-3.60 (96H, m, -C(O)OC*H*$_2$CH$_2$-), 3.34 (1H, t, $^3J_{H-H}$ = 6.0 Hz, RSC(S)S-C*H*RCH$_2$-), 3.20 (2H, t, $^3J_{H-H}$ = 6.0 Hz, CH$_3$(CH$_2$)$_{10}$C*H*$_2$SC(S)S-), 2.55-2.40 (2H, m, RSC(S)S-CHRC*H*$_2$CHR-), 2.40-2.05 (48H, m, -CH$_2$C*H*RCH$_2$-), 2.05-1.78 (23H, m, -CHRC*H*$_2$CHR- *meso*), 1.80-1.40 (99H, m, -CHRC*H*$_2$CHR-*racemo*; -SCH$_2$C*H*$_2$(CH$_2$)$_9$CH$_3$; -SCH$_2$CH$_2$C*H*$_2$(CH$_2$)$_8$CH$_3$; -C(O)OCH$_2$C*H*RCH$_2$-; *H*OCH$_2$AR), 1.40-0.98 (423H, m, -CHRC*H*$_2$CHR- *meso*; -CH$_2$C*H*$_2$CH$_2$-; -S(CH$_2$)$_3$(C*H*$_2$)$_8$CH$_3$), 0.88 (288H, m, -CH$_2$C*H*$_3$), 0.67 (3H, t, $^3J_{H-H}$ = 6.0 Hz, -CH$_2$C*H*$_3$).

DP 25 Poly(Isodecyl acrylate): ^{1}H NMR: δ_H (300 MHz, CDCl$_3$) = 7.36-7.10 (4H, dd, $^3J_{H-H}$ = 6.0 Hz, Ar*H*), 4.90-4.75 (2H, m, HOC*H*$_2$Ar), 4.65 (2H, s, ArC*H*$_2$CH$_2$R), 4.4-3.60 (50H, m, -C(O)OC*H*$_2$CH$_2$-), 3.34 (1H, t, $^3J_{H-H}$ = 6.0 Hz, RSC(S)S-C*H*RCH$_2$-), 3.20 (2H, t, $^3J_{H-H}$ = 6.0 Hz, CH$_3$(CH$_2$)$_{10}$C*H*$_2$SC(S)S-), 2.55-2.40 (2H, m, RSC(S)S-CHRC*H*$_2$CHR-), 2.40-2.05 (24H, m, -CH$_2$C*H*RCH$_2$-), 2.05-1.78 (12H, m, -CHRC*H*$_2$CHR- *meso*), 1.80-1.40 (103H, m, -CHRC*H*$_2$CHR-*racemo*; -SCH$_2$C*H*$_2$(CH$_2$)$_9$CH$_3$; -SCH$_2$CH$_2$C*H*$_2$(CH$_2$)$_8$CH$_3$; -C(O)OCH$_2$C*H*$_2$CH$_2$-; *H*OCH$_2$AR), 1.40-0.98 (228H, m, -CHRC*H*$_2$CHR- *meso*; -C(O)OCH$_2$CH$_2$(C*H*$_2$)$_4$CH$_2$CH(CH$_3$)$_2$; -S(CH$_2$)$_3$(C*H*$_2$)$_8$CH$_3$), 0.88 (225H, m, -C*H*$_2$C*H*(CH$_3$)$_2$), 0.67 (3H, t, $^3J_{H-H}$ = 6.0 Hz, -CH$_2$C*H*$_3$).

DP 20 Poly(Lauryl acrylate): ^{1}H NMR: δ_H (300 MHz, CDCl$_3$) = 7.36-7.10 (4H, dd, $^3J_{H-H}$ = 6.0 Hz, Ar*H*), 4.90-4.75 (2H, m, HOC*H*$_2$Ar), 4.65 (2H, s, ArC*H*$_2$CH$_2$R), 4.4-3.70 (40H, m, -C(O)OC*H*$_2$CH$_2$-), 3.70-3.55 (1H, m, RSC(S)S-C*H*RCH$_2$-), 3.40-3.20 (2H, m, CH$_3$(CH$_2$)$_{10}$C*H*$_2$SC(S)S-), 2.55-2.40 (2H, m, RSC(S)S-CHRC*H*$_2$CHR-), 2.40-2.05 (19H, m, -CH$_2$C*H*RCH$_2$-), 2.05-1.78 (9H, m, -CHRC*H*$_2$CHR- *meso*), 1.75-1.50 (83H, m, -CHRC*H*$_2$CHR-*racemo*; -SCH$_2$C*H*$_2$(CH$_2$)$_9$CH$_3$; -SCH$_2$CH$_2$C*H*$_2$(CH$_2$)$_8$CH$_3$; -C(O)OCH$_2$C*H*$_2$CH$_2$-; *H*OCH$_2$AR), 1.40-0.98 (386H, m, -CHRC*H*$_2$CHR- *meso*; -CH$_2$C*H*$_2$CH$_2$-; -S(CH$_2$)$_3$(C*H*$_2$)$_8$CH$_3$), 0.88 (60H, t, $^3J_{H-H}$ = 6.0 Hz, -CH$_2$C*H*$_3$), 0.67 (3H, t, $^3J_{H-H}$ = 6.0 Hz, -CH$_2$C*H*$_3$).

DP 327 Poly(Stearyl acrylate): ^{1}H NMR: δ_H (300 MHz, CDCl$_3$) = 7.36-7.10 (4H, dd, $^3J_{H-H}$ = 6.0 Hz, Ar*H*), 5.05 (2H, m, HOC*H*$_2$Ar), 4.90-4.65 (2H, s, ArC*H*$_2$CH$_2$R), 4.4-3.70 (654H, m, -C(O)OC*H*$_2$CH$_2$-), 3.70-3.55 (1H, m, RSC(S)S-C*H*RCH$_2$-), 3.40-3.20 (2H, m, CH$_3$(CH$_2$)$_{10}$C*H*$_2$SC(S)S-), 2.55-2.40 (1H, m, RSC(S)S-CHRC*H*$_2$CHR-), 2.40-2.05 (326H, m, -CH$_2$C*H*RCH$_2$-), 2.05-1.78 (163H, m, -CHRC*H*$_2$CHR- *meso*), 1.75-1.50 (985H, m, -CHRC*H*$_2$CHR- *racemo*; -SCH$_2$C*H*$_2$(CH$_2$)$_9$CH$_3$; -SCH$_2$CH$_2$C*H*$_2$(CH$_2$)$_8$CH$_3$; -C(O)OCH$_2$C*H*$_2$CH$_2$-; *H*OCH$_2$AR), 1.40-0.98 (9989H, m, -CHRC*H*$_2$CHR- *meso*; -C(O)OCH$_2$CH$_2$(C*H*$_2$)$_{15}$CH$_3$; -

S(CH$_2$)$_3$(C*H*$_2$)$_8$CH$_3$), 0.88 (981H, t, $^3J_{H-H}$ = 6.0 Hz, -CH$_2$C*H*$_3$), 0.67 (3H, t, $^3J_{H-H}$ = 6.0 Hz, -CH$_2$C*H*$_3$).

General Protocol for the Preparation of Block Copolymers of PPDL *via* the RAFT Process using 2 as a macro-CTA

Methyl acrylate (1.14 mL, 12.54 mmol), macro-CTA **2** (50 mg, 12.54 x 10^{-3} mmol), and anhydrous toluene (1.11 mL, 50 wt.%) were combined in an ampoule equipped with magnetic stirring, degassed *via* three freeze-pump-thaw cycles, and refilled with argon. The ampoule was immersed in an 80 ºC oil bath with stirring for approximately 1 hour. Thereafter AIBN (0.212 mL of a degassed 10 mg ml^{-1} AIBN stock solution in toluene, 12.54 x 10^{-4} mmol) was injected into the reaction mixture and aliquots of the reaction mixture were removed at regular time intervals for ^{1}H NMR spectroscopy (CDCl$_3$), GPC (CHCl$_3$/THF), MALDI-ToF, and DSC analysis. Other acrylic or styrenic monomers were similarly polymerized, with the exception of NIPAM, which was polymerization in chloroform at 60 ºC. Furthermore, additional reactions were performed varying [M]/[I], [M], temperature, and initiator.

PPDL-b-(DP 32 PEHA): ^{1}H NMR: δ_H (300 MHz, CDCl$_3$) = 7.28-7.08 (4H, dd, $^3J_{H-H}$ = 6.0 Hz, Ar*H*), 5.05 (2H, s, RC(O)OC*H*$_2$Ar), 4.95-4.70 (2H, m, ArC*H*$_2$CH$_2$R), 4.05 (32H, t, $^3J_{H-H}$ = 6.0 Hz, -CH$_2$C(O)OC*H*$_2$-), 4.20-3.68 (64H, m, -HC(O)OC*H*$_2$CH$_2$-), 3.64 (1H, t, $^3J_{H-H}$ = 6.0 Hz, RSC(S)S-C*H*RCH$_2$-), 3.40-3.22 (2H, t, $^3J_{H-H}$ = 6.0 Hz, CH$_3$(CH$_2$)$_{10}$C*H*$_2$SC(S)S-), 2.55-2.45 (2H, m, RSC(S)S-CHRC*H*$_2$CHR-), 2.28 (65H, t, $^3J_{H-H}$ = 6.0 Hz, -C*H*$_2$C(O)OCH$_2$-; -CH$_2$C*H*RCH$_2$-; *H*OCH$_2$-), 2.05-1.75 (15H, m, -CHRC*H*$_2$CHR- *meso*), 1.75-1.50 (131H, m, -CHRC*H*$_2$CHR- *racemo*; -SCH$_2$C*H*$_2$(CH$_2$)$_9$CH$_3$; -SCH$_2$CH$_2$C*H*$_2$(CH$_2$)$_8$CH$_3$; -C(O)OCH$_2$C*H*$_2$CH$_2$-; -CH$_2$C*H*$_2$CH$_2$C(O)O-; -C(O)OCH$_2$C*H*RCH$_2$-), 1.45-0.97 (608H, m, -CHRC*H*$_2$CHR- *meso*; -C*H*$_2$-; -S(CH$_2$)$_3$(C*H*$_2$)$_8$CH$_3$), 0.97-0.75 (192H, m, C*H*$_3$CH$_2$-), 0.75-0.54 (3H, m, C*H*$_3$(CH$_2$)$_{11}$SC(S)S-).

PPDL-b-(DP 17 PIDA): ^{1}H NMR: δ_H (300 MHz, CDCl$_3$) = 7.28-7.08 (4H, dd, $^3J_{H-H}$ = 6.0 Hz, Ar*H*), 5.05 (2H, s, RC(O)OC*H*$_2$Ar), 4.95-4.70 (2H, m, ArC*H*$_2$CH$_2$R), 4.05 (32H, t, $^3J_{H-H}$ = 6.0 Hz, -CH$_2$C(O)OC*H*$_2$-), 4.20-3.68 (34H, m, -HC(O)OC*H*$_2$CH$_2$-), 3.64 (1H, t, $^3J_{H-H}$ = 6.0 Hz, RSC(S)S-C*H*RCH$_2$-), 3.40-3.22 (2H, m, -CH$_3$(CH$_2$)$_{10}$C*H*$_2$SC(S)S-), 2.65-2.45 (2H, m, RSC(S)S-CHRC*H*$_2$CHR-), 2.28 (49H, t, $^3J_{H-H}$ = 6.0 Hz, -C*H*$_2$C(O)OCH$_2$-; -CH$_2$C*H*RCH-; *H*OCH$_2$-), 2.00-1.80 (8H, m, -CHRC*H*$_2$CHR- *meso*), 1.80-1.50 (118H, m, -CHRC*H*$_2$CHR- *racemo*; -SCH$_2$C*H*$_2$(CH$_2$)$_9$CH$_3$; -SCH$_2$CH$_2$C*H*$_2$(CH$_2$)$_8$CH$_3$; -C(O)OCH$_2$C*H*$_2$CH$_2$-; -CH$_2$C*H*$_2$CH$_2$C(O)O-),

1.50-0.97 (480H, m, -CHRCH_2CHR- *meso*, -CH_2-; -S(CH$_2$)$_3$(CH_2)$_8$CH$_3$), 0.97-0.68 (153H, m, CH_3CH$_2$-; CH$_3$CH-; CH$_3$CHCH_2-), 0.68-0.54 (3H, m, CH_3(CH$_2$)$_{11}$SC(S)S-).

PPDL-b-(DP 30 PLA): ^{1}H NMR: δ_H (300 MHz, CDCl$_3$) = 7.28-7.08 (4H, dd, $^3J_{\text{H-H}}$ = 6.0 Hz, ArH), 5.05 (2H, s, RC(O)OCH_2Ar), 4.95-4.70 (2H, m, ArCH_2CH$_2$R), 4.05 (32H, t, $^3J_{\text{H-H}}$ = 6.0 Hz, -CH$_2$C(O)OCH_2-), 4.20-3.68 (60H, m, -HC(O)OCH_2CH$_2$-), 3.68-3.59 (1H, m, RSC(S)S-CHRCH$_2$-), 3.40-3.22 (2H, m, CH$_3$(CH$_2$)$_{10}$CH_2SC(S)S-), 2.65-2.45 (2H, m, RSC(S)S-CHRCH_2CHR-), 2.28 (62H, t, $^3J_{\text{H-H}}$ = 6.0 Hz, -CH_2C(O)OCH$_2$-; -CH$_2$CHRCH-; HOCH$_2$-), 2.15-1.75 (14H, m, -CHRCH_2CHR- *meso*), 1.75-1.49 (157H, m, -CHRCH_2CHR- *racemo*, -SCH$_2$CH_2(CH$_2$)$_9$CH$_3$; -SCH$_2$CH$_2$CH_2(CH$_2$)$_8$CH$_3$; -C(O)OCH$_2$CH_2CH$_2$-; -CH$_2$CH_2CH$_2$C(O)O-), 1.44-0.98 (891H, m, -CHRCH_2CHR- *meso*; -CH_2-; -S(CH$_2$)$_3$(CH_2)$_8$CH$_3$); 0.98-0.75 (90H, m, CH_3CH$_2$-), 0.72-0.63 (3H, m, CH_3(CH$_2$)$_{11}$SC(S)S-).

PPDL-b-(DP 47 PSA): ^{1}H NMR: δ_H (300 MHz, CDCl$_3$) = 7.28-7.08 (4H, dd, $^3J_{\text{H-H}}$ = 6.0 Hz, ArH), 5.05 (2H, s, RC(O)OCH_2Ar), 4.95-4.70 (2H, m, ArCH_2CH$_2$R), 4.05 (32H, t, $^3J_{\text{H-H}}$ = 6.0 Hz, -CH$_2$C(O)OCH_2-), 4.20-3.68 (94H, m, -HC(O)OCH_2CH$_2$-), 3.64 (1H, t, $^3J_{\text{H-H}}$ = 6.0 Hz, RSC(S)S-CHRCH$_2$-), 3.38-3.22 (2H, m, CH$_3$(CH$_2$)$_{10}$CH_2SC(S)S-), 2.65-2.45 (2H, m, RSC(S)S-CHRCH_2CHR-), 2.28 (79H, t, $^3J_{\text{H-H}}$ = 6.0 Hz, -CH_2C(O)OCH$_2$-; -CH$_2$CHRCH-; HOCH$_2$-), 2.25-1.75 (23H, m, -CHRCH_2CHR- *meso*), 1.75-1.50 (208H, m, -CHRCH_2CHR- *racemo*, -SCH$_2$CH_2(CH$_2$)$_9$CH$_3$; -SCH$_2$CH$_2$CH_2(CH$_2$)$_8$CH$_3$; -C(O)OCH$_2$CH_2CH$_2$-; -CH$_2$CH_2CH$_2$C(O)O-), 1.50-0.98 (1769H, m, -CHRCH_2CHR- *meso*; -CH_2-; -S(CH$_2$)$_3$(CH_2)$_8$CH$_3$); 0.88 (141H, t, $^3J_{\text{H-H}}$ = 6.0 Hz, CH_3CH$_2$-), 0.72-0.63 (3H, m, CH_3(CH$_2$)$_{11}$SC(S)S-).

PPDL-b-(DP 43 PMA): ^{1}H NMR: δ_H (300 MHz, CDCl$_3$) = 7.40-7.10 (4H, m, ArH), 5.06 (2H, s, RC(O)OCH_2Ar), 4.95-4.70 (2H, m, ArCH_2CH$_2$R), 4.05 (32H, t, $^3J_{\text{H-H}}$ = 6.0 Hz, -CH$_2$C(O)OCH_2-), 3.66 (129H, bs, -C(O)OCH_3), 3.58-3.44 (1H, m, RSC(S)S-CHRCH$_2$-), 3.38-3.22 (2H, m, CH$_3$(CH$_2$)$_{10}$CH_2SC(S)S-), 2.45-2.35 (2H, m, RSC(S)S-CHRCH_2CHR-), 2.28 (75H, t, $^3J_{\text{H-H}}$ = 6.0 Hz, -CH_2C(O)OCH$_2$-; -CHC(O)OCH$_3$; HOCH$_2$-), 2.05-1.80 (21H, m, -CHRCH_2CHR- *meso*), 1.75-1.56 (110H, m, -CHRCH_2CHR- *racemo*, -SCH$_2$CH_2(CH$_2$)$_9$CH$_3$; -SCH$_2$CH$_2$CH_2(CH$_2$)$_8$CH$_3$; -C(O)OCH$_2$CH_2CH$_2$-; -CH$_2$CH_2CH$_2$C(O)O-), 1.40-1.20 (357H, m, -CHRCH_2CHR- *meso*, -CH_2-; -S(CH$_2$)$_3$(CH_2)$_8$CH$_3$), 0.95-0.80 (3H, m, CH_3(CH$_2$)$_{11}$SC(S)S-).

PPDL-b-(DP 27 P(NIPAM)): ^{1}H NMR: δ_H (300 MHz, CDCl$_3$) = 7.40-7.10 (4H, m, ArH), 7.05-5.70 (27H, bs, -C(O)NHCH(CH$_3$)$_2$), 5.05 (2H, s, RC(O)OCH_2Ar), 4.70-4.50 (2H, m, ArCH_2CH$_2$R), 4.05 (32H, t, $^3J_{\text{H-H}}$ = 6.0 Hz, -CH$_2$C(O)OCH_2-), 4.16-3.88 (27H, -C(O)NHCH(CH$_3$)$_2$), 3.63 (1H, t, $^3J_{\text{H-H}}$ = 6.0 Hz, RSC(S)S-CHRCH$_2$-), 3.40-3.20 (2H, m, CH$_3$(CH$_2$)$_{10}$CH_2SC(S)S-), 2.50-2.40 (2H, m, RSC(S)S-CHRCH_2CHR-), 2.28 (59H, t, $^3J_{\text{H-H}}$ = 6.0

Hz, -CH_2C(O)OCH$_2$-; -CHC(O)OCH$_3$; HOCH$_2$-), 2.23-1.98 (13H, m, -CHRCH_2CHR- *meso*), 1.75-1.50 (94H, m, -CHRCH_2CHR- *racemo*, -SCH$_2$CH_2(CH$_2$)$_9$CH$_3$; -SCH$_2$CH$_2$CH_2(CH$_2$)$_8$CH$_3$; -C(O)OCH$_2$CH_2CH$_2$-; -CH$_2$CH_2CH$_2$C(O)O-), 1.40-1.25 (349H, m, -CHRCH_2CHR- *meso*; -CH_2-; -S(CH$_2$)$_3$(CH_2)$_8$CH$_3$), 1.25-1.10 (162H, bs, -CHCH_3), 0.80 (3H, t, $^3J_{H-H}$ = 6.0 Hz, CH_3(CH$_2$)$_{11}$SC(S)S-).

PPDL-b-(DP 31 PS): ^{1}H NMR: δ_H (300 MHz, CDCl$_3$) = 7.25-6.15 (155H, m, ArH), 5.15-4.95 (2H, s, RC(O)OCH_2Ar), 4.75-4.55 (2H, m, ArCH_2CH$_2$R), 4.05 (32H, t, $^3J_{H-H}$ = 6.0 Hz, -CH$_2$C(O)OCH_2-), 3.64 (1H, t, $^3J_{H-H}$ = 6.0 Hz, RSC(S)S-CHRCH$_2$-), 3.40-3.15 (2H, m, CH$_3$(CH$_2$)$_{10}$CH_2SC(S)S-), 2.29 (33H, t, $^3J_{H-H}$ = 6.0 Hz, -CH_2C(O)OCH$_2$-; HOCH$_2$-), 2.45-1.70 (30H, m, -CH$_2$CHRCH$_2$-), 1.70-1.50 (144H, m, -CHRCH_2CHR-, -SCH$_2$CH_2(CH$_2$)$_9$CH$_3$; -SCH$_2$CH$_2$CH_2(CH$_2$)$_8$CH$_3$; -C(O)OCH$_2$CH_2CH$_2$-; -CH$_2$CH_2CH$_2$C(O)O-), 1.50-1.15 (336H, m, -CH_2-; -S(CH$_2$)$_3$(CH_2)$_8$CH$_3$), 0.88 (3H, t, $^3J_{H-H}$ = 6.0 Hz, CH_3(CH$_2$)$_{11}$SC(S)S-).

6.4 Experimental Details for Chapter 3

Preparation of PPDL macro-CTA 3

Working in a glovebox, *lipase* (100.0 mg, 1 wt.%), dodecyl 4-(hydroxymethyl) benzyl carbonotrithioate (**1**) (806.0 mg, 0.208 mmol), and PDL in toluene (41.6 mmol, 46 mL of a 25 wt.% PDL stock solution in anhydrous toluene) were combined in a Schlenk flask equipped with magnetic stirring. The flask was immersed in a 60 °C oil bath with stirring, stopped after 165 minutes, and an aliquot analysed by ^{1}H NMR spectroscopy (CDCl$_3$) to evaluate percent monomer conversion. The mixture was quenched with cold chloroform, filtered to remove the enzyme, concentrated, recrystallized from ethyl acetate, and dried *in vacuo*. The resulting polymer was analysed by ^{1}H NMR spectroscopy (CDCl$_3$) and GPC (CHCl$_3$).

Preparation of PPDL-*b*-PEHA Copolymers for Fuels Testing

DP 19 PPDL macro-CTA **3**, AIBN, 2-ethylhexyl acrylate, and anhydrous toluene were combined in an ampoule equipped with magnetic stirring according to the quantities outlined in Table 6.1, degassed *via* three freeze-pump-thaw cycles, and refilled with nitrogen. The ampoule was immersed in an 80 °C oil bath with stirring and stopped at the specified time. The reaction mixture was precipitated twice in methanol, dried *in vacuo*, and analysed by ^{1}H NMR spectroscopy (CDCl$_3$) and GPC (CHCl$_3$).

Table 6.1: Reagent quantities for the preparation of PPDL-*b*-PEHA copolymers.

Entry	Macro-CTA	2-EHA	AIBN	Toluene	Time (min)
1	0.75 g (15.15×10^{-2} mmol)	3.22 mL (15.15 mmol)	2.49 mg (15.15×10^{-3} mmol)	12.51 mL	42
2	0.75 g (15.15×10^{-2} mmol)	3.22 mL (15.15 mmol)	2.49 mg (15.15×10^{-3} mmol)	12.51 mL	82
3	0.5 g (10.1×10^{-2} mmol)	2.15 mL (10.1 mmol)	1.66 mg (10.1×10^{-3} mmol)	8.34 mL	162
4	0.5 g (10.1×10^{-2} mmol)	2.15 mL (10.1 mmol)	1.66 mg (10.1×10^{-3} mmol)	8.34 mL	1200
5	0.5 g (10.1×10^{-2} mmol)	4.29 mL (20.19 mmol)	1.66 mg (10.1×10^{-3} mmol)	4.97 mL	75
6	0.5 g (10.1×10^{-2} mmol)	4.29 mL (20.19 mmol)	1.66 mg (10.1×10^{-3} mmol)	4.97 mL	80
7	0.5 g (10.1×10^{-2} mmol)	4.29 mL (20.19 mmol)	1.66 mg (10.1×10^{-3} mmol)	4.97 mL	370

Preparation of PPDL macro-CTA 4

Working in a glovebox, *lipase* (1.21 g, 1 wt.%) and dodecyl 4-(hydroxymethyl) benzyl carbonotrithioate (**1**) (10.0 g, 25.08 mmol, [M]/[I] = 20) were combined in a Schlenk flask equipped with magnetic stirring. PDL in toluene (501.64 mmol, 554.69 mL of a 25 wt.% PDL stock solution in anhydrous toluene) was transferred into the reaction flask using a cannula, and the resulting mixture was stirred until homogeneous. The flask was immersed in a 60 ℃ oil bath with stirring for 175 minutes, after which the resulting mixture was diluted with cold chloroform, filtered to remove the enzyme, concentrated by rotoevaporation, and dried *in vacuo*. The product was analysed by ^{1}H NMR spectroscopy (CDCl$_3$), GPC (CHCl$_3$), MALDI-ToF mass spectrometry, and DSC. Although the crude product was utilized for further experiments, it however was purified *via* precipitation in methanol from chloroform for DSC analysis.

Preparation of PPDL-*b*-Poly(acrylate) Copolymers for Fuels Testing

Acrylate, PPDL macro-CTA **4**, and anhydrous toluene (50 wt.%) were combined in a Schlenk tube equipped with magnetic stirring according to the quantities outlined in Table 6.2, degassed *via* three freeze-pump-thaw cycles, and refilled with argon. The Schlenk tube was immersed in an 80 ℃ oil bath with stirring for approximately 1 hour. Thereafter, the required amount of degassed AIBN stock solution in anhydrous toluene (10 g L^{-1}) was injected, and the reaction was permitted to stir for the indicated amount of time. An aliquot was analysed by ^{1}H NMR spectroscopy (CDCl$_3$), after which the mixture was taken up in cold chloroform, filtered to remove the enzyme, concentrated *in vacuo*, precipitated in methanol, and analysed by ^{1}H NMR spectroscopy (CDCl$_3$), GPC (CHCl$_3$), DSC, and MALDI-ToF mass spectrometry where indicated.

Table 6.2: Reagent quantities for the preparation of PPDL-*b*-poly(acrylate) copolymers.

Entry	Macro-CTA	Acrylate	AIBN	Toluene (mL)	Time (min)
		2-EHA			
1	9.0 g (1.27 mmol)	26.96 mL (126.86 mmol)	20.83 mg (12.7×10^{-2} mmol)	37.93	8
2	9.0 g (1.27 mmol)	26.96 mL (126.86 mmol)	20.83 mg (12.7×10^{-2} mmol)	37.93	11
3	4.0 g (5.64×10^{-1} mmol)	11.98 mL (56.4 mmol)	9.26 mg (5.64×10^{-2} mmol)	16.85	28
4	2.0 g (2.82×10^{-1} mmol)	17.97 mL (84.6 mmol)	4.63 mg (2.82×10^{-2} mmol)	20.66	15
5	2.5 g (3.52×10^{-1} mmol)	22.46 mL (105.72 mmol)	5.79 mg (3.52×10^{-2} mmol)	25.82	29
		IDA			
6	6.2 g (8.74×10^{-1} mmol)	21.21 mL (87.4 mmol)	14.35 mg (8.74×10^{-2} mmol)	28.58	10
7	4.2 g (5.92×10^{-1} mmol)	14.37 mL (59.2 mmol)	9.72 mg (5.92×10^{-2} mmol)	19.36	17
8	2.6 g (3.67×10^{-1} mmol)	8.90 mL (36.7 mmol)	6.02 mg (3.67×10^{-2} mmol)	11.97	31
9	1.8 g (2.54×10^{-1} mmol)	18.48 mL (76.13 mmol)	4.17 mg (2.54×10^{-2} mmol)	20.73	15
		LA			
10	6.5 g (2.54×10^{-1} mmol)	27.69 mL (91.6 mmol)	15.05 mg (9.16×10^{-2} mmol)	35.75	10
11	4.5 g (63.4×10^{-1} mmol)	19.17 mL (63.4 mmol)	10.42 mg (6.34×10^{-2} mmol)	24.79	17
12	3.0 g (42.3×10^{-1} mmol)	12.78 mL (42.3 mmol)	6.95 mg (4.23×10^{-2} mmol)	16.51	31
13	2.0 g (2.82×10^{-1} mmol)	25.56 mL (84.59 mmol)	4.63 mg (2.82×10^{-2} mmol)	28.37	23
14	2.0 g (2.82×10^{-1} mmol)	25.56 mL (84.59 mmol)	4.63 mg (2.82×10^{-2} mmol)	28.37	23
		SA			
15	6.0 g (8.46×10^{-1} mmol)	35.38 mL (84.6 mmol)	13.9 mg (8.46×10^{-2} mmol)	39.57	9
16	7.0 g (9.87×10^{-1} mmol)	41.28 mL (98.7 mmol)	16.2 mg (9.87×10^{-2} mmol)	46.18	17
17	4.5 g (6.34×10^{-1} mmol)	26.53 mL (63.4 mmol)	10.42 mg (6.34×10^{-2} mmol)	29.69	27
18	1.5 g (2.1×10^{-1} mmol)	26.53 mL (63.4 mmol)	3.47 (2.1×10^{-2} mmol)	26.22	21

Preparation of Block Copolymer Stock Solutions to Treat Diesel

Block copolymer (1 g) was dissolved in Solvesso 150 (100 mL) and held at room temperature overnight. The appearance of the solution was noted both upon initial mixing and following standing at room temperature overnight. The solutions were used to treat diesel fuel

with up to 400 ppm of the block copolymer per fuel sample in order to prepare samples for CFPP testing and cold temperature analysis (specifically, to evaluate wax dispersion and visualize wax crystal size and morphology *via* microscopy).

Cold Temperature Analysis of Diesel Fuel Samples

Treated fuel samples (80 g) were cooled in a Clive Hurley Cold Room. The cold room was rapidly cooled from ambient temperature to 7 ℃, and cooled 1 ℃ per hour thereafter, equilibrating at -18 ℃ overnight. The percent wax settling was noted for every sample. Furthermore, wax crystals were imaged for every sample using an optical microscope, and photographs of the wax crystals were taken at different magnifications, as indicated by scale bars.

Determination of the Cold Filter Plugging Point (CFPP)

The cold filter plugging point test was carried out at the Analytical Testing Laboratory according to Infineum UK Ltd procedures, specifically IP309. A 40 mL fuel sample was cooled at a rate of 1 °C per minute in 1 °C intervals using a cooling bath. At each 1 °C interval, the fuel was passed through a 45 µm gauze filter and into a bulb pipette under vacuum. The time taken for the pipette to fill with fuel was recorded. The fuel was then passed back through the filter and into the fuel reservoir to be further cooled by the cooling bath. This process was repeated until the time taken to fill the bulb pipette exceeded 60 seconds or the fuel failed to pass back into the reservoir, at which point the test was terminated. The temperature at which the test was terminated was taken as the CFPP temperature. CFPP tests were run in duplicate, and where the results differed by >2 °C, the samples are tested an additional 2 times. The averages of the different runs were calculated and quoted as the CFPP temperature.

6.5 Experimental Details for Chapter 4

Preparation of Triphenylstannane dithiobenzylester (5)

Anhydrous stannous chloride (1.0 g, 5.17 mmol) was weighed into a Schlenk flask equipped with magnetic stirring under an inert atmosphere. Dry, degassed tetrahydrofuran (100 mL) was transferred into the Schlenk flask using a cannula. The resulting solution was cooled in a dry ice/acetone bath, and a degassed solution of phenyllithium (15.51 mmol) in dibutyl ether was added drop wise, turning the mixture yellow, red, and finally purple. The mixture was permitted to warm to 0 ℃ with stirring over approximately two hours, after which dry, degassed 1,4-dioxane (1.03 mL, 10.34 mmol) and carbon disulfide (1.27 mL, 10.34 mmol) were added drop

wise with cooling in an ice bath. The resulting red mixture was permitted to warm to room temperature with stirring over approximately two hours, after which dry, degassed benzyl bromide (0.94 mL, 7.75 mmol) was added drop wise. The resulting mixture was permitted to stir overnight, after which it was filtered and concentrated *in vacuo* to yield a dark purple solid. The mixture was taken up in petroleum ether, filtered, concentrated, and dried *in vacuo*, after which it was recrystallized repeatedly from acetone to yield purple crystals (0.70 g, 32%):[3-5] ^{1}H NMR δ_H (400 MHz, CDCl$_3$) = 7.85-7.00 (20H, m, ArH), 4.68 (2H, s, -CH_2Ph); ^{13}C NMR δ_C (400 MHz, CDCl$_3$) = 137.5, 137.2, 137.2, 129.8, 129.5, 129.3, 129.0, 128.8, 128.6, 127.6, 39.0; m.p.= 94.8 °C; UV (λ_{max}, CHCl$_3$) = 317 nm; IR (neat, ν_{max} cm^{-1}) = 1048 (CS$_2$ $\nu_{assymetric}$), 809 (CS$_2$ $\nu_{symmetric}$); TGA = 229.8 °C (78.9 % total mass loss).

Preparation of Triphenylstannane dithioisopropylester (6)

Anhydrous stannous chloride (1.0 g, 5.17 mmol) was weighed into a Schlenk flask equipped with magnetic stirring under an inert atmosphere. Dry, degassed tetrahydrofuran (100 mL) was transferred into the Schlenk flask using a cannula. The resulting solution was cooled in a dry ice/acetone bath, after which a degassed solution of phenyllithium (15.51 mmol) in dibutyl ether was added drop wise, turning the mixture yellow, red, and finally purple. The mixture was permitted to warm to 0 °C with stirring over approximately two hours, after which dry, degassed 1,4-dioxane (1.03 mL, 10.34 mmol) and carbon disulfide (1.27 mL, 10.34 mmol) were added drop wise with cooling in an ice bath. The resulting red mixture was stirred at room temperature for approximately two hours, after which dry, degassed 2-iodopropane (0.77 mL, 7.75 mmol) was added drop wise. The resulting mixture was permitted to stir overnight, after which it was filtered, concentrated, and dried *in vacuo* to yield a dark purple solid. The mixture was taken up in petroleum ether, filtered, concentrated, and dried *in vacuo*, after which it was recrystallized repeatedly from acetone and petroleum ether to yield purple crystals (0.18 g, 13%):[6,7] ^{1}H NMR δ_H (300 MHz, CDCl$_3$) = 7.88-7.28 (15H, m, ArH), 4.58 (1H, sept, $^3J_{H-H}$ = 6.0 Hz, -CH(CH$_3$)$_2$), 1.35 (6H, d, $^3J_{H-H}$ = 6.0 Hz, -CH(CH_3)$_2$); ^{13}C NMR δ_C (500 MHz, CDCl$_3$) = 266.0, 137.8, 137.3, 137.2, 137.0, 136.5, 129.7, 129.6, 129.5, 129.0, 128.8, 128.6, 38.5, 21.3; m.p.= 131.4 °C; UV (λ_{max}, CHCl$_3$) = 318 nm; IR (neat, ν_{max} cm^{-1}) = 1032 (CS$_2$ $\nu_{assymetric}$), 804 (CS$_2$ $\nu_{symmetric}$); TGA = 219.8 °C (80.4 % total mass loss).

Polymerization of Styrene using Triphenylstannane dithiobenzylester (5) as a CTA

Styrene (2.22mL, 19.3 mmol), triphenylstannane dithiobenzylester (**5**) (100.0 mg, 0.19 mmol), and AIBN (3.2 mg, 0.02 mmol) were combined in an ampoule equipped with magnetic

stirring, degassed *via* three freeze-pump-thaw cycles, and refilled with argon. The ampoule was immersed in a 60 ° C oil bath with stirring and aliquots were taken at regular intervals for ^{1}H NMR spectroscopy (CDCl$_3$) and GPC (THF) analysis.

DP 6 Polystyrene: ^{1}H NMR: δ_H (300 MHz, CDCl$_3$) = 8.20-6.20 (50H, m, Ar*H*), 3.10-2.96, (1H, dd, $^3J_{H-H}$ = 6.0 Hz, Ph$_3$SnC(S)S-C*H*RCH$_2$-), 2.45-1.75 (5H, m, -CH$_2$C*H*RCH$_2$-), 1.75-1.00 (12H, -CHRC*H$_2$*CHR-), 1.34-1.26 (2H, t, $^3J_{H-H}$ = 6.0 Hz, Ar-C*H$_2$*CH$_2$R).

Polymerization of Methyl acrylate using Triphenylstannane dithiobenzylester (5) as a CTA

Methyl acrylate (1.76 mL, 19.3 mmol), triphenylstannane dithiobenzylester (**5**) (100.0 mg, 0.19 mmol), and AIBN (3.2 mg, 0.02 mmol) were combined in an ampoule equipped with magnetic stirring, degassed *via* three freeze-pump-thaw cycles, and refilled with argon. The ampoule was immersed in a 60 ℃ oil bath with stirring and aliquots were taken at regular intervals for ^{1}H NMR spectroscopy (CDCl$_3$) and GPC (THF) analysis.

DP 11 Poly(methyl acrylate): ^{1}H NMR: δ_H (300 MHz, CDCl$_3$) = 7.85-6.85 (20H, m, Ar*H*), 3.95-3.35 (33H, s, -OC*H$_3$*), 3.22-3.02 (1H, dd, $^3J_{H-H}$ = 6.0 Hz, Ph$_3$SnC(S)S-C*H*CH$_2$-), 2.61-2.52 (2H, m, Ph$_3$SnC(S)S-CHRC*H$_2$*-), 2.47-2.17 (10H, bs, -CH$_2$C*H*RCH$_2$-), 2.10-1.85 (5H, m, -CHRC*H$_2$*CHR- *meso*), 1.85-1.55 (10H, m, -CHRC*H$_2$*CHR- *racemo*), 1.55-1.38 (5H, m, -CHRC*H$_2$*CHR- *meso*), 1.38-1.28 (2H, t, $^3J_{H-H}$ = 6.0 Hz, Ar-C*H$_2$*CH$_2$-).

Synthesis of MDO (7)

Preparation of 2-chloromethyl-1,3-dioxepane

Chloroacetaldehyde dimethyl acetal (69.90 g, 550.0 mmol), 1,4-butanediol (50.0 g, 550.0 mmol), and a catalytic amount of *p*-toluenesulfonic acid were combined in a round bottom flask equipped with magnetic stirring, an oil bath, and a distillation apparatus. The mixture was heated to 120 ^{o}C for three hours during which time methanol was distilled from the reaction mixture. The resulting clear, yellow mixture was further heated to 140 ^{o}C for four hours to drive off residual methanol. The product was distilled under reduced pressure (1.3 Torr) at 30 ^{o}C to yield a clear, colourless liquid (78 %). ^{1}H NMR spectroscopy data matches reported values:[8] δ_H (300 MHz, CDCl$_3$) = 4.87-4.81 (2H, t, -OC*H*CH$_2$Cl), 3.98-3.57 (4H, dm, 22-OC*H$_2$*CH$_2$), 3.46-3.42 (2H, d, -C*H$_2$*Cl), 2.82-1.58 (4H, m, 2-OCH$_2$C*H$_2$*).

Preparation of 2-methylene-1,3-dioxepane

Potassium *t*-butoxide (69.65 g, 620.08 mmol) was degassed *via* three vacuum/nitrogen cycles in a one litre three-necked flask equipped with a heating mantle, magnetic stirring, a

condenser, and a Schlenk line. Degassed, anhydrous tetrahydrofuran (450 mL) was transferred into the reaction mixture using a cannula, and 2-chloromethyl-1,3-dioxepane (46.74 g, 310.39 mmol) was injected. The reaction mixture was refluxed at 85 $^{\circ}$C under $N_{2\,(g)}$ for 18 hours, after which the resulting tan coloured mixture was filtered and distilled from CaH_2 under reduced pressure (6.0 Torr) at 30 $^{\circ}$C to yield a clear, colourless liquid (82 %). NMR spectroscopy data match reported values:[8] δ_H (400 MHz, CDCl$_3$) = 3.88-3.74 (4H, m, 2 -OCH_2CH$_2$-), 3.34 (2H, s, C=CH_2), 1.75-1.61 (4H, m, 2 -OCH$_2$CH_2-); δ_C (400 MHz, CDCl$_3$) = 163.9, 70.1, 67.1, 28.8.

Polymerization of MDO (7) using Triphenylstannane dithioisopropylester (6) as a CTA

MDO (0.98 mL, 8.76 mmol), triphenylstannane dithioisopropylester (**6**) (41.1 mg, 8.76 x 10^{-2} mmol), and AIBN (1.44 mg, 8.76 x 10^{-3} mmol) were combined in an ampoule equipped with magnetic stirring, degassed *via* three freeze-pump-thaw cycles, and refilled with argon. Additional ampoules were similarly prepared for individual kinetic points. The ampoules were immersed in an oil bath (60, 100, or 150 ºC) with stirring and stopped at different time intervals (72, 48, and 24 hours, respectively). Aliquots were removed for direct ^{1}H NMR spectroscopy (CDCl$_3$) and GPC (CHCl$_3$) analysis. Free radical control polymerizations were similarly performed in the absence of AIBN.

Polymerization of Isoprene using Triphenylstannane dithioisopropylester (6) as a CTA

Working in a glovebox, isoprene (3.67 mL, 36.7 mmol), AIBN (6.0 mg, 0.04 mmol), and triphenylstannane dithioisopropylester (**6**) (172.2 mg, 0.37 mmol) were combined in a vial equipped with magnetic stirring until homogenous. Approximately 0.6 mL aliquots were rapidly transferred to 5 ampoules equipped with magnetic stirring. The ampoules were degassed *via* three freeze-pump-thaw cycles, refilled with argon, immersed in a 60 $^{\circ}$C oil bath, and stopped at regular time intervals by freezing in $N_{2\,(l)}$. Monomer conversion was analysed by gravimetry. Thereafter, the residue was taken up twice in dichloromethane and dried *in vacuo* to remove isoprene. Residual material was analysed by ^{1}H NMR spectroscopy (CDCl$_3$) and GPC (THF). Free radical control polymerizations were similarly performed in the absence of AIBN.

DP 6 Poly(isoprene): ^{1}H NMR: δ_H (300 MHz, CDCl$_3$) = 7.85-7.30 (15H, m, ArH), 6.00-4.50 (6H, m, -C=CHCCH$_2$-), 3.30-2.95 (2H, m, -SCH_2C-), 2.95-2.50 (1H, m, -CH(CH$_3$)$_2$), 2.35-1.65 (12H, m, -CCH_2C-), 1.65-1.28 (18H, m, -C(CH_3)), 1.29-0.80 (6H, m, -CH(CH_3)$_2$).

6.6 References

(1)   Still, W. C.; Kahn, M.; Mitra, A. *J. Org. Chem.* **1978**, *43*, 2923.

(2)   Petzetakis, N.; Dove, A. P.; O'Reilly, R. K. *Chem. Sci.* **2011**, *2*, 955.

(3)   Carr, S. W.; Colton, R.; Dakternieks, D.; Hoskins, B. F.; Steen, R. *J. Inorg. Chem.* **1983**, *22*, 3700.

(4)   Hiller, W.; Kunze, U.; Tischer, R. *Inorg. Chim. Acta* **1987**, *133*, 51.

(5)   Kunze, U.; Tischer, R. *Chem. Ber. Recl.* **1987**, *120*, 1099.

(6)   Kunze, U.; Bolz, P. R.; Winter, W. *Chem. Ber. Recl.* **1981**, *114*, 2744.

(7)   Kunze, U.; Hattich, T. *Chem. Ber. Recl.* **1982**, *115*, 3663.

(8)   Taskinen, E.; Pentikäinen, M.-L. *Tetrahedron* **1978**, *34*, 2365.